UNIVERSITÉ DE STRASBOURG

ÉCOLE DOCTORALE DES SCIENCES CHIMIQUES

Institut de Chimie, UMR 7177

THÈSE présentée par :

Fan HE

soutenue le : **23 septembre 2015**

pour obtenir le grade de : **Docteur de l'université de Strasbourg**

Discipline/ Spécialité : Chimie

Complexes de métaux de transition avec des ligands carbènes N-hétérocycliques : synthèse et réactivité

THÈSE dirigée par :
M. BRAUNSTEIN Pierre Directeur de recherche, CNRS, Université de Strasbourg
Codirecteur de thèse :
M. DANOPOULOS Andreas Fellow USIAS, Université de Strasbourg

RAPPORTEURS :
M. ALBRECHT Martin Professeur, Université de Bern
M. LE GENDRE Pierre Professeur, Université de Bourgogne

AUTRES MEMBRES DU JURY :
M.BRÄSE Stephan Professeur, Karlsruher Institut für Technologie
M. WESOLEK Marcel Chargé de recherche, CNRS, Université de Strasbourg

REMERCIEMENTS

Je tiens tout d'abord à remercier Dr. Pierre BRAUNSTEIN, mon directeur de thèse, pour son accueil au sein du laboratoire de Chimie de Coordination à l'université de Strasbourg. Je le remercie plus particulièrement pour son soutien et ses précieux conseils. Je lui exprime toute ma reconnaissance pour avoir valorisé au mieux les travaux réalisés.

Je tiens à remercier Dr. Andréas DANOPOULOS, mon codirecteur de thèse, pour ses précieux conseils et pour m'avoir initié aux techniques de travail en milieu inerte pour les produits sensibles.

Je souhaite remercier les professeurs Martin ALBRECHT, Pierre LE GENDRE et Stephan BRÄSE ainsi que le Dr. Marcel WESOLEK de me faire l'honneur de juger mon travail.

Je remercie le professeur Laurent RUHLMANN, Dr. Jean-Paul GISSELBRECHT, Dr. Sylvie CHOUA ainsi que Dr. Maylis ORIO pour leurs précieuses collaborations

Je tiens à remercier les services communs de l'Université de Strasbourg et plus particulièrement le service de radiocristallographie aux rayons-X, le service de RMN, celui d'analyse élémentaire et le magasin de chimie.

Un grand merci à Nadia Bouaouina, Sandrine Garcin et Soumia Hnini pour leur aide dans tous les aspects administratifs de la thèse.

Tous les membres du laboratoire (passé ou présent) sont chaleureusement remerciés : (dans le désordre)

Dr. Jacky Rosé, Marc Mermillon-Fournier, Mélanie Boucher, Dr. Lucie Routaboul, Dr. Alessio Ghisolfi, Dr. Sophie Hameury, Thomas Simler, Minghui Yuan, Pengfei Ai, Xiaoyu Ren, Dr. Paulin Buchwalter, Dr. Martin Jagenbrein, Dr. Serena Orbisaglia, Mary E Garner, Dr. Valentine Charra, Dr. Béatrice Jacques, Dr. Pierre de Frémont, Dr. Kirill Monakhov, Dr. Alexandre Massard, Venkatesh Subbiah…

Enfin un dernier mot pour ma famille et tout particulièrement pour mes parents, toute ma gratitude va vers eux.

Merci à tous !

TABLE DES MATIERES

ABBREVIATIONS

d	chemical shift
1D	one dimensial
2D	two dimensial
Ad	adamantyl
anal. calcd.	analysis caclulated
Ar	aryl
br	broad
CCDC	Cambridge Crystallographic Data Centre
COESY	correlation spectroscopy
CIF	crystallographic information file
coa	cyclooctane
cod	cyclooctadiene
coe	cyclooctene
Cp	cyclopentadienyl
Cp*	pentamethylcyclopentadienyl
Cy	cyclohexyl
d	doublet
DCM	dichloromethane
DFT	density functional theory
Dipp	2,6-diisopropylphenyl
DMA	dimethylacetamide
DMSO	dimethylsulfoxide
EPR	electron paramagnetic resonance

equiv.	equivlent
ESI	electronic supplementry information
Et	ethyl
FTIR	fourier transform infrared spectroscopy
GC	gas chromatography
h	hour(s)
HMBC	heteronuclear multiple bond correlation
HSQC	heteronuclear single-quantum correlation
Hz	hertz
i-Pr	isopropyl
IR	infrared
KHMDS	potassium bis(trimethylsilyl)amide
m	multiplet
m-	meta-
MAO	methylaluminoxane
Me	methyl
Mes	mesityl
min	minute(s)
NaHMDS	sodium bis(trimethylsilyl)amide
n-Bu	*n*-butyl
NHC	N-heterocyclic carbene
NOESY	nuclear overhauser effect spectroscopy
o-	ortho-
OTf	trifluoromethanesulfonate

p-	para-
Ph	phenyl
ppm	parts per million
PTSA	*p*-toluenesulfonic acid
Py	pyridine
q	quartet
RCM	ring closing metathesis
RT	room temperature
s	singlet
sept	septuplet
t	triplet
TBA	2,2-dimethylbutane
TBE	3,3-dimethyl-1-butene
t-Bu	*tert*-butyl
THF	tetrahydrofuran
TMS	trimethylsilyl
TOF	turnover frequency
TON	turnover number

Introduction générale

Introduction générale

Le sujet de cette thèse est la synthèse de complexes contenant des ligands carbènes de type N-hétérocyclique protique (pNHC) fonctionnalisé par une imine dans le but de développer des méthodologies synthétiques permettant d'avoir accès aux complexes avec des pNHC, des imidazolides 'anioniques' ainsi que leurs complexes homo- et hétéro-nucléaires correspondants. Dans cette introduction, nous présenterons brièvement différents ligands tels que les NHCs, les NHCs fonctionnalisés avec une imine, les NHCs protiques et les ligands polyfonctionnels en chimie de coordination et organométallique.

1 Les ligands Carbènes-N-Hétérocycliques (NHCs)

L'isolement par Arduengo et collaborateurs de carbènes N-hétérocycliques stables grâce à des N substituants volumineux sur le cycle imidazole (Schéma 1),[1] a déclenché un engouement croissant pour ce type de ligand, en particulier dans le domaine de la chimie organométallique.

Schéma 1. Synthèse permettant l'isolement du premier carbène N-hétérocyclique stable **2** par Arduengo.

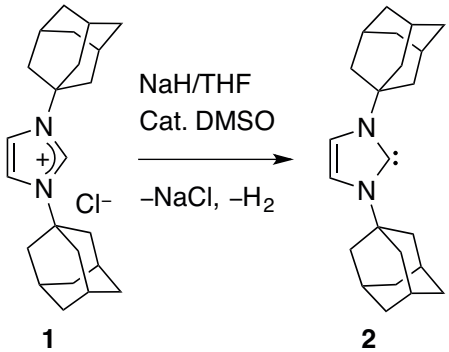

De nombreux aspects de la chimie des NHCs ont été passés en revue. La première description exhaustive des méthodes de synthèse des NHCs ainsi que de leur chimie de coordination a été publiée par Herrmann et Köcher.[2] Tous les types de carbènes stables incluant les dérivés acycliques ont fait l'objet d'une revue par Bertrand.[3] La coordination des ligands NHC aux alcalins, alcalino-terreux et aux métaux de transition des groupes 3 à 7,[4] des métaux de transition des groupes 8 à 11,[5]

Références p 11

ainsi qu'au éléments des groupes 13 et 14[6] ont fait respectivement l'objet de différents articles de revues très détaillés. En particulier les réactions de couplage C-C catalysées par des complexes Pd NHC[7] et l'utilisation des complexes carbéniques du Ru dans la réaction catalytique de métathèse des oléfines[8] ont fait l'objet de revues exhaustives.

2 Ligands polyfonctionnels

La conception des ligands est devenue une part importante dans la chimie organométallique étant donné que les ligands contrôlent de façon subtile la géométrie et les propriétés du centre métallique dans les complexes. En particulier les ligands possédant différents groupes fonctionnels tel que des donneurs dur et mou (ligand hybride, Schéma 2) ont été utilisés de façon croissante en chimie. Des propriétés tout à fait inhabituelles peuvent être obtenues pour ces complexes métalliques quand des caractéristiques comparables mais différentes sont combinées dans un même ligand.[9]

Schéma 2. Modes de coordination d'un ligand hybride.

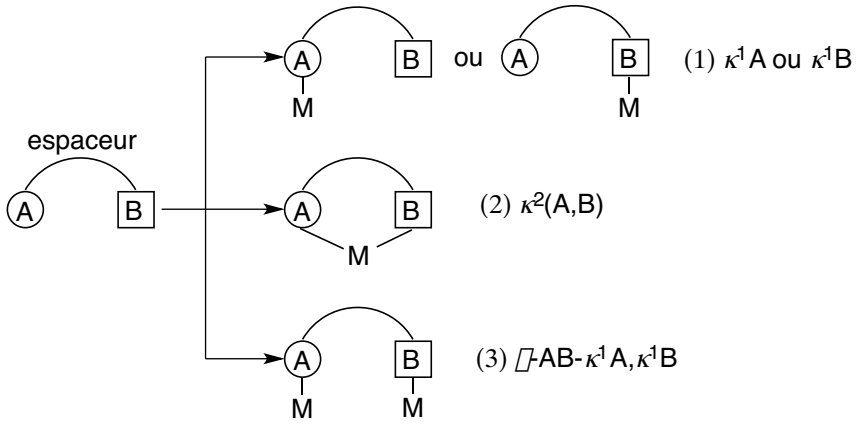

Si le pouvoir donneur de ces deux fonctionnalités est différent, une discrimination avec le centre métallique est anticipée (Schéma 2). Ces fonctionnalités peuvent à leur tour influencer les propriétés des liaisons et la réactivité du ou des ligands liés au même centre métallique et tout particulièrement celui en position *trans*. Un concept utile a vu le jour à partir de l'étude des propriétés dynamiques des interactions induites avec le centre métallique impliquant des ligands hybrides et il a été nommé hémilabilité.[10]

En plus de la capacité donneur du carbone des ligands NHC, leurs N-substituants

Références p 11

jouent un rôle essentiel dans les modifications de la stabilité, des propriétés électroniques, de la géométrie ainsi que des propriétés catalytiques impliquant ces complexes NHC.[11] Ci-après sont décrits des ligands NHC fonctionnels.

3 Ligand hybride NHC avec une fonction imine

Au regard des propriétés catalytiques remarquables des complexes[12] α-diimine et pyridine diimine, il apparaît judicieux d'élaborer des complexes métalliques possédant des ligands NHC fonctionnalisés[16] par un groupement imine. Les propriétés intéressantes des ligands imino-NHCs en tant que donneurs hybrides sont basées sur l'association d'un groupement imine σ-donneur/π-accepteur avec un groupement NHC, puissant σ-donneur/faible π-accepteur. Un accomplissement remarquable des complexes NHC fonctionnalisés avec une imine a été obtenu avec un complexe Rh(I) NHC fonctionnalisé avec une imine chélatante[13] qui donne des activités et sélectivités très élevées dans la réaction catalytique de cyclopropanation des alcènes. Les ligands NHC fonctionnalisés avec une imine seront introduits de façon plus détaillée dans le chapitre 1.

4 Carbènes N-hétérocycliques protiques

Dans la plupart de leurs complexes avec les métaux, les deux sites N de l'hétérocycle comportent un substituant R (R = R' ou R ≠ R' pour **3**) qui permet des variations subtiles tant stériques qu'électroniques des ligands NHC. Les complexes avec des NHC protiques (pNHC) (représentation **4** où R peut aussi être un H) sont moins répandus. Cependant le fragment NH peut être un site réactif et peut permettre d'intéressantes interactions hydrogène intra- ou inter-moléculaires, ces dernières sont essentielles pour la reconnaissance de substrat en catalyse homogène.[14]

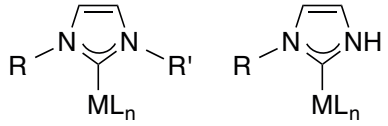

3 **4**

Possédant un groupe acide N-H, les pNHCs ne peuvent généralement pas être obtenus par simple déprotonation de leurs sels d'imidazolium correspondants. Les

Références p 11

pNHCs libres ne sont pas stables et tendent à s'isomériser en leurs imidazoles correspondants.[15] Ceci a suscité le développement de différentes méthodes d'accès aux complexes des métaux pNHC qui ont fait récemment l'objet d'une revue exhaustive.[14b,14c,16] Le premier complexe de métal de transition comportant un 1H-imidazol-2-ylidene (R = H in **4**) a été obtenu par réarrangement d'un complexe Ru(II)-imidazole (**5**) en un complexe Ru(II)-pNHC (**6**) par catalyse acide[17] (Schéma 1). Récemment, la préparation des complexes similaires de type (benz)imidazole pNHC (**8**) via l'addition oxydante des 2-halogenoazoles (**7**) envers un métal de transition zéro-valent a été décrite par Hahn (Schéma 3).[18]

Schéma 3. Exemples de complexes de métaux de transition possédant un ligand 1H-(benz)imidazol-2-ylidène.[17-18]

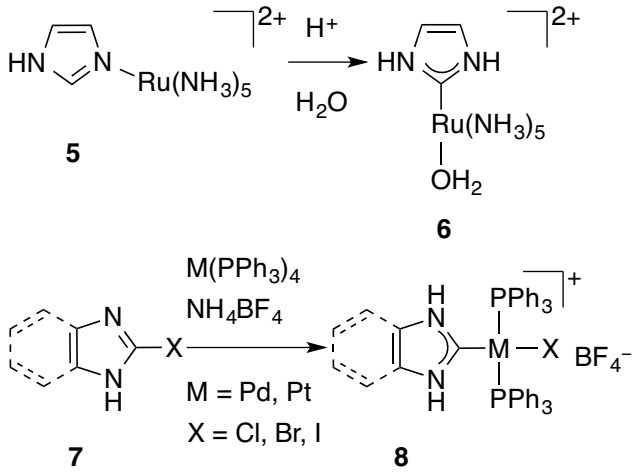

En plus de la capacité donneur du ligand NHC, le substituant R sur N dans **4** peut jouer un rôle majeur envers les propriétés électroniques et de coordination du ligand. Le complexe métallique résultant[11] possède ainsi une stabilité et des propriétés catalytiques particulières. Dans la plupart des complexes métalliques possédant un ligand pNHC, le substituant R est un groupe alkyle ou aryle et il y a relativement peu d'exemples où une fonctionnalité supplémentaire a été incorporée dans le N-substituant qui pourrait donner lieu à une propriété bidente pour le ligand pNHC. Les quelques complexes avec ce type de ligands pNHC fonctionnel possèdent des propriétés intéressantes (Schéma 4).

Références p 11

Schéma 4. Complexes de métaux de transition avec des ligands bidentes pNHC fonctionnels.

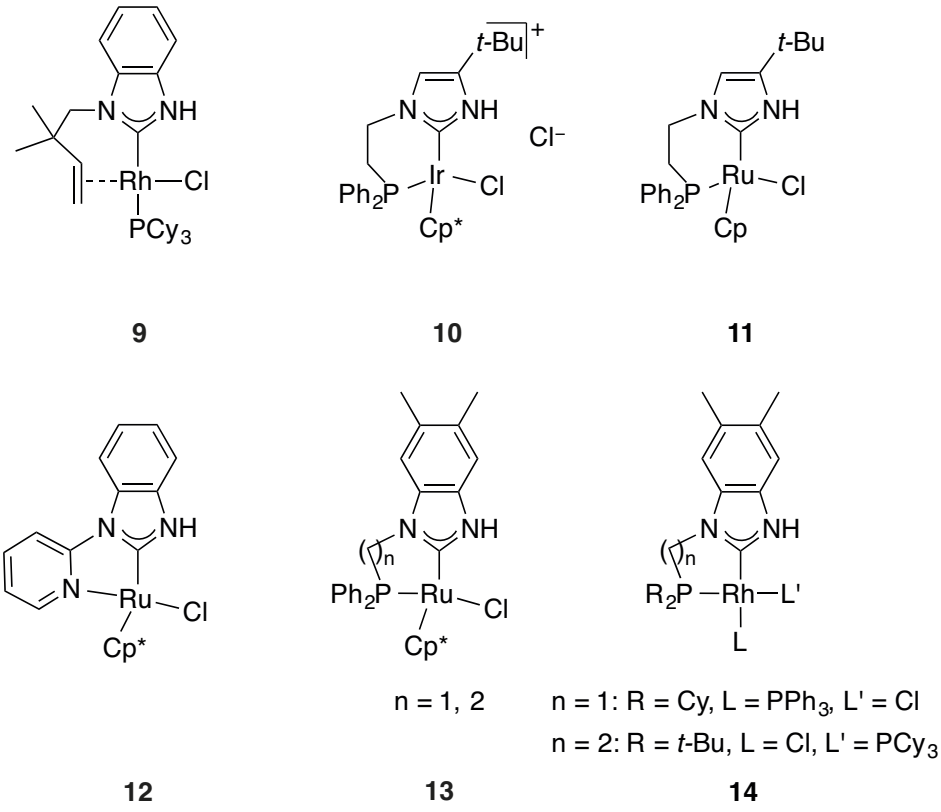

9 **10** **11**

12 **13** **14**

Ainsi, Bergman, Ellman, et leurs collaborateurs ont décrit une réaction intramoléculaire de couplage des alcènes pour former des hétérocycles donnant accès aux azoles fonctionnalisés en position 2. Dans cette réaction un complexe du Rh(I) comportant un ligand pNHC fonctionnalisé avec un alcène **9** a été isolé en tant qu'intermédiaire (Scheme 4).[19] Cette réaction intramoléculaire a été étendue à une réaction de couplage intermoléculaire.[10] Le complexe du Ru(II) possédant un ligand pNHC fonctionnalisé avec un groupement pyridyle **12** décrit par Kuwata et Ikariya (Schéma 4) a été utilisé avec succès dans la réaction catalytique de condensation de la *N*-(2-pyridyl)benzimidazole avec un alcool allylique avec élimination d'eau.[20] Les complexes de l'Ir(III) **10** et du Ru(II) **11** possédant un ligand pNHC fonctionnalisé avec une phosphine décrits par Grotjahn (Schéma 4) sont efficaces dans les réactions d'activation de l'hydrogène moléculaire et de transfert d'hydrogène.[21] Les complexes du Ru(II) possédant eux aussi un ligand pNHC fonctionnalisé avec une phosphine **13**, décrits par Hahn ont révélé des liaisons hydrogène entre le groupe NH et l'accepteur de liaison hydrogène la 1,3-dimethyltetrahydropyrimidin-2(1H)-one (DMAU).[22] Cette propriété pourrait être utilisée pour la reconnaissance d'un substrat et la catalyse

Références p 11

régiosélective à l'aide de complexes possédant des ligands pNHC.[14b,14c] Dans les complexes du Rh(I) possédant des ligands pNHC fonctionnalisés par un groupement phosphine **14**, décrits par Hahn, et qui possèdent des encombrements stériques sur les substituants des ligands phosphines PR_3 et P^C, des isomères à géométrie *cis*-P,P et *trans*-P,P ont pu être isolés.[23]

Références p 11

Références

(1) Arduengo, A. J., III; Harlow, R. L.; Kline, M., *J. Am. Chem. Soc.* **1991,** *113*, 361–363.

(2) Herrmann, W. A.; Köcher, C., *Angew. Chem. Int. Ed. Engl.* **1997,** *36*, 2162–2187.

(3) Bourissou, D.; Guerret, O.; Gabbaï, F. P.; Bertrand, G., *Chem. Rev.* **2000,** *100*, 39–92.

(4) Bellemin-Laponnaz, S.; Dagorne, S., *Chem. Rev.* **2014,** *114*, 8747–8774.

(5) (a) Díez-González, S.; Marion, N.; Nolan, S. P., *Chem. Rev.* **2009,** *109*, 3612–3676. (b) Riener, K.; Haslinger, S.; Raba, A.; Högerl, M. P.; Cokoja, M.; Herrmann, W. A.; Kühn, F. E., *Chem. Rev.* **2014,** *114*, 5215–5272.

(6) (a) Asay, M.; Jones, C.; Driess, M., *Chem. Rev.* **2011,** *111*, 354–396. (b) Fliedel, C.; Schnee, G.; Avilés, T.; Dagorne, S., *Coord. Chem. Rev.* **2014,** *275*, 63–86.

(7) (a) Kantchev, E. A. B.; O'Brien, C. J.; Organ, M. G., *Angew. Chem. Int. Ed.* **2007,** *46*, 2768–2813. (b) Marion, N.; Nolan, S. P., *Acc. Chem. Res.* **2008,** *41*, 1440–1449. (c) Würtz, S.; Glorius, F., *Acc. Chem. Res.* **2008,** *41*, 1523–1533.

(8) (a) Fürstner, A., *Angew. Chem. Int. Ed.* **2000,** *39*, 3012–3043. (b) Trnka, T. M.; Grubbs, R. H., *Acc. Chem. Res.* **2001,** *34*, 18–29. (c) Connon, S. J.; Blechert, S., *Angew. Chem. Int. Ed.* **2003,** *42*, 1900–1923. (d) Clavier, H.; Grela, K.; Kirschning, A.; Mauduit, M.; Nolan, S. P., *Angew. Chem. Int. Ed.* **2007,** *46*, 6786–6801. (e) Samojłowicz, C.; Bieniek, M.; Grela, K., *Chem. Rev.* **2009,** *109*, 3708–3742.

(9) Braunstein, P., *J. Organomet. Chem.* **2004,** *689*, 3953–3967.

(10) Braunstein, P.; Naud, F., *Angew. Chem. Int. Ed.* **2001,** *40*, 680–699.

(11) Tornatzky, J.; Kannenberg, A.; Blechert, S., *Dalton Trans.* **2012,** *41*, 8215–8225.

(12) (a) Johnson, L. K.; Killian, C. M.; Brookhart, M., *J. Am. Chem. Soc.* **1995,** *117*, 6414–6415. (b) Small, B. L.; Brookhart, M.; Bennett, A. M. A., *J. Am. Chem. Soc.* **1998,** *120*, 4049–4050. (c) J. P. Britovsek, G.; C. Gibson, V.; J. McTavish, S.; A. Solan, G.; J. P. White, A.; J. Williams, D.; J. P. Britovsek, G.; S. Kimberley, B.; J. Maddox, P., *Chem. Commun.* **1998**, 849–850.

(13) (a) Rosenberg, M. L.; Krivokapic, A.; Tilset, M., *Org. Lett.* **2009,** *11*, 547–550. (b) Rosenberg, M. L.; Vlašaná, K. r.; Gupta, N. S.; Wragg, D.; Tilset, M., *J. Org. Chem.* **2011,** *76*, 2465–2470.

(14) (a) Meier, N.; Hahn, F. E.; Pape, T.; Siering, C.; Waldvogel, S. R., *Eur. J. Inorg. Chem.* **2007,** *2007*, 1210–1214. (b) Hahn, F. E., *ChemCatChem* **2013,** *5*, 419–430. (c) Jahnke, M. C.; Hahn, F. E., *Coord. Chem. Rev.* **2015,** *293–294*, 95–115.

(15) Karmakar, S.; Datta, A., *Angew. Chem. Int. Ed.* **2014,** *53*, 9587–9591.

(16) Hahn, F. E., Advances in Organometallic Chemistry and Catalysis, **2013**, 111–132.

(17) Sundberg, R. J.; Bryan, R. F.; Taylor, I. F.; Taube, H., *J. Am. Chem. Soc.* **1974,** *96*, 381–392.

(18) (a) Das, R.; Daniliuc, C. G.; Hahn, F. E., *Angew. Chem. Int. Ed.* **2014,** *53*, 1163–1166. (b) Das, R.; Hepp, A.; Daniliuc, C. G.; Hahn, F. E., *Organometallics* **2014,** *33*, 6975–6987.

(19) (a) Tan, K. L.; Bergman, R. G.; Ellman, J. A., *J. Am. Chem. Soc.* **2001,** *123*, 2685–2686. (b) Tan, K. L.; Bergman, R. G.; Ellman, J. A., *J. Am. Chem. Soc.* **2002,** *124*, 3202–3203. (c) Tan, K. L.; Vasudevan, A.; Bergman, R. G.; Ellman, J. A.; Souers, A. J., *Org. Lett.* **2003,** *5*, 2131–2134.

(20) Araki, K.; Kuwata, S.; Ikariya, T., *Organometallics* **2008,** *27*, 2176–2178.

(21) (a) Miranda-Soto, V.; Grotjahn, D. B.; DiPasquale, A. G.; Rheingold, A. L., *J. Am. Chem. Soc.* **2008,** *130*, 13200–13201. (b) Miranda-Soto, V.; Grotjahn, D. B.; Cooksy, A. L.; Golen, J. A.; Moore, C. E.; Rheingold, A. L., *Angew. Chem. Int. Ed.* **2011,** *50*, 631–635.

(22) Hahn, F. E.; Naziruddin, A. R.; Hepp, A.; Pape, T., *Organometallics* **2010,** *29*, 5283–5288.

(23) Naziruddin, A. R.; Hepp, A.; Pape, T.; Hahn, F. E., *Organometallics* **2011,** *30*, 5859–5866.

Chapitre 1

Bibliographie

Résumé du Chapitre 1

Dans ce chapitre sont passés en revue les complexes possédant un ligand NHC fonctionnalisé par un ou deux groupements imine. La réactivité de ces complexes est mentionnée ainsi que les différentes réactions catalytiques dans lesquelles ils sont impliqués.

En plus des complexes NHC-imine de l'Ag et du Cu utilisés aussi pour la transmétallation y figurent les métaux de transition de la première sous-période à l'exception du Sc, V, Mn, Zn.

Le métalloïde Ge y est aussi décrit.

Concernant la deuxième sous-période le Pd et le Rh y tiennent une place de choix, deux autres métaux y sont aussi cités, le Zr et le Ru, tandis que les autres en sont absents.

Références: p 24

Introduction

As stated in the general introduction, the interesting features of the imino-NHCs as hybrid donor ligands are based on the association of a σ-donor/π-acceptor imine with a strong σ-donor/poor π-acceptor NHC functionality. The purpose of this chapter is to survey the literature concerning the research and development of this type of ligands and their metal complexes.

Références: p 24

1 Mono(imino)-NHC ligands and metal complexes

In 2003 Coleman reported the imino-NHC ligand precursor **1** (Z/E isomers) and Ag(I) complex **2**, but transfer of the ligand from Ag(I) to Pd(II) and Rh(I) led to the tautomerisation of the imine moiety to the enamine, affording complexes **3** and **4** (Scheme 1).[1]

Scheme 1.

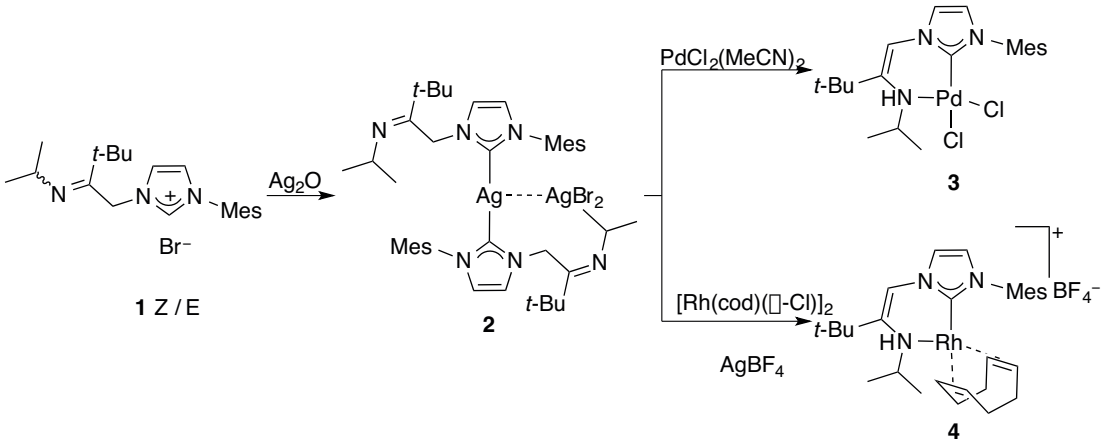

In the study of Bildstein in 2004, a 1,2-rearrangement was observed after deprotonation of the imidazoliun salts **5a**/**b** and 2-iminoyl(benz)imidazoles **6a**/**b** were isolated as the products (Scheme 2).[2]

Scheme 2.

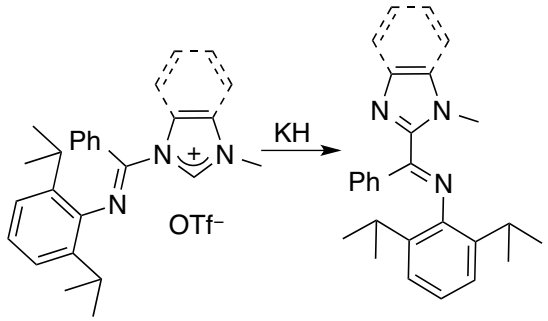

5a: imidazole
5b: benzimindazole

6a: imidazole
6b: benzimindazole

In 2006, the imino-NHC ligand **8** (Z/E isomers) reported by Coleman was the first example of a stable crystalline noncyclic imino-NHC and the Ag(I) complex **9** was also prepared. The Pd(II) complexes **10** and **11**, the Rh(I) complexes **12** and **13** were prepared by the reaction of **8** with the corresponding metal precursors (Scheme 3). The Pd(II) complexes showed moderate activity in Suzuki type C-C cross-coupling reactions, while the Rh(I) complexes were active in the

Références: p 24

hydroformylation of 1-octene.[3]

Scheme 3.

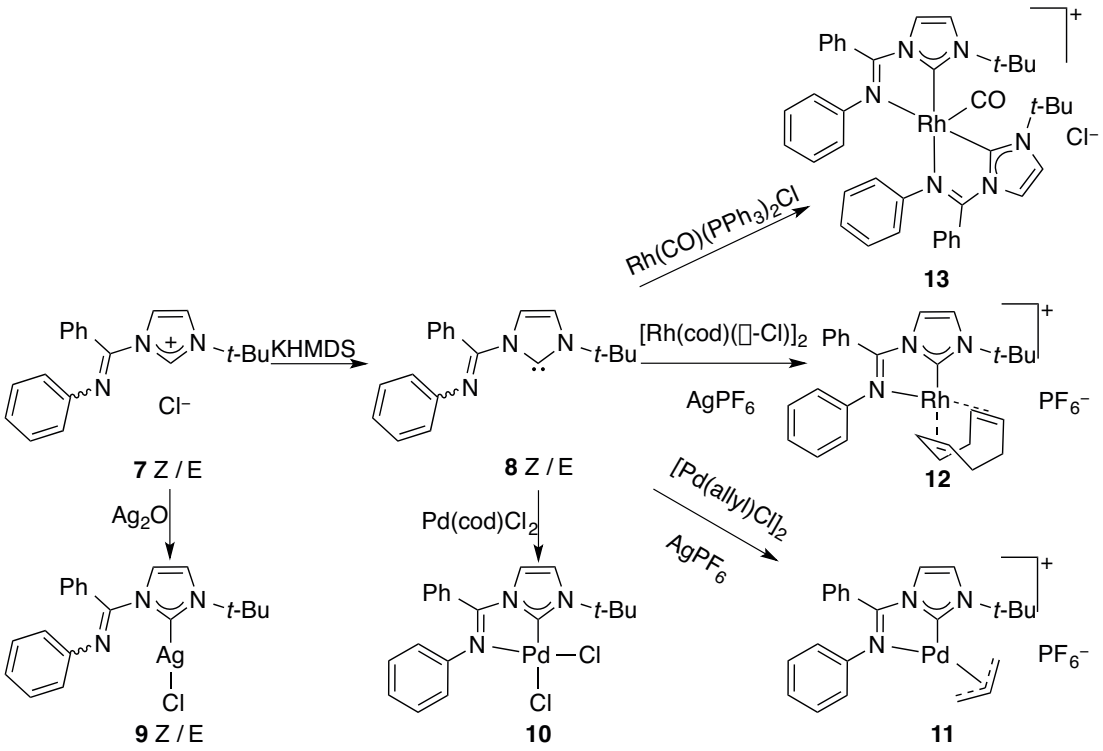

In 2009, a remarkable achievement of imine-functionalized NHC complexes in catalysis was reported by Tilset with the high activity (up to 99%) and *cis*-selectivity (higher than 99%) in the catalytic cyclopropanation of alkenes with the chelated imine-functionalized NHC Rh(I) complex **14** (Scheme 4).[4]

Scheme 4.

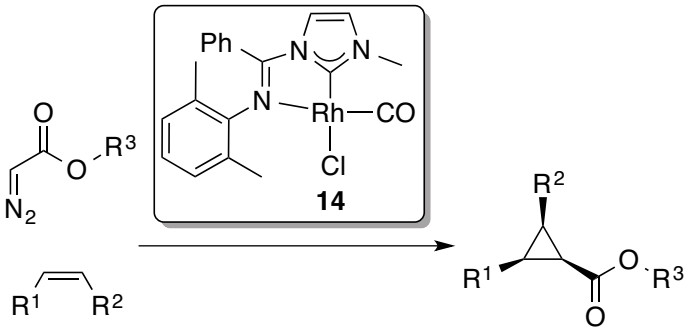

In 2010 the first aryl-substituted imino-NHC ligand precursor **15** was prepared by Lavoie, along with the corresponding Ag(I) and Cu(I) chloride complexes **16** and **17**. An unusual T-shape coordination mode for the copper center in **17** was observed (Scheme 5).[5]

Références: p 24

Scheme 5.

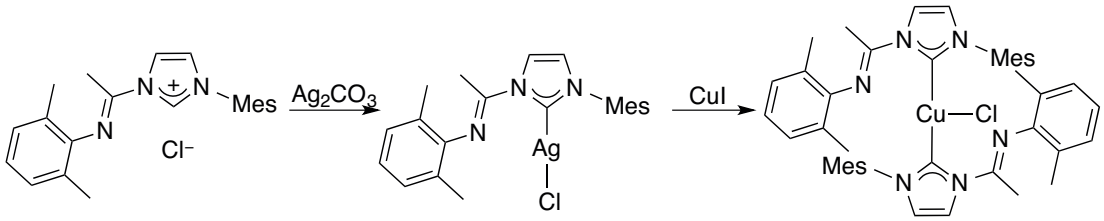

15 **16** **17**

In 2011 Lavoie reported the synthesis of the bulky 1-(1-arylimino-2,2-dimethylpropyl)-3-(aryl)imidazolium salt **19** from the corresponding imidazole and the activated imidoyl chloride. The absence of acidic protons adjacent to the iminic carbon allowed for the first time the isolation of an imino-NHC of this ligand class. The isolated free carbene was coordinated to titanium, zirconium, hafnium and chromium. The resulting metal halide complexes were tested at room temperature and atmospheric pressure in the catalytic polymerization reaction of ethylene. The Zr(IV) complex **22a** was found to be the most active with a productivity of 140 kg(PE) mol^{-1}(Zr) h^{-1} (Scheme 6).[6]

Scheme 6.

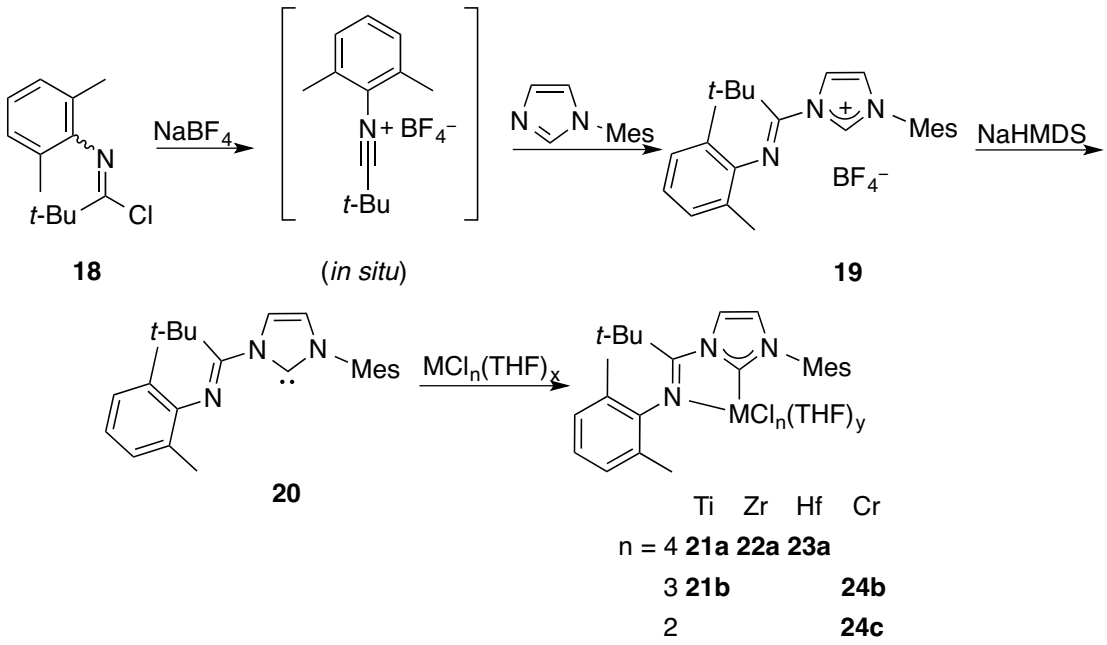

18 (*in situ*) **19**

20

	Ti	Zr	Hf	Cr
n = 4	**21a**	**22a**	**23a**	
3	**21b**			**24b**
2				**24c**

In the case of Ni(II) complexes, the oxidative addition of the imidazolium salt **15** to $Ni(cod)_2$ led to the isolation of the unexpected bis(carbene)$NiCl_2$ complex **26**, presumably through a putative nickel hydride intermediate **25** (Scheme 7). [7]

Références: p 24

Scheme 7.

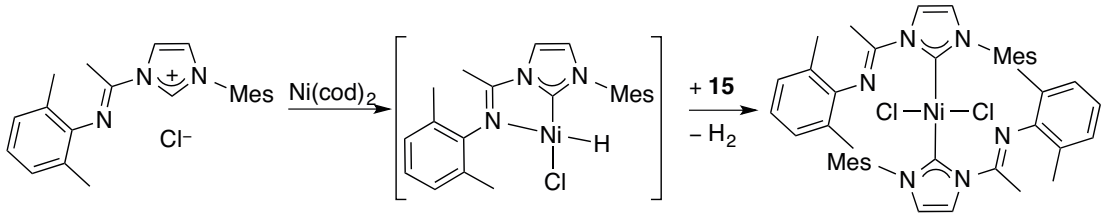

15 **25** **26**

When the Cu(I) complexes **27a**/**b** were used as transmetalating agents, the chelated Ni(II) complexes **28a**/**b** bis(carbene)$NiBr_2$ complex **29** were isolated (Scheme 8).[7]

Scheme 8.

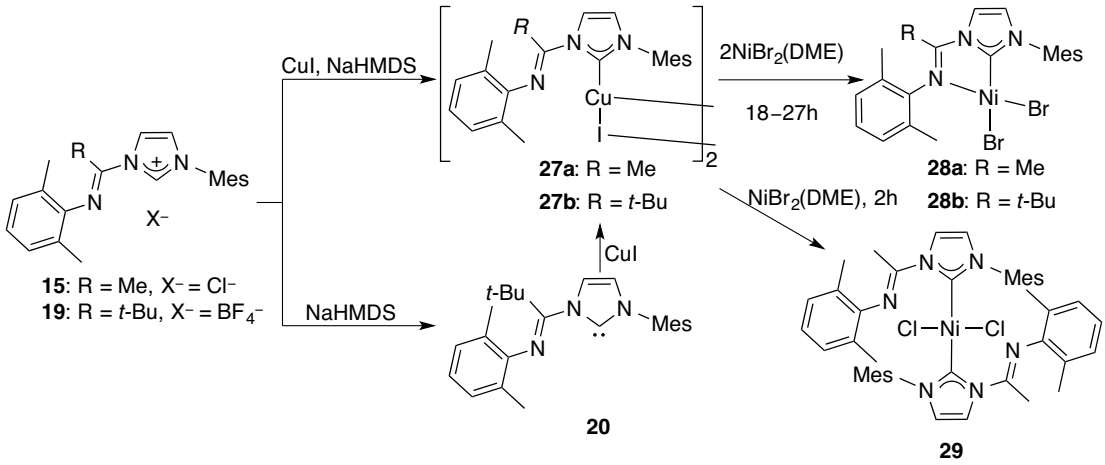

15: R = Me, X^- = Cl^-
19: R = *t*-Bu, X^- = BF_4^-

27a: R = Me
27b: R = *t*-Bu

28a: R = Me
28b: R = *t*-Bu

20

29

In the case of Pd(II) imino-NHC complexes, reactivity studies,[8] catalytic behavior in norbornene polymerization[9] and arylation of electron-deficient fluoroarenes[10] have been reported. While inactive for ethylene polymerization, the palladium methyl complex **30** reacted with CO to afford the insertion product **31** (Scheme 9).

Scheme 9.

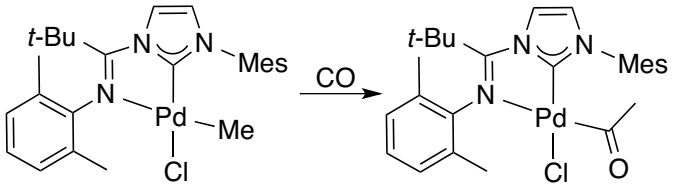

30 **31**

When the ruthenium imino-NHC complex **32** was reacted with $AgPF_6$ with the objective to generate a four-coordinate complex, an unexpected dicationic ruthenium benzyl degradation product **33** was obtained through insertion of the benzylidene in

Références: p 24

the NHC-Ru bond with concomitant reduction of Ru(IV) to Ru(II) (Scheme 10).[11]

Scheme 10.

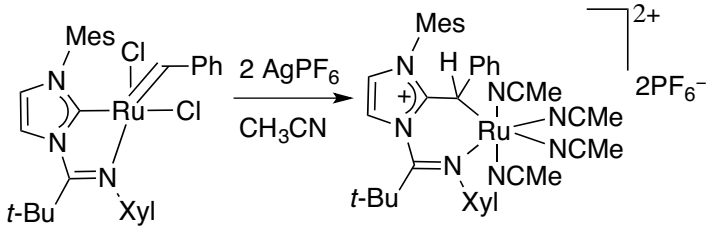

32 **33**

In the study reported by Kinjo, the autoionization of germanium dichloride/dioxane complex with an imino-NHC ligand **34** afforded a novel germanium NHC-imine ion **35**. Its reduction with potassium graphite produced a cyclic species **36**, which can be viewed as both a Ge^0 species **36a** and a mesoionic germylene **36b**. An X-ray diffraction analysis and computational studies revealed that one of the lone pairs on the Ge atom is involved in the π system of the GeC_2N_2 five-membered ring. The nucleophilic behavior of **36** was associated with the presence of two lone-pairs on Ge (Scheme 11).[12]

Scheme 11.

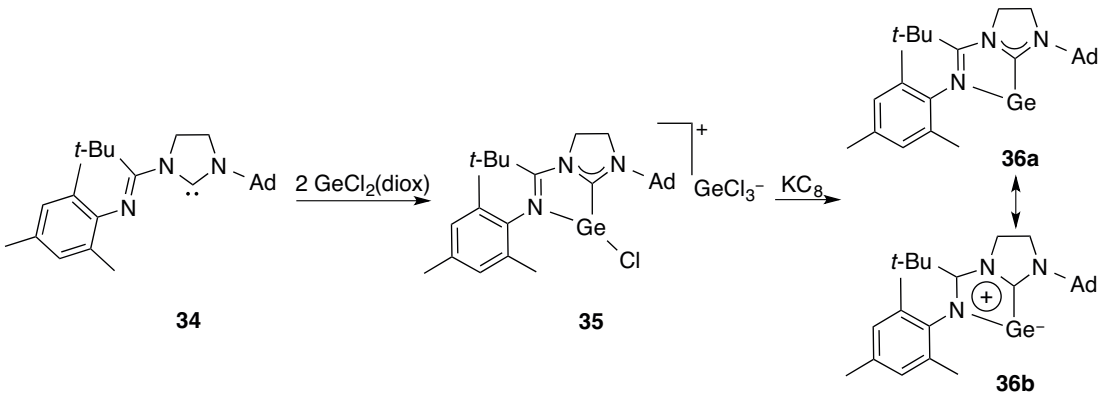

34 **35** **36a** **36b**

2 Bis(imino)-NHC ligands and metal complexes

2.1 Imidazole-type bis(imino)-NHC ligands and metal complexes

The first isolation of Cu(I) complexes containing bis(imino)-NHC ligands was reported by Lavoie in 2010,[13] but the free carbenes could not be isolated and it was suggested that this was due to intermolecular rearrangements. Then the Fe(II) (**37a**), Co(II) (**37b**) and Cr(III) (**38**) complexes were prepared from the corresponding silver or copper complex as transmetalating agent or from *in situ* deprotonation of the

Références: p 24

imidazolium salt in the presence of metal precursors. The catalytic activities of all three complexes were evaluated for ethylene polymerization at atmospheric pressure and room temperature by activation with MAO. The Cr(III) complexes were found to be the most active, with a productivity of 35 kg(PE) mol^{-1}(Cr) h^{-1} (Scheme 12).[14]

Scheme 12.

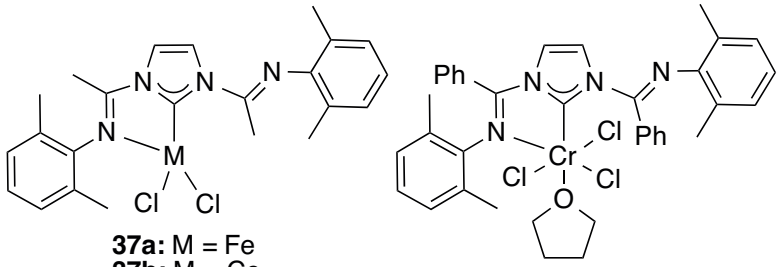

Danopoulos and Braunstein reported the isolation of the first bis(imino)-NHC free carbene **39**. When deprotonation of the imidazolium salt was performed at room temperature, **40** was isolated as the main product, resulting formally from the insertion of the carbon atom of the free NHC **39** into the C2−H bond of N-arylimine-functionalized imidazole (Scheme 13).[15]

Scheme 13.

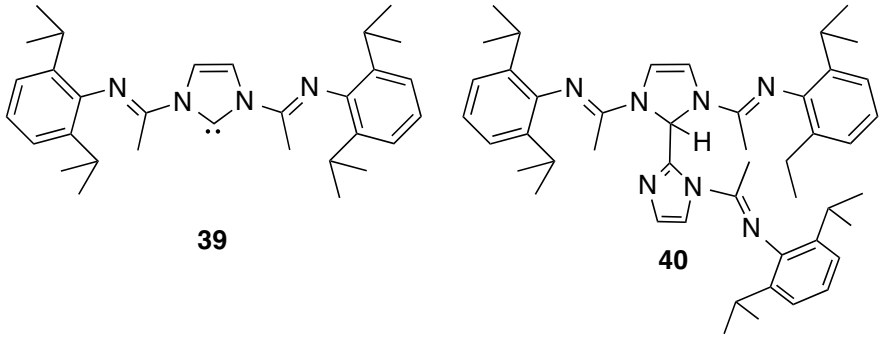

2.2 4,5,6-trihydropyrimidine-type bis(imino)-NHC ligands and metal complexes

In 2012, Lavoie reported the preparation of Cr(III), Fe(II) and Co(II) complexes of bis(imino)pyrimidin-2-ylidene.[16] The Cr(III) complex **43** was prepared by transmetalation of Cu(I) complex **42** and $CrCl_3 \cdot 3THF$, while Fe(II) and Co(II) complexes **44a** and **44b** were prepared by the reaction of the pyrimidinium salt **41**, KHMDS and the corresponding metal precursors (Scheme 14). In complex **43**, the ligand was shown to coordinate to Cr(III) in a tridentate fashion. This is the first

Références: p 24

demonstration of such a binding capability for bis(imino)carbene ligands. Spectroscopic evidence (magnetic susceptibility and FTIR) pointed to the coordination of the ligand to Fe(II) and Co(II) in **44a** and **44b** exclusively in a bidentate fashion. The Cr(III) complex **43** was found to be active in ethylene polymerization.

Scheme 14.

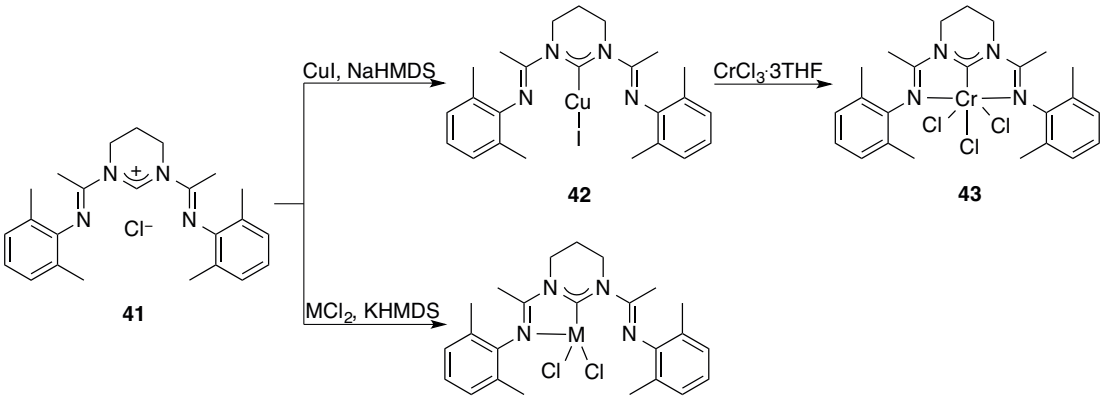

In the same year, the isolation of the Fe(II) complex **46** was reported by Byers (Scheme 15).[17] The structure of **46** was confirmed crystallographically. The NHC ligand in **46** adopted a tridentate conformation with a rather short Fe–C_{NHC} bond distance of 1.812(2) Å.

Scheme 15.

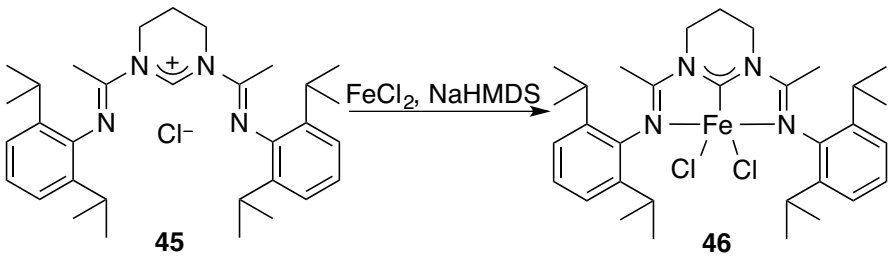

In the study reported by Roesler in 2015, the reaction of the pyrimidinium salt **47** with $Ni(cod)_2$ afforded the Ni(II) complex **48**. The Ni^0 pincer-type NHC complex **49** was prepared by deprotonation of **48**. It retained a chloride in the square-planar coordination sphere of nickel. Complex **48** could rapidly activate ammonia at room temperature, in a ligand-assisted process where the NHC carbon atom played the unprecedented role of proton acceptor. For the first time, complex **50** with the coordinated ammonia and the activated amido species **51** were observed together in

Références: p 24

solution, in a solvent-dependent equilibrium (Scheme 16).[18]

Scheme 16.

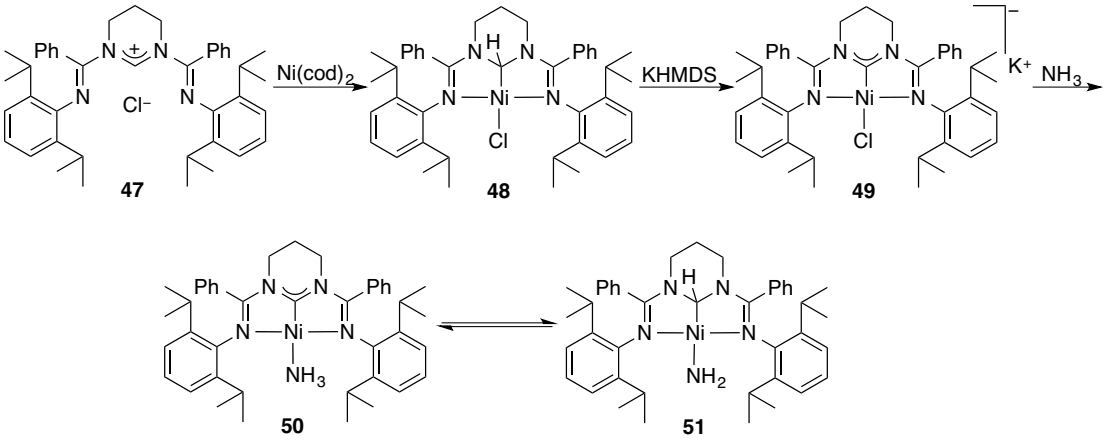

Conclusion

This short overview on imino-NHC ligands and complexes has shown the additional versatility brought about by the imino functionality(ies). Whereas chelation of the ligand tends to increase stability, numerous examples have been reported of dangling behaviour for this function, in particular in the case of the bis(imino)-NHC ligands where only one imino group may form a chelate. The stereoelectronic modifications at the metal centre upon binding of the imino-NHC ligands have an obvious impact on both its stoichiometric and catalytic its reactivity. Obviously, more research is needed in this area to expand the scope of the current studies and better understand the nature of the interactions between the ligands and the metal centre and their consequences on the reactivity of the metal complexes.

Références: p 24

References

(1) Coleman, K. S.; Chamberlayne, H. T.; Turberville, S.; Green, M. L. H.; Cowley, A. R., *Dalton Trans.* **2003**, 2917–2922.

(2) Steiner, G.; Krajete, A.; Kopacka, H.; Ongania, K.-H.; Wurst, K.; Preishuber-Pflügl, P.; Bildstein, B., *Eur. J. Inorg. Chem.* **2004**, 2827–2836.

(3) (a) Coleman, K. S.; Dastgir, S.; Barnett, G.; Alvite, M. J. P.; Cowley, A. R.; Green, M. L. H., *J. Organomet. Chem.* **2005,** *690*, 5591–5596. (b) Dastgir, S.; Coleman, K. S.; Cowley, A. R.; Green, M. L. H., *Organometallics* **2006,** *25*, 300–306.

(4) (a) Rosenberg, M. L.; Krivokapic, A.; Tilset, M., *Org. Lett.* **2009,** *11*, 547–550. (b) Rosenberg, M. L.; Vlašaná, K. r.; Gupta, N. S.; Wragg, D.; Tilset, M., *J. Org. Chem.* **2011,** *76*, 2465–2470.

(5) Badaj, A. C.; Dastgir, S.; Lough, A. J.; Lavoie, G. G., *Dalton Trans.* **2010,** *39*, 3361–3365.

(6) Larocque, T. G.; Badaj, A. C.; Dastgir, S.; Lavoie, G. G., *Dalton Trans.* **2011,** *40*, 12705–12712.

(7) Badaj, A. C.; Lavoie, G. G., *Organometallics* **2012,** *31*, 1103–1111.

(8) Badaj, A. C.; Lavoie, G. G., *Organometallics* **2013,** *32*, 4577–4590.

(9) Deng, J.; Gao, H.; Zhu, F.; Wu, Q., *Organometallics* **2013,** *32*, 4507–4515.

(10) Zhou, Q.; Wang, Y.-N.; Guo, X.-Q.; Zhu, X.-H.; Li, Z.-M.; Hou, X.-F., *Organometallics* **2015,** *34*, 1021–1028.

(11) Larocque, T. G.; Badaj, A. C.; Lavoie, G. G., *Dalton Trans.* **2013,** *42*, 14955–14958.

(12) Su, B.; Ganguly, R.; Li, Y.; Kinjo, R., *Angew. Chem. Int. Ed.* **2014,** *53*, 13106–13109.

(13) Al Thagfi, J.; Dastgir, S.; Lough, A. J.; Lavoie, G. G., *Organometallics* **2010,** *29*, 3133–3138.

(14) Al Thagfi, J.; Lavoie, G. G., *Organometallics* **2012,** *31*, 2463–2469.

(15) Liu, P.; Wesolek, M.; Danopoulos, A. A.; Braunstein, P., *Organometallics* **2013,** *32*, 6286–6297.

(16) Thagfi, J. A.; Lavoie, G. G., *Organometallics* **2012,** *31*, 7351–7358.

(17) Kaplan, H. Z.; Li, B.; Byers, J. A., *Organometallics* **2012,** *31*, 7343–7350.

(18) Brown, R. M.; Borau Garcia, J.; Valjus, J.; Roberts, C. J.; Tuononen, H. M.; Parvez, M.; Roesler, R., *Angew. Chem. Int. Ed.* **2015,** *54*, 6274–6277.

Chapitre 2

Dinuclear iridium and rhodium complexes with bridging arylimidazolide-N^3,C^2 ligands: synthetic, structural, reactivity, electrochemical and spectroscopic studies

Résumé

La déprotonation des 1-arylimidazoles (aryl = mésityl (Mes), 2,6-diisopropylphenyl (Dipp)), avec le *n*-butyl lithium a permis l'obtention des dérivés (1-aryl-1*H*-imidazol-2-yl)lithiés correspondants (**1a**, Ar = Mes; **1b**, Ar = Dipp) avec de bons rendements (Schéma 1).

Schéma 1.

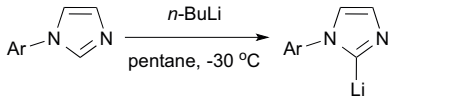

1a Ar = Mes, yield 70%
1b Ar = Dipp, yield 92%

La réaction de **1a** avec 0.5 équiv. de $[Ir(cod)(\mu\text{-}Cl)]_2$ permet l'obtention de deux complexes di-nucléaires doublement pontés-C2,N3 qui sont des isomères géométriques - $[Ir(cod)\{\mu\text{-}C_3H_2N_2(Mes)\text{-}\kappa C2,\kappa N3\}]_2$ (**3**), $\mathbf{3_{H\text{-}H}}$, étant l'isomère "tête-tête" noté (H-H) de symétrie C_S, et $\mathbf{3_{H\text{-}T}}$, l'isomère thermodynamiquement favorable "tête-queue" noté (H-T) de symétrie C_2 (Schéma 2). Le carbone métallé du ligand pontant donneur de quatre électrons a partiellement un caractère carbénique qui rappelle les complexes métallés avec des ligand NHC protiques.

Schéma 2.

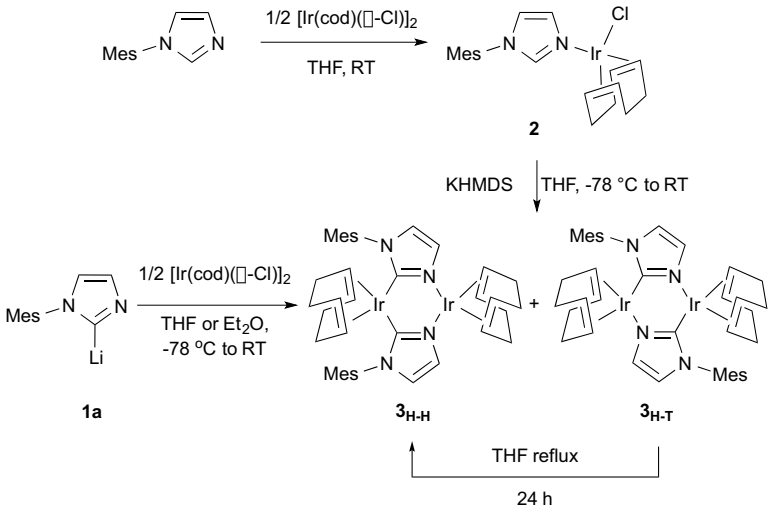

La substitution des ligands cod par des CO dans $\mathbf{3_{H\text{-}H}}$ et $\mathbf{3_{H\text{-}T}}$ a permis l'obtention des complexes tétracarbonylés $[Ir(CO)_2\{\mu\text{-}C_3H_2N_2(Mes)\text{-}\kappa C2,\kappa N3\}]_2$ $\mathbf{4_{H\text{-}H}}$ et $\mathbf{4_{H\text{-}T}}$, respectivement. La réaction avec PMe_3 donne seulement un complexe,

 References: p 44

$[Ir(CO)(PMe_3)\{\mu\text{-}C_3H_2N_2(Mes)\text{-}\kappa C2,\kappa N3\}]_2$ (**5**), ceci montre que l'isomérisation de la structure centrale $Ir[\mu\text{-}C_3H_2N_2(Mes)\text{-}\kappa C2,\kappa N3]_2Ir$ ($\mathbf{4_{H\text{-}H}}$) pour donner **5** se fait dans des conditions douces grâce à la substitution par une phosphine. L'addition oxydante de MeI au complexe **5** permet l'obtention d'un complexe bimétallique d^7-d^7 ayant formellement une liaison métal-métal $[Ir_2(CO)_2(PMe_3)_2(Me)I\{\mu\text{-}C_3H_2N_2(Mes)\text{-}\kappa C2,\kappa N3\}_2]$ (**6**) pour satisfaire la règle des 18 électrons (Schéma 3).

Schéma 3.

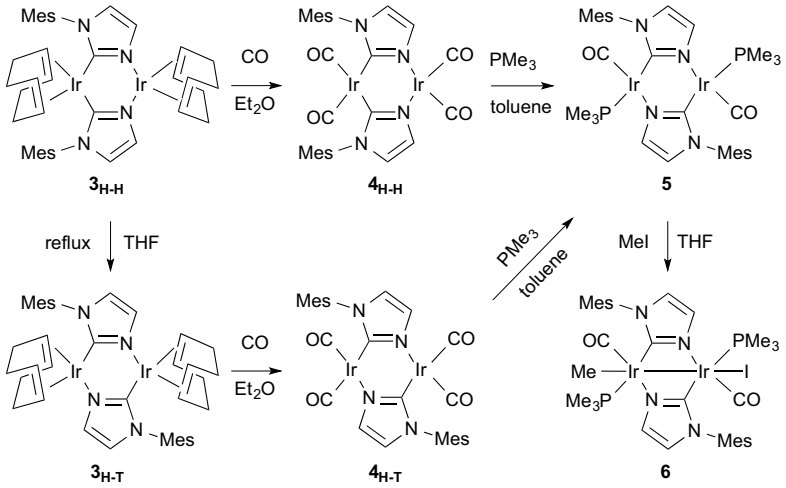

Le complexe de couleur bleue $[Ir(C_2H_4)_2\{\mu\text{-}C_3H_2N_2(Mes)\text{-}\kappa C2,\kappa N3\}]_2$ (**7**) et le complexe violet $[Rh(C_2H_4)_2\{\mu\text{-}C_3H_2N_2(Dipp)\text{-}\kappa C2,\kappa N3\}]_2$ (**9**) qui sont des complexes tetraéthylèniques sont eux aussi obtenus seulement avec la configuration "tête à queue" H-T des ligands pontants (Schéma 4).

Schéma 4.

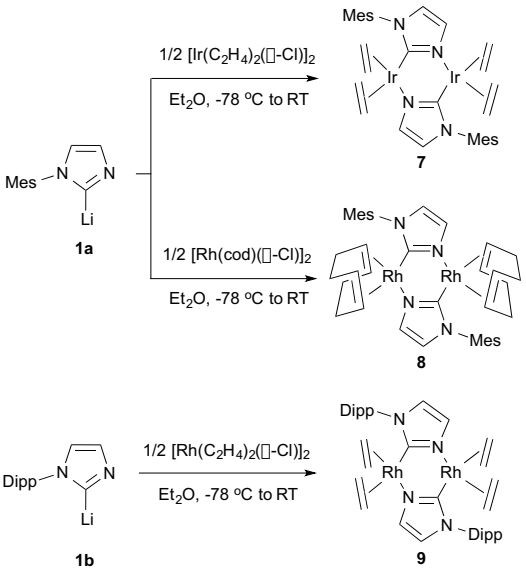

References: p 44

Bien que modestement performant dans la déshydrogénation catalytique des alcanes, le complexe **7** s'avère être un précurseur plus actif que $\mathbf{3_{H\text{-}T}}$, $\mathbf{4_{H\text{-}T}}$ and **5**, la labilité plus importante des ligands éthylène étant probablement dans ce cas un facteur déterminant. Les études de voltamétrie cyclique couplée à l'analyse spectrale UV-vis-proche-IR ainsi qu'une étude coulométrique approfondie ont permis de mettre en évidence que le complexe $\mathbf{3_{H\text{-}T}}$ donnait lieu à une oxydation à un électron générant un système à valence mixte Ir(I)/Ir(II). L'énergie de la bande d'inter-valence du complexe orange du dirhodium $[Rh(cod)\{\mu\text{-}C_3H_2N_2(Mes)\text{-}\kappa C2,\kappa N3\}]_2$ (**8**) est déplacée vers les basses énergies en comparaison avec $\mathbf{3_{H\text{-}T}}$ reflétant ainsi la diminution énergétique avec la distance intermétallique. L'étude RPE a permis de mettre en évidence que les centres métalliques Ir et Rh contribuent considérablement à l'anisotropie magnétique observée expérimentalement et donc à l'orbitale moléculaire occupée par un électron (SOMO) dans les systèmes à valence mixte Ir(I)/Ir(II) et Rh(I)/Rh(II). Les structures moléculaires des complexes $\mathbf{3_{H\text{-}H}}$, $\mathbf{3_{H\text{-}T}}$, **8** et **9** ont été déterminées par diffraction des rayons-X.

References: p 44

Références et synopsis

Dinuclear iridium and rhodium complexes with bridging arylimidazolide-N^3,C^2 ligands: synthetic, structural, reactivity, electrochemical and spectroscopic studies

Ce chapitre a été rédigé sous forme d'une publication qui vient d'être acceptée tout récemment.

He, F.; Ruhlmann, L.; Gisselbrecht, J.-P.; Choua, S.; Orio, M.; Wesolek, M.; Danopoulos, A.; Braunstein, P., *Dalton Trans.* **2015**, *44*, 17030–17044. Selected as inside front cover and a *Dalton Transactions* Hot Article in September 2015.

Ma contribution a porté sur la recherche bibliographique, la synthèse des ligands et complexes qui y sont décrits ainsi que dans la rédaction de la version préliminaire.

References: p 44

Volume 44 | Number 39 | 21 October 2015 | Pages 16967–17416

Dalton Transactions

An international journal of inorganic chemistry

www.rsc.org/dalton

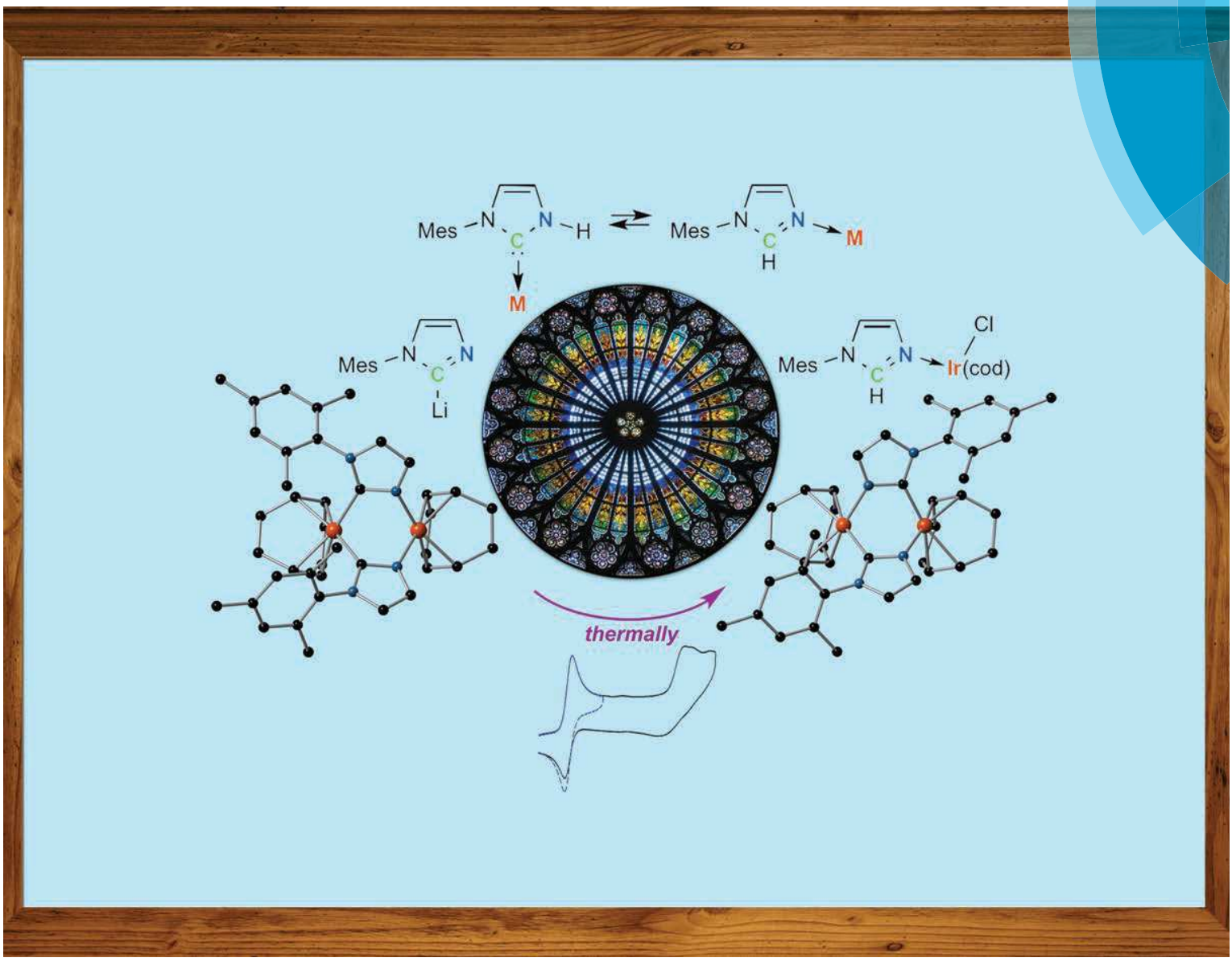

ISSN 1477-9226

ROYAL SOCIETY OF CHEMISTRY

PAPER

Andreas A. Danopoulos, Pierre Braunstein *et al.*

Dinuclear iridium and rhodium complexes with bridging arylimidazolide-N^3,C^2 ligands: synthetic, structural, reactivity, electrochemical and spectroscopic studies

 References: p 44

Dalton Transactions

PAPER

View Article Online
View Journal | View Issue

Cite this: *Dalton Trans.*, 2015, **44**, 17030

Dinuclear iridium and rhodium complexes with bridging arylimidazolide-N^3,C^2 ligands: synthetic, structural, reactivity, electrochemical and spectroscopic studies†

Fan He,[a] Laurent Ruhlmann,[b] Jean-Paul Gisselbrecht,[b] Sylvie Choua,[c] Maylis Orio,[d] Marcel Wesolek,[a] Andreas A. Danopoulos*[a,e] and Pierre Braunstein*[a]

Deprotonation of 1-arylimidazoles (aryl = mesityl (Mes), 2,6-diisopropylphenyl (Dipp)), with *n*-butyl lithium afforded the corresponding derivatives (1-aryl-1*H*-imidazol-2-yl)lithium (**1a**, Ar = Mes; **1b**, Ar = Dipp) in good yield. Reaction of **1a** with 0.5 equiv. of $[Ir(cod)(\mu\text{-}Cl)]_2$ yielded two geometrical isomers of a doubly C2,N3-bridged dinuclear complex $[Ir(cod)\{\mu\text{-}C_3H_2N_2(Mes)\text{-}\kappa C2,\kappa N3\}]_2$ (**3**), $\mathbf{3_{H-H}}$, a head-to-head (H–H) isomer of C_S symmetry, and $\mathbf{3_{H-T}}$, the thermodynamically preferred head-to-tail (H–T) isomer of C_2 symmetry. The metallated carbon of the 4 electron donor anionic bridging ligands has some carbene character, reminiscent of the situation in N-metallated protic NHC complexes. Displacement of cod ligands from $\mathbf{3_{H-H}}$ and $\mathbf{3_{H-T}}$ afforded the tetracarbonyl complexes $[Ir(CO)_2\{\mu\text{-}C_3H_2N_2(Mes)\text{-}\kappa C2,\kappa N3\}]_2$ $\mathbf{4_{H-H}}$ and $\mathbf{4_{H-T}}$, respectively. The reaction with PMe_3, which gave only one complex, $[Ir(CO)(PMe_3)\{\mu\text{-}C_3H_2N_2(Mes)\text{-}\kappa C2,\kappa N3\}]_2$ (**5**), demonstrates that the isomerization of the central core $Ir[\mu\text{-}C_3H_2N_2(Mes)\text{-}\kappa C2,\kappa N3]_2Ir$ from H–H to H–T on going from $\mathbf{4_{H-H}}$ to **5** is readily triggered by phosphine substitution under mild conditions. Oxidative-addition of MeI to **5** afforded the formally metal–metal bonded d^7–d^7 complex $[Ir_2(CO)_2(PMe_3)_2(Me)I\{\mu\text{-}C_3H_2N_2(Mes)\text{-}\kappa C2,\kappa N3\}_2]$ (**6**). The blue $[Ir(C_2H_4)_2\{\mu\text{-}C_3H_2N_2(Mes)\text{-}\kappa C2,\kappa N3\}]_2$ (**7**) and purple $[Rh(C_2H_4)_2\{\mu\text{-}C_3H_2N_2(Dipp)\text{-}\kappa C2,\kappa N3\}]_2$ (**9**) tetraethylene complexes were also obtained with only a H–T arrangement of the bridging ligands. Although only modestly efficient in alkane dehydrogenation, complex **7** was found to be a more active pre-catalyst than $\mathbf{3_{H-T}}$, $\mathbf{4_{H-T}}$ and **5**, probably because of the favorable lability of the ethylene ligands. From cyclic voltammetry, exhaustive coulometry and spectroelectrochemistry studies, it was concluded that $\mathbf{3_{H-T}}$ undergoes a metal-based one electron oxidation to generate the mixed-valent Ir(I)/Ir(II) system. The energy of the intervalence band for the orange dirhodium complex $[Rh(cod)\{\mu\text{-}C_3H_2N_2(Mes)\text{-}\kappa C2,\kappa N3\}]_2$ (**8**) is shifted toward lower energies in comparison with $\mathbf{3_{H-T}}$, reflecting the decrease of the energy with the intermetallic distance. It was concluded from the EPR study that the Ir and Rh centres contribute substantially to the experimental magnetic anisotropy and thus to the singly occupied molecular orbital (SOMO) in the mixed-valent Ir(I)/Ir(II) and Rh(I)/Rh(II) systems. The molecular structures of $\mathbf{3_{H-H}}$, $\mathbf{3_{H-T}}$, **8** and **9** have been determined by X-ray diffraction.

Received 24th June 2015,
Accepted 23rd July 2015

DOI: 10.1039/c5dt02403j

www.rsc.org/dalton

[a]*Laboratoire de Chimie de Coordination, Institut de Chimie (UMR 7177 CNRS), Université de Strasbourg, 4 rue Blaise Pascal, 67081 Strasbourg Cedex, France. E-mail: braunstein@unistra.fr, danopoulos@unistra.fr*
[b]*Laboratoire d'Electrochimie et de Chimie Physique du Corps Solide, Institut de Chimie (UMR 7177 CNRS), Université de Strasbourg, 4 rue Blaise Pascal, 67081 Strasbourg Cedex, France*
[c]*Institut de Chimie, Université de Strasbourg, 1 rue Blaise Pascal, BP 296 R8, F-67008 Strasbourg, Cedex, France*
[d]*Institut des Sciences Moléculaires de Marseille, Aix Marseille Université, CNRS, Centrale Marseille, ISM2 UMR 7313, 13397 Marseille, France*
[e]*Université de Strasbourg, Institute for Advanced Study (USIAS), Strasbourg, France*

† Electronic supplementary information (ESI) available: Table S1 containing the crystal data for $\mathbf{3_{H-H}}$, $\mathbf{3_{H-T}}$, **8** and **9**, figures showing UV-visible-NIR spectra (S1, S3), ^{1}H NMR spectra (S2, S4), cyclic voltammograms (S5–S7), time-resolved UV-visible-NIR absorption spectra (S8, S9), EPR spectra (S10), the optimized structures (S11, S13), spin population distribution and SOMO (S12, S14). CCDC 1052655–1052658. For ESI and crystallographic data in CIF or other electronic format see DOI: 10.1039/c5dt02403j

Introduction

The isolation by Arduengo and co-workers of stable N-heterocyclic carbenes (NHCs) of the imidazole type with bulky *N*-substituents,[1] has triggered a fast growing interest for this class of ligands, in particular in organometallic chemistry.[2] Protic NHCs (pNHCs) are characterised by the presence of a N-bound H atom and have been comparatively much less investigated, despite their strong σ-donor character and the possibility for the *N*H group to be involved in secondary interactions of potential relevance to bifunctional catalysis,[3] substrate recognition[4] and biological systems.[5]

Different synthetic methodologies allow access to pNHC metal complexes: building the C-bound heterocycle in the metal coordination sphere,[6] using suitable N-protecting groups that are removed after metal coordination,[7] or facilitating the kinetic formation of the M–C_{NHC} bond by the oxidative-addition of the C–X bond of halo-imidazoles (X = halide).[8] Most recently, we found that *N*-arylimine-functionalized pNHC Ir(I) and Ir(III) complexes could be readily obtained from cationic or neutral Ir(I) imidazole complexes using excess $TlPF_6$ or $[Ir(cod)(\mu\text{-}Cl)]_2$, respectively.[9] Deprotonation of such a pNHC Ir(I) complex was shown to give rise to an equilibrium between a mononuclear complex containing a C-bound 'anionic' imidazolide and its dimer in which this moiety binds in a μ-C,N bridging mode (Scheme 1).[9]

Anionic imidazolides possess interesting properties. Lithium 1-methyl-(4-*t*-butyl)imidazolide was found by Boche and co-workers to have carbene character, as supported by the ^{13}C NMR chemical shift of its C2 atom (δ 195.9) and an X-ray diffraction study.[10] Kostyuk and co-workers reported a method to synthesize N-phosphorylated carbenes by the reaction between lithium imidazolides, bearing a bulky N-bound *t*-butyl or adamantyl group, and di(*t*-butyl)chlorophosphine.[11] Furthermore, an imidazolide can act as a *N*,*C*-bidentate ligand, comparable to a pyrazolide. While dinuclear bis(μ-pyrazolido) iridium(I) complexes have been widely investigated in oxidative addition reactions,[12] substitution chemistry,[13] kinetic[14] and theoretical studies,[15] no extensive study on dinuclear iridium complexes bearing imidazolides has yet been carried out.[16] A brief report described in 1983 the synthesis of dinuclear imidazolide Rh(I) complexes by deprotonation with MeLi of a mononuclear imidazole complex.[17] As part of our current investigations on the tautomerism/metallotropism between pNHC and imidazole ligands in iridium complexes (Scheme 2),[9] we describe herein the synthesis, structural and spectroscopic characterisation, reactivity and electrochemical properties of a series of doubly C,N-bridged dinuclear iridium and rhodium complexes bearing 1-arylimidazolide ligands.

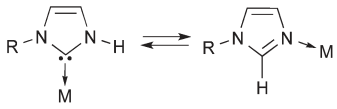

Scheme 2 Tautomerism/metallotropism between pNHC and imidazole ligands.[9]

Results and discussion

Synthesis and characterisation of the di-iridium complexes

Starting from 1-arylimidazoles (aryl = mesityl (Mes), 2,6-diisopropylphenyl (Dipp)), the corresponding derivatives (1-aryl-1*H*-imidazol-2-yl)lithium (1a, Ar = Mes; 1b, Ar = Dipp) were prepared in good yield by deprotonation with a stoichiometric amount of *n*-butyl lithium in pentane at −30 °C (Scheme 3).

In their NMR spectra in THF-d_8, the absence of the ^1H NMR resonance of the proton at C2 and the values of the $^{13}C\{^1H\}$ NMR resonance due to the C2 carbon, at δ 205.8 for (1-mesityl-1*H*-imidazol-2-yl)lithium (**1a**) and δ 202.3 for

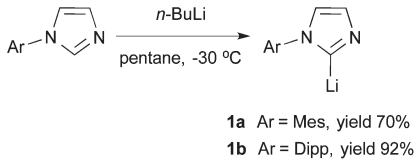

Scheme 3 Synthesis of (1-aryl-1*H*-imidazol-2-yl)lithium (**1a,b**).

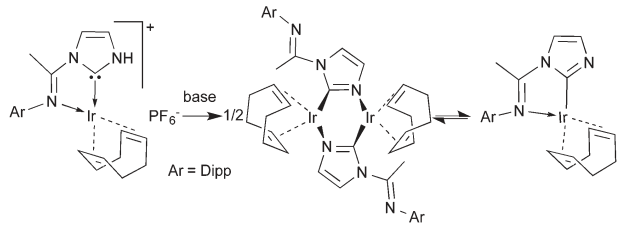

Scheme 1 Deprotonation of a protic NHC (pNHC) Ir(I) complex leading to an equilibrium between a mononuclear complex containing a C-bound 'anionic' imidazolide and its dimer.[9]

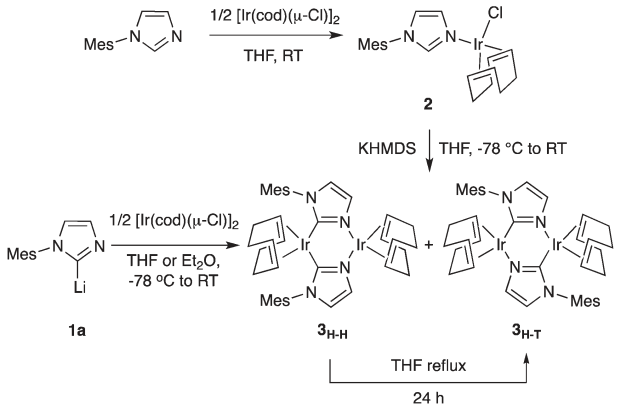

Scheme 4 Stepwise or direct synthesis of the two isomers of the dinuclear complexes $\mathbf{3_{H-H}}$ and $\mathbf{3_{H-T}}$.

(1-(2,6-diisopropylphenyl)-1*H*-imidazol-2-yl)lithium (**1b**), consistent with the metallation of this carbon.

Treatment of **1a** with 0.5 equiv. of $[Ir(cod)(\mu\text{-}Cl)]_2$ at −78 °C in THF led to the formation of the doubly C,N-bridged dinuclear complex $[Ir(cod)\{\mu\text{-}C_3H_2N_2(Mes)\text{-}\kappa C2,\kappa N3\}]_2$ (**3**) as a red solid in nearly quantitative yield (Scheme 4). Its ^1H and $^{13}C\{^1H\}$ NMR spectra in C_6D_6 revealed the presence of a *ca.* 40 : 60 mixture of two constitutional isomers, $\mathbf{3_{H-H}}$, a head-to-head isomer of C_S symmetry, and $\mathbf{3_{H-T}}$, a head-to-tail isomer of C_2 symmetry. In the NMR spectra of the mixture in C_6D_6, each isomer displays one set of mesityl, imidazolide and cod signals. The chemical shifts of the $^{13}C\{^1H\}$ NMR resonance due to the C2 carbon (δ 171.3 and 172.0) are considerably upfield-shifted when compared to the value of 205.8 ppm in **1a**. It turned out to be difficult to efficiently separate and isolate each isomer pure out of this mixture because of their similar solubilities. Another procedure to prepare doubly C,N-bridged dinuclear complexes was found to consist of the deprotonation of 1-mesitylimidazolyl(cycloocta-1,5-diene) iridium(I) chloride $[Ir(cod)Cl\{C_3H_3N_2(Mes)\text{-}\kappa N3\}]$ (**2**) with a stoichiometric amount of potassium bis(trimethylsilyl)amide (KHMDS) in THF at −78 °C. According to the NMR spectra, a *ca.* 40 : 60 mixture of the same two isomers $\mathbf{3_{H-H}}$ and $\mathbf{3_{H-T}}$ was again obtained. However, when the reaction using **1a** was repeated in Et_2O,[16b] the resulting red suspension was found to consist of a *ca.* 90 : 10 mixture of $\mathbf{3_{H-H}}$ and $\mathbf{3_{H-T}}$, after dissolution in toluene and ^1H NMR analysis. This difference in proportions obtained in THF is likely due to the lower solubility of $\mathbf{3_{H-H}}$ in Et_2O. After recrystallization from a toluene/Et_2O solution at −30 °C, deep red crystals of one pure isomer were obtained in 80% yield. In its ^1H NMR spectrum (C_6D_6), the C4 and C5 imidazolyl protons gave rise to an AX pattern at δ 7.20 (d) and 6.42 (d, ^3J = 1.4 Hz). In the $^{13}C\{^1H\}$ NMR spectrum, the three resonances at δ 171.3, 125.5 and 122.4 are assigned to the C2, C4 and C5 imidazolyl carbons, respectively. However, a definitive assignment of this isomer as H–H or H–T was impossible on the exclusive basis of the spectroscopic data. Fortunately, its structure was elucidated by X-ray diffraction analysis and established its H–H arrangement. The molecular structure of $\mathbf{3_{H-H}}$ is shown in Fig. 1, with selected bond lengths and angles. The C_s molecular symmetry of the complex in solution is almost retained in the solid state, as indicated by NMR spectroscopy. The boat conformation of $\mathbf{3_{H-H}}$ is similar to that of the analogous bridged pyrazolido complex.[12b] There is no direct iridium-iridium interaction since the separation between the metal atoms is 3.1844(9) Å. The iridium(I) centres adopt an approximate square planar coordination geometry, defined by two olefinic bonds of the 1,5-cyclooctadiene ligand and two carbon atoms (or two nitrogen atoms) from the imidazolide bridging ligands. The latter can be formally considered as 4 electron anionic donors toward Ir(I) centres. The electronic environment at the metals is unsymmetrical and Ir(1) is more electron-rich than Ir(2) since it is bound to two carbanionic donors. This is also supported by the difference in redox potentials between the isomers $\mathbf{3_{H-H}}$ and $\mathbf{3_{H-T}}$ (Table 1) although in the case of $\mathbf{3_{H-H}}$ the redox waves are irreversible. The C1–N1 [1.35(2) Å] and C21–N3 [1.35(2) Å] bond lengths are not significantly shorter (within 3σ) than those of C1–N2 [1.38(2) Å] and C21–N4 [1.39 (2) Å]. This is indicative of electronic delocalization between the N1, C1 and N2 atoms (N3, C21 and N4, respectively) and of a carbene character for C1 and C21, respectively (Scheme 5).

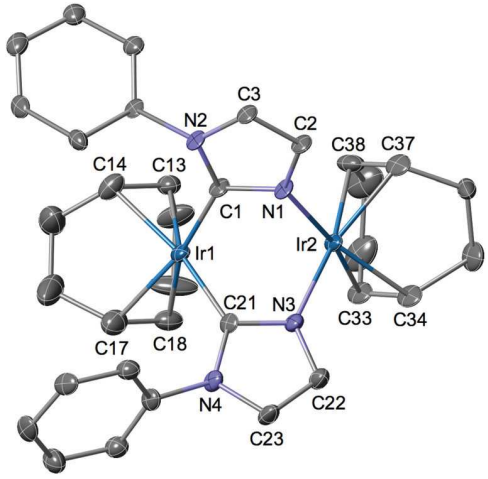

Fig. 1 View of the molecular structure of $\mathbf{3_{H-H}}$, H atoms and methyl groups are omitted for clarity. Thermal ellipsoids are at the 30% level. Selected bond lengths (Å) and angles (°): Ir1···Ir2 3.1844(9), C1–N1 1.35(2), C1–N2 1.38(2), Ir1–C1 2.05(1), Ir1–C21 2.05(1), Ir1–C13 2.14(1), Ir1–C14 2.18(1), Ir1–C17 2.17(2), Ir1–C18 2.16(2), C13–C14 1.38(2), C17–C18 1.36(3), C21–N3 1.35(2), C21–N4 1.39(2), Ir2–N1 2.07(1), Ir2–N3 2.06(1), Ir2–C33 2.10(1), Ir2–C34 2.09(1), Ir2–C37 2.11(2), Ir2–C38 2.10(2), C33–C34 1.39(3), C37–C38 1.40(3); N1–C1–N2 106(1), N3–C21–N4 105(1), C1–Ir1–C21 87.4(6), C13–Ir1–C14 37.2(6), C14–Ir1–C17 80.6(7), C17–Ir1–C18 36.5(7), C18–Ir1–C13 81.4(6), N1–Ir2–N3 86.5(5), C33–Ir2–C34 38.7(7), C34–Ir2–C37 82.8(6), C37–Ir2–C38 38.7(7), C38–Ir2–C33 81.3(7).

The complex $\mathbf{3_{H-H}}$ can be thermally converted to its isomer $\mathbf{3_{H-T}}$ upon refluxing a THF solution for 24 h (Scheme 4). In the ^1H NMR spectrum of $\mathbf{3_{H-T}}$ in C_6D_6, the protons at the imidazolide backbone carbons C4 and C5 give rise to an AX pattern at δ 7.02 (d) and 6.09 (d, ^3J = 1.6 Hz). In the $^{13}C\{^1H\}$ NMR spectrum, the resonances at δ 125.4 and 121.3 are assigned to C4 and C5, respectively. The $^{13}C\{^1H\}$ NMR resonance of the imidazolide C2 carbon (C1 and C21 in Fig. 2) in $\mathbf{3_{H-T}}$ (δ 172.0) is downfield shifted compared to that in $\mathbf{3_{H-H}}$ (δ 171.3) (C1 and C21 in Fig. 1). The UV-visible-NIR absorption spectrum of $\mathbf{3_{H-T}}$ in CH_2Cl_2 is shown in Fig. S1 (see ESI†). Single crystals of $\mathbf{3_{H-T}}$ suitable for X-ray diffraction were obtained by slow diffusion of a layer of Et_2O into a THF solution of $\mathbf{3_{H-T}}$ at room temperature under argon. The molecular structure of $\mathbf{3_{H-T}}$ is shown in Fig. 2, with selected bond lengths and angles.

A boat conformation is observed for the structure of $\mathbf{3_{H-T}}$, similar to that of its isomer $\mathbf{3_{H-H}}$. The distance between two iridium atoms (3.1407(2) Å) is shorter than in $\mathbf{3_{H-H}}$ but still too long to represent a direct metal–metal interaction. Each iridium atom has a 16 valence electron configuration and adopts an approximate square planar coordination geometry,

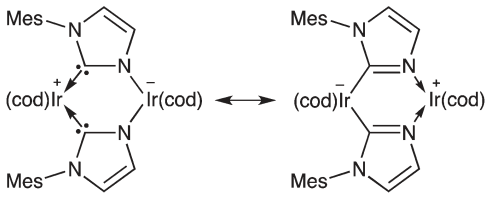

Scheme 5 Limiting resonance structures for the diiridium(I) complex $\mathbf{3_{H-H}}$ emphasising the dipolar nature of this isomer.

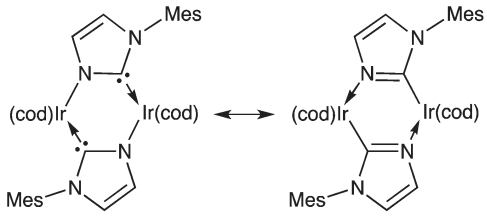

Scheme 6 Limiting resonance structures for $\mathbf{3_{H-T}}$.

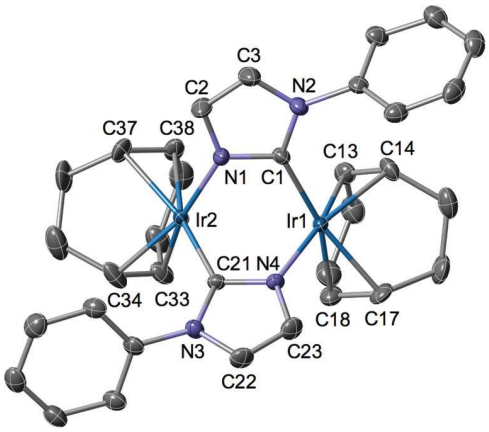

Fig. 2 View of the molecular structure of $\mathbf{3_{H-T}}$, H atoms and methyl groups are omitted for clarity. Thermal ellipsoids are at the 30% level. Selected bond lengths (Å) and angles (°): Ir1···Ir2 3.1407(2), C1–N1 1.349(5), C1–N2 1.373(5), Ir1–C1 2.058(4), Ir1–N4 2.068(3), Ir1–C13 2.121(4), Ir1–C14 2.112(4), Ir1–C17 2.166(4), Ir1–C18 2.158(4), C13–C14 1.409(6), C17–C18 1.390(6), C21–N3 1.378(5), C21–N4 1.335(5), Ir2–N1 2.067(3), Ir2–C21 2.043(4), Ir2–C33 2.135(4), Ir2–C34 2.118(4), Ir2–C37 2.168(4), Ir2–C38 2.159(4), C33–C34 1.404(7), C37–C38 1.395(6); N1–C1–N2 106.1(3), N3–C21–N4 106.7(3), C1–Ir1–N4 86.9(1), C13–Ir1–C14 38.9(2), C14–Ir1–C17 82.0(2), C17–Ir1–C18 37.5(2), C18–Ir1–C13 81.2(2), N1–Ir2–C21 86.6(1), C33–Ir2–C34 38.6(2), C34–Ir2–C37 82.0(2), C37–Ir2–C38 37.6(2), C38–Ir2–C33 81.2(2).

defined by two olefinic bonds of the 1,5-cyclooctadiene ligand, one carbon atom of one imidazolide and one nitrogen atom of the other bridging imidazolide ligand. The C1–N1 and C21–N4 distances of 1.349(5) Å and 1.335(5) Å, respectively, are almost identical to the corresponding distances in $\mathbf{3_{H-H}}$ (1.35(2) Å). A similar comment applies to the bond lengths C1–N2 1.373(5) and C21–N3 1.378(5) which compare with the corresponding values of 1.38(2) and 1.39(2) Å in $\mathbf{3_{H-H}}$. This, together with the similarity between the C–N bond lengths in $\mathbf{3_{H-T}}$, is consistent with the resonance structures shown in Scheme 6.

Displacement reactions of the cod ligands

With the original aim to prepare derivatives of $\mathbf{3_{H-H}}$ and $\mathbf{3_{H-T}}$ in which replacement of the cod ligands with two-electron donor ligands could modify the redox properties, as monitored by cyclic voltammetry, the tetracarbonyl derivatives $[Ir(CO)_2\{\mu\text{-}C_3H_2N_2(Mes)\text{-}\kappa C2,\kappa N3\}]_2$ ($\mathbf{4_{H-H}}$ and $\mathbf{4_{H-T}}$, respectively) were readily synthesized by reaction with carbon monoxide in Et_2O (Scheme 7). While a clear brown Et_2O solution of $\mathbf{4_{H-T}}$ was obtained, the reaction with $\mathbf{3_{H-H}}$ led to a yellow suspension. The higher solubility of $\mathbf{4_{H-T}}$ in Et_2O compared to that of $\mathbf{4_{H-H}}$ is consistent with their different polarity. Indeed, $\mathbf{4_{H-T}}$ has a good solubility in nonpolar solvents such as pentane or *n*-hexane. The $^{13}C\{^1H\}$ NMR spectroscopic data for $\mathbf{4_{H-H}}$ and $\mathbf{4_{H-T}}$ in C_6D_6 show for each isomer one set of mesitylimidazolide and two CO signals, consistent with either a C_s or C_2 molecular symmetry. Compared to the cod precursors ($\mathbf{3_{H-H}}$ and $\mathbf{3_{H-T}}$), the $^{13}C\{^1H\}$ NMR resonances of the imidazolide C2 are downfield shifted (δ 172.8 in $\mathbf{4_{H-H}}$ and δ 175.1 in $\mathbf{4_{H-T}}$). The IR spectra of $\mathbf{4_{H-H}}$ and $\mathbf{4_{H-T}}$ show three ν(CO) bands at 2060, 2037, 1954 and 2059, 2041, 1968 cm^{-1}, respectively, corresponding to the pattern for a dinuclear, folded tetracarbonyl framework.

The reaction of $\mathbf{4_{H-H}}$ or $\mathbf{4_{H-T}}$ with 2.0 equiv. of trimethylphosphine in toluene at room temperature afforded the same red solid $[Ir(CO)(PMe_3)\{\mu\text{-}C_3H_2N_2(Mes)\text{-}\kappa C2,\kappa N3\}]_2$ (**5**), which shows two ν(CO) bands at 2000 and 1911 cm^{-1} in the infra-red spectrum (Scheme 7). According to the NMR spectra in C_6D_6, this complex contains one set of mesitylimidazolide, trimethylphosphine and CO signals. The imidazolide backbone protons at C4 and C5 are observed at δ 6.89 (d) and 6.68 (d, ^3J = 0.9 Hz) and the corresponding $^{13}C\{^1H\}$ NMR resonances at δ 128.3 and 120.1. In the $^{13}C\{^1H\}$ NMR spectrum, the resonances due to the CO and $C_{imidazolide}$ carbons are found at δ 181.4 (d, J_{C-P} = 10.0 Hz) and 177.1 (d, J_{C-P} = 112.0 Hz), respectively. The coordinated trimethylphosphine ligands give rise to a ^1H NMR resonance at δ 1.13 (d, $^2J_{H-P}$ = 8.7 Hz), a $^{13}C\{^1H\}$ NMR signal at δ 17.0 (d, J_{C-P} = 31.6 Hz) and a singlet in $^{31}P\{^1H\}$ NMR at δ −24.1. All these data are consistent with a C_2 molecular symmetry for **5**, *i.e.* a H–T arrangement. The isomerization of the central core $Ir[\mu\text{-}C_3H_2N_2(Mes)\text{-}\kappa C2,\kappa N3]_2Ir$ from H–H to H–T on going from $\mathbf{4_{H-H}}$ to **5** has thus been triggered by phosphine substitution under mild conditions. The preference for the H–T arrangement is consistent with $\mathbf{3_{H-T}}$ being the thermodynamically favoured isomer of **3**.

Oxidative-addition of MeI

Treatment of **5** with a slight excess of MeI afforded the yellow complex $[Ir_2(CO)_2(PMe_3)_2(Me)I\{\mu\text{-}C_3H_2N_2(Mes)\text{-}\kappa C2,\kappa N3\}_2]$ (**6**) corresponding to a 1 : 1 addition product (Scheme 7). The observation in C_6D_6 of two sets of ^1H NMR signals for the mesitylimidazolide and trimethylphosphine protons and of $^{13}C\{^1H\}$ NMR signals for the CO ligands is consistent with a

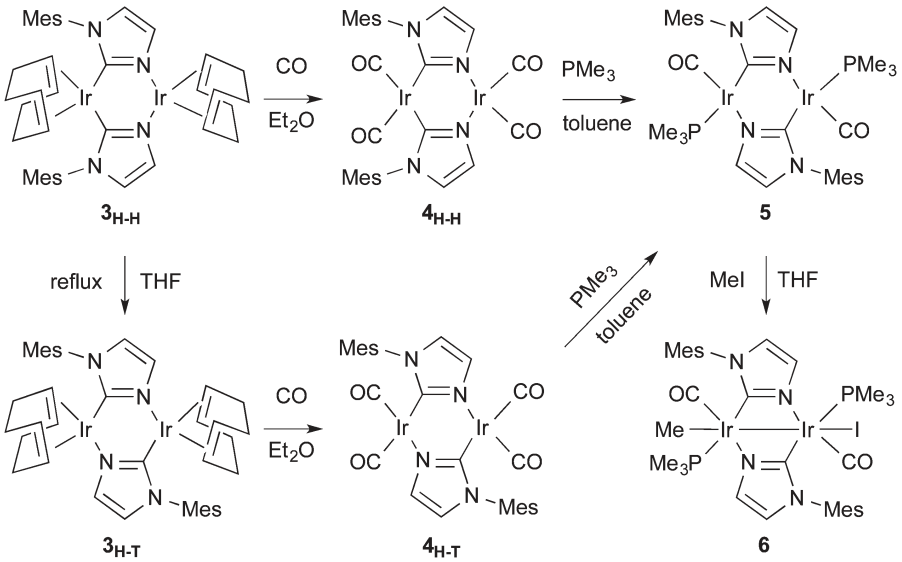

Scheme 7 Reactions of $\mathbf{3_{H-H}}$ and $\mathbf{3_{H-T}}$ with CO or PMe_3.

non-symmetric system. In the $^{13}C\{^1H\}$ NMR spectrum, the resonances of the $C_{imidazolide}$ carbons are significantly upfield shifted (δ 142.8 and 140.8 *vs.* δ 177.1 in **5**). The $^{31}P\{^1H\}$ NMR spectrum shows two close resonances at δ −46.6 and −48.9, consistent with similarly bonded but inequivalent phosphine ligands.[12a] Attempts to crystallize **6** were unsuccessful. The IR spectrum of **6** shows two ν(CO) bands at 2019 and 1952 cm^{-1}, indicative of weaker back-bonding from the metal to the CO ligands compared to **5** and consistent with the presence of iridium(II) centres in **6** where a formal metal–metal bond leads to a 18 electron count to each metal centre. In contrast to **5**, an NMR experiment showed that $\mathbf{3_{H-T}}$ reacted reversibly with MeI since placing a solution of the oxidative-addition product, obtained in the presence of excess MeI, under reduced pressure regenerated $\mathbf{3_{H-T}}$. Such a behaviour has been previously observed with diiridium pyrazolido-bridged complexes and explained by the steric hindrance caused by the cod ligands that prevents the iridium centres to get closer to each other in the oxidised product.[12h]

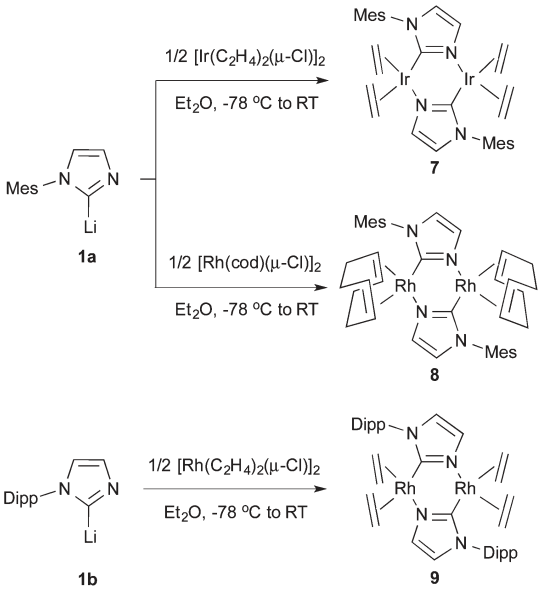

Scheme 8 Synthesis of the isolated dinuclear olefinic complexes **7–9**.

Synthesis and characterisation of diiridium tetraethylene complexes

Treatment of **1a** with 0.5 equiv. $[Ir(C_2H_4)_2(\mu\text{-}Cl)]_2$ at −78 °C in Et_2O led to the formation of the doubly C,N-bridged imidazolide dinuclear complex $[Ir(C_2H_4)_2\{\mu\text{-}C_3H_2N_2(Mes)\text{-}\kappa C2,\kappa N3\}]_2$ (**7**) as a blue solid in 77% yield (Scheme 8).

The colour of **7** is similar to that of other tetraethylene diiridium complexes reported in the literature.[13c] Its NMR spectra in C_6D_6 only showed one set of mesitylimidazolide signals. In the $^{13}C\{^1H\}$ NMR spectrum, the resonance of the $C_{imidazolide}$ is observed at δ 171.5. The imidazolide protons at C4 and C5 gave rise to an AX pattern at δ 7.09 (d) and 6.49 (d, ^3J = 1.5 Hz) and the corresponding $^{13}C\{^1H\}$ NMR resonances occurred at δ 124.6 and 122.0, respectively. In the ^1H NMR spectrum, two AA'BB' patterns are anticipated for the chemically-distinct coordinated ethylene ligands (*trans* to C and *trans* to N).[13c,18] The resolution of the spectra did not allow to extract all the corresponding coupling constants. Nevertheless, one AA'BB' pattern with δ_B 3.13 and δ_A 2.89 and a second AA'BB' pattern with δ_B 2.63 and δ_A 2.36 were observed (Fig. S2†).[19] Since the ^1H NMR chemical shifts of the mesityl and imidazolide groups are similar to those of $\mathbf{3_{H-T}}$, the arrangement of **7** should also be H–T but attempts to crystallize **7** were unsuccessful.

Synthesis and characterisation of dirhodium cod and tetraethylene complexes

To extend the scope of the reactivity of **1a**, it was treated with 0.5 equiv. of $[Rh(cod)(\mu\text{-}Cl)]_2$, and the new complex $[Rh(cod)\{\mu\text{-}C_3H_2N_2(Mes)\text{-}\kappa C2,\kappa N3\}]_2$ (**8**) was isolated (Scheme 8). As for **8**, the $^{13}C\{^1H\}$ NMR spectrum of **8** in C_6D_6 only showed one set of mesitylimidazolyl signals and a doublet due to C2 at δ 176.2 (J_{C-Rh} = 50.4 Hz). The protons at C4 and C5 were observed in the ^1H NMR spectrum at δ 6.96 and 6.51 as two broad singlets (the $^3J_{H-H}$ coupling was not resolved) and the corresponding $^{13}C\{^1H\}$ resonances were found at δ 126.8 and 120.3. The UV-visible-NIR absorption spectrum of **8** in CH_2Cl_2 is shown in Fig. S3.† Orange single crystals of **8** suitable for X-ray diffraction were grown from a toluene solution at 0 °C under argon. The molecular structure of **8** is shown in Fig. 3, with selected bond lengths and angles. This complex adopts a H–T arrangement and the same boat conformation as its iridium analog. The separation between the two Rh atoms is 3.2117(4) Å, which is too long to represent a direct metal–metal interaction. Each rhodium atom is in a 16 valence electron configuration and adopts an approximate square planar geometry, defined by two olefinic bonds of the 1,5-cyclooctadiene ligand, one carbon atom of one imidazolide and one nitrogen atom of the another bridging imidazolide ligand.

The reaction of **1b** with $[Rh(C_2H_4)_2(\mu\text{-}Cl)]_2$ at −78 °C in Et_2O afforded $[Rh(C_2H_4)_2\{\mu\text{-}C_3H_2N_2(Dipp)\text{-}\kappa C2,\kappa N3\}]_2$ (**9**) (Scheme 8). Its NMR spectrum in C_6D_6 only showed one set of Dipp imidazolide signals and a doublet due to C2 at δ 175.1 (J_{C-Rh} = 49.0 Hz). The resonances of the H atoms at the backbone carbons C4 and C5 were observed at δ 7.02 and 6.64, respectively, as two singlets, and the corresponding $^{13}C\{^1H\}$ NMR resonances at δ 125.9 and 122.8. In the ^1H NMR spectrum, like in **7**, two AA'BB' patterns are anticipated for the chemically distinct coordinated ethylene ligands.[13c,18] However, the resolution of the spectra did not allow extraction of all the corresponding coupling constants. Nevertheless one AA'BB' pattern with δ_B 3.65 and δ_A 3.58 and a second AA'BB' pattern with δ_B 2.86 and δ_A 2.62 were observed (Fig. S4†).[19] Purple single crystals of **9** suitable for X-ray diffraction were grown from *n*-hexane solution at −30 °C under ethylene atmosphere. A similar reaction using **1a** instead of **1b** proceeded similarly (^1H monitoring) although a well-characterised solid product could not be obtained due to limited solubility in hexane from which **9** could be crystallised. The molecular structure of **9** is shown in Fig. 4, with selected bond lengths and angles. The structure of **9** adopts a boat conformation and like in **8**, the arrangement of the bridging ligands is of the H–T type. The separation between two Rh atoms is 3.3146(9) Å, which is again too long to represent a direct bonding interaction. Each 16 electron rhodium atom adopts an approximately square planar geometry, defined by two ethylene ligands, one carbon atom of one imidazolido and one nitrogen atom of the other bridging imidizolido ligand. Like in $\mathbf{3_{H-T}}$, the metrical data indicate a more pronounced double bond character for the N–C bond located in the bridging part of the ligands.

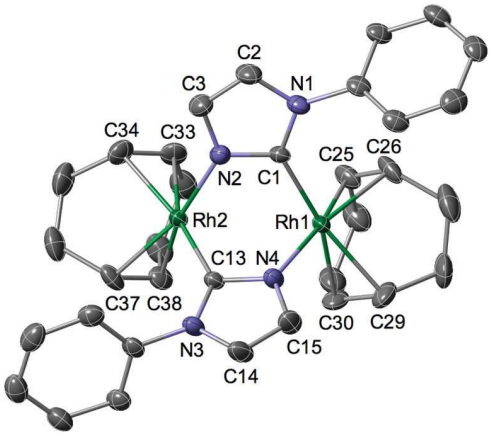

Fig. 3 View of the molecular structure of **8**, H atoms and methyl groups are omitted for clarity. Thermal ellipsoids are at the 30% level. Selected bond lengths (Å) and angles (°): Rh1···Rh2 3.2117(4), C1–N1 1.376(3), C1–N2 1.342(3), Rh1–C1 2.045(2), Rh1–N4 2.079(2), Rh1–C25 2.135(3), Rh1–C26 2.117(3), Rh1–C29 2.188(3), Rh1–C30 2.171(3), C25–C26 1.382(4), C29–C30 1.372(4), C13–N3 1.378(3), C13–N4 1.345(3), Rh2–N2 2.067(3), Rh2–C13 2.043(4), Rh2–C33 2.172(3), Rh2–C34 2.183(3), Rh2–C37 2.118(3), Rh2–C38 2.122(3), C33–C34 1.376(4), C37–C38 1.392(4); N1–C1–N2 106.7(2), N3–C13–N4 106.3(2), C1–Rh1–N4 85.73(9), C25–Rh1–C26 37.9(1), C26–Rh1–C29 82.3(1), C29–Rh1–C30 36.7(1), C30–Rh1–C25 81.4(1), N2–Rh2–C13 86.27(9), C33–Rh2–C34 36.8(1), C34–Rh2–C37 82.1(1), C37–Rh2–C38 38.3(1), C38–Rh2–C33 81.5(1).

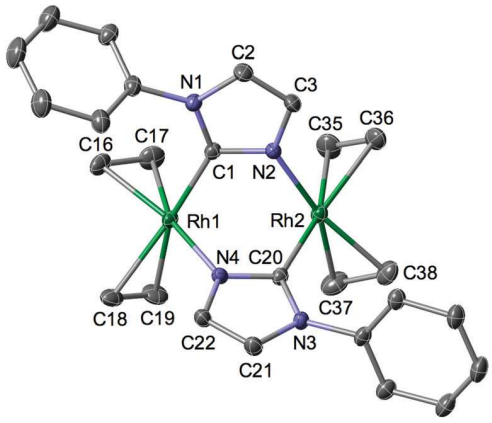

Fig. 4 View of the molecular structure of **9**, H atoms and isopropyl groups are omitted for clarity. Thermal ellipsoids are at the 30% level. Selected bond lengths (Å) and angles (°): Rh1···Rh2 3.3146(9), C1–N1 1.372(3), C1–N2 1.344(3), Rh1–C1 2.040(3), Rh1–N4 2.081(2), Rh1–C16 2.141(3), Rh1–C17 2.125(3), Rh1–C18 2.208(3), Rh1–C19 2.192(3), C16–C17 1.369(5), C18–C19 1.351(5), C20–N3 1.379(3), C20–N4 1.342(3), Rh2–N2 2.080(2), Rh2–C20 2.041(3), Rh2–C35 2.202(3), Rh2–C36 2.211(3), Rh2–C37 2.129(3), Rh2–C38 2.124(3), C35–C36 1.354(5), C37–C38 1.385(5); N1–C1–N2 106.7(2), N3–C20–N4 106.4(2), C1–Rh1–N4 84.6(1), C16–Rh1–C17 37.4(1), C17–Rh1–C19 89.2(2), C18–Rh1–C19 35.8(1), C16–Rh1–C18 86.9(1), N2–Rh2–C20 84.9(1), C35–Rh2–C36 35.7(1), C36–Rh2–C38 87.0(1), C37–Rh2–C38 38.0(1), C35–Rh2–C37 89.1(2).

Electrochemical investigations

Since a two-electron oxidation of the dinuclear unit could formally give an Ir(II)–Ir(II) complex or a mixed-valence Ir(I)/Ir(III) complex in which only one metal centre would have been formally oxidised, we became interested in studying the redox behaviour of representatives of these dinuclear complexes, in particular, with respect to the two possible H–T or H–H arrangements of the bridging ligands, since they lead to a symmetrical or unsymmetrical electronic environment of the metal centres, respectively. An electrochemical investigation of complexes $\mathbf{3_{H-T}}$ and **8** was carried out by cyclic voltammetry and rotating disk voltammetry in CH_2Cl_2 + 0.1 M $[n\text{-}Bu_4N]PF_6$. Cyclic voltammograms of $\mathbf{3_{H-T}}$ and **8** with added ferrocene are presented in Fig. S5 and S6 (see ESI†) and show reversible processes. In contrast, irreversible oxidation was observed by cyclic voltammetry in the case of complex $\mathbf{3_{H-H}}$ (see Fig. S7 in ESI†)

As shown in Fig. 5 and Table 1, two successive oxidations have been detected in the case of $\mathbf{3_{H-T}}$. The first oxidation step occurs at −0.45 V *vs.* Fc^+/Fc and corresponds to a reversible electron transfer, while the second step presents an irreversible oxidation peak at +0.67 V *vs.* Fc^+/Fc.

The number of electrons exchanged during the first oxidation step was determined by exhaustive coulometry. During the electrolysis, the oxidation current decreased exponentially with time. When this current reached the residual value measured in the absence of electroactive material, typically after 4 h under the above conditions, the number of electrons transferred was 0.9/molecule of $\mathbf{3_{H-T}}$, which strongly suggests that oxidation of only one Ir(I) centre to Ir(II) has occurred, leading to the mixed-valent Ir(I)/Ir(II) intermediate. Attempts to chemically oxidize $\mathbf{3_{H-T}}$ using AgOTf in CH_2Cl_2 gave intractable mixture of species.

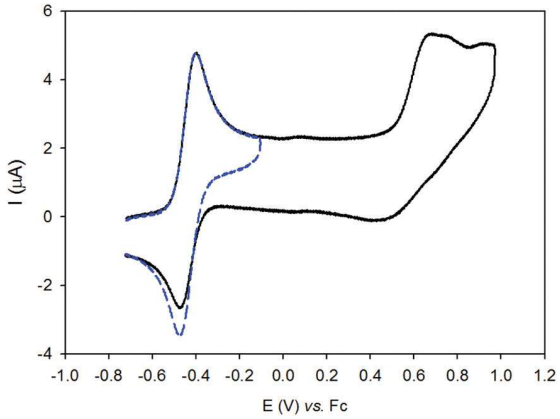

Fig. 5 Cyclic voltammograms of $\mathbf{3_{H-T}}$ (CH_2Cl_2 + 0.1 M $[n\text{-}Bu_4N]PF_6$, glassy carbon electrode, scan rate 0.1 V s^{-1}, *vs.* Fc^+/Fc).

Table 1 Electrochemical data for $\mathbf{3_{H-T}}$, $\mathbf{3_{H-H}}$ and **8**[a]

Complex		
$\mathbf{3_{H-T}}$	−0.45 (64)	+0.67[b]
$\mathbf{3_{H-H}}$	−1.23[b]	−0.39[b]
8	−0.40 (63)	+0.58[b]

[a] All potentials in V *vs.* Fc^+/Fc were obtained from cyclic voltammetry in CH_2Cl_2 containing 0.1 mol L^{-1} $[n\text{-}Bu_4N]PF_6$. Scan rate = 0.1 V s^{-1}. Working electrode: glassy carbon electrode. The given half-wave potentials in the case of the reversible couple are equal to $E_{1/2} = (E_{pa} - E_{pc})/2$. In bracket: ($\Delta E_p$, peak splitting in mV at a scan rate of 0.1 V s^{-1}). [b] Irreversible electron transfer.

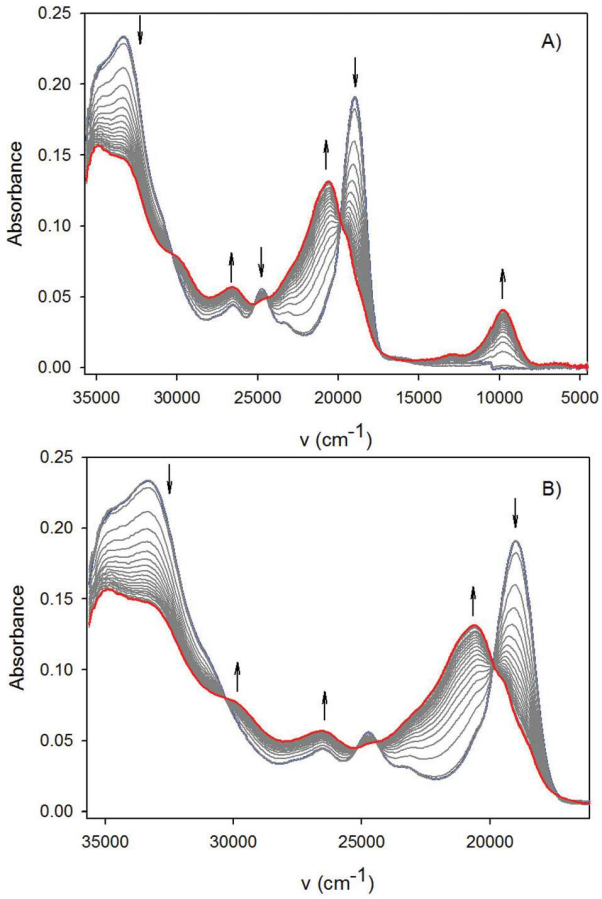

Fig. 6 (A) Time-resolved UV-visible-NIR spectra of $\mathbf{3_{H-T}}$ for the first oxidation step (transition Ir(I)/Ir(I) to Ir(I)/Ir(II)) in CH_2Cl_2 + 0.1 M $[n\text{-}Bu_4N]PF_6$ (spectra recorded every 5 s). (B) UV-visible spectral evolution for the first oxidation step.

For $\mathbf{3_{H-T}}$, time resolved UV-Vis-NIR spectroelectrochemistry data were recorded during cyclic voltammetry between −0.70 V and +0.20 V *vs.* Fc^+/Fc (scan rate 20 mV s^{-1}). As seen from the array of spectra depicted in Fig. 6 (and Fig. S8† for the plot *versus* λ (nm)), during the oxidation the generated Ir(I)/Ir(II) species is characterised by low-energy intervalence charge transfer (IVCT) bands in the near infrared region at 1024 nm. On the reverse potential scan, a decrease of the intensity for

this IVCT band was observed and the oxidized Ir(I)/Ir(II) system reverted quantitatively to the initial Ir(I)/Ir(I) species.

From the results obtained by cyclic voltammetry (reversible oxidation at −0.45 V *vs.* Fc^+/Fc), exhaustive coulometry (one-electron process) and spectroelectrochemistry (new NIR band at λ_{max} = 1024 nm for the oxidized system), it can be concluded that $\mathbf{3_{H-T}}$ undergoes a one electron oxidation on the metal generating the mixed-valent Ir(I)/Ir(II) system, in equilibrium with Ir(II)/Ir(I), and giving rise to an IVCT band in the NIR region.

For comparison, we examined a H–T dirhodium complex. Features similar to those for $\mathbf{3_{H-T}}$ were observed with **8** and the mixed-valent system Rh(I)/Rh(II). The cyclic voltammogram shows two successive oxidations, the first at −0.40 V *vs.* Fc^+/Fc corresponds to a reversible electron transfer, while the second step is associated to an irreversible oxidation process at +0.58 V *vs.* Fc^+/Fc (Fig. 7). Again, exhaustive coulometry indicated a number of electrons transferred of 0.9/molecule for **8**, leading to the mixed-valent intermediate Rh(I)/Rh(II).

Spectroelectrochemistry measurements at the first oxidation process evidenced a new low-energy intervalence charge transfer (IVCT) band around 1073 nm, which is in good agreement with the formation of a mixed-valent intermediate Rh(I)/Rh(II) (Fig. 8 and S9† for the plot *versus* λ (nm)). The new band at 612 nm might correspond to the Rh(II).

For **8** and for $\mathbf{3_{H-T}}$, we observed one additional band at 612 nm and 781 nm, respectively. In studies on mixed-valent Ir(I)/Ir(II) or Rh(I)/Rh(II) intermediates, similar bands were also observed, but not at the same wavelength, because of the presence of different ligands.[20] Such bands may be attributed to the Ir(II) or Rh(II) component of the complexes.

For a dinuclear system, the electronic coupling calculated from the Hush equation[21] decreases with the distance between the metal centres. Hush proposed that the electronic coupling could be extracted from the intervalence band shape according to eqn (1):

$$H_{ab} = 0.0206(\varepsilon_{max}\Delta\nu_{1/2}\lambda)^{1/2}/d_{ab} \quad (1)$$

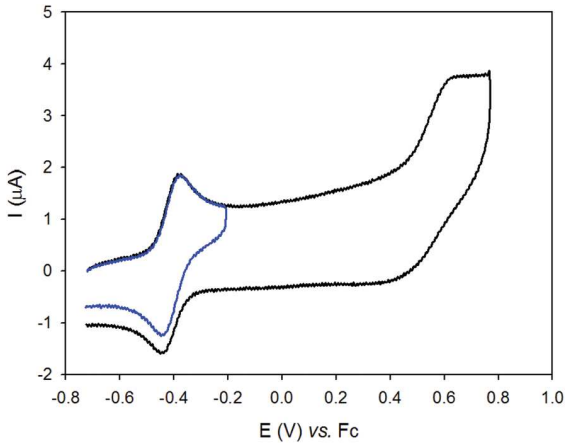

Fig. 7 Cyclic voltammograms of **8** (CH_2Cl_2 + 0.1 M $[n\text{-}Bu_4N]PF_6$, Glassy carbon electrode, scan rate 0.1 V s^{-1}, *vs.* Fc^+/Fc).

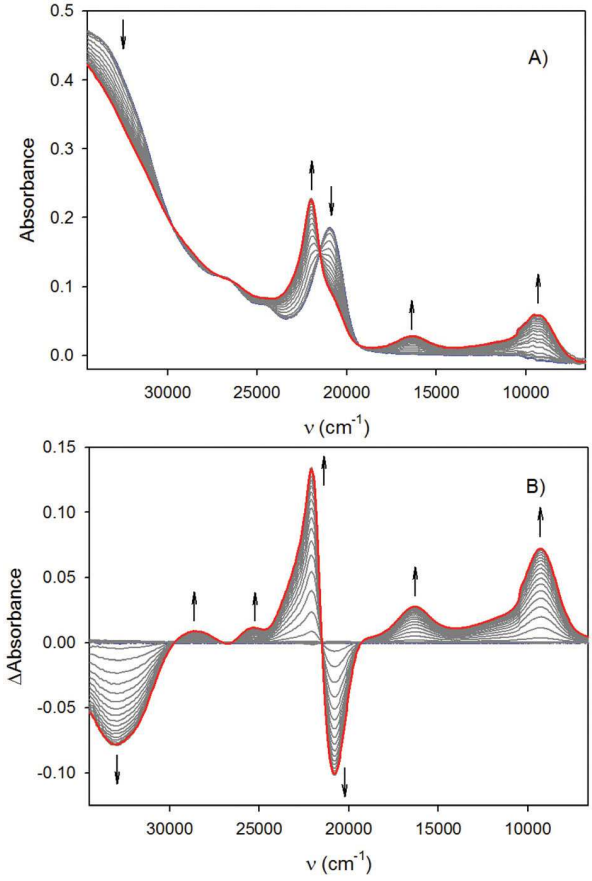

Fig. 8 (A) Time-resolved UV-visible-NIR spectra of **8** for the first oxidation step (transition Rh(I)/Rh(I) to Rh(I)/Rh(II)) in CH_2Cl_2 + 0.1 M $[n\text{-}Bu_4N]PF_6$ (spectra recorded every 5 s). (B) Time-resolved UV-visible-NIR differential spectra for the first oxidation step.

where ε_{max} (M^{-1} cm^{-1}) is the maximum intensity, $\Delta\nu_{1/2}$ (cm^{-1}) is the width at half-height, λ (cm^{-1}) is the energy maximum band (E_{op}), and d_{ab} (Å) is the diabatic electron-transfer distance. E_{op} occurs at 9823 cm^{-1} (λ_{max} = 1018 nm) and at 9320 cm^{-1} (λ_{max} = 1073 nm) for $\mathbf{3_{H-T}}$ and **8**. The measured $\Delta\nu_{1/2}$ values for $\mathbf{3_{H-T}}$ and **8** are 47 393 cm^{-1} and 40 486 cm^{-1}, respectively. According to eqn (1), the corresponding calculated electronic couplings are H_{Ir-Ir} = 3960 cm^{-1} and H_{Rh-Rh} = 4746 cm^{-1}. Thus, the energy of the intervalence band for **8** is shifted toward lower energies in comparison with $\mathbf{3_{H-T}}$, reflecting the decrease of the energy with the intermetallic distance (d_{Ir-Ir} = 3.141 Å, d_{Rh-Rh} = 3.212 Å).

The transition from charge localized to charge-delocalized (which are also called class II and class III, respectively, in the Robin–Day terminology)[22] occurs at $\lambda = 2H_{ab}$, so mixed-valent (MV) compounds with $\lambda > 2H_{ab}$ are charge-localized and those with $\lambda \sim 2H_{ab}$ are charge-delocalized. In our case:

$$\mathbf{3_{H-T}}: \ \lambda(9823\ cm^{-1}) > 2H_{ab}\ (2 \times 3960 = 7920\ cm^{-1})$$

$$\mathbf{8}: \ \lambda(9320\ cm^{-1}) \text{ is } \sim 2H_{ab}\ (2 \times 4746 = 9492\ cm^{-1})$$

These data thus suggest that $\mathbf{3_{H-T}}$ is a charge-localized while **8** is a charge-delocalized system under the conditions of our room temperature measurements.

EPR measurements

EPR spectroscopy constitutes a highly suitable tool to evaluate the electronic structure of metal complexes with unpaired electrons, especially on heavy metal centres. At low temperature, the average <*g*> value and the anisotropy (Δg) calculated from the principal values of the *g*-tensor afford a qualitative estimate of the extent of electron localization over the metal and/or over the ligand.[23] We thus wanted to examine in more detail the electronic structure of the mixed-valent Ir(I)/Ir(II) and Rh(I)/Rh(II) species. The oxidized species were generated at room temperature by electrolysis after consumption of about 0.9 electron/molecule and the resulting solutions were transferred into an EPR tube under argon. The X-band EPR spectrum in frozen CH_2Cl_2 solution of Ir(I)/Ir(II) (the oxidized species of $\mathbf{3_{H-T}}$) exhibited a signal with an axial symmetry (Fig. 9) with $g_1 = g_2 =$ 1.987 and $g_3 = 2.123$ values (see Table 2). Increasing the temperature to ambient caused the EPR signal to disappear. In the case of the Rh(I)/Rh(II) system obtained by oxidation of **8**, the EPR spectrum at low temperature displayed a rhombic signal (Fig. S10 in ESI†). At room temperature, a very weak EPR signal is recorded with only one line centred at around $g = 2.00$ without hyperfine structure. Satisfying simulations were obtained with one or two equivalent ^{103}Rh nucleus ($I = 1/2$ isotopic abundance 100%) and in order to discriminate between the two possibilities DFT calculations were performed. The structure of the Rh(I)/Rh(II) complex was subjected to geometry optimization (Fig. S11†) and its electronic structure was investigated (Fig. S12†). Mulliken population analysis indicates an equally distributed spin density between the two rhodium atoms with positive spin populations found at Rh(1) (0.49) and Rh(2) (0.49). The spin density of the Rh atoms accounts for 90% of the total spin density and the remaining 10% are spread over the ligands. The Singly Occupied Molecular Orbital (SOMO) of the complex displays 90% Rh character and features the σ antibonding interaction between the Rh $3d_{z^2}$ orbitals. The EPR parameters arising from the spectral simulation for two equivalent ^{103}Rh nuclei are reported in Table 2. The results of the DFT calculations for the Ir(I)/Ir(II) system are similar to those obtained for Rh(I)/Rh(II) and also suggest a delocalized mixed-valent species (Fig. S13 and S14†).

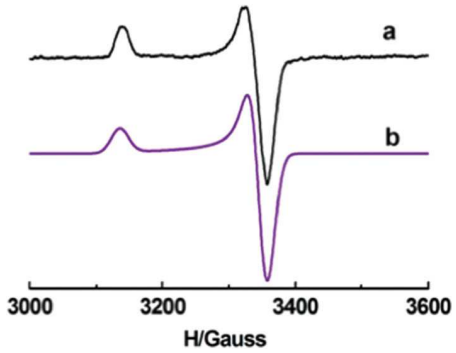

Fig. 9 EPR spectra of the Ir(I)/Ir(II) system electrochemically generated from $\mathbf{3_{H-T}}$ system electrochemically generated in CH_2Cl_2 at 100 K: (a) Experimental spectrum (b) Simulated spectrum.

Table 2 EPR parameters of the oxidized complexes

	g_1	g_2	g_3	<g>[a]	Δg[b]	A_1/G	A_2/G	A_3/G
Ir(I)/Ir(II)	1.987	1.987	2.123	2.033	0.136	—	—	—
Rh(I)/Rh(II)	1.993	2.031	2.105	2.043	0.112	33	18	27

[a] $\langle g\rangle = [(g_1^2 + g_2^2 + g_3^2)/3]^{1/2}$. [b] $\Delta g = g_3 - g_1$.

The oxidized forms are characterised by a *g* anisotropy and the average *g* values are significantly larger than for the free electron (2.0023). Such features may imply that the Ir and Rh centres contribute substantially to the experimental magnetic anisotropy and thus to the SOMO.

Attempted catalytic transfer dehydrogenation of cyclooctane using iridium complexes $\mathbf{3_{H-T}}$, $\mathbf{4_{H-T}}$, **5** and **7** as precatalysts.

Iridium pincer complexes have shown very promising catalytic properties in alkane dehydrogenation reactions,[24] due to their high thermal stability and high efficiency. The synergistic action of two reactive sites in close proximity could be seen as a key element in the design of powerful catalysts. This prompted us to explore the catalytic activity of these dinuclear iridium complexes towards alkane dehydrogenation. The reaction of cyclooctane (COA) and *t*-butylethylene (TBE), as sacrificial olefin, to form cyclooctene (COE) and *t*-butylethane (TBA) catalyzed by the POCOP iridium pincer complex[25] was employed in the benchmark reaction.

The results of preliminary experiments on the catalytic transfer dehydrogenation of COA to COE are summarized in Table 3. Using complex **7** as precursor gave better results and 2.06% of the cyclooctane was converted to *cis*-cyclooctene at a TOF of 6.24 h^{-1}. This higher value compared to the other precatalysts is probably due to the easier de-coordination of the ethylene ligands from the iridium centres, which facilitates the metal–alkane interactions.

Table 3 Catalytic transfer dehydrogenation of cyclooctane in the presence of *t*-butylethylene with $\mathbf{3_{H-T}}$, $\mathbf{4_{H-T}}$, **5** and **7** [a]

Entry	Catalyst	TON[b]	TOF[c]/h^{-1}
1	$\mathbf{3_{H-T}}$	4.6	0.46
2	$\mathbf{4_{H-T}}$	—	—
3	**5**	5.8	0.58
4	**7**	62.4	6.24

[a] Reaction conditions: [Ir_2] catalyst (0.010 mmol), COA (4.0 mL, 30.3 mmol), TBE (0.40 mL, 3.1 mmol), 200 °C, 10 h. [b] The number of moles of COA that a mole of [Ir_2] catalyst can convert in 10 h. [c] Turnover number per hour.

Conclusions

In this work, we have provided a more detailed investigation on dinuclear Ir(I) and Rh(I) complexes containing a bridging 1-arylimidazolide ligand, C2 and N3-bound to the metals.[16b] Initial deprotonation of 1-arylimidazoles (aryl = mesityl (Mes), 2,6-diisopropylphenyl (Dipp)) by *n*-butyl lithium in pentane at −30 °C was carried out to afford the corresponding derivatives (1-aryl-1*H*-imidazol-2-yl)lithium (**1a,b**) which were then used to prepare the doubly C,N-bridged dinuclear Ir(I) complexes **3**. These Ir(I) complexes exist in two isomeric forms, $\mathbf{3_{H-H}}$ which is the head-to-head isomer of C_S symmetry, and $\mathbf{3_{H-T}}$, the head-to-tail isomer of C_2 symmetry, which is thermodynamically more stable. The X-ray diffraction data suggest electron delocalisation within the N⋯C⋯N system and thus some carbene character for the Ir-bound imidazolide carbon atom, that is more pronounced in $\mathbf{3_{H-H}}$. The metal-bound imidazolide may be viewed as a deprotonated pNHC system. When the tetracarbonyl derivatives $\mathbf{4_{H-H}}$ and $\mathbf{4_{H-T}}$ were reacted with PMe_3, one CO ligand was displaced from each Ir centre and only one isomer was formed, **5**, in which the imidazolide ligands are bound in a H–T manner This ligand arrangement was retained in the formally metal–metal bonded, d^7–d^7 Ir(II)–Ir(II) complex, **6**, resulting from oxidative-addition of MeI across **5**. From the results obtained by cyclic voltammetry, exhaustive coulometry and spectroelectrochemistry, it was concluded that $\mathbf{3_{H-T}}$ undergoes a metal-based one electron oxidation to generate the mixed-valent Ir(I)/Ir(II) system, in equilibrium with Ir(II)/Ir(I), characterised by an IVCT band in the NIR region.

EPR studies combined with DFT calculations suggested that the Ir and Rh centres contribute substantially to the experimental magnetic anisotropy in the oxidized species and thus to the SOMO. These data evidenced that both Ir(II)/Ir(I) and Rh(II)/Rh(I) complexes are delocalized mixed-valent species.

The dinuclear iridium complexes were found to be only moderately active pre-catalysts in the reaction of cyclooctane and *t*-butylethylene to form cyclooctene and *t*-butylethane. Whether these results are directly linked to a difficulty to access coordinatively unsaturated and reactive species or to an inhibiting effect of the cod ligands cannot be stated at this stage. In favour of the latter hypothesis is that slightly better performances were obtained with the tetraethylene complex **7**, may be due to the favourable lability of the ethylene ligands.

Experimental

General considerations

All manipulations involving organometallics were performed under argon in a Braun glove-box or using standard Schlenk techniques. Solvents were dried using standard methods and distilled over sodium/benzophenone under argon prior use or passed through columns of activated alumina and subsequently purged with argon. The starting materials $[Rh(cod)(\mu\text{-}Cl)]_2$,[26] $[Ir(C_2H_4)_2(\mu\text{-}Cl)]_2$ [12h] and $[Rh(C_2H_4)_2(\mu\text{-}Cl)]_2$ [27] were prepared according to the literature and $[Ir(cod)(\mu\text{-}Cl)]_2$ is commercially available from Johnson Matthey PLC. NMR spectra of complexes were recorded on a Bruker 300 MHz, 400 MHz, 500 MHz or 600 MHz instrument at ambient temperature and referenced using the proton (^{1}H) or carbon (^{13}C) resonance of the residual solvent, with downfield shifts reported as positive. Assignments are based on ^{1}H, ^{1}H-COSY, ^{1}H-NOESY, ^{1}H/^{13}C-HSQC, and ^{1}H/^{13}C-HMBC experiments. ^{31}P{^{1}H} NMR spectra were recorded on a Bruker Avance 300 instrument at 121.49 MHz using H_3PO_4 (85% in D_2O) as external standard. IR spectra were recorded in the region 4000–100 cm^{-1} on a Nicolet 6700 FT-IR spectrometer (ATR mode, diamond crystal). Elemental analyses were performed by the "Service de microanalyses", Université de Strasbourg.

Synthetic procedures

(1-Mesityl-1*H*-imidazol-2-yl)lithium (1a). To a stirred solution of 1-mesitylimidazole (1.49 g, 8.0 mmol) in pentane (30 mL) was added dropwise a solution of *n*-BuLi (1.6 M in *n*-hexane, 5.0 mL, 8.0 mmol) at −78 °C over 2 min. The reaction mixture was stirred for 1 h at −30 °C, then allowed to warm to room temperature and stirred for another 2 h. The resulting clear orange solution was evaporated *in vacuo*. The residue was washed with pentane (3 × 5 mL) to yield a white powder which was collected by filtration and dried *in vacuo* (1.08 g, 70%). ^{1}H NMR (500 MHz, THF-d_8): δ 7.04 (s, 1H, NC*H*CHN$_{(mesityl)}$), 6.83 (s, 2H, aryl-*H*), 6.70 (s, 1H, NCHC*H*N$_{(mesityl)}$), 2.25 (s, 3H, *p*-C*H*$_{3(mesityl)}$), 1.95 (s, 6H, *o*-C*H*$_{3(mesityl)}$). ^{13}C{^{1}H} NMR (125 MHz, THF-d_8): δ 205.8 (N*C*N$_{(mesityl)}$), 142.3 (*C*$_{(mesityl)}$), 136.5 (*C*$_{(mesityl)}$), 135.5 (*C*$_{(mesityl)}$) 128.3 (*C*H$_{(mesityl)}$), 127.9 (N*C*HCHN$_{(mesityl)}$), 116.8 (NCH*C*HN$_{(mesityl)}$), 20.9 (*p*-*C*H$_{3(mesityl)}$), 18.2 (*o*-*C*H$_{3(mesityl)}$).

(1-(2,6-Diisopropylphenyl)-1*H*-imidazol-2-yl)lithium (1b). To a stirred solution of 1-(2,6-diisopropylphenyl)-imidazole (1.83 g, 8.0 mmol) in pentane (30 mL) was added dropwise a solution of *n*-BuLi (1.6 M in *n*-hexane, 5.0 mL, 8.0 mmol) at −78 °C over 2 min. Then the reaction mixture was allowed to warm to room temperature and stirred for another 2 h. The precipitate was collected by filtration, washed with pentane and dried *in vacuo* to obtain a white powder (1.72 g, 92%). ^{1}H NMR (500 MHz, THF-d_8): δ 7.19 (t, ^3J = 7.6 Hz, 1H, *p*-aryl-*H*), 7.11 (d, ^3J = 7.6 Hz, 2H, *m*-aryl-*H*), 7.04 (s, 1H, NC*H*CHN$_{(Dipp)}$), 6.81 (s, 1H, NCHC*H*N$_{(Dipp)}$), 2.72 (sept, ^3J = 6.9 Hz, 2H, C*H*(CH$_3$)$_2$), 1.04 (d, ^3J = 6.9 Hz, 6H, CH(C*H*$_3$)$_2$), 1.03 (d, ^3J = 6.9 Hz, 6H, CH(C*H*$_3$)$_2$). ^{13}C{^{1}H} NMR (125 MHz, THF-d_8): δ 202.3 (N*C*N$_{(Dipp)}$), 147.4 (*C*$_{(Dipp)}$), 142.2 (*C*$_{(Dipp)}$), 127.4 (N*C*HCHN$_{(Dipp)}$), 127.1 (*C*H$_{(Dipp)}$), 123.0 (*C*H$_{(Dipp)}$), 119.0 (NCH*C*HN$_{(Dipp)}$), 28.3 (*C*H(CH$_3$)$_2$), 25.1 (CH(*C*H$_3$)$_2$), 24.3 (CH(*C*H$_3$)$_2$).

1-Mesitylimidazolyl(cycloocta-1,5-diene)iridium(I) chloride [Ir(cod)Cl{$C_3H_3N_2$(Mes)-κN3}] (2). A solution of 1-mesitylimidazole (0.028 g, 0.15 mmol) in THF (2 mL) was added to a stirred solution of $[Ir(cod)(\mu\text{-}Cl)]_2$ (0.050 g, 0.074 mmol) in THF (2 mL). The mixture was stirred for 1 h at room temperature and then the volatiles were removed *in vacuo*. The residue

was washed with pentane (3 × 2 mL) and dried under vacuum to give a yellow powder (0.074 g, 0.14 mmol, 94%). ^{1}H NMR (500 MHz, CD_2Cl_2): δ 8.27 (apparent t, ^4J = 1.4 Hz, 1H, NC*H*N), 7.28 (apparent t, $^{3,4}J$ = 1.4 Hz, 1H, NC*H*CHN$_{(mesityl)}$), 6.99 (s, 2H, aryl-*H*), 6.96 (apparent t, $^{3,4}J$ = 1.4 Hz, 1H, NCHC*H*N$_{(mesityl)}$), 4.20 (br s, 2H, C*H*$_{(cod)}$), 3.71 (br s, 2H, C*H*$_{(cod)}$), 2.33 (s, 3H, *p*-C*H*$_{3(mesityl)}$), 2.27 (m, 4H, C*H*$_{2(cod)}$), 1.98 (s, 6H, *o*-C*H*$_{3(mesityl)}$), 1.62 (m, 2H, C*H*$_{2(cod)}$), 1.51 (m, 2H, C*H*$_{2(cod)}$). ^{13}C{^{1}H} NMR (125 MHz, CD_2Cl_2): δ 140.4 (N*C*HN), 140.3 (*p*-*C*$_{(mesityl)}$), 135.3 (*o*-*C*$_{(mesityl)}$), 132.6 (*ipso*-*C*$_{(mesityl)}$), 129.5 (*m*-*C*$_{(mesityl)}$), 126.9 (N*C*HCHN$_{(mesityl)}$), 121.5 (NCH*C*HN$_{(mesityl)}$), 67.1 (*C*H$_{(cod)}$), 58.2 (*C*H$_{(cod)}$), 32.3 (*C*H$_{2(cod)}$), 31.5 (*C*H$_{2(cod)}$), 21.2 (*p*-*C*H$_{3(mesityl)}$), 17.5 (*o*-*C*H$_{3(mesityl)}$). Anal. Calcd for $C_{20}H_{26}ClIrN_2$ (%): C, 46.01; H, 5.02; N, 5.37. Found: C, 45.79; H, 5.11; N, 5.90.

[Ir(cod){μ-C$_3$H$_2$N$_2$(Mes)-κC2,κN3}]$_2$ ($\mathbf{3_{H-H}}$). To a stirred solution of **1a** (0.100 g, 0.52 mmol) in Et_2O (10 mL) was added a solution of [Ir(cod)(μ-Cl)]$_2$ (0.168 g, 0.25 mmol) in Et_2O (5 mL) at −78 °C. The reaction mixture was allowed to warm to room temperature gradually and was stirred for 12 h. After removal of the volatiles under vacuum, the residue was extracted with toluene and the solution was filtered through Celite. The filtrate was concentrated to *ca.* 2 mL, Et_2O (3 mL) was added and this solution was cooled to −30 °C to yield a dark red crystalline solid (0.194 g, 80%) which was collected by filtration and dried *in vacuo*. ^{1}H NMR (400 MHz, C_6D_6): δ 7.20 (d, ^3J = 1.4 Hz, 2H, NC*H*CHN$_{(mesityl)}$), 6.74 (s, 2H, aryl-*H*), 6.68 (s, 2H, aryl-*H*), 6.42 (d, ^3J = 1.4 Hz, 2H, NCHC*H*N$_{(mesityl)}$), 4.24 (m, 2H, C*H*$_{(cod)}$), 3.89 (m, 4H, C*H*$_{(cod)}$), 3.55 (m, 2H, C*H*$_{(cod)}$), 2.65–2.31 (m, 8H, C*H*$_{2(cod)}$), 2.10 (s, 12H, *o*-C*H*$_{3(mesityl)}$), 1.91 (s, 6H, *p*-C*H*$_{3(mesityl)}$), 1.85 (m, 4H, C*H*$_{2(cod)}$), 1.64 (m, 4H, C*H*$_{2(cod)}$). ^{13}C{^{1}H} NMR (100 MHz, C_6D_6): δ 171.3 (N*C*N$_{(mesityl)}$), 138.5 (*C*$_{(mesityl)}$), 137.3 (*C*$_{(mesityl)}$), 136.9 (*C*$_{(mesityl)}$), 135.8 (*C*$_{(mesityl)}$), 128.9 (*C*H$_{(mesityl)}$), 128.8 (*C*H$_{(mesityl)}$), 125.5 (N*C*HCHN$_{(mesityl)}$), 122.4 (NCH*C*HN$_{(mesityl)}$), 69.4, 69.0, 65.2 and 59.5 (*C*H$_{(cod)}$), 32.9, 32.7, 32.5 and 32.1 (*C*H$_{2(cod)}$), 21.0 (*p*-*C*H$_{3(mesityl)}$), 20.2 (*o*-*C*H$_{3(mesityl)}$), 18.3 (*o*-*C*H$_{3(mesityl)}$). Anal. Calcd for $C_{40}H_{50}Ir_2N_4$ (%): C, 49.46; H, 5.19; N, 5.77. Found: C, 48.68; H, 5.00; N, 5.72.

From **2**: To a stirred solution of **2** (0.052 g, 0.10 mmol) in THF (5 mL) was added a solution of KHMDS (0.020 g, 0.10 mmol) in THF (2 mL) at −78 °C. The reaction mixture was allowed to warm to room temperature gradually and was stirred for 12 h. After removal of the volatiles under vacuum, the residue was extracted with toluene and the solution was filtered through Celite. The filtrate was evaporated to dryness under reduced pressure to yield a red solid (0.044 g, 91%). ^{1}H NMR analysis of the resulting red solid revealed a *ca.* 40 : 60 mixture of $\mathbf{3_{H-H}}$ and $\mathbf{3_{H-T}}$.

[Ir(cod){μ-C$_3$H$_2$N$_2$(Mes)-κC2,κN3}]$_2$ ($\mathbf{3_{H-T}}$). A solution of $\mathbf{3_{H-H}}$ (0.048 g, 0.050 mmol) in THF (5 mL) was refluxed for 24 h. After removal of the solvent under vacuum, the residue was washed with pentane (2 × 1 mL) to yield a purple crystalline solid (0.046 g, 96%) which was collected by filtration and dried *in vacuo*. ^{1}H NMR (300 MHz, C_6D_6): δ 7.02 (d, ^3J = 1.1 Hz, 2H, NC*H*CHN$_{(mesityl)}$), 6.89 (s, 2H, aryl-*H*), 6.77 (s, 2H, aryl-*H*), 6.53 (d, ^3J = 1.1 Hz, 2H, NCHC*H*N$_{(mesityl)}$), 4.32 (m, 2H, C*H*$_{(cod)}$), 3.85 (m, 2H, C*H*$_{(cod)}$), 3.66 (m, 4H, C*H*$_{(cod)}$), 2.67–2.27 (m, 8H, C*H*$_{2(cod)}$), 2.21 (s, 6H, *o*-C*H*$_{3(mesityl)}$), 2.18 (s, 6H, *o*-C*H*$_{3(mesityl)}$), 1.97 (s, 6H, *p*-C*H*$_{3(mesityl)}$), 1.81–1.49 (m, 8H, C*H*$_{2(cod)}$). ^{13}C{^{1}H} NMR (75 MHz, C_6D_6): δ 172.0 (N*C*N$_{(mesityl)}$), 138.3 (*C*$_{(mesityl)}$), 137.2 (*C*$_{(mesityl)}$), 136.8 (*C*$_{(mesityl)}$), 135.0 (*C*$_{(mesityl)}$), 129.3 (*C*H$_{(mesityl)}$), 128.1 (*C*H$_{(mesityl)}$), 125.4 (N*C*HCHN$_{(mesityl)}$), 121.3 (NCH*C*HN$_{(mesityl)}$), 75.7, 73.8, 59.8 and 56.0 (*C*H$_{(cod)}$), 35.4, 33.4, 32.4, 29.4 (*C*H$_{2(cod)}$), 21.1 (*p*-*C*H$_{3(mesityl)}$), 19.2 (*o*-*C*H$_{3(mesityl)}$), 18.2 (*o*-*C*H$_{3(mesityl)}$). Anal. Calcd for $C_{40}H_{50}Ir_2N_4$ (%): C, 49.46; H, 5.19; N, 5.77. Found: C, 49.21; H, 4.96; N, 5.60.

[Ir(CO)$_2${μ-C$_3$H$_2$N$_2$(Mes)-κC2,κN3}]$_2$ ($\mathbf{4_{H-H}}$). A suspension of $\mathbf{3_{H-H}}$ (0.097 g, 0.100 mmol) in Et_2O (5 mL) was stirred under CO (1 bar) at room temperature and the color turned from red to yellow immediately. The suspension was further stirred for 30 min. After removal of the volatiles under vacuum, the residue was washed with pentane (2 × 1 mL) to yield a yellow crystalline solid which was collected by filtration and dried *in vacuo* (0.070 g, 81%). ^{1}H NMR (500 MHz, C_6D_6): δ 7.11 (d, ^3J = 1.5 Hz, 2H, NC*H*CHN$_{(mesityl)}$), 6.67 (s, 4H, aryl-*H*), 6.33 (d, ^3J = 1.5 Hz, 2H, NCHC*H*N$_{(mesityl)}$), 2.04 (s, 6H, C*H*$_{3(Mes)}$), 1.96 (s, 6H, C*H*$_{3(Mes)}$), 1.82 (s, 6H, C*H*$_{3(Mes)}$). ^{13}C{^{1}H} NMR (125 MHz, C_6D_6): δ 181.4 (*C*O), 175.5 (*C*O), 172.8 (N*C*N$_{(mesityl)}$), 138.7 (*C*$_{(mesityl)}$), 136.8 (*C*$_{(mesityl)}$), 136.4 (*C*$_{(mesityl)}$), 136.1 (*C*$_{(mesityl)}$), 131.4 (N*C*HCHN$_{(mesityl)}$), 129.4 (*C*H$_{(mesityl)}$), 129.0 (*C*H$_{(mesityl)}$), 123.0 ((NCH*C*HN$_{(mesityl)}$)), 21.0 (*C*H$_{3(mesityl)}$), 19.6 (*C*H$_{3(mesityl)}$), 18.1 (*C*H$_{3(mesityl)}$). IR (pure, orbit diamond): ν_{CO} = 2060, 2037, 1954 cm^{-1}. Anal. Calcd for $C_{28}H_{26}Ir_2N_4O_4$ (%): C, 38.79; H, 3.02; N, 6.46. Found: C, 38.53; H, 3.15; N, 6.29.

[Ir(CO)$_2${μ-C$_3$H$_2$N$_2$(Mes)-κC2,κN3}]$_2$ ($\mathbf{4_{H-T}}$). A procedure similar to that used for the synthesis of $\mathbf{4_{H-H}}$ but starting from $\mathbf{3_{H-T}}$ yielded a brown solid (0.065 g, 75%). ^{1}H NMR (300 MHz, C_6D_6): δ 6.95 (d, ^3J = 1.6 Hz, 2H, NC*H*CHN$_{(mesityl)}$), 6.79 (s, 2H, aryl-*H*), 6.77 (s, 2H, aryl-*H*), 6.41 (d, ^3J = 1.6 Hz, 2H, NCHC*H*N$_{(mesityl)}$), 2.09 (s, 6H, *p*-C*H*$_{3(mesityl)}$), 1.95 (s, 12H, *o*-C*H*$_{3(mesityl)}$). ^{13}C{^{1}H} NMR (75 MHz, C_6D_6): δ 183.7 (*C*O), 175.7 (*C*O), 175.1 (N*C*N$_{(mesityl)}$), 138.7 (*C*$_{(mesityl)}$), 136.5 (*C*$_{(mesityl)}$), 135.6 (*C*$_{(mesityl)}$), 130.5 (N*C*HCHN$_{(mesityl)}$), 129.4 (*C*H$_{(mesityl)}$), 129.3 (*C*H$_{(mesityl)}$), 122.1 (NCH*C*HN$_{(mesityl)}$), 21.1 (*p*-*C*H$_{3(mesityl)}$), 18.7 (*o*-*C*H$_{3(mesityl)}$), 18.0 (*o*-*C*H$_{3(mesityl)}$). IR (pure, orbit diamond): ν_{CO} = 2059, 2041, 1968 cm^{-1}. Anal. Calcd for $C_{28}H_{26}Ir_2N_4O_4$ (%): C, 38.79; H, 3.02; N, 6.46. Found: C, 38.42; H, 3.22; N, 6.63.

[Ir(CO)(PMe$_3$){μ-C$_3$H$_2$N$_2$(Mes)-κC2,κN3}]$_2$ (5). This complex can be synthesized by reaction of either $\mathbf{4_{H-T}}$ or $\mathbf{4_{H-H}}$ with 2.0 equiv. of trimethylphosphine.

From $\mathbf{4_{H-T}}$: To a solution of $\mathbf{4_{H-T}}$ (0.043 g, 0.05 mmol) in toluene (5 mL) was added a solution of PMe_3 (0.1 M in Et_2O, 1.0 mL, 0.1 mmol). The mixture was stirred for 4 h and the initially yellow solution became red. After removal of the volatiles under vacuum, the residue was washed with pentane (2 × 1 mL) to yield a red crystalline solid which was collected by filtration and dried *in vacuo* (0.045 g, 93%). ^{1}H NMR (500 MHz, C_6D_6): δ 6.90 (s, 2H, aryl-*H*), 6.89 (d, ^3J = 1.0 Hz, 2H, NC*H*CHN$_{(mesityl)}$), 6.77 (s, 2H, aryl-*H*), 6.68 (apparent t, $^3J_{H-H}$, $^5J_{H-P}$ = 1.0 Hz, 2H, NCHC*H*N$_{(mesityl)}$), 2.28 (s, 6H, *o*-C*H*$_{3(mesityl)}$),

2.18 (s, 6H, *o*-C$H_{3(\text{mesityl})}$), 2.08 (s, 6H, *p*-C$H_{3(\text{mesityl})}$), 1.13 (d, $^2J_{H-P}$ = 8.7 Hz, 18H, PCH_3). ^{31}P{^{1}H} NMR (121.5 MHz, C_6D_6): δ −24.1. ^{13}C{^{1}H} NMR (125 MHz, C_6D_6): δ 181.4 (d, $^2J_{C-P}$ = 10.0 Hz, *C*O), 177.1 (d, $^2J_{C-P}$ = 112.0 Hz, N*C*N$_{(\text{mesityl})}$), 138.3 (*C*$_{(\text{mesityl})}$), 137.5 (*C*$_{(\text{mesityl})}$), 136.7 (*C*$_{(\text{mesityl})}$), 135.5 (*C*$_{(\text{mesityl})}$), 129.4 (*C*H$_{(\text{mesityl})}$), 128.9 (*C*H$_{(\text{mesityl})}$), 128.0 (d, $^4J_{C-P}$ = 5.2 Hz, NC*H*CHN$_{(\text{mesityl})}$), 120.1 (d, $^4J_{C-P}$ = 2.0 Hz, NCH*C*HN$_{(\text{mesityl})}$), 21.1 (*p*-*C*H$_{3(\text{mesityl})}$), 18.9 (*o*-*C*H$_{3(\text{mesityl})}$), 18.3 (*o*-*C*H$_{3(\text{mesityl})}$), 17.0 (d, $^1J_{C-P}$ = 31.6 Hz, P*C*H$_3$). IR (pure, orbit diamond): ν_{CO} = 2000, 1911 cm^{-1}. Anal. Calcd for $C_{32}H_{44}Ir_2N_4O_2P_2$ (%): C, 39.91; H, 4.60; N, 5.82. Found: C, 39.88; H, 4.70; N, 5.75.

From $\mathbf{4_{H-H}}$: A procedure similar to that used with $\mathbf{4_{H-T}}$ was employed to yield the same red crystalline solid (0.046 g, 96%).

[Ir$_2$(CO)$_2$(PMe$_3$)$_2$(Me)I{μ-C$_3$H$_2$N$_2$(Mes)-κC2,κN3}$_2$] (6). To a stirred solution of **5** (0.030 g, 0.032 mmol) in THF (5 mL) was added dropwise over 2 min a solution of MeI (0.1 M in Et_2O, 0.4 mL, 0.04 mmol) and the mixture was stirred for 5 min. Concentration of the solution under vacuum to 2 mL followed by addition of pentane (5 mL) afforded the product as a yellow powder (0.032 g, 90%). ^{1}H NMR (500 MHz, C_6D_6): δ 7.87 (d, ^3J = 1.2 Hz, 1H, NC*H*CHN$_{(\text{mesityl})}$), 6.97 (s, 1H, aryl-*H*), 6.89 (s, 1H, aryl-*H*), 6.75 (s, 2H, aryl-*H*), 6.73 (d, ^3J = 1.2 Hz, 1H, NC*H*CHN$_{(\text{mesityl})}$), 6.19 (t, J_{H-H}, J_{H-P} = 1.2 Hz, 1H, NCHC*H*N$_{(\text{mesityl})}$), 6.04 (t, J_{H-H}, J_{H-P} = 1.2 Hz, 1H, NCHC*H*N$_{(\text{mesityl})}$), 2.26 (s, 3H, C$H_{3(\text{mesityl})}$), 2.22 (s, 3H, C$H_{3(\text{mesityl})}$), 2.15 (s, 3H, C$H_{3(\text{mesityl})}$), 2.12 (s, 3H, C$H_{3(\text{mesityl})}$), 1.96 (s, 3H, C$H_{3(\text{mesityl})}$), 1.74 (s, 3H, C$H_{3(\text{mesityl})}$), 1.51 (d, $^2J_{H-P}$ = 9.6 Hz, 9H, PCH_3), 1.02 (d, $^2J_{H-P}$ = 9.6 Hz, 9H, PCH_3), 0.71 (d, $^3J_{H-P}$ = 5.7 Hz, 3H, IrCH_3). ^{31}P{^{1}H} NMR (121.5 MHz, C_6D_6): δ −46.6, −48.9. ^{13}C{^{1}H} NMR (125 MHz, C_6D_6): δ 181.5 (d, $^2J_{C-P}$ = 10.5 Hz, *C*O), 180.0 (d, $^2J_{C-P}$ = 9.6 Hz, *C*O), 142.8 (d, $^2J_{C-P}$ = 136.7 Hz, N*C*N$_{(\text{mesityl})}$), 140.8 (d, $^2J_{C-P}$ = 141.1 Hz, N*C*N$_{(\text{mesityl})}$), 138.2, 138.1, 137.9, 136.8, 136.7, 136.5, 135.2 and 135.0 (*C*$_{(\text{mesityl})}$), 131.9 (d, $^4J_{C-P}$ = 4.6 Hz, N*C*HCHN$_{(\text{mesityl})}$), 129.8, 129.1, 129.0 and 128.9 (*C*H$_{(\text{mesityl})}$), 122.2 (d, $^4J_{C-P}$ = 3.8 Hz, NCH*C*HN$_{(\text{mesityl})}$), 121.5 (d, $^4J_{C-P}$ = 3.8 Hz, NC*H*CHN$_{(\text{mesityl})}$), 121.0 (d, $^4J_{C-P}$ = 3.7 Hz, NCH*C*HN$_{(\text{mesityl})}$), 21.4 (*C*H$_{3(\text{mesityl})}$), 21.2 (*C*H$_{3(\text{mesityl})}$), 18.7 (*C*H$_{3(\text{mesityl})}$), 18.6 (d, $^1J_{C-P}$ = 34.9 Hz, P*C*H$_3$), 18.4 (*C*H$_{3(\text{mesityl})}$), 17.8 (*C*H$_{3(\text{mesityl})}$), 17.3 (*C*H$_{3(\text{mesityl})}$), 14.8 (d, $^1J_{C-P}$ = 33.5 Hz, P*C*H$_3$), −31.8 (d, $^2J_{C-P}$ = 2.3 Hz, Ir*C*H$_3$). IR (pure, orbit diamond): ν_{CO} = 2019, 1952 cm^{-1}. Anal. Calcd for $C_{33}H_{47}IIr_2N_4O_2P_2$ (%): C, 35.87; H, 4.29; N, 5.07. Found: C, 35.33; H, 4.02; N, 5.21.

[Ir(C$_2$H$_4$)$_2${μ-C$_3$H$_2$N$_2$(Mes)-κC2,κN3}]$_2$ (7). To a stirred solution of **1a** (0.100 g, 0.52 mmol) in Et_2O (10 mL) was added a solution of [Ir(C$_2$H$_4$)$_2$(μ-Cl)]$_2$ (0.142 g, 0.25 mmol) in Et_2O (5 mL) at −78 °C. The reaction mixture was allowed to warm to room temperature gradually and was further stirred for 4 h. After removal of volatiles *in vacuo*, the residue was extracted with toluene and the solution was filtered through Celite. After evaporation of the toluene, the solid was washed with pentane (2 × 1 mL) at 0 °C and dried *in vacuo* to yield a blue solid, which was stored at −30 °C (0.167 g, 77%). ^{1}H NMR (600 MHz, C_6D_6): δ 7.09 (d, ^3J = 1.5 Hz, 2H, NC*H*CHN$_{(\text{mesityl})}$), 6.80 (s, 2H, aryl-*H*), 6.74 (s, 2H, aryl-*H*), 6.49 (d, ^3J = 1.5 Hz, 2H, NCHC*H*N$_{(\text{mesityl})}$), 3.13 (broad B part of an AA'BB' spin system, 4H, C$H_{2(\text{ethylene})}$) and 2.89 (broad A part of an AA'BB' spin system, 4H, C$H_{2(\text{ethylene})}$), 2.63 (B part of an AA'BB' spin system with |N| ≈ 8.2 Hz, 4H, C$H_{2(\text{ethylene})}$) and 2.36 (A part of an AA'BB' spin system with |N| ≈ 8.2 Hz, 4H, C$H_{2(\text{ethylene})}$), 2.11 (s, 6H, *o*-C$H_{3(\text{mesityl})}$), 2.08 (s, 6H, *o*-C$H_{3(\text{mesityl})}$), 1.97 (s, 6H, *p*-C$H_{3(\text{mesityl})}$). ^{13}C{^{1}H} NMR (150 MHz, C_6D_6): δ 171.5 (N*C*N$_{(\text{mesityl})}$), 137.8 (*C*$_{(\text{mesityl})}$), 137.5 (*C*$_{(\text{mesityl})}$), 136.7 (*C*$_{(\text{mesityl})}$), 134.8 (*C*$_{(\text{mesityl})}$), 129.7 (*C*H$_{(\text{mesityl})}$), and 128.8 (*C*H$_{(\text{mesityl})}$), 124.6 (N*C*HCHN$_{(\text{mesityl})}$), 122.0 (NCH*C*HN$_{(\text{mesityl})}$), 60.5 (*C*H$_{2(\text{ethylene})}$), 42.3 (*C*H$_{2(\text{ethylene})}$), 21.5 (*p*-*C*H$_{3(\text{mesityl})}$), 19.0 (*o*-*C*H$_{3(\text{mesityl})}$), 18.1 (*o*-*C*H$_{3(\text{mesityl})}$). Calcd for $C_{32}H_{42}Ir_2N_4$ (%): C, 44.32; H, 4.88; N, 6.46. Found: C, 43.88; H, 4.95; N, 6.73.

[Rh(cod){μ-C$_3$H$_2$N$_2$(Mes)-κC2,κN3}]$_2$ (8). A procedure similar to that used for the synthesis of $\mathbf{3_{H-H}}$ was used but starting from [Rh(cod)(μ-Cl)]$_2$. Treatment of **1a** (0.100 g, 0.52 mmol) with [Rh(cod)(μ-Cl)]$_2$ (0.123 g, 0.25 mmol) afforded an orange solid (0.168 g, 85%). ^{1}H NMR (500 MHz, C_6D_6): δ 6.96 (an overlap of two s, 4H, NC*H*CHN$_{(\text{mesityl})}$ and aryl-*H*), 6.77 (s, 2H, aryl-*H*), 6.51 (s, 2H, NCHC*H*N$_{(\text{mesityl})}$), 4.72 (m, 2H, C$H_{(\text{cod})}$), 4.48 (m, 2H, C$H_{(\text{cod})}$), 4.09 (m, 2H, C$H_{(\text{cod})}$), 3.76 (m, 2H, C$H_{(\text{cod})}$), 2.73–2.55 (m, 4H, C$H_{2(\text{cod})}$), 2.31 (s, 6H, *o*-C$H_{3(\text{mesityl})}$), 2.20 (s, 6H, *o*-C$H_{3(\text{mesityl})}$), 2.09–1.96 (m, 8H, C$H_{2(\text{cod})}$), 1.94 (s, 6H, *p*-C$H_{3(\text{mesityl})}$), 1.86–1.77 (m, 4H, C$H_{2(\text{cod})}$). ^{13}C{^{1}H} NMR (125 MHz, C_6D_6): δ 176.2 (d, $^1J_{C-Rh}$ = 50.4 Hz, N*C*N$_{(\text{mesityl})}$), 138.8 (*C*$_{(\text{mesityl})}$), 137.2 (*C*$_{(\text{mesityl})}$), 137.0 (*C*$_{(\text{mesityl})}$), 135.1 (*C*$_{(\text{mesityl})}$), 129.3 (*C*H$_{(\text{mesityl})}$), 128.6 (*C*H$_{(\text{mesityl})}$), 126.8 (N*C*HCHN$_{(\text{mesityl})}$), 120.3 (NCH*C*HN$_{(\text{mesityl})}$), 90.3 (d, $^1J_{C-Rh}$ = 8.4 Hz, *C*H$_{(\text{cod})}$), 89.3 (d, $^1J_{C-Rh}$ = 7.3 Hz, *C*H$_{(\text{cod})}$), 79.2 (d, $^1J_{C-Rh}$ = 12.9 Hz, *C*H$_{(\text{cod})}$), 72.0 (d, $^1J_{C-Rh}$ = 11.9 Hz, *C*H$_{(\text{cod})}$), 33.4, 33.3, 30.7 and 29.6 (*C*H$_{2(\text{cod})}$), 21.1 (*p*-*C*H$_{3(\text{mesityl})}$), 19.5 (*o*-*C*H$_{3(\text{mesityl})}$), 18.2 (*o*-*C*H$_{3(\text{mesityl})}$). Calcd for $C_{40}H_{50}Rh_2N_4$ (%): C, 60.61; H, 6.36; N, 7.07. Found: C, 60.13; H, 6.48; N, 7.32.

[Rh(C$_2$H$_4$)$_2${μ-C$_3$H$_2$N$_2$(Dipp)-κC2,κN3}]$_2$ (9). To a stirred solution of **1b** (0.120 g, 0.51 mmol) in Et_2O (10 mL) was added a solution of [Rh(C$_2$H$_4$)$_2$(μ-Cl)]$_2$ (0.085 g, 0.25 mmol) in Et_2O (5 mL) at −78 °C. The reaction mixture was allowed to warm to room temperature gradually and was further stirred for 4 h. After removal of the volatiles under vacuum, the residue was extracted with *n*-hexane and the solution was filtered through Celite. The filtrate was concentrated to *ca.* 4 mL under reduced presssure and then was cooled to −30 °C in an ethylene atmosphere to obtain purple crystals, which were stored at −30 °C (0.135 g, 70%). ^{1}H NMR (400 MHz, C_6D_6): δ 7.28 (d, ^3J = 4.4 Hz, 4H, *m*-aryl-*H*), 7.08 (t, ^3J = 4.4 Hz, 2H, *p*-aryl-*H*), 7.02 (s, 2H, NC*H*CHN$_{(\text{Dipp})}$), 6.64 (s, 2H, NCHC*H*N$_{(\text{Dipp})}$), 3.65 (B part of a broad poorly resolved AA'BB' spin system, 4H, C$H_{2(\text{ethylene})}$) and 3.58 (A part of a broad poorly resolved AA'BB' spin system, 4H, C$H_{2(\text{ethylene})}$), 3.25 (sept, ^3J = 6.8 Hz, 2H, C*H*(CH$_3$)$_2$), 2.86 (B part of an AA'BB' spin system with |N| ≈ 7.5 Hz and poorly resolved Rhodium coupling, 4H, C$H_{2(\text{ethylene})}$) and 2.62 (A part of an AA'BB' spin system with |N| ≈ 7.5 Hz and poorly resolved rhodium coupling, 4H, C$H_{2(\text{ethylene})}$), 2.48 (sept, ^3J = 6.8 Hz, 2H, C*H*(CH$_3$)$_2$), 1.73 (d, ^3J = 6.8 Hz, 6H, CH(C*H*$_3$)$_2$), 1.16 (d, ^3J = 6.8 Hz, 6H, CH(C*H*$_3$)$_2$), 1.06 (d, ^3J = 6.8 Hz, 6H, CH(C*H*$_3$)$_2$), 0.80 (d, ^3J = 6.8 Hz, 6H, CH(C*H*$_3$)$_2$). ^{13}C{^{1}H} NMR (100 MHz, C_6D_6):

δ 175.1 (d, $^1J_{C-Rh}$ = 49.0 Hz, N*C*N$_{(Dipp)}$), 147.1 (*C*$_{(Dipp)}$), 146.1 (*C*$_{(Dipp)}$), 137.8 (*C*$_{(Dipp)}$), 128.9 (*C*H$_{(Dipp)}$), 125.9 (N*C*HCHN$_{(Dipp)}$), 124.1 (*C*H$_{(Dipp)}$), 123.8 (*C*H$_{(Dipp)}$), 122.8 (NCH*C*HN$_{(Dipp)}$), 78.7 (d, $^1J_{C-Rh}$ = 6.6 Hz, *C*H$_{2(ethylene)}$), 58.0 (d, $^1J_{C-Rh}$ = 12.1 Hz, *C*H$_{2(ethylene)}$), 28.8 (*C*H(CH$_3$)$_2$), 28.3(*C*H(CH$_3$)$_2$), 26.3, 24.9, 24.2 and 23.4 (CH(*C*H$_3$)$_2$). Calcd for $C_{38}H_{54}Rh_2N_4$ (%): C, 59.07; H, 7.04; N, 7.25. Found: C, 58.63; H, 6.87; N, 7.42.

Catalytic transfer dehydrogenation of cyclooctane

In a preliminary investigation, a red suspension of complex $\mathbf{3_{H-T}}$ (9.7 mg, 0.010 mmol) in a mixture of COA (4.0 mL, 30.3 mmol) and TBE (0.40 mL, 3.1 mmol), in a sealed tube under argon, was heated at 200 °C for 10 h (Table 3, entry 1). Gas chromatographic (GC) analysis of the products indicated 0.15% of the cyclooctane was converted to *cis*-cyclooctene at a turnover frequency (TOF) 0.46 h^{-1}. The formation of TBA, confirmed by GC and ^{1}H NMR analysis, also indicated that the transfer dehydrogenation reaction did occur. When complex $\mathbf{4_{H-T}}$ was used as the precatalyst under the same reaction conditions (Table 3, entry 2), no catalytic activity was observed. In the catalytic reaction using complex **5** (Table 3, entry 3), in which two CO ligands of complex **4** are replaced by two molecules of PMe_3, GC analysis of the products indicated that 0.19% of the cyclooctane was converted to *cis*-cyclooctene at a TOF of 0.58 h^{-1}. Better results were obtained with complex **7** where 2.06% of the cyclooctane was converted to *cis*-cyclooctene at a TOF of 6.24 h^{-1}.

X-ray data collection, structure solution, and refinement for all compounds

Suitable crystals for the X-ray analysis of all compounds were obtained as described above. Data for $\mathbf{3_{H-H}}$, $\mathbf{3_{H-T}}$ and **8** were collected on an APEX-II CCD (graphite-monochromated Mo-Kα radiation, λ = 0.71073 Å) at 173(2) K and data for **9** were collected on a Kappa CCD diffractometer (graphite-monochromated Mo-Kα radiation, λ = 0.71073 Å) at 173(2) K. Crystallographic and experimental details for these structures are summarized in Table S1 (see ESI†). The structures were solved by direct methods (SHELXS-97 [28]) and refined by full-matrix least-squares procedures (based on F^2, SHELXL-97) with anisotropic thermal parameters for all the non-hydrogen atoms. The hydrogen atoms were introduced into the geometrically calculated positions (SHELXS-97 procedures). The SQUEEZE instruction in PLATON was applied for **9** and the residual electron density was assigned to half a molecule of disordered *n*-hexane. In **9**, one methyl group (C11) was found disordered over two positions.

Electrochemistry

All compounds were studied in CH_2Cl_2 + 0.1 mM [*n*-Bu$_4$N]PF$_6$. [*n*-Bu$_4$N]PF$_6$ (Fluka, electrochemical grade) and CH_2Cl_2 (Merck, UVasol®) were used as received. The electrochemical measurements were carried out at room temperature (20 °C) in CH_2Cl_2 containing 0.1 M [*n*-Bu$_4$N]PF$_6$ in a classical three-electrode cell. The electrolyte was degassed by bubbling argon through the solution for at least 5 min, and an argon flow was kept over the solution during measurements. The electrochemical cell was connected to a computerized multipurpose electrochemical device (Autolab, Eco Chemie BV, The Netherlands) controlled by a GPES software (v. 4.7) running on a PC computer. The working electrode was a glassy carbon (GC) disk electrode (diameter: 3 mm), used either motionless for cyclic voltammetry (100 mV s^{-1} to 10 V s^{-1}) or as a rotating disk electrode. The auxiliary electrode was a Pt wire, and the pseudo reference electrode a Pt wire. All potentials are given *vs.* Fc^+/Fc used as internal reference in agreement with the IUPAC recommendation[29] and are uncorrected from ohmic drop.

The number of exchanged electrons for the first oxidation step was determined by exhaustive electrolysis. Prior to electrolysis, the corresponding mixtures were stirred and degassed by bubbling argon through the solution for 10 min. Then, the desired working potential was applied. During anodic oxidation, the electrolyzed solution was continuously stirred and maintained under argon. Coulometric measurements were performed in a standard 40 mL cell. The working and the auxiliary electrodes were a platinum wire (o.d. 0.8 mm) of 15 cm length. For the controlled-potential electrolysis, the anodic and cathodic compartments were separated by a fritted-glass disk to prevent diffusion of the electrogenerated species.

The reference electrode was a saturated calomel electrode (SCE) that was electrically connected to the studied solution by a junction bridge filled with the corresponding solvent-supporting electrolyte solution.

Spectroelectrochemical experiments were carried out as described elsewhere,[30] using a Zeiss MCS 601 UV–vis–NIR diode array spectrometer.

UV-visible-NIR spectroscopy

UV–Vis absorption spectra have been recorded for 4.41 × 10^{-5} mol L^{-1} ($\mathbf{3_{H-T}}$) and 8.07 × 10^{-5} mol L^{-1} (**8**) solutions in CH_2Cl_2 on a Perkin-Elmer Lambda 35 spectrophotometer in quartz cells (1 cm). The UV-visible-NIR absorption spectroscopic measurements were performed in CH_2Cl_2. The optical absorption spectrum of $\mathbf{3_{H-T}}$ (Fig. S1 in ESI†) was characterised by a band in the visible domain around 525 nm ($\varepsilon_{525\ nm}$ = 3648 dm^3 mol^{-1} cm^{-1}). In the case of the **8** (Fig. S3 in ESI†), the band was observed at 476 nm ($\varepsilon_{476\ nm}$ = 4585 dm^3 mol^{-1} cm^{-1}).

EPR experiments

EPR spectra were recorded with an EMX spectrometer (Bruker) operating at X-band and equipped with a standard HSN cavity and a variable temperature attachment. Computer simulations of the EPR spectra were performed with the help of Easy Spin software.[31]

DFT calculations

All theoretical calculations were performed with the ORCA program package.[32] Geometry optimization was carried out using the GGA functional BP86[33] and by taking advantage of

the resolution of the identity (RI) approximation in the Split-RI-J[34] variant with the appropriate Coulomb fitting sets.[35] Increased integration grids (Grid4 and GridX4 in ORCA convention) and tight SCF convergence criteria were used. Solvent effects were accounted for according to the experimental conditions. For that purpose, we used the CH_2Cl_2 (ε = 9.08) solvent within the framework of the conductor like screening (COSMO) dielectric continuum approach.[36] Electronic structures were obtained from single-point calculations using the B3LYP[37] functional. Scalar relativistic effects were included using the scalar relativisitc zero-order regular approximation (ZORA)[38] and the scalar relativistically recontracted (SARC)[39] version of the def2-TZVP(-f) basis set together with the decontracted def2-TZVP/J Coulomb fitting basis sets for all atoms. Spin density and molecular orbitals were plotted using the orca_plot utility program and visualized with Chemcraft[40] software.

Acknowledgements

The USIAS, CNRS, UdS, Région Alsace and Communauté Urbaine de Strasbourg are gratefully acknowledged for the award of fellowships and a Gutenberg Excellence Chair (2010–11) to AAD and support. We also thank the ucFRC (http://www.icfrc.fr) for support and the China Scholarship Council for a PhD grant to F. H., and the Service de Radiocristallographie (Institut de Chimie, Strasbourg) for the determination of the crystal structures.

Notes and references

1 (*a*) A. J. Arduengo III, R. L. Harlow and M. Kline, *J. Am. Chem. Soc.*, 1991, **113**, 361; (*b*) A. J. Arduengo, H. V. R. Dias, R. L. Harlow and M. Kline, *J. Am. Chem. Soc.*, 1992, **114**, 5530.

2 (*a*) M. Melaimi, M. Soleilhavoup and G. Bertrand, *Angew. Chem., Int. Ed.*, 2010, **49**, 8810; (*b*) P. de Frémont, N. Marion and S. P. Nolan, *Coord. Chem. Rev.*, 2009, **253**, 862; (*c*) F. E. Hahn and M. C. Jahnke, *Angew. Chem., Int. Ed.*, 2008, **47**, 3122; (*d*) D. Bourissou, O. Guerret, F. P. Gabbaï and G. Bertrand, *Chem. Rev.*, 2000, **100**, 39.

3 (*a*) S. Kuwata and T. Ikariya, *Chem. – Eur. J.*, 2011, **17**, 3542; (*b*) S. Kuwata and T. Ikariya, *Chem. Commun.*, 2014, **50**, 14290.

4 F. E. Hahn, *ChemCatChem*, 2013, **5**, 419.

5 (*a*) C.-H. Hsieh, R. Pulukkody and M. Y. Darensbourg, *Chem. Commun.*, 2013, **49**, 9326; (*b*) D. Brackemeyer, A. Hervé, C. Schulte to Brinke, M. C. Jahnke and F. E. Hahn, *J. Am. Chem. Soc.*, 2014, **136**, 7841.

6 (*a*) F. E. Hahn, V. Langenhahn, T. Lügger, T. Pape and D. Le Van, *Angew. Chem., Int. Ed.*, 2005, **44**, 3759; (*b*) F. E. Hahn, V. Langenhahn and T. Pape, *Chem. Commun.*, 2005, 5390; (*c*) J. Ruiz, G. García, M. E. G. Mosquera, B. F. Perandones, M. P. Gonzalo and M. Vivanco, *J. Am. Chem. Soc.*, 2005, **127**, 8584.

7 (*a*) G. E. Dobereiner, C. A. Chamberlin, N. D. Schley and R. H. Crabtree, *Organometallics*, 2010, **29**, 5728; (*b*) P. C. Kunz, C. Wetzel, S. Kogel, M. U. Kassack and B. Spingler, *Dalton Trans.*, 2011, **40**, 35.

8 (*a*) T. Kösterke, T. Pape and F. E. Hahn, *J. Am. Chem. Soc.*, 2011, **133**, 2112; (*b*) T. Kösterke, J. Kösters, E.-U. Würthwein, C. Mück-Lichtenfeld, C. Schulte to Brinke, F. Lahoz and F. E. Hahn, *Chem. – Eur. J.*, 2012, **18**, 14594; (*c*) R. Das, C. G. Daniliuc and F. E. Hahn, *Angew. Chem., Int. Ed.*, 2014, **53**, 1163; (*d*) R. Das, A. Hepp, C. G. Daniliuc and F. E. Hahn, *Organometallics*, 2014, **33**, 6975.

9 F. He, P. Braunstein, M. Wesolek and A. A. Danopoulos, *Chem. Commun.*, 2015, **51**, 2814.

10 (*a*) C. Hill, F. Bosold, K. Harms, J. C. W. Lohrenz, M. Marsch, M. Schmieczek and G. Boche, *Chem. Ber.*, 1997, **130**, 1201; (*b*) C. Hilf, F. Bosold, K. Harms, M. Marsch and G. Boche, *Chem. Ber.*, 1997, **130**, 1213.

11 A. P. Marchenko, H. N. Koidan, I. I. Pervak, A. N. Huryeva, E. V. Zarudnitskii, A. A. Tolmachev and A. N. Kostyuk, *Tetrahedron Lett.*, 2012, **53**, 494.

12 (*a*) K. A. Beveridge, G. W. Bushnell, K. R. Dixon, D. T. Eadie, S. R. Stobart, J. L. Atwood and M. J. Zaworotko, *J. Am. Chem. Soc.*, 1982, **104**, 920; (*b*) A. W. Coleman, D. T. Eadie, S. R. Stobart, M. J. Zaworotko and J. L. Atwood, *J. Am. Chem. Soc.*, 1982, **104**, 922; (*c*) G. W. Bushnell, D. O. K. Fjeldsted, S. R. Stobart and M. J. Zaworotko, *J. Chem. Soc., Chem. Commun.*, 1983, 580; (*d*) J. L. Atwood, K. A. Beveridge, G. W. Bushnell, K. R. Dixon, D. T. Eadie, S. R. Stobart and M. J. Zaworotko, *Inorg. Chem.*, 1984, **23**, 4050; (*e*) G. W. Bushnell, M. J. Decker, D. T. Eadie, S. R. Stobart, R. Vefghi, J. L. Atwood and M. J. Zaworotko, *Organometallics*, 1985, **4**, 2106; (*f*) D. O. K. Fjeldsted, S. R. Stobart and M. J. Zaworotko, *J. Am. Chem. Soc.*, 1985, **107**, 8258; (*g*) G. W. Bushnell, D. O. K. Fjeldsted, S. R. Stobart and J. Wang, *Organometallics*, 1996, **15**, 3785; (*h*) M. A. Arthurs, J. Bickerton, S. R. Stobart and J. Wang, *Organometallics*, 1998, **17**, 2743.

13 (*a*) K. A. Beveridge, G. W. Bushnell, S. R. Stobart, J. L. Atwood and M. J. Zaworotko, *Organometallics*, 1983, **2**, 1447; (*b*) G. W. Bushnell, D. O. K. Fjeldsted, S. R. Stobart, M. J. Zaworotko, S. A. R. Knox and K. A. MacPherson, *Organometallics*, 1985, **4**, 1107; (*c*) Y. Yuan, M. V. Jiménez, E. Sola, F. J. Lahoz and L. A. Oro, *J. Am. Chem. Soc.*, 2002, **124**, 752.

14 (*a*) R. D. Brost and S. R. Stobart, *Inorg. Chem.*, 1989, **28**, 4307; (*b*) R. D. Brost, D. O. K. Fjeldsted and S. R. Stobart, *J. Chem. Soc., Chem. Commun.*, 1989, 488.

15 D. L. Lichtenberger, A. S. Copenhaver, H. B. Gray, J. L. Marshall and M. D. Hopkins, *Inorg. Chem.*, 1988, **27**, 4488.

16 (*a*) J. Müller, C. Hänsch and J. Pickardt, *J. Organomet. Chem.*, 1983, **259**, C21; (*b*) F. Bonati, L. A. Oro, M. T. Pinillos, C. Tejel and B. Bovio, *J. Organomet. Chem.*, 1994, **465**, 267.

17 J. Müller and R. Stock, *Angew. Chem., Int. Ed. Engl.*, 1983, **22**, 993.

18 R. Cramer, J. B. Kline and J. D. Roberts, *J. Am. Chem. Soc.*, 1969, **91**, 2519.
19 The AA'BB' pattern can be treated with a good approximation as an AA'XX'. See: H. Günther, *NMR Spectroscopy: Basic Principles, Concepts, and Applications in Chemistry*, Wiley-VCH Verlag GmbH & Co, Weinheim, Germany, 3rd edn, 2013.
20 (*a*) W. Kaim, S. Berger, S. Greulich, R. Reinhardt and J. Fiedler, *J. Organomet. Chem.*, 1999, **582**, 153; (*b*) S. Frantz, R. Reinhardt, S. Greulich, M. Wanner, J. Fiedler, C. Duboc-Toia and W. Kaim, *Dalton Trans.*, 2003, 3370; (*c*) W. Kaim and J. Fiedler, *Chem. Soc. Rev.*, 2009, **38**, 3373.
21 N. S. Hush, *Electrochim. Acta*, 1968, **13**, 1005.
22 M. B. Robin and P. Day, in *Advances in Inorganic Chemistry and Radiochemistry*, ed. H. J. Emeléus and A. G. Sharpe, Academic Press, 1968, vol. 10, pp. 247.
23 (*a*) V. Kasack, W. Kaim, H. Binder, J. Jordanov and E. Roth, *Inorg. Chem.*, 1995, **34**, 1924; (*b*) S. Patra, B. Sarkar, S. Ghumaan, J. Fiedler, W. Kaim and G. K. Lahiri, *Dalton Trans.*, 2004, 754.
24 J. Choi, A. H. R. MacArthur, M. Brookhart and A. S. Goldman, *Chem. Rev.*, 2011, **111**, 1761.
25 I. Göttker-Schnetmann, P. White and M. Brookhart, *J. Am. Chem. Soc.*, 2004, **126**, 1804.
26 G. Giordano, R. H. Crabtree, R. M. Heintz, D. Forster and D. E. Morris, *Inorg. Synth.*, 1990, **28**, 88.
27 R. Cramer, *Inorg. Chem.*, 1962, **1**, 722.
28 G. M. Sheldrick, *SHELXL-97, Program for crystal structure refinement*, University of Göttingen, Göttingen, Germany, 1997.
29 G. Gritzner and J. Kuta, *Pure Appl. Chem.*, 1984, **56**, 461.
30 J. Bley-Escrich, J.-P. Gisselbrecht, E. Vogel and M. Gross, *Eur. J. Inorg. Chem.*, 2002, 2829.
31 S. Stoll and A. Schweiger, *J. Magn. Reson.*, 2006, **178**, 42.
32 F. Neese, *WIREs Comput. Mol. Sci.*, 2012, **2**, 73.
33 (*a*) J. P. Perdew, *Phys. Rev. B: Condens. Matter*, 1986, **33**, 8822; (*b*) J. P. Perdew, *Phys. Rev. B: Condens. Matter*, 1986, **34**, 7406; (*c*) A. D. Becke, *Phys. Rev. A*, 1988, **38**, 3098.
34 F. Neese, *J. Comput. Chem.*, 2003, **24**, 1740.
35 F. Weigend, *Phys. Chem. Chem. Phys.*, 2006, **8**, 1057.
36 A. Klamt and G. Schüürmann, *J. Chem. Soc., Perkin Trans. 2*, 1993, 799.
37 (*a*) A. D. Becke, *J. Chem. Phys.*, 1993, **98**, 1372; (*b*) C. Lee, W. Yang and R. G. Parr, *Phys. Rev. B: Condens. Matter*, 1988, **37**, 785.
38 (*a*) C. Chang, M. Pelissier and P. Durand, *Phys. Scr.*, 1986, **34**, 394; (*b*) J.-L. Heully, I. Lindgren, E. Lindroth, S. Lundqvist and A.-M. Martensson-Pendrill, *J. Phys. B: At. Mol. Phys.*, 1986, **19**, 2799; (*c*) E. van Lenthe, E. J. Baerends and J. G. Snijders, *J. Chem. Phys.*, 1993, **99**, 4597; (*d*) B. A. Hess, *Phys. Rev. A*, 1986, **33**, 3742.
39 (*a*) D. A. Pantazis, X.-Y. Chen, C. R. Landis and F. Neese, *J. Chem. Theor. Comput.*, 2008, **4**, 908; (*b*) D. A. Pantazis and F. Neese, *J. Chem. Theor. Comput.*, 2009, **5**, 2229.
40 *Chemcraft* http://chemcraftprog.com.

Dinuclear Iridium and Rhodium Complexes with Bridging Arylimidazolide-N^3,C^2 Ligands: Synthetic, Structural, Reactivity, Electrochemical and Spectroscopic Studies

Fan He,[a] Laurent Ruhlmann,[b] Jean-Paul Gisselbrecht,[b] Sylvie Choua,[c] Maylis Orio,[e] Marcel Wesolek,[a] Andreas A. Danopoulos,*[a,d] Pierre Braunstein*[a]

[a] Laboratoire de Chimie de Coordination, Institut de Chimie (UMR 7177 CNRS), Université de Strasbourg, 4 rue Blaise Pascal, 67081 Strasbourg Cedex (France)

[b] Laboratoire d'Electrochimie et de Chimie Physique du Corps Solide, Institut de Chimie (UMR 7177 CNRS), Université de Strasbourg, 4 rue Blaise Pascal, 67081 Strasbourg Cedex (France)

[c] Institut de Chimie, Université de Strasbourg, 1 rue Blaise Pascal, BP 296 R8, 67008 Strasbourg, Cedex (France)

[d] Université de Strasbourg, Institute for Advanced Study (USIAS), Strasbourg (France)

[e] Institut des Sciences Moléculaires de Marseille, Aix Marseille Université, CNRS, Centrale Marseille, ISM2 UMR 7313, 13397, Marseille, France

E-mails: danopoulos@unistra.fr, braunstein@unistra.fr

Contents

oxidation step.

Fig. S10 EPR spectra of the Rh(I)/Rh(II) system **8** electrochemically generated in CH_2Cl_2 at 100 K: a) Experimental spectrum b) Simulated spectrum with one ^{103}Rh nucleus (left) and two equivalent ^{103}Rh nuclei (right).

Fig. S11 Optimized structure of the Rh(I)/Rh(II) system with relevant interatomic distances.

Fig. S12 Spin population distribution (left) and Singly Occupied Molecular Orbital (SOMO) of the Rh(I)/Rh(II) system (right).

Fig. S13 Optimized structure of the Ir(I)/Ir(II) system with relevant interatomic distances.

Fig. S14 Spin population distribution (left) and Single Occupied Molecular Orbital (SOMO) of the Ir(I)/Ir(II) system (right).

Table S1. Crystal data and structure refinement for $\mathbf{3_{H\text{-}H}}$, $\mathbf{3_{H\text{-}T}}$, **8** and **9**.

	$\mathbf{3_{H\text{-}H}}$	$\mathbf{3_{H\text{-}T}}$	**8**	**9**
Empirical formula	$C_{40}H_{50}Ir_2N_4$	$C_{40}H_{50}Ir_2N_4$	$C_{40}H_{50}Rh_2N_4$	$C_{38}H_{54}N_4Rh_2$
Fw	971.24	971.24	792.66	772.67
T/K	173(2)	173(2)	173(2)	173(2)
Crystal system	Triclinic	Monoclinic	Monoclinic	Triclinic
Space group	*P* -1	*P* 2_1/c	*P* 2_1/c	*P* -1
a/Å	10.533(3)	12.3621(4)	12.4452(7)	8.5688(17)
b/Å	12.162(3)	18.9590(6)	18.7469(10)	14.354(3)
c/Å	14.504(4)	17.3685(5)	17.5877(7)	16.312(3)
α/°	86.570(6)	90	90	93.13(3)
β/°	85.210(6)	119.356(2)	119.594(3)	91.35(3)
γ/°	69.345(6)	90	90	95.87(3)
V/Å^3	1731.5(7)	3547.99(19)	3568.1(3)	1991.9(7)
Z	2	4	4	2
μ/mm^{-1}	7.712	7.528	0.958	0.856
No. of rflns collected	35403	37595	32340	20590
No. unique rflns	10116	12351	10482	9057
R(int)	0.0643	0.0273	0.0358	0.0519
Goodness of fit on F^2	1.137	1.111	1.025	1.012
Final *R* indices [$I>2\sigma(I)$]	R1 = 0.0855 wR2 = 0.2408	R1 = 0.0332 wR2 = 0.0580	R1 = 0.0347 wR2 = 0.0695	R1 = 0.0363 wR2 = 0.1021
R indices (all data)	R1 = 0.1050 wR2 = 0.2547	R1 = 0.0561 wR2 = 0.0674	R1 = 0.0671 wR2 = 0.0815	R1 = 0.0413 wR2 = 0.1062

References: p 44

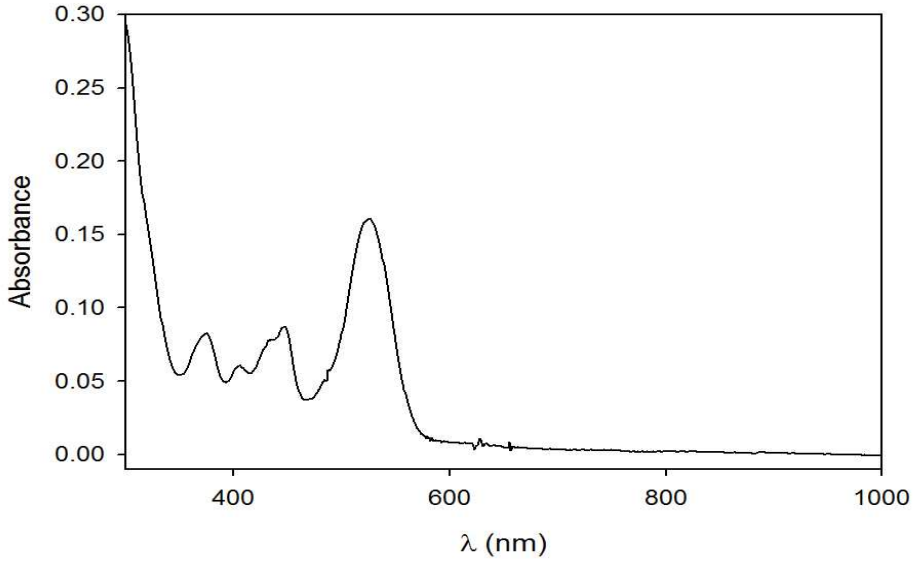

Fig S1 UV-visible-NIR absorption spectrum of $\mathbf{3_{H\text{-}T}}$ in CH_2Cl_2 (c = 4.408 10^{-5} mol L^{-1}).

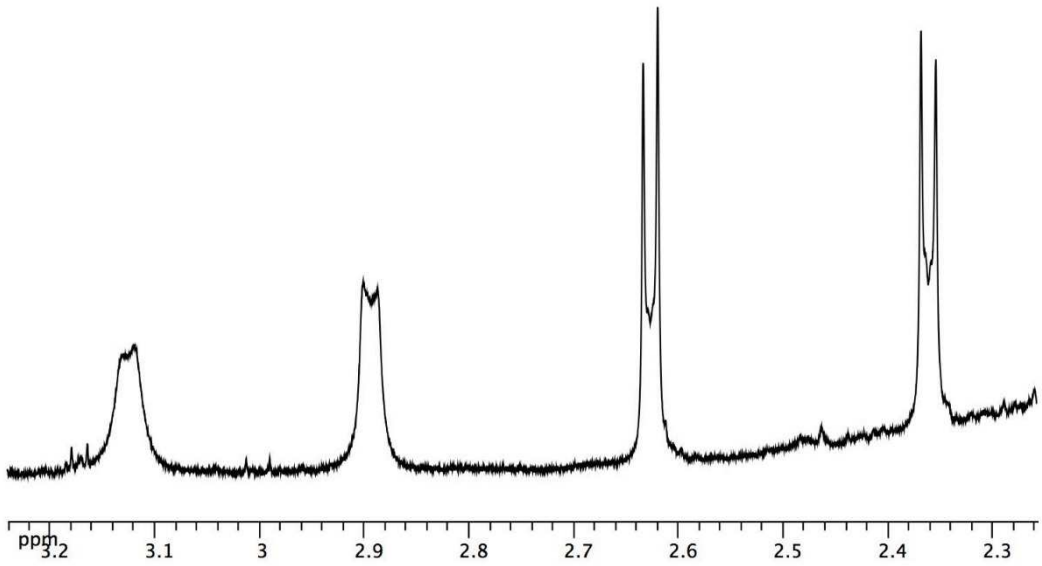

Fig. S2 ^{1}H NMR signals (600 MHz, C_6D_6) of the ethylene ligands in complex **7**.

References: p 44

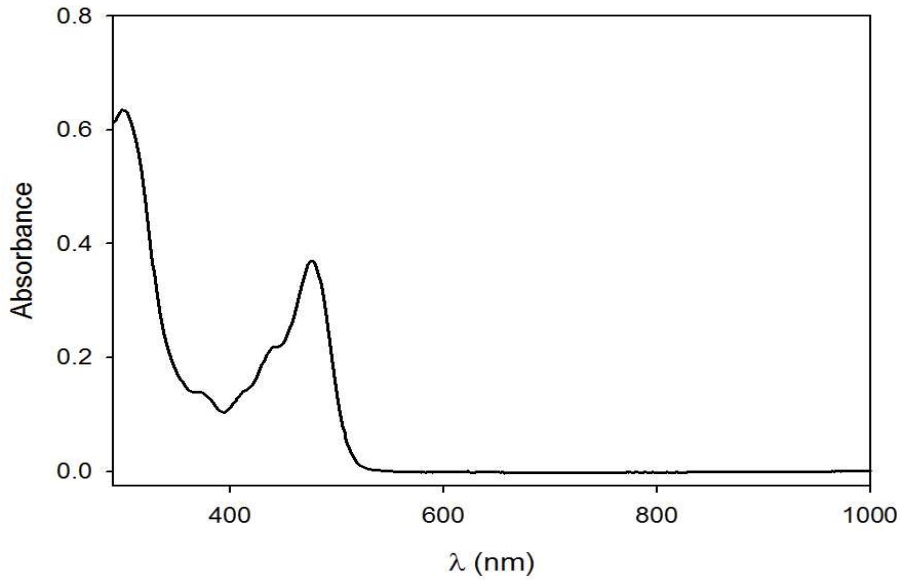

Fig. S3 UV-visible-NIR absorption spectrum of **8** in CH_2Cl_2 (c = 8.074 10^{-5} mol L^{-1}).

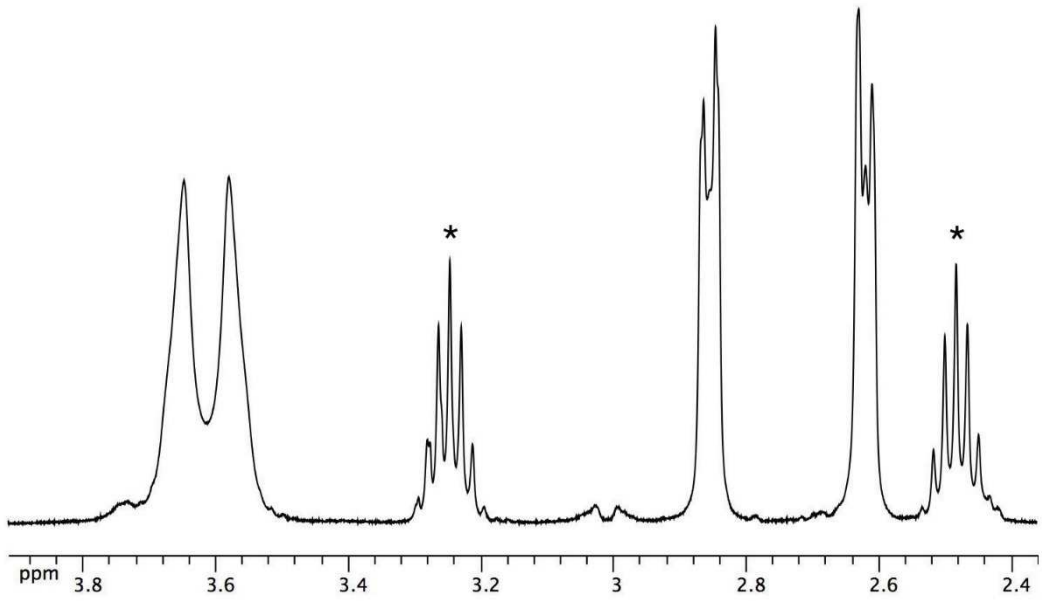

Fig. S4 ^{1}H NMR signals (400 MHz, C_6D_6) of the ethylene ligands in complex **9**. (* for C*H*$(CH_3)_2$ of Dipp)

References: p 44

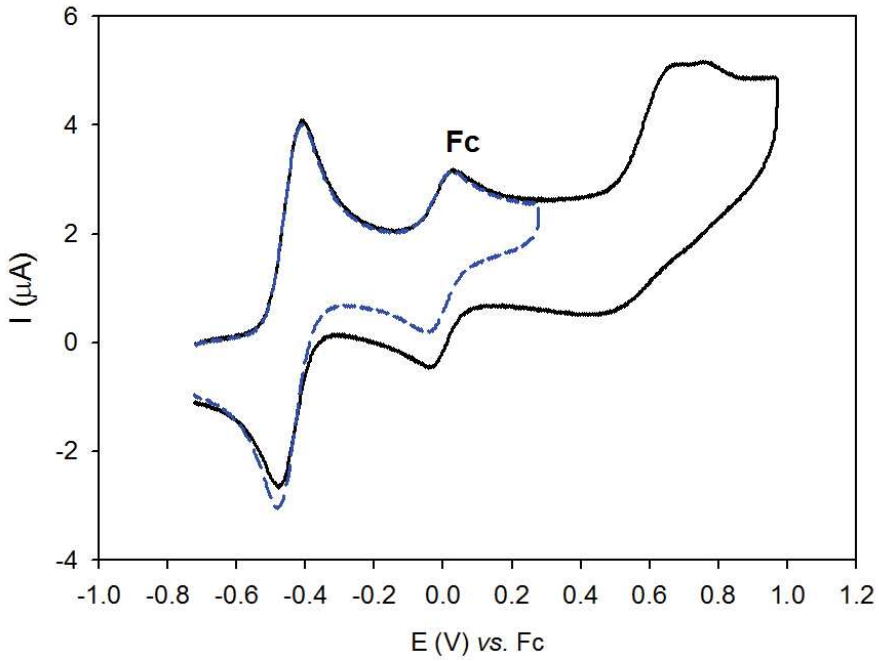

Fig. S5 Cyclic voltammograms of $\mathbf{3_{H\text{-}T}}$ with added ferrocene (CH_2Cl_2 + 0.1 M [*n*-Bu_4N]PF_6, glassy carbon electrode, scan rate 0.1 Vs^{-1}, *vs*. Fc^+/Fc).

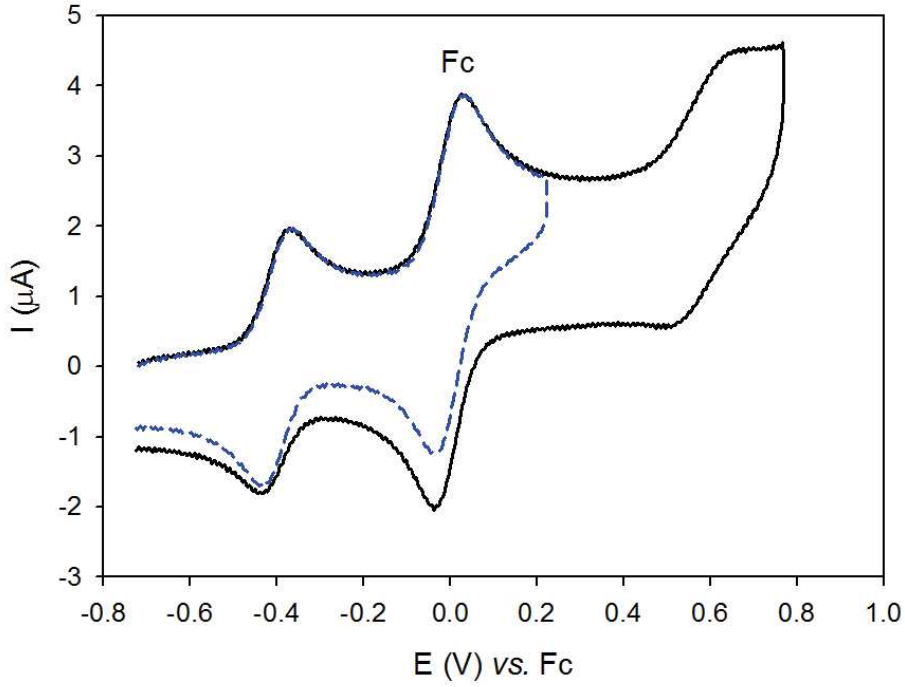

Fig. S6 Cyclic voltammograms of **8** with added ferrocene (CH_2Cl_2 + 0.1 M [*n*-Bu_4N]PF_6, glassy carbon electrode, scan rate 0.1 Vs^{-1}, *vs*. Fc^+/Fc).

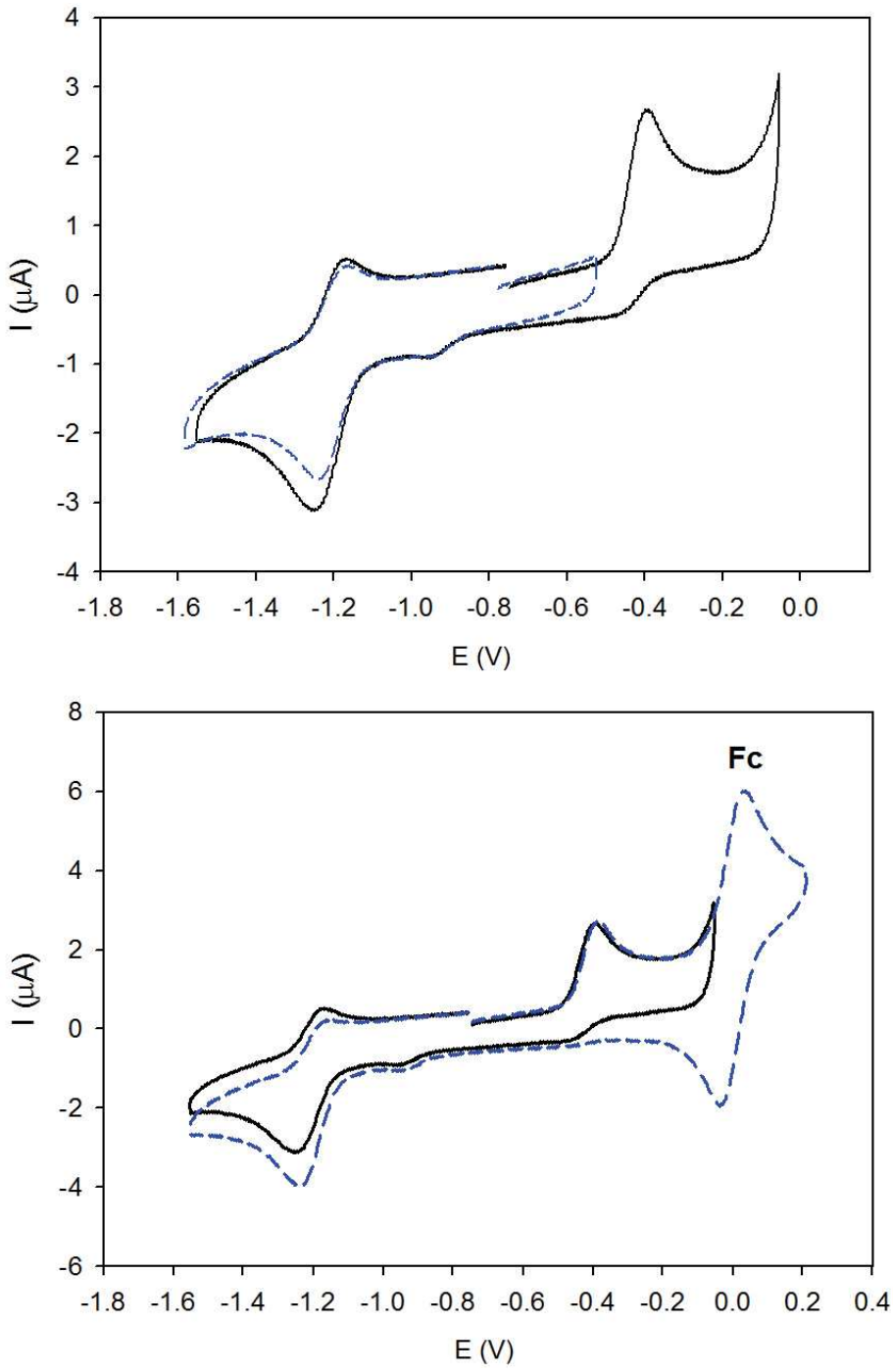

Fig. S7 Cyclic voltammograms of $\mathbf{3_{H\text{-}H}}$ (top) and $\mathbf{3_{H\text{-}H}}$ with added ferrocene (bottom) (CH_2Cl_2 + 0.1 M [*n*-Bu_4N]PF_6, glassy carbon electrode, scan rate 0.1 Vs^{-1}, *vs.* Fc^+/Fc).

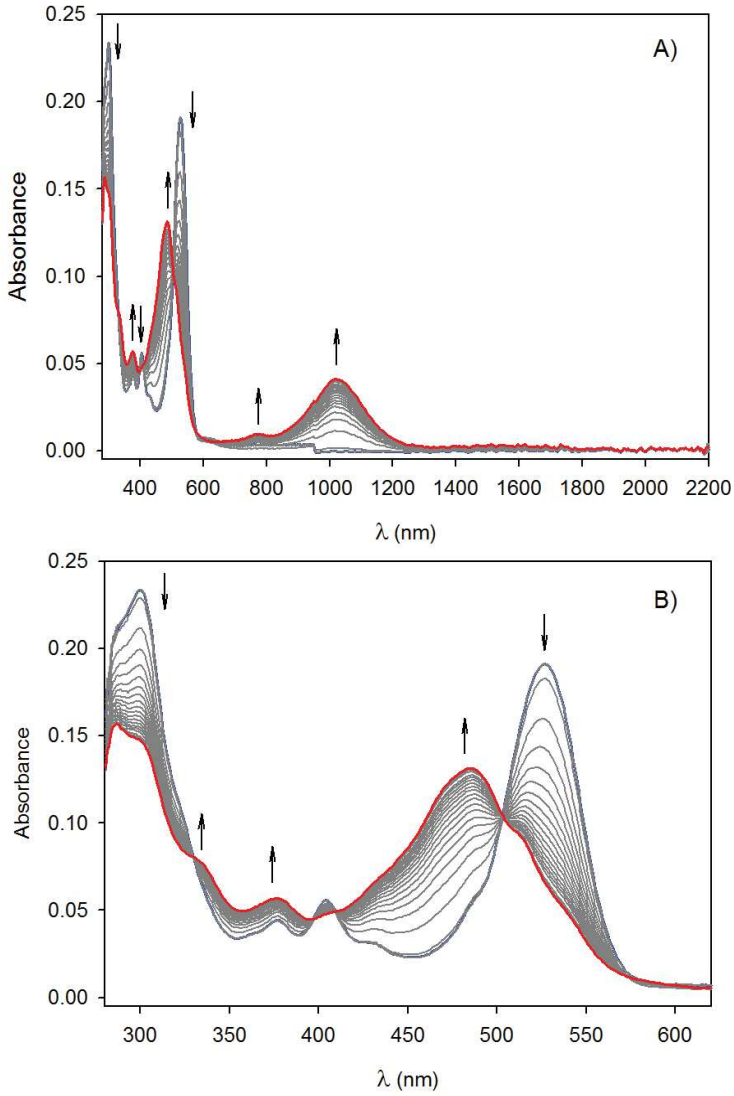

Fig. S8 A) Time-resolved UV-visible-NIR spectra of $\mathbf{3_{H\text{-}T}}$ for the first oxidation step (transition Ir(I)/Ir(I) to Ir(I)/Ir(II)) in CH_2Cl_2 + 0.1 M [*n*-Bu_4N]PF_6 (spectra recorded every 5 s). B) UV-visible spectral evolution for the first oxidation step.

References: p 44

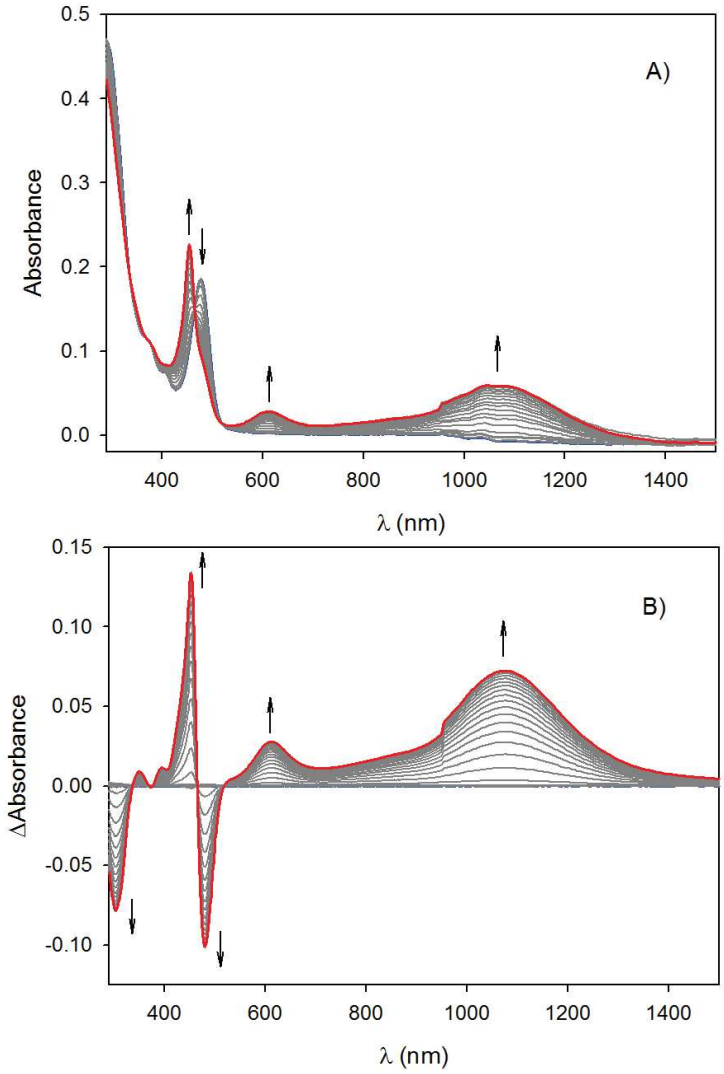

Fig. S9 A) Time-resolved UV-visible-NIR spectra of **8** for the first oxidation step (transition Rh(I)/Rh(I) to Rh(I)/Rh(II)) in CH_2Cl_2 + 0.1 M [*n*-Bu_4N]PF_6 (spectra recorded every 5 s). B) Time-resolved UV-visible-NIR differential spectra for the first oxidation step.

References: p 44

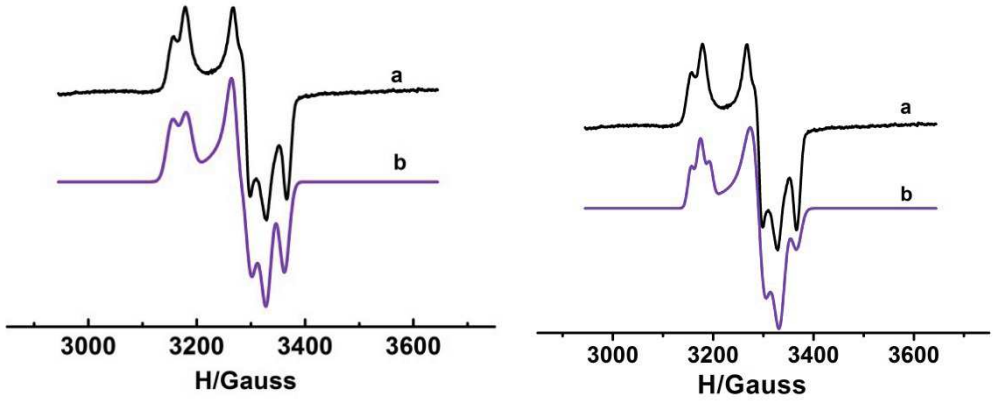

Fig. S10 EPR spectra of the Rh(I)/Rh(II) system **8** electrochemically generated in CH_2Cl_2 at 100 K: a) Experimental spectrum b) Simulated spectrum with one ^{103}Rh nucleus (left) and two equivalent ^{103}Rh nuclei (right).

References: p 44

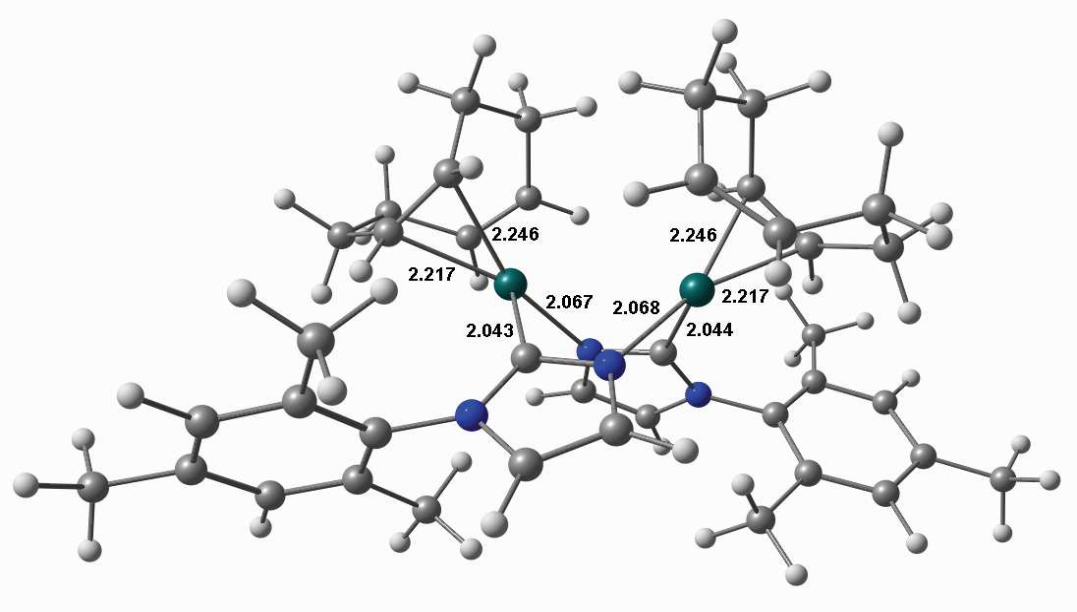

Fig. S11 Optimized structure of the Rh(I)/Rh(II) system with relevant interatomic distances.

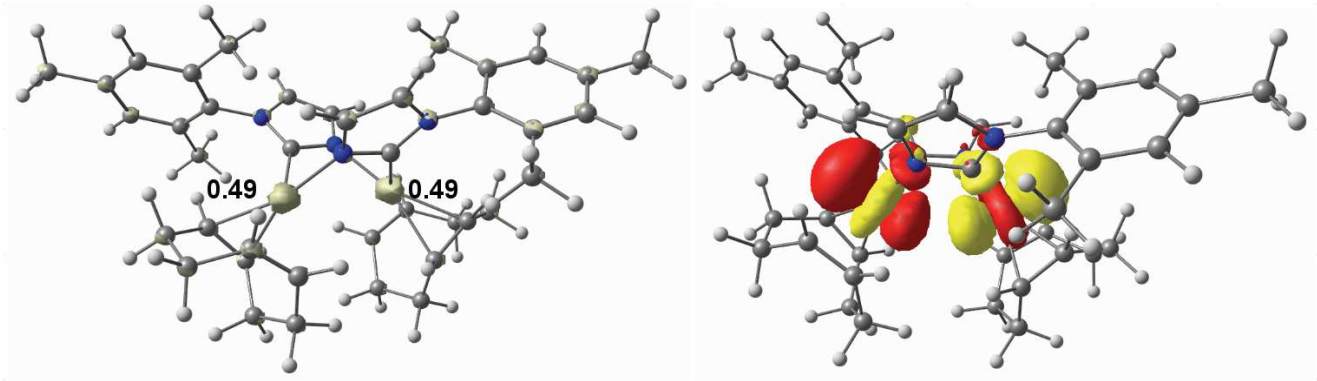

Fig. S12 Spin population distribution (left) and Singly Occupied Molecular Orbital (SOMO) of the Rh(I)/Rh(II) system (right).

References: p 44

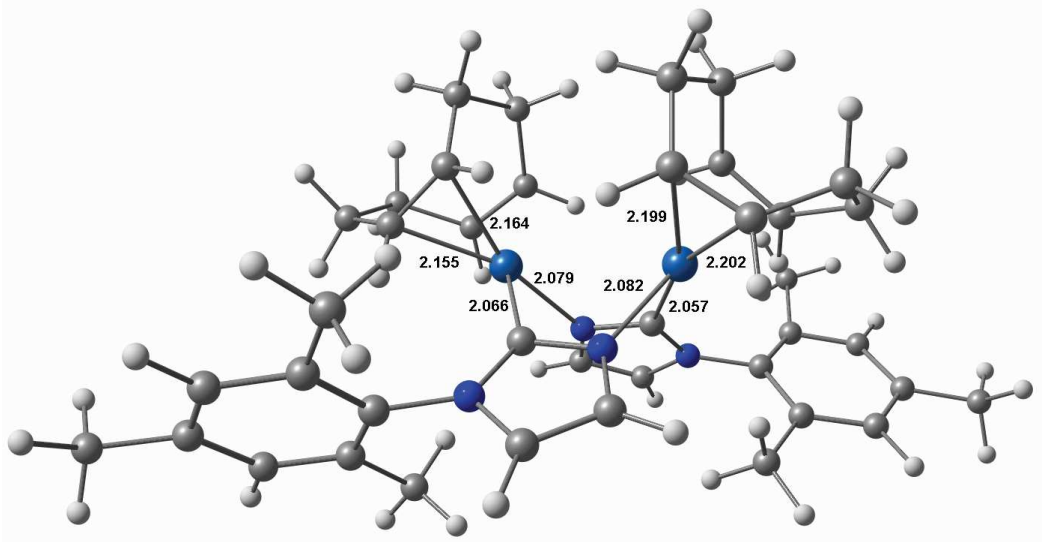

Fig. S13 Optimized structure of the Ir(I)/Ir(II) system with relevant interatomic distances.

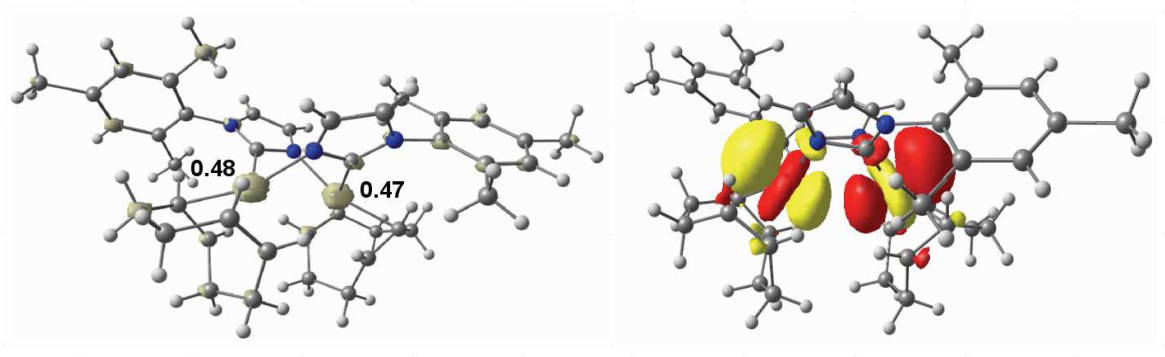

Fig. S14 Spin population distribution (left) and Singly Occupied Molecular Orbital (SOMO) of the Ir(I)/Ir(II) system (right).

References: p 44

Chapire 3

Imine-functionalised protic NHC complexes of Ir: direct formation by C-H activation

Résumé

Le complexe 1-(2,6-diisopropylphenylimino)ethylimidazolyle (cycloocta-1,5-diene)iridium(I) chlorure, [Ir(cod)Cl{$C_3H_3N_2$(DippN=CMe)-κN3}] (**1**) a été préparé en faisant réagir le 1-(2,6-diisopropylphenylimino)ethylimidazole (**L**) avec 0.5 équivalent de [Ir(cod)(μ-Cl)]$_2$. La réaction ultérieure de **1** avec un demi équivalent supplémentaire de [Ir(cod)(μ-Cl)]$_2$, ou la réaction directe de **L** avec 1.0 équivalent de [Ir(cod)(μ-Cl)]$_2$ a permis l'obtention du complexe [Ir_2(cod)$_2$$HCl_2${μ-$C_3H_2N_2$(DippN=CMe)-$\kappa^2$(C2,$N_{imine}$),$\kappa$N3}] (**2**), un complexe homobinucléaire à valence mixte comportant un Ir(I) lié à N de l'imidazolyle et un Ir(III) lié au C2 de l'imidazolyle suite à l'activation de la liaison C-H. Le complexe NHC protique (pNHC) avec une fonctionnalité imine de l'Ir(I) [Ir(cod){$C_3H_3N_2$(DippN=CMe)-κ^2(C2,N_{imine})}]$^+$[PF_6]$^-$ (**3**$^+$[PF_6]$^-$) a été obtenu à partir de la réaction de **1** ou **2** avec respectivement 1 ou 0,5 équivalent de $TlPF_6$ (Schéma 1).

Schéma 1.

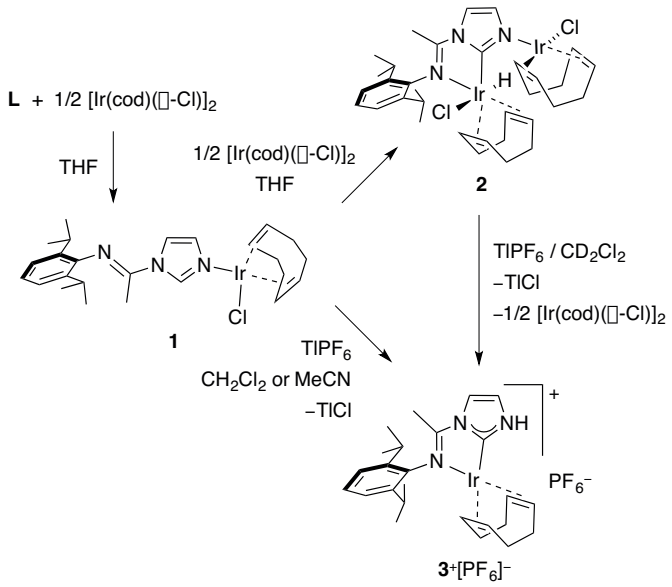

La déprotonation du complexe **3**$^+$[PF_6]$^-$ donne lieu à un équilibre entre un complexe mononucléaire où l'iridium est lié au C 'anionique' d'un fragment imidazolide [Ir(cod){$C_3H_2N_2$(DippN=CMe)-κ^2(C2,N_{imine})}] (**5**) et son dimère [Ir(cod){μ-$C_3H_2N_2$(DippN=CMe)-κC2,κN3}]$_2$ (**4**) dont chaque moitié est liée par un pont μ-C,N (Schéma 2).

 References: p 66

Schéma 2.

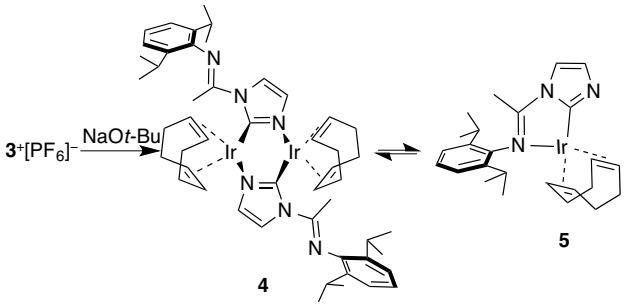

La réaction de **L** avec HCl ou $HBF_4 \cdot Et_2O$ conduit respectivement aux sels d'imidazolium $\mathbf{6}^+Cl^-$ et $\mathbf{6}^+[BF_4]^-$. La réaction de $\mathbf{6}^+Cl^-$ avec 0.5 équivalent de $[Ir(cod)(\mu\text{-}Cl)]_2$ permet l'isolement de $[Ir(cod)HCl_2\{C_3H_3N_2(DippN{=}CMe)\text{-}\kappa N3\}]$ (**7**), un complexe issu de l'insertion de l'Ir dans la liaison N-H, cependant que la réaction de $\mathbf{6}^+[BF_4]^-$ menée dans les mêmes conditions donne $[Ir(cod)HCl\{C_3H_3N_2(DippN{=}CMe)\text{-}\kappa^2(C2,N_{imine})\}]^+[BF_4]^-$ ($\mathbf{8}^+[BF_4]^-$), un complexe issu d'une activation C-H (Schéma 3).

Schéma 3.

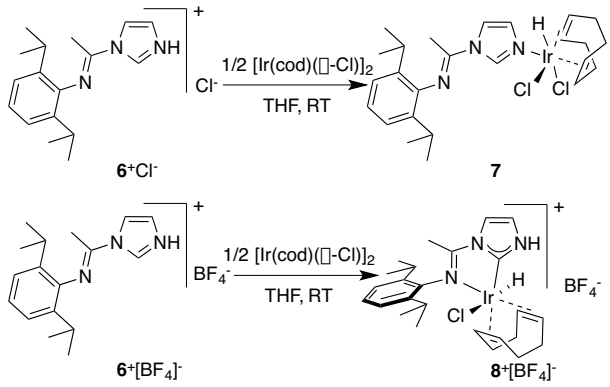

Les structures moléculaires des complexes **1**, **2**, $\mathbf{3}^+[PF_6]^-$, **4** et $\mathbf{8}^+[BF_4]^-$ ont été déterminées par diffraction des rayons-X.

References: p 66

Références et synopsis

Imine-functionalised protic NHC complexes of Ir: direct formation by C-H activation

Ce chapitre a été rédigé sous forme d'une publication.

He, F.; Braunstein, P.; Wesolek, M.; Danopoulos, A. A., *Chem. Commun.* **2015,** *51*, 2814–2817.

Ma contribution a porté sur la recherche bibliographique, la partie expérimentale ainsi que la rédaction de la version préliminaire.

References: p 66

ChemComm

COMMUNICATION

View Article Online
View Journal | View Issue

Imine-functionalised protic NHC complexes of Ir: direct formation by C–H activation†

Fan He,[a] Pierre Braunstein,*[a] Marcel Wesolek[a] and Andreas A. Danopoulos*[ab]

Cite this: *Chem. Commun.*, 2015, 51, 2814

Received 18th December 2014,
Accepted 6th January 2015

DOI: 10.1039/c4cc10109j

www.rsc.org/chemcomm

***N*-Arylimine-functionalised protic NHC (pNHC) Ir(I) and Ir(III) complexes are obtained directly from neutral or cationic Ir(I) imidazole complexes using excess $[Ir(cod)(\mu\text{-}Cl)]_2$ or $TlPF_6$, respectively. *N*-Arylimine-functionalised imidazolium salts lead to imidazole or pNHC complexes by competing N–H or C–H bond activation depending on the type of imidazolium counterion.**

The landmark isolation of stable NHCs of the imidazole type made use of bulky *N*-substituents for the successful kinetic and thermodynamic stabilisation of the reactive carbene species.[1] Since then, bulky alkyl and aryl substituents have been used routinely in the NHC coordination chemistry, exerting also subtle electronic and steric tuning of the C_{NHC}–metal interactions. In contrast, 1*H*-imidazol-2-ylidene, the simplest parent (R = H) imidazole-type protic NHC (pNHC), has only recently been stabilised by coordination to transition metals (**I**),[2] and the resulting carbene complex may be transformed into its imidazole tautomer (**II**).[3]

pNHCs constitute versatile spectator ligands, which, in addition to their strong σ-donor character, provide the option of secondary interactions, (*i.e.* H-bonding), which could be of importance in the design of bifunctional catalysts,[4] substrate recognition[5] and of relevance to biological systems.[6]

The coordination chemistry of pNHCs is a topical area of interest, thanks to the successful development of versatile synthetic methodologies based on building the C-bound heterocycle at the metal coordination sphere,[7] or using suitable *N*-protecting groups that are removed after coordination,[8] or by facilitating kinetic formation of the $M–C_{NHC}$ bond by C–X bond (X = halide) oxidative-addition of halo-imidazoles.[2a,9] Conceptually simpler is the *direct* pNHC formation.

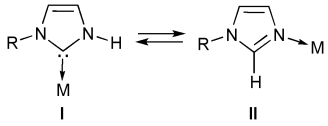

Scheme 1 Tautomerism/metallotropism involving protic NHC (pNHC) and imidazole ligands (M = metal; R = H, alkyl, aryl, functional group).

It has been established computationally that 1*H*-imidazole is more stable than the tautomeric 1*H*-imidazol-2-ylidene by *ca.* 30 kcal mol^{-1}.[3a] However, this energy difference can be suppressed and reversed upon metal coordination of the 1*H*-imidazol-2-ylidene. Analogous comments apply to 1*R*-imidazole (**III**) and tautomeric pNHCs 1*R*-imidazol-2-ylidenes (**IV**).

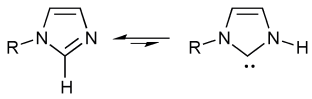

The conversion of coordinated *R*-imidazole to pNHC (**II** → **I**) was firstly demonstrated experimentally by the acid-catalyzed rearrangement of Ru–imidazole to Ru–pNHC[10] and, more recently, by deprotonation with an external base of imidazoles coordinated to mononuclear, inert 6-coordinate d^6 Re(I) and Mn(I) carbonyls[11] and $Fe(NO)_2(CO)$,[6a] followed by quenching of the resultant imidazolide with a suitable acid. Conversely, transformation of Ru-coordinated NHC following N–C bond activation to a mixture of coordinated imidazole and pNHC tautomers was studied by experimental and computational means.[3b,c] Similar rearrangements involving related benzimidazole[12] or pyridine[13] heterocycles have been observed, and associated with catalytic transformations.

From these limited available examples, it appears that the elementary steps involved in C–H and N–H bond cleavage/formation, which may be responsible for tautomerism, may be mechanistically diverse. Furthermore, the presence of functionalities capable of stabilising and directing C *vs.* N metalation has not been thoroughly examined, except in the context of the formation of heteroatom-functionalised NHC spectator ligands.[14]

[a] *Laboratoire de Chimie de Coordination, Institut de Chimie (UMR 7177 CNRS), Université de Strasbourg, 4 rue Blaise Pascal, 67081 Strasbourg Cedex, France. E-mail: braunstein@unistra.fr*

[b] *Institute for Advanced Study (USIAS), Université de Strasbourg, 4 rue Blaise Pascal, 67081 Strasbourg Cedex, France. E-mail: danopoulos@unistra.fr*

† Electronic supplementary information (ESI) available: Experimental and X-ray crystallographic data. CCDC 1039710–1039714. For ESI and crystallographic data in CIF or other electronic format see DOI: 10.1039/c4cc10109j

Herein, we report preliminary studies aimed at the synthesis of *N*-arylimine-functionalised imidazole and pNHC complexes of iridium (type **I**, R = arylimino, M = Ir), and at gaining insight into the elementary steps that may operate during imidazole to pNHC tautomerism (from **II** to **I** in Scheme 1). The arylimine functional group was selected by virtue of its comparable donor characteristics with the κ^1-*N*-imidazole ligand and the possible *reversible* formation of chelates.

The reaction of 1-(2,6-diisopropylphenylimino)ethylimidazole (**L**)[15] with 0.5 equiv. of $[Ir(cod)(\mu\text{-}Cl)]_2$ in THF led to the isolation of **1** (Scheme 2). Both analytical and spectroscopic (^1H–$^{13}C\{^1H\}$-NMR and IR) data point to the presence of a N-bound Ir(cod)Cl fragment (see the ESI† for synthetic details and full characterisation). Particularly diagnostic is a broad peak at δ 8.88 assignable to C2–*H* (*cf.* δ 8.11 in **L**). N-coordination was further corroborated crystallographically (Fig. S1 in the ESI†). Importantly, the arylimino functional group (in *E* configuration in **1**) is dangling.

Further reaction of **1** with $[Ir(cod)(\mu\text{-}Cl)]_2$ (0.5 equiv.) or reaction of **L** with 1.0 equiv. of $[Ir(cod)(\mu\text{-}Cl)]_2$ (THF, RT) gave **2** (Scheme 2). Its ^1H NMR spectrum (THF-d_8) contains a hydride signal at δ −14.74 and in the ^{13}C NMR spectrum, signals at δ 166.6 and 158.7 are assignable to $C_{(imine)}$ and C-$2_{(NHC)}$, respectively. The IR ν(Ir–H) band is observed at 2200 cm^{-1}. The structure of **2** (Fig. 1) revealed a binuclear complex comprising one N-bound Ir(I) centre (*cf.* **1**) and one C2-bound Ir(III) center, formally originating from the second half-equivalent of $[Ir(cod)(\mu\text{-}Cl)]_2$; crucially, the *N*-arylimino group is also coordinated to Ir(III) as part of a 5-membered chelate. One can thus consider the N-bound Ir(cod)Cl moiety as a $N_{(imidazole)}$ *'metalla protecting and activating group'*, which in cooperation with the directing effect of the *N*-arylimine, facilitates C2 metalation. The latter may involve C–H oxidative addition,[16] in line with the observed *cis* Ir–C and Ir–H bond disposition.

With the hope to access a pNHC Ir complex by tautomerism of a more reactive species (*e.g.* $[\mathbf{1}\text{–}Cl^-]^+$), **1** was treated with chloride abstracting $TlPF_6$ (in CH_2Cl_2 or MeCN, RT) and, gratifyingly, this led to the isolation of salt $\mathbf{3}^+[PF_6]^-$. Its ^1H NMR spectrum contains a characteristic new broad singlet at δ 10.36, and the signal of C2–*H* of the starting material disappeared, while in the ^{13}C NMR spectrum the N*C*N and *C*=N signals shifted considerably downfield (from δ 138.3 and 148.9 to 173.6 and 168.0, respectively). The IR absorptions at 3359 and 1613 cm^{-1} are assignable to N–H[8a] and coordinated C=N, respectively.

The structure of $\mathbf{3}^+[PF_6]^-$ was elucidated crystallographically (see Fig. 2 for the cation and ESI† for details). Ir adopts a distorted square-planar coordination geometry defined by a κ^2(N,C)-bound novel imino-functionalised pNHC and a cod ligand.

The Ir–C_{pNHC} bond distance (1.984(3) Å) is shorter than the average found in other Ir(I)–NHC complexes[17] (2.038 Å, ranging 1.895–2.194 Å, with shorter bond lengths associated with chelating NHC ligands), probably due to the chelate formation and the small hydrogen substituent at the N1 atom. The closest N–H···F(PF_5) distances of 2.37(5) and 2.49(5) Å are consistent with hydrogen bonding interactions.

The tautomerism (**II** → **I** in Scheme 1) of transient $[\mathbf{1}\text{–}Cl^-]^+$ to $\mathbf{3}^+$, which provides an alternative to the recently reported metalation of 2-chloro-benzimidazole heterocycles and the formation of anionic and pNHC ligands,[9b] may involve concerted, dyotropic-type

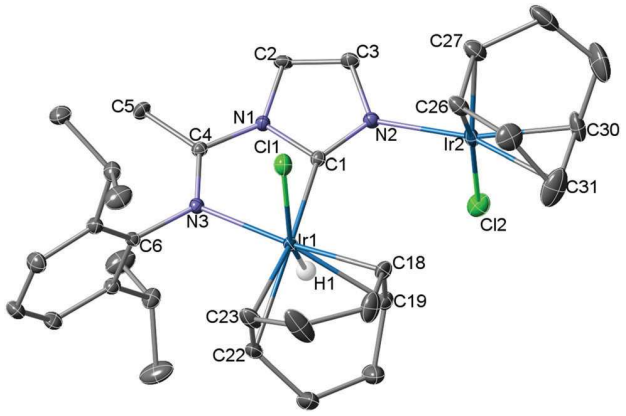

Fig. 1 Molecular structure of **2**. H atoms are omitted for clarity, except H1(Ir). Thermal ellipsoids are at the 30% level.

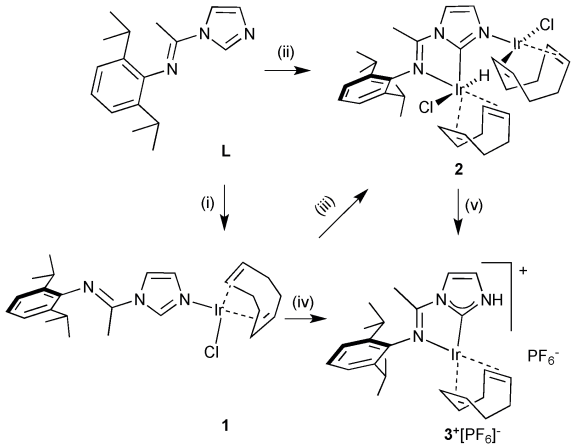

Scheme 2 Synthesis of complexes **1**, **2** and $\mathbf{3}^+[PF_6]^-$. *Reagents and conditions*: (i) 0.5 equiv. of $[Ir(cod)(\mu\text{-}Cl)]_2$, THF, RT, 97% yield; (ii) 1.0 equiv. of $[Ir(cod)(\mu\text{-}Cl)]_2$, THF, RT, 86% yield; (iii) 0.5 equiv. of $[Ir(cod)(\mu\text{-}Cl)]_2$, THF, RT, 86% yield; (iv) 1.0 equiv. of $TlPF_6$, CH_2Cl_2 or MeCN, RT, 85% yield; (v) 1.0 equiv. of $TlPF_6$, −0.5 equiv. $[Ir(cod)(\mu\text{-}Cl)]_2$, CD_2Cl_2, RT.

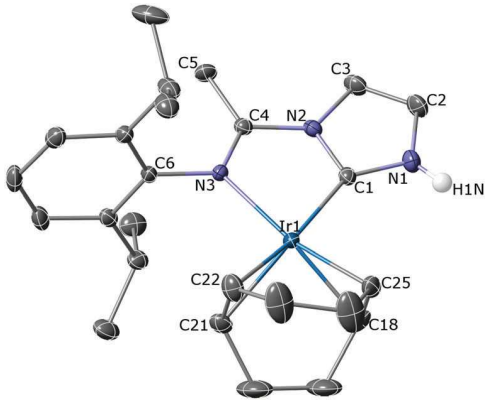

Fig. 2 Molecular structure of the cation in $\mathbf{3}^+[PF_6]^-$. H atoms are omitted for clarity, except H1(N1). Thermal ellipsoids are at the 30% level.

metalation/H transfer and be driven by the thermodynamic stability of $\mathbf{3}^+$ due to Ir–C bond or/and chelate ring formation.‡ It has been reported that the increased electrophilicity (going from Ir(I) to Ir(III) and Ir–Cl to Ir^+) favours the formation of the pNHC over imidazole complexes.[3a] Interestingly, abstraction with 1.0 equiv. of $TlPF_6$ of a chloride ligand in **2**, most likely from the Ir(III) centre, also gave $\mathbf{3}^+[PF_6]^-$, together with 0.5 equiv. $[Ir(cod)(\mu\text{-}Cl)]_2$ which originates from the N-bound Ir(cod)Cl moiety, in quantitative NMR yield (Scheme 2).

In an attempt to establish experimentally whether discrete deprotonation/protonation steps may model the reverse reaction, *i.e.* the transformation from pNHC to *N*-imidazole, the pNHC in $\mathbf{3}^+$ was deprotonated with 1.0 equiv. of NaO*t*-Bu (Scheme 3).

A mononuclear complex with C-coordinated 'anionic' imidazolide[9b,14a] was not obtained, but rather a mixture of two different iridium species (in a ratio of *ca.* 25 : 75 by ^{1}H NMR in CD_2Cl_2 at RT). The ^{13}C NMR spectrum of the mixture showed signals due to N*C*N and *C*=N at δ 174.8 and 156.2, δ 179.3 and 166.3, respectively. Attempts to separate the mixture by crystallisation led to the isolation of **4** (the ^{1}H NMR spectrum of which is assignable to the minor component of the mixture) in the form of dark red crystals (Fig. 3).

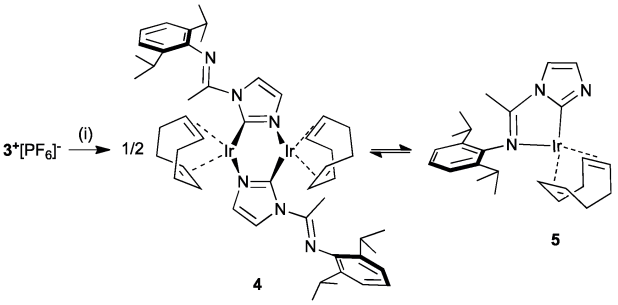

Scheme 3 Syntheses of **4** and **5**. *Reagents and conditions*: (i) 1.0 equiv. of NaO*t*-Bu, CH_2Cl_2, 0 °C, 70% yield.

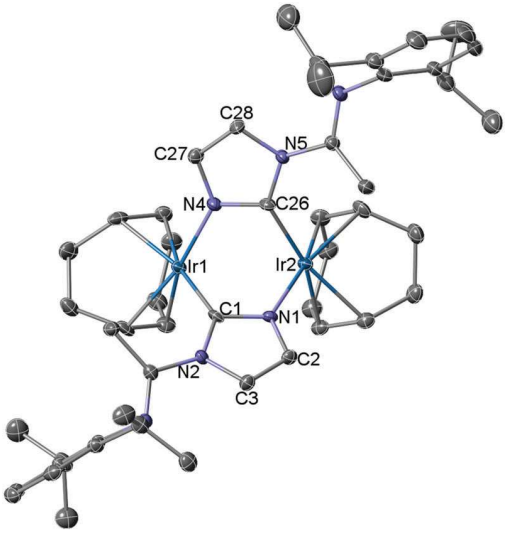

Fig. 3 Molecular structure of **4**. H atoms are omitted for clarity. Thermal ellipsoids are at the 30% level.

Its structure features a diiridium core with two bridging monoanionic imidazolides in a symmetrical 'boat-like' conformation and no direct Ir–Ir interaction (d(Ir–Ir) = 3.1844(3) Å).†

Both Ir centres adopt a square planar coordination geometry, defined by the olefinic bonds of the cod ligand, one carbon atom and one nitrogen atom of the imidazolide. Interestingly, the *N*-arylimine functionality has become dangling. In the supernatant solution after isolation of **4** the same ratio of species was observed (by NMR), and dissolution of crystals of **4** resulted again in the same mixture. This points to the presence of a chemical equilibrium with another (major) partner, the nature of which can be inferred by NMR spectroscopy: on the basis of the general appearance of the spectrum and since the chemical shift of *C*=N of the major partner is similar to the corresponding value for $\mathbf{3}^+$, we suggest that this partner is neutral, mononuclear complex **5** depicted in Scheme 3. Attempts to protonate the mixture **4** and **5** or deprotonate **1** led to intractable product mixtures.

The role of the '$[Ir(cod)]^+$' fragment in $[\mathbf{1}\text{–}Cl^-]^+$ as a 'metalla-protecting and -directing group' for the direct metallation of the C2–H imidazole, raised the question whether non-metal electrophiles, such as a proton, could undertake similar roles. In preliminary experiments, the simple imidazolium salts $\mathbf{L}H^+X^-$ ($\mathbf{6}^+Cl^-$ and $\mathbf{6}^+[BF_4]^-$) (see the ESI† for synthetic details and full characterisation data) were reacted with $[Ir(cod)(\mu\text{-}Cl)]_2$ (Scheme 4).

Unexpectedly, the selectivity of the reactions is dependent on the nature of X^-. The reaction of $\mathbf{6}^+Cl^-$ with 0.5 equiv. of $[Ir(cod)(\mu\text{-}Cl)]_2$ in THF at room temperature gave the Ir hydride complex **7**, formally a product from the oxidative addition of the N–H bond to Ir(cod)Cl (Ir–*H* at δ −12.10 in CD_2Cl_2, ν(Ir–H) at 2206 cm^{-1}). In contrast, the reaction of $\mathbf{6}^+[BF_4]^-$ with 0.5 equiv. of $[Ir(cod)(\mu\text{-}Cl)]_2$ under the same conditions yielded the Ir hydride complex salt $\mathbf{8}^+[BF_4]^-$ (Ir–*H* at δ −14.50 in CD_2Cl_2, ν(Ir–H) at 2211 cm^{-1}, ν(N–H) at 3241 cm^{-1}). Cation $\mathbf{8}^+$ (Fig. 4)† formally arises from the oxidative-addition of the C2–H bond to Ir(I). Similarly to the Ir(III) centre in **2**, the Ir in $\mathbf{8}^+$ is in a distorted octahedral coordination geometry defined by a κ^2(C,N) pNHC–imino chelate, one cod ligand and *trans* hydride and chloride ligands. The presence of a N–H···F(BF_3) hydrogen bond can also be deduced from the metrical data (N–H···F distance 2.721(3) Å). The underlying reason behind the anion-dependent selectivity

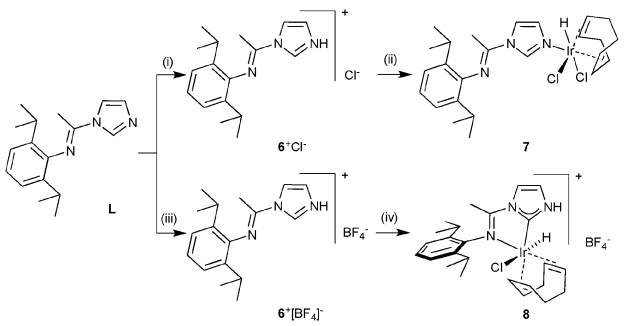

Scheme 4 Reactions of $(\mathbf{L}H^+)X^-$ with $[Ir(cod)(\mu\text{-}Cl)]_2$. *Reagents and conditions*: (i) 1.0 equiv. of HCl (a solution in Et_2O), Et_2O, RT, 85% yield; (ii) 0.5 equiv. of $[Ir(cod)(\mu\text{-}Cl)]_2$, THF, RT, 85% yield; (iii) 1.0 equiv. of $HBF_4{\cdot}Et_2O$, Et_2O, RT, 73% yield; (iv) 0.5 equiv. of $[Ir(cod)(\mu\text{-}Cl)]_2$, THF, RT, 82% yield.

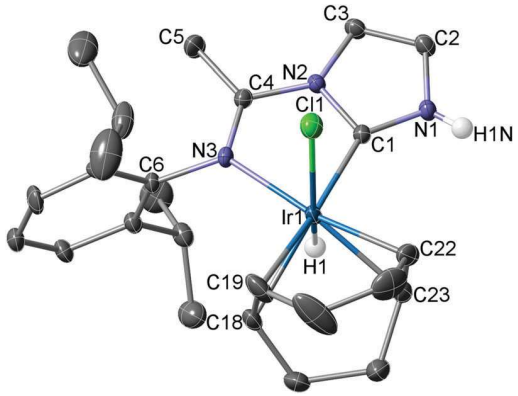

Fig. 4 Molecular structure of $\mathbf{8}^{+}$ in $\mathbf{8}^{+}[BF_4]^{-}$. H atoms are omitted for clarity, except H1(N1) and H1(Ir). Thermal ellipsoids are at the 30% level.

is under investigation but it is clear that the presence of a coordinating anion (Cl^{-} *vs.* BF_4^{-}) favors the monodentate behaviour of ligand **L**.

In conclusion, we have isolated and characterised novel Ir(I) and Ir(III) intermediates involved in the formation of *N*-arylimine-functionalised pNHC complexes of Ir by the direct C–H activation of the corresponding imidazoles and imidazolium salts. These results highlight the importance of the imidazole pre-coordination or the use of the imidazolium salts for successful pNHC isolation. In the former case, binuclear or cationic Ir species are implicated in the C2–H metalation, in the latter, counterion effects influence the selectivity for N–H *vs.* C–H activation. The insight provided may be useful in understanding subtle mechanistic details and developing simpler synthetic methodologies relevant to pNHC complex formation. These targets are being further pursued in our laboratory.

A.A.D. thanks the CNRS, the Région Alsace, the Département du Bas-Rhin and the Communauté Urbaine de Strasbourg for a Gutenberg Excellence Chair (2010–2011) and the USIAS for the award of a fellowship. F.H. is grateful to the China Scholarship Council for a PhD grant. We thank the CNRS and the MESR (Paris) for support and the Service de Radiocristallographie (Institut de Chimie, Strasbourg) for the determination of the crystal structures and Johnson Matthey PLC for a generous loan of Ir precursor complexes.

Notes and references

‡ The role of chelate ring formation in addition to the difference or Ir–N *vs.* Ir–C bond energies may be important in rationalising the relative thermodynamic stability of the complexes studied. To estimate these key factors, we initiated the study of the N to C rearrangement in Ir(I) complexes with 1,4-di(arylimino)imidazoles; preliminary experimental results support the fact that Ir–C bond strength is an important factor contributing to the thermodynamic stability.

1 (*a*) A. J. Arduengo, III, R. L. Harlow and M. Kline, *J. Am. Chem. Soc.*, 1991, **113**, 361; (*b*) A. J. Arduengo, H. V. R. Dias, R. L. Harlow and M. Kline, *J. Am. Chem. Soc.*, 1992, **114**, 5530; (*c*) D. Bourissou, O. Guerret, F. P. Gabbaï and G. Bertrand, *Chem. Rev.*, 2000, **100**, 39.
2 (*a*) R. Das, C. G. Daniliuc and F. E. Hahn, *Angew. Chem., Int. Ed.*, 2014, **53**, 1163; (*b*) R. Das, A. Hepp, C. G. Daniliuc and F. E. Hahn, *Organometallics*, 2014, **33**, 6975.
3 (*a*) G. Sini, O. Eisenstein and R. H. Crabtree, *Inorg. Chem.*, 2002, **41**, 602; (*b*) S. Burling, M. F. Mahon, R. E. Powell, M. K. Whittlesey and J. M. J. Williams, *J. Am. Chem. Soc.*, 2006, **128**, 13702; (*c*) L. J. L. Häller and S. A. Macgregor, *Eur. J. Inorg. Chem.*, 2009, 2000.
4 (*a*) S. Kuwata and T. Ikariya, *Chem. – Eur. J.*, 2011, **17**, 3542; (*b*) S. Kuwata and T. Ikariya, *Chem. Commun.*, 2014, **50**, 14290.
5 F. E. Hahn, *ChemCatChem*, 2013, **5**, 419.
6 (*a*) C.-H. Hsieh, R. Pulukkody and M. Y. Darensbourg, *Chem. Commun.*, 2013, **49**, 9326; (*b*) D. Brackemeyer, A. Hervé, C. Schulte to Brinke, M. C. Jahnke and F. E. Hahn, *J. Am. Chem. Soc.*, 2014, **136**, 7841.
7 (*a*) F. E. Hahn, V. Langenhahn, T. Lügger, T. Pape and D. Le Van, *Angew. Chem., Int. Ed.*, 2005, **44**, 3759; (*b*) F. E. Hahn, V. Langenhahn and T. Pape, *Chem. Commun.*, 2005, 5390; (*c*) J. Ruiz, G. García, M. E. G. Mosquera, B. F. Perandones, M. P. Gonzalo and M. Vivanco, *J. Am. Chem. Soc.*, 2005, **127**, 8584.
8 (*a*) G. E. Dobereiner, C. A. Chamberlin, N. D. Schley and R. H. Crabtree, *Organometallics*, 2010, **29**, 5728; (*b*) P. C. Kunz, C. Wetzel, S. Kogel, M. U. Kassack and B. Spingler, *Dalton Trans.*, 2011, **40**, 35.
9 (*a*) T. Kösterke, T. Pape and F. E. Hahn, *J. Am. Chem. Soc.*, 2011, **133**, 2112; (*b*) T. Kösterke, J. Kösters, E.-U. Würthwein, C. Mück-Lichtenfeld, C. Schulte to Brinke, F. Lahoz and F. E. Hahn, *Chem. – Eur. J.*, 2012, **18**, 14594.
10 R. J. Sundberg, R. F. Bryan, I. F. Taylor and H. Taube, *J. Am. Chem. Soc.*, 1974, **96**, 381.
11 (*a*) M. A. Huertos, J. Pérez, L. Riera and A. Menéndez-Velázquez, *J. Am. Chem. Soc.*, 2008, **130**, 13530; (*b*) M. A. Huertos, J. Pérez, L. Riera, J. Díaz and R. López, *Angew. Chem., Int. Ed.*, 2010, **49**, 6409; (*c*) J. Ruiz and B. F. Perandones, *J. Am. Chem. Soc.*, 2007, **129**, 9298; (*d*) J. Ruiz, A. Berros, B. F. Perandones and M. Vivanco, *Dalton Trans.*, 2009, 6999; (*e*) J. Ruiz, B. F. Perandones, J. F. Van der Maelen and S. García-Granda, *Organometallics*, 2010, **29**, 4639.
12 (*a*) K. L. Tan, R. G. Bergman and J. A. Ellman, *J. Am. Chem. Soc.*, 2002, **124**, 3202; (*b*) J. C. Lewis, S. H. Wiedemann, R. G. Bergman and J. A. Ellman, *Org. Lett.*, 2004, **6**, 35; (*c*) S. H. Wiedemann, J. C. Lewis, J. A. Ellman and R. G. Bergman, *J. Am. Chem. Soc.*, 2006, **128**, 2452; (*d*) J. C. Lewis, R. G. Bergman and J. A. Ellman, *Acc. Chem. Res.*, 2008, **41**, 1013.
13 (*a*) E. Alvarez, S. Conejero, M. Paneque, A. Petronilho, M. L. Poveda, O. Serrano and E. Carmona, *J. Am. Chem. Soc.*, 2006, **128**, 13060; (*b*) E. Álvarez, S. Conejero, P. Lara, J. A. López, M. Paneque, A. Petronilho, M. L. Poveda, D. del Río, O. Serrano and E. Carmona, *J. Am. Chem. Soc.*, 2007, **129**, 14130; (*c*) M. L. Buil, M. A. Esteruelas, K. Garcés, M. Oliván and E. Oñate, *J. Am. Chem. Soc.*, 2007, **129**, 10998; (*d*) D. Kunz, *Angew. Chem., Int. Ed.*, 2007, **46**, 3405; (*e*) S. Conejero, P. Lara, M. Paneque, A. Petronilho, M. L. Poveda, O. Serrano, F. Vattier, E. Álvarez, C. Maya, V. Salazar and E. Carmona, *Angew. Chem., Int. Ed.*, 2008, **47**, 4380.
14 (*a*) V. Miranda-Soto, D. B. Grotjahn, A. G. DiPasquale and A. L. Rheingold, *J. Am. Chem. Soc.*, 2008, **130**, 13200; (*b*) V. Miranda-Soto, D. B. Grotjahn, A. L. Cooksy, J. A. Golen, C. E. Moore and A. L. Rheingold, *Angew. Chem., Int. Ed.*, 2011, **50**, 631; (*c*) F. E. Hahn, A. R. Naziruddin, A. Hepp and T. Pape, *Organometallics*, 2010, **29**, 5283; (*d*) A. R. Naziruddin, A. Hepp, T. Pape and F. E. Hahn, *Organometallics*, 2011, **30**, 5859; (*e*) K. Araki, S. Kuwata and T. Ikariya, *Organometallics*, 2008, **27**, 2176.
15 P. Liu, M. Wesolek, A. A. Danopoulos and P. Braunstein, *Organometallics*, 2013, **32**, 6286.
16 (*a*) D. S. McGuinness, K. J. Cavell and B. F. Yates, *Chem. Commun.*, 2001, 355; (*b*) M. A. Duin, N. D. Clement, K. J. Cavell and C. J. Elsevier, *Chem. Commun.*, 2003, 400; (*c*) N. D. Clement, K. J. Cavell, C. Jones and C. J. Elsevier, *Angew. Chem., Int. Ed.*, 2004, **43**, 1277; (*d*) E. Mas-Marzá, M. Sanaú and E. Peris, *Inorg. Chem.*, 2005, **44**, 9961; (*e*) M. Viciano, M. Poyatos, M. Sanaú, E. Peris, A. Rossin, G. Ujaque and A. Lledós, *Organometallics*, 2006, **25**, 1120; (*f*) F. E. Hahn and M. C. Jahnke, *Angew. Chem., Int. Ed.*, 2008, **47**, 3122.
17 The Cambridge Structural Database, updated in Feb. 7, 2014.

SUPPORTING INFORMATION

Imine-functionalised protic NHC complexes of Ir: Direct formation by C-H activation

Fan He,[a] Pierre Braunstein,*[a] Marcel Wesolek,[a] and Andreas A. Danopoulos*[a, b]

[a] Laboratoire de Chimie de Coordination, Institut de Chimie (UMR 7177 CNRS), Université de Strasbourg, 4 rue Blaise Pascal, 67081 Strasbourg Cedex (France)

[b] Institute for Advanced Study (USIAS), Université de Strasbourg, 4 rue Blaise Pascal, 67081 Strasbourg Cedex, (France)

E-mail: braunstein@unistra.fr; danopoulos@unistra.fr

References: p 66

1 Synthesis and characterization

1.1 General methods

All manipulations involving organometallics were performed under argon in a Braun glove box or using standard Schlenk techniques. Solvents were dried using standard methods and distilled under argon prior use or passed through columns of activated alumina and subsequently purged with argon. NMR spectra of complexes were recorded on Bruker a AVANCE I 300 MHz, AVANCE III 400 MHz or AVANCE I 500 MHz instrument at ambient temperature and referenced using the proton (^{1}H) or carbon (^{13}C) resonance of the residual solvent. Assignments are based on ^{1}H, ^{1}H-COSY, ^{1}H-NOESY, ^{1}H/^{13}C-HSQC, and ^{1}H/^{13}C-HMBC experiments. IR spectra were recorded in the region 4000–100 cm^{-1} on a Nicolet 6700 FT-IR spectrometer (ATR mode, diamond crystal). Elemental analyses were performed by the "Service de microanalyses", Université de Strasbourg.

1.2 Synthesis of 1

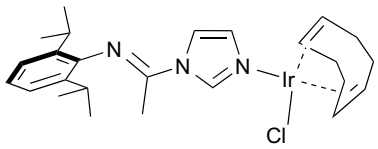

A solution of 1-(2,6-diisopropylphenylimino)ethylimidazole (81 mg, 0.30 mmol) in THF (5 mL) was added to a solution of [Ir(cod)(μ-Cl)]$_2$ (100 mg, 0.15 mmol) in THF (5 mL). The mixture was stirred for 1 h at room temperature and then concentrated under reduced pressure to *ca.* 1 mL. A yellow precipitate was formed after pentane (5 mL) was added to the solution. The precipitate was filtered, washed with pentane (2 × 3 mL) and dried under vacuum to give a yellow solid (175 mg, 0.29 mmol, 97%). ^{1}H NMR (500 MHz, CD_2Cl_2): δ 8.88 (s, 1H, NC*H*N), 7.87 (t, 1H, ^{3}J = 1.5 Hz, NCHC*H*N$_{(imine)}$), 7.20–7.10 (m, 4H, NC*H*CHN$_{(imine)}$ and aryl-*H*), 4.55–3.96 (br s, 2H, C*H*$_{(cod)}$), 3.96–3.44 (br s, 2H, C*H*$_{(cod)}$), 2.68 (sept, ^{3}J = 6.9 Hz, 2H, C*H*(CH$_3$)$_2$), 2.27 (m, 4H, C*H*$_{2(cod)}$), 2.20 (s, 3H, C*H*$_{3(imine)}$), 1.59 (m, 4H, C*H*$_{2(cod)}$), 1.14 (d, ^{3}J = 6.9 Hz, 6H, CH(C*H*$_3$)$_2$), 1.11 (d, ^{3}J = 6.9 Hz, 6H, CH(C*H*$_3$)$_2$). ^{13}C{^{1}H} NMR (125 MHz, CD_2Cl_2): δ 148.9 (*C*=N), 142.1 (*ipso*-*C*$_{(dipp)}$), 138.3 (N*C*HN), 137.2 (*o*-*C*$_{(dipp)}$), 127.7 (N*C*HCHN$_{(imine)}$), 125.1 (*p*-*C*$_{(dipp)}$), 123.7 (*m*-*C*$_{(dipp)}$), 117.2 (NCH*C*HN$_{(imine)}$), 68.0 (br s, *C*H$_{(cod)}$), 58.6 (br s, *C*H$_{(cod)}$), 31.9 (br s, *C*H$_{2(cod)}$), 28.8

($CH(CH_3)_2$), 23.4 ($CH(CH_3)_2$), 23.0 ($CH(CH_3)_2$), 16.5 ($CH_{3(imine)}$). IR: ν_{max} (pure, orbit diamond)/cm^{-1} 1687 ν(C=N) and 291 ν(Ir-Cl). Anal. calcd for $C_{25}H_{35}ClIrN_3$ (%): C, 49.61; H, 5.83; N, 6.94. Found: C, 49.38; H, 5.72; N, 7.06.

1.3 Synthesis of 2

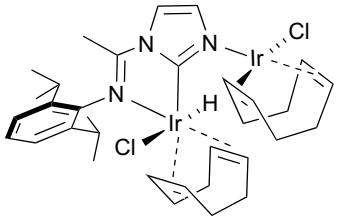

The synthesis of complex **2** can be performed by reaction of 1-(2,6-diisopropylphenylimino) ethylimidazole with 1.0 equiv. of $[Ir(cod)(\mu\text{-}Cl)]_2$ or by reaction of complex **1** with 0.5 equiv. of $[Ir(cod)(\mu\text{-}Cl)]_2$.

a) Addition of 1.0 equiv of $[Ir(cod)(\mu\text{-}Cl)]_2$ to 1-(2,6-diisopropylphenylimino)ethylimidazole.

To a solution of 1-(2,6-diisopropylphenylimino)ethylimidazole (40 mg, 0.15 mmol) in THF (4 mL) was added $[Ir(cod)(\mu\text{-}Cl)]_2$ (100 mg, 0.15 mmol) under magnetic stirring in a glove box. The mixture was stirred for 3 h at room temperature and then concentrated under reduced pressure to *ca.* 0.5 mL. Yellow-green crystals suitable for X-ray analysis were obtained after 2-3 days and a crystalline product was isolated (120 mg, 0.13mmol, 86%).

b) Addition of 0.5 equiv. of $[Ir(cod)(\mu\text{-}Cl)]_2$ to complex **1**.

To a solution of complex **1** (90 mg, 0.15 mmol) in THF (4 mL) was added $[Ir(cod)(\mu\text{-}Cl)]_2$ (50 mg, 0.075 mmol) under magnetic stirring in a glove box. The same product was obtained as in a) with an identical work-up. ^{1}H NMR (400 MHz, THF-d_8): δ 7.43 (d, ^3J = 2.1 Hz, 1H, NC*H*CHN$_{(imine)}$), 7.29–6.26 (m, 3H, aryl-*H*), 7.15 (d, ^3J = 2.1 Hz, 1H, NCHC*H*N$_{(imine)}$), 6.28 (m, 1H, C*H*$_{(cod)}$), 6.10 (m, 1H, C*H*$_{(cod)}$), 4.25 (m, 1H, C*H* $_{(cod)}$), 4.15-4.04 (m, 3H, C*H* $_{(cod)}$), 4.02 (sept, ^3J = 6.7 Hz, 1H, C*H*$(CH_3)_2$), 3.89 (m, 1H, C*H* $_{(cod)}$), 3.24 (m, 1H, C*H* $_{(cod)}$), 3.19 (sept, ^3J = 6.7 Hz, 1H, C*H*$(CH_3)_2$), 2.98–2.87 (m, 1H, C$H_{2(cod)}$), 2.81–2.71 (m, 2H, C$H_{2(cod)}$), 2.50–2.37 (m, 1H, C$H_{2(cod)}$), 2.42 (s, 3H, C$H_{3(imine)}$), 2.33-2.04 (m, 8H, C$H_{2(cod)}$), 2.00–1.90 (m, 1H, C$H_{2(cod)}$)1.90–1.79 (m, 1H, C$H_{2(cod)}$), 1.60–1.45 (m, 2H, C$H_{2(cod)}$), 1.42 (d, ^3J = 6.7 Hz, 3H, CH(C$H_3)_2$), 1.28 (d, ^3J = 6.7 Hz, 3H, CH(C$H_3)_2$), 1.11 (d, ^3J = 6.7 Hz, 3H, CH(C$H_3)_2$), 1.00 (d, ^3J = 6.7 Hz, 3H, CH(C$H_3)_2$), -14.74 (d, ^4J = 1.8Hz, 1H, Ir-H).

$^{13}C\{^1H\}$ NMR (125 MHz, THF-d_8): δ 166.6 (*C*=N), 158.7 (N*C*N$_{(imine)}$), 144.4 (*o*-*C*$_{(dipp)}$), 143.2 (*o*-*C*$_{(dipp)}$), 139.9 (*ipso*-*C*$_{(dipp)}$), 130.7 (N*C*HCHN$_{(imine)}$), 129.3 (*p*-*C*$_{(dipp)}$), 125.7 (*m*-*C*$_{(dipp)}$), 125.2 (*m*-*C*$_{(dipp)}$), 117.0 (NCH*C*HN$_{(imine)}$), 96.0, 94.3, 78.4, 76.9, 68.4, 66.6, 60.8 and 57.1 (*C*H$_{(cod)}$), 37.4, 33.7, 32.8, 32.5, 31.1, 29.8, 29.2 and 28.2 (*C*H$_{2(cod)}$), 28.4 and 28.1 (*C*H(CH$_3$)$_2$), 25.7, 25.5, 25.1 and 23.6 (CH(*C*H$_3$)$_2$), 16.1 (*C*H$_{3(imine)}$). IR (CsI, Nujol mull): ν(Ir-H) = 2200 cm^{-1}, ν(C=N) = 1621 cm^{-1}, *ν*(Ir-Cl) = 290 cm^{-1}. Anal. Calcd for $C_{33}H_{47}Cl_2Ir_2N_3$ (941.09): C, 42.12; H, 5.03; N, 4.47. Found: C, 41.98, H, 5.03; N, 4.32.

1.4 Synthesis of $3^+[PF_6]^-$

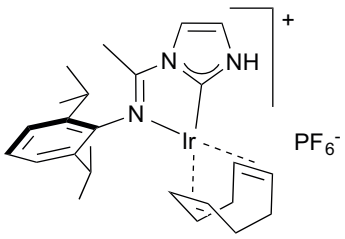

The synthesis of complex $\mathbf{3}^+[PF_6]^-$ can be performed by reaction of either complex **1** or complex **2** with 1.0 equiv. of $TlPF_6$.

a) Reaction of complex **1** with $TlPF_6$. To a solution of **1** (121 mg, 0.20 mmol) in CH_2Cl_2 or CH_3CN (5 mL), was added $TlPF_6$ (70 mg, 0.20 mmol). The reaction mixture was stirred for 12 h at room temperature. After filtration through Celite, the filtrate was concentrated under reduced pressure to *ca.* 2 mL and then was stratified with Et_2O to yield dark green crystals, which were collected by filtration and dried in vacuo (122 mg, 0.17 mmol, 85%). ^1H NMR (500 MHz, CD_2Cl_2): δ 10.36 (br s, 1H, N*H*), 7.38–7.29 (m, 4H, NHCHC*H*N$_{(imine)}$ and aryl-*H*), 7.25 (t, ^3J = 2.0 Hz, 1H, NHC*H*CHN$_{(imine)}$), 4.35 (m, 2H, C*H*$_{(cod)}$), 4.17 (m, 2H, C*H*$_{(cod)}$), 3.02 (sept, ^3J = 6.8 Hz, 2H, C*H*(CH$_3$)$_2$), 2.36 (s, 3H, C*H*$_{3(imine)}$), 2.27–1.96 (m, 8H, C*H*$_{2(cod)}$), 1.34 (d, ^3J = 6.8 Hz, 6H, CH(C*H*$_3$)$_2$), 1.13 (d, ^3J = 6.8 Hz, 6H, CH(C*H*$_3$)$_2$). $^{13}C\{^1H\}$ NMR (125 MHz, CD_2Cl_2): δ 173.6 (NH*C*N$_{(imine)}$), 168.0 (*C*=N), 141.3 (*o*-*C*$_{(dipp)}$), 138.2 (*ipso*-*C*$_{(dipp)}$), 129.1 (*p*-*C*$_{(dipp)}$), 124.8 (*m*-*C*$_{(dipp)}$), 122.2 (NH*C*HCHN$_{(imine)}$), 116.6 (NHCH*C*HN$_{(imine)}$), 95.9 (*C*H$_{(cod)}$), 65.4 (*C*H$_{(cod)}$), 33.2 (*C*H$_{2(cod)}$), 30.3 (*C*H$_{2(cod)}$), 28.9 (*C*H(CH$_3$)$_2$), 25.1 (CH(*C*H$_3$)$_2$), 23.4 (CH(*C*H$_3$)$_2$), 16.2 (*C*H$_{3(imine)}$). $^{31}P\{^1H\}$ NMR (121.5 MHz, CD_2Cl_2): δ −144.3 (sept, $^1J_{P,F}$ = 712 Hz, *P*F_6^-). $^{19}F\{^1H\}$ NMR (282.4 MHz, CD_2Cl_2): δ −73.3 (d, $^1J_{F,P}$ = 712 Hz, P*F*$_6^-$). IR: ν_{max} (pure, orbit diamond)/cm^{-1} 3359 *ν*(N-H), 1613 *ν*(C=N) and 832 *ν*(P-F). Anal. calcd for $C_{25}H_{35}F_6IrN_3P$ (%): C, 42.01; H, 4.94; N, 5.88. Found: C, 41.73; H, 4.83; N, 5.84.

b) Reaction of complex **2** with $TlPF_6$. Complex **2** (5.4 mg, 0.0057 mmol), $TlPF_6$ (2.0 mg, 0.0057mmol) and CD_2Cl_2 (0.5 mL) were added into a Young NMR tube in a glove box. After 12 h, the colour of this solution turned to dark green. $\mathbf{3}^+[PF_6]^-$ and $[Ir(cod)(\mu\text{-}Cl)]_2$ were obtained in quantitative NMR yields.

1.5 Synthesis of 4 and 5

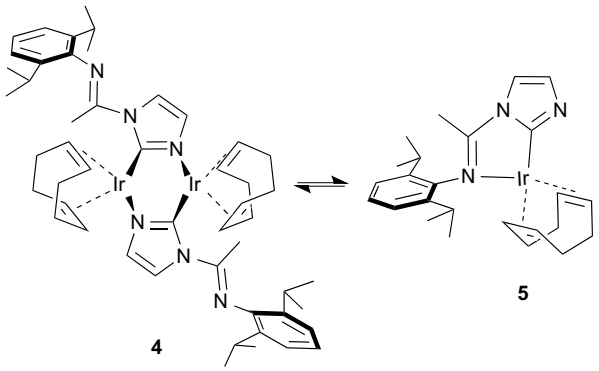

To a solution of $\mathbf{3}^+[PF_6]^-$ (50 mg, 0.070 mmol) in CH_2Cl_2 (5 mL) at 0 ºC, was added NaO*t*-Bu (7.0 mg, 0.073 mmol). The reaction mixture was stirred for 10 min at 0 ºC. Then the reaction mixture was allowed to warm to room temperature and was stirred for another 20 min. After filtration through Celite, the filtrate was evaporated to *ca.* 1 mL under reduced pressure. After Et_2O (2 mL) was added, the solution was cooled to -30 ºC to yield dark red crystals that were collected by filtration and dried in vacuo (28 mg, 0.049 mmol, 70%). Anal. calcd for $C_{25}H_{34}IrN_3$ (%): C, 52.79; H, 6.03; N, 7.39. Found: C, 52.30; H, 6.24; N, 7.45. The spectroscopic analysis of the crystals at room temperature revealed a mixture of two complexes **4** and **5** with a molar ratio 14:86 in CD_2Cl_2 (by ^{1}H NMR integration of 1:3) and with a molar ratio 80:20 in toluene-d_8 (by ^{1}H NMR integration of 8:1), respectively. The assignment to **4** or **5** was made on the basis of the chemical shift of *C*=N in the ^{13}C NMR spectrum, which if different for a coordinated and a dangling imine group. **4**: ^{1}H NMR (500 MHz, CD_2Cl_2): δ 7.65 (d, ^3J = 1.5 Hz, 2H, NC*H*CHN$_{(imine)}$), 7.19 (m, 2H, aryl-*H*), 7.10 (m, 4H, aryl-*H*), 6.90 (d, ^3J = 1.5 Hz, 2H, NCHC*H*N$_{(imine)}$), 4.48 (m, 2H, C*H*$_{(cod)}$), 3.55 (m, 2H, C*H*$_{(cod)}$), 3.49 (m, 4H, C*H*$_{(cod)}$), 3.02 (sept, ^3J = 7.0 Hz, 2H, C*H*(CH$_3$)$_2$), 2.95 (s, 6H, C*H*$_{3(imine)}$), 2.68 (sept, ^3J = 7.0 Hz, 2H, C*H*(CH$_3$)$_2$), 2.51–2.29 (m, 12H, C*H*$_{2(cod)}$), 2.22 (m, 4H, C*H*$_{2(cod)}$), 1.32 (d, ^3J = 7.0 Hz, 12H, CH(C*H*$_3$)$_2$), 1.13 (d, ^3J = 7.0 Hz, 12H, CH(C*H*$_3$)$_2$). ^{13}C{^{1}H} NMR (125 MHz, CD_2Cl_2): δ 174.8 (N*C*N$_{(imine)}$), 156.2 (*C*=N), 143.9 (*ipso*-*C*$_{(dipp)}$), 137.7 (*o*-*C*$_{(dipp)}$), 136.9 (*o*-*C*$_{(dipp)}$), 128.7 (*p*-*C*$_{(dipp)}$), 125.5 (N*C*HCHN$_{(imine)}$), 123.6 (*m*-*C*$_{(dipp)}$), 123.4 (*m*-*C*$_{(dipp)}$), 120.3 (NCH*C*HN$_{(imine)}$), 77.8

($CH_{(cod)}$), 73.6 ($CH_{(cod)}$), 61.2 ($CH_{(cod)}$), 58.8 ($CH_{(cod)}$), 34.3 ($CH_{2(cod)}$), 33.3 ($CH_{2(cod)}$), 31.5 ($CH_{2(cod)}$), 30.1 ($CH_{2(cod)}$), 28.5 ($CH(CH_3)_2$), 28.4 ($CH(CH_3)_2$), 23.9 ($CH(CH_3)_2$), 23.8 ($CH(CH_3)_2$), 22.6 ($CH(CH_3)_2$), 20.8 ($CH_{3(imine)}$). **5**: ^{1}H NMR (500 MHz, CD_2Cl_2): δ 7.24 (m, 3H, aryl-*H*), 6.98 (d, ^3J = 1.7 Hz, 1H, NC*H*CHN$_{(imine)}$), 6.88 (d, ^3J = 1.7 Hz, 1H, NCHC*H*N$_{(imine)}$), 4.22 (m, 2H, C*H*$_{(cod)}$), 3.35 (m, 2H, C*H*$_{(cod)}$), 3.22 (sept, ^3J = 6.7 Hz, 2H, C*H*$(CH_3)_2$), 2.25 (s, 3H, C*H*$_{3(imine)}$), 2.21–2.01 (m, 4H, C*H*$_{2(cod)}$), 1.90–1.68 (m, 4H, C*H*$_{2(cod)}$), 1.34 (d, ^3J = 6.7 Hz, 6H, CH(C*H*$_3)_2$), 1.10 (d, ^3J = 6.7 Hz, 6H, CH(C*H*$_3)_2$). ^{13}C{^{1}H} NMR (125 MHz, CD_2Cl_2): δ 179.3 (N*C*N$_{(imine)}$), 166.3 (*C*=N), 142.1 (*o*-*C*$_{(dipp)}$), 139.6 (*ipso*-*C*$_{(dipp)}$), 133.4 (N*C*HCHN$_{(imine)}$), 127.7 (*p*-*C*$_{(dipp)}$), 124.2 (*m*-*C*$_{(dipp)}$), 114.3 (NCH*C*HN$_{(imine)}$), 83.3 ($CH_{(cod)}$), 62.6 ($CH_{(cod)}$), 32.8 ($CH_{2(cod)}$), 30.7 ($CH_{2(cod)}$), 28.5 ($CH(CH_3)_2$), 25.1 ($CH(CH_3)_2$), 23.5 ($CH(CH_3)_2$), 15.5 ($CH_{3(imine)}$).

1.6 Synthesis of 6^+Cl^-

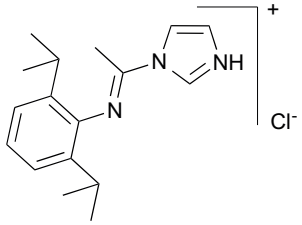

To a solution of 1-(2,6-diisopropylphenylimino) ethylimidazole (540 mg, 2.0 mmol) in Et_2O (30 mL) was added dropwise a solution of HCl (1.0 M in Et_2O, 2.0 mL, 2.0 mmol). The reaction mixture was stirred for 1 h at room temperature. Then the resultant precipitate was collected by filtration, washed with Et_2O and dried in vacuo to obtain a white powder (520 mg, 1.7 mmol, 85%). ^{1}H NMR (500 MHz, $CDCl_3$): δ 15.02 (br s, 1H, N*H*), 10.73 (s, 1H, NC*H*N), 8.13 (s, 1H, NCHC*H*N$_{(imine)}$), 7.51 (s, 1H, NC*H*CHN$_{(imine)}$), 7.17 (m, 3H, aryl-*H*), 2.62 (sept, ^3J = 6.9 Hz, 2H, C*H*$(CH_3)_2$), 2.54 (s, 3H, C*H*$_{3(imine)}$), 1.15 (d, ^3J = 6.9 Hz, 6H, CH(C*H*$_3)_2$), 1.11 (d, ^3J = 6.9 Hz, 6H, CH(C*H*$_3)_2$). ^{13}C{^{1}H} NMR (125 MHz, $CDCl_3$): δ 147.7 (*C*=N), 139.9 (*ipso*-*C*$_{(dipp)}$), 135.6 (*o*-*C*$_{(dipp)}$), 135.1 (N*C*HN), 124.6 (*p*-*C*$_{(dipp)}$), 122.6 (*m*-*C*$_{(dipp)}$), 119.4 (N*C*HCHN$_{(imine)}$), 116.2 (NCH*C*HN$_{(imine)}$), 27.6 ($CH(CH_3)_2$), 22.3 ($CH(CH_3)_2$), 21.9 ($CH(CH_3)_2$), 16.1 ($CH_{3(imine)}$). IR: ν_{max}(pure, orbit diamond)/cm^{-1} 3368 *v*(N-H) and 1694 *v*(C=N). Anal. calcd for $C_{17}H_{24}ClN_3$ (%): C, 66.76; H, 7.91; N, 13.74. Found: C, 66.44; H, 7.76; N, 13.89.

1.7 Synthesis of $6^{+}[BF_4]^{-}$

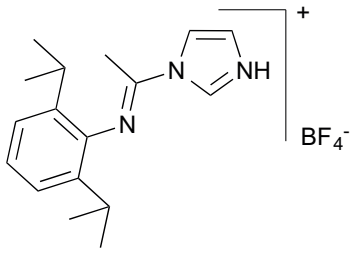

To a solution of 1-(2,6-diisopropylphenylimino) ethylimidazole (600 mg, 2.2 mmol) in Et_2O (30 mL) was added dropwise a solution of $HBF_4 \cdot Et_2O$ (0.30 mL, 357 mg, 2.2 mmol) in Et_2O (5 mL). The reaction mixture was stirred for 12 h at room temperature. Then the resultant precipitate was collected by filtration, washed with Et_2O and dried in vacuo to obtain a white powder (572 mg, 1.6 mmol, 73%). ^{1}H NMR (500 MHz, $CDCl_3$): δ 12.45 (br s, 1H, N*H*), 9.43 (s, 1H, NC*H*N), 8.17 (s, 1H, NCHC*H*$N_{(imine)}$), 7.67 (s, 1H, NC*H*CH$N_{(imine)}$), 7.18 (m, 3H, aryl-*H*), 2.65 (sept, ^3J = 6.9 Hz, 2H, C*H*$(CH_3)_2$), 2.38 (s, 3H, C$H_{3(imine)}$), 1.16 (d, ^3J = 6.9 Hz, 6H, CH(C$H_3)_2$), 1.12 (d, ^3J = 6.9 Hz, 6H, CH(C$H_3)_2$). ^{13}C{^{1}H} NMR (125 MHz, $CDCl_3$): δ 148.2 (*C*=N), 140.8 (*ipso*-$C_{(dipp)}$), 136.8 (*o*-$C_{(dipp)}$), 135.3 (N*C*HN), 125.6 (*p*-$C_{(dipp)}$), 123.6 (*m*-$C_{(dipp)}$), 121.2 (N*C*HCH$N_{(imine)}$), 117.5 (NCH*C*$HN_{(imine)}$), 28.6 (*C*H$(CH_3)_2$), 23.4 (CH(*C*$H_3)_2$), 22.9 (CH(*C*$H_3)_2$), 15.8 (*C*$H_{3(imine)}$). IR: ν_{max} (pure, orbit diamond)/cm^{-1} 3326 *ν*(N-H) and 1705 *ν*(C=N). Anal. calcd for $C_{17}H_{24}BF_4N_3$ (%): C, 57.16; H, 6.77; N, 11.76. Found: C, 57.38; H, 6.52; N, 12.30.

1.8 Synthesis of 7

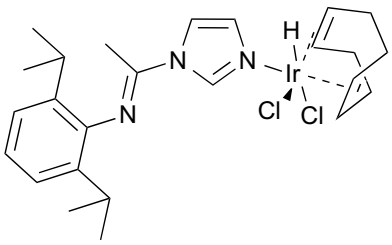

To a solution of $\mathbf{6}^{+}Cl^{-}$ (46 mg, 0.15 mmol) in THF (5 mL) was added a solution of $[Ir(cod)(\mu\text{-}Cl)]_2$ (50 mg, 0.075 mmol) in THF (5 mL). The mixture was stirred for 4 h at room temperature and then was concentrated under reduced pressure to ca. 1 mL. A yellow precipitate was formed after 5 mL of pentane was added to the solution. The precipitate was filtered, washed with pentane (2 × 3 mL) and dried under vacuum to give a yellow solid (82 mg, 0.13 mmol, 85%). ^{1}H NMR (500 MHz, CD_2Cl_2): δ 8.90 (s, 1H, NC*H*N), 7.83 (t, 1H, ^3J = 1.6 Hz, NCHC*H*$N_{(imine)}$), 7.39 (t, 1H, ^3J = 1.6 Hz, NC*H*CH$N_{(imine)}$), 7.16 (m, 3H, aryl-*H*), 4.88 (m, 1H, C$H_{(cod)}$), 4.76 (m, 1H, C$H_{(cod)}$), 4.37 (m, 1H, C$H_{(cod)}$), 4.26 (m, 1H, C$H_{(cod)}$), 3.07–2.79 (m, 2H, C$H_{2(cod)}$), 2.76–2.52 (m, 4H, C$H_{2(cod)}$ and C*H*$(CH_3)_2$), 2.39–2.15 (m, 5H, C$H_{2(cod)}$ and C$H_{3(imine)}$), 2.11–1.89 (m, 2H, C$H_{2(cod)}$), 1.15 (d, ^3J = 6.9 Hz, 6H, CH(C$H_3)_2$), 1.11 (d, ^3J = 6.9 Hz, 6H,

$CH(CH_3)_2$), -12.10 (s, 1H, Ir-H). $^{13}C\{^1H\}$ NMR (125 MHz, CD_2Cl_2): δ 148.6 (*C*=N), 141.9 (*ipso*-$C_{(dipp)}$), 138.8 (N*C*HN), 137.2 (*o*-$C_{(dipp)}$), 131.8 (N*C*HCHN$_{(imine)}$), 125.2 (*p*-$C_{(dipp)}$), 123.7 (*m*-$C_{(dipp)}$), 117.3 (NCH*C*HN$_{(imine)}$), 83.5 ($CH_{(cod)}$), 81.7 ($CH_{(cod)}$), 79.5 ($CH_{(cod)}$), 76.2 ($CH_{(cod)}$), 35.3 ($CH_{2(cod)}$), 32.3 ($CH_{2(cod)}$), 29.9 ($CH_{2(cod)}$), 29.6 ($CH_{2(cod)}$), 28.7 ($CH(CH_3)_2$), 23.4 ($CH(CH_3)_2$), 23.0 ($CH(CH_3)_2$), 16.4 ($CH_{3(imine)}$). IR: ν_{max}(pure, orbit diamond)/cm^{-1} 2206 *v*(Ir-H), 1687 *v*(C=N) and 294 *v*(Ir-Cl). Anal. calcd for $C_{25}H_{36}Cl_2IrN_3$ (%): C, 46.79; H, 5.65; N, 6.55. Found: C, 46.32; H, 5.52; N, 6.52.

1.9 Synthesis of $8^+[BF_4]^-$

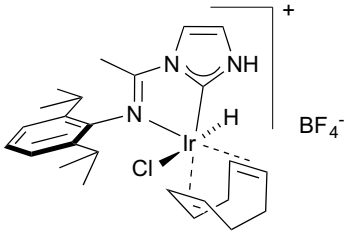

To a solution of $\mathbf{6}^+[BF_4]^-$ (54 mg, 0.15 mmol) in THF (5 mL) was added to a solution of $[Ir(cod)(\mu\text{-}Cl)]_2$ (50 mg, 0.075 mmol) in THF (5 mL). The mixture was stirred for 12 h at room temperature and then the volatiles was removed under reduced pressure. The residue was dissolved in 2 mL of dichloromethane and stratified with Et_2O to yield light green crystals, which were collected by filtration and dried in vacuo (85 mg, 0.12 mmol, 82%). ^1H NMR (500 MHz, CD_2Cl_2): δ 11.84 (br s, 1H, N*H*), 7.50 (t, ^3J = 1.7 Hz, 1H, NHCHC*H*N$_{(imine)}$), 7.44–7.22 (m, 4H, NHC*H*CHN$_{(imine)}$ and aryl-*H*), 5.21 (m, 1H, C*H*$_{(cod)}$), 4.78 (m, 1H, C*H*$_{(cod)}$), 4.45 (m, 1H, C*H*$_{(cod)}$), 4.10 (m, 1H, C*H*$_{(cod)}$), 3.72 (sept, ^3J = 6.9 Hz, 1H, C*H*$(CH_3)_2$), 2.94 (m, 3H, C*H*$(CH_3)_2$ and C*H*$_{2(cod)}$), 2.36 (s, 3H, C*H*$_{3(imine)}$), 2.70–2.46 (m, 5H, C*H*$_{3(imine)}$ and C*H*$_{2(cod)}$), 2.30–2.16 (m, 2H, C*H*$_{2(cod)}$), 1.90–1.76 (m, 2H, C*H*$_{2(cod)}$), 1.41 (d, ^3J = 6.9 Hz, 3H, CH(C*H*$_3)_2$), 1.32 (d, ^3J = 6.9 Hz, 3H, CH(C*H*$_3)_2$), 1.12 (d, ^3J = 6.9 Hz, 3H, CH(C*H*$_3)_2$), 1.07 (d, ^3J = 6.9 Hz, 3H, CH(C*H*$_3)_2$), -14.50 (d, ^4J = 1.6Hz, 1H Ir-H). $^{13}C\{^1H\}$ NMR (125 MHz, CD_2Cl_2): δ 167.3 (*C*=N), 161.3 (NH*C*N$_{(imine)}$), 142.8 (*o*-$C_{(dipp)}$), 141.3 (*o*-$C_{(dipp)}$), 138.1 (*ipso*-$C_{(dipp)}$), 129.9 (*p*-$C_{(dipp)}$), 125.9 (*m*-$C_{(dipp)}$), 125.3 (*m*-$C_{(dipp)}$), 122.5 (NH*C*HCHN$_{(imine)}$), 117.8 (NHCH*C*HN$_{(imine)}$), 99.8 ($CH_{(cod)}$), 98.4 ($CH_{(cod)}$), 78.9 ($CH_{(cod)}$), 77.6 ($CH_{(cod)}$), 37.5 ($CH_{2(cod)}$), 29.1 ($CH_{2(cod)}$), 28.3 ($CH_{2(cod)}$), 28.2 ($CH(CH_3)_2$), 28.0 ($CH_{2(cod)}$), 27.9 ($CH(CH_3)_2$), 25.6 ($CH(CH_3)_2$), 25.4 ($CH(CH_3)_2$), 24.6 ($CH(CH_3)_2$), 23.3 ($CH(CH_3)_2$), 16.9 ($CH_{3(imine)}$). IR: ν_{max} (pure, orbit diamond)/cm^{-1} 3241 *v*(N-H), 2211 *v*(Ir-H), 1627 *v*(C=N) and 445 *v*(Ir-Cl). Anal. calcd

for $C_{25}H_{36}BClF_4IrN_3$ (%): C, 43.33; H, 5.24; N, 6.06. Found: C, 42.97; H, 5.25; N, 6.02.

2 X-ray crystallography

2.1 General methods

Suitable crystals for the X-ray analysis of all compounds were obtained as described above. Data for **1**, **2**, **3** and **8** were collected on an APEX-II CCD (graphite-monochromated Mo-Kα radiation, λ = 0.71073 Å) at 173(2) K, data for **4** was collected on a Kappa CCD diffractometer (graphite-monochromated Mo-Kα radiation, λ = 0.71073 Å) at 173(2) K. Crystallographic and experimental details for these structures are summarized in Table S1. The structures were solved by direct methods (SHELXS-97[1]) and refined by full-matrix least-squares procedures (based on F^2, SHELXL-97) with anisotropic thermal parameters for all the non-hydrogen atoms. The hydrogen atoms were introduced into the geometrically calculated positions (SHELXS-97 procedures).

CCDC 1039710-1039714

The following specific comments apply for the structures:

Complex 3: Instead of placed in a calculated position, the hydrogen atom H1N was found.

Complex 4: The SQUEEZE instruction in PLATON was applied for **4**. The residual electron density was assigned to four molecules of disordered diethyl ether for **4**.

Complex 8: Instead of placed in a calculated position, the hydrogen atom H1N and the hydride atom H1 on the iridium atom were found. The SQUEEZE instruction in PLATON was applied for **8**. The residual electron density was assigned to one molecule of disordered diethyl ether for **8**.

2.2 Summary of crystal data

Table S1. Crystal data and structure refinement for **1**, **2**, **3**, **4** and **8**

ompound number	**1**	**2**	**3**	**4**	**8**
ıternal code	pbad121109	pbmw140303	pbfh140623	pbfh140901	pbfh141126
CDC	1039710	1039712	1039714	1039713	1039711
mpirical formula	$C_{25}H_{35}ClIrN_3$	$C_{33}H_{47}Cl_2Ir_2N_3$	$C_{25}H_{35}F_6IrN_3P$	$C_{50}H_{68}Ir_2N_6$	$C_{25}H_{36}BClF_4IrN_3$
w	605.21	941.03	714.73	1137.50	693.03
/K	173(2)	173(2)	173(2)	173(2)	173(2)
rystal system	Triclinic	Monoclinic	Triclinic	Triclinic	Monoclinic
pace group	P -1	P 21/c	P -1	P -1	C 2/c
/Å	8.5409(4)	8.7044(3)	10.2750(4)	12.2904(3)	22.1698(9)
/Å	11.3926(5)	21.9069(8)	10.7121(4)	13.3290(5)	20.5501(8)
/Å	13.7162(6)	19.1631(6)	13.6503(5)	19.4944(6)	14.5843(6)
/°	69.6340(10)	90	105.8340(10)	86.542(2)	90
/°	87.7630(10)	115.4070(10)	110.0360(10)	72.600(2)	110.9360(10)
°	71.5300(10)	90	97.4030(10)	62.575(4)	90
/Å^3	1182.94(9)	3300.7(2)	1316.23(9)	2693.61(17)	6205.8(4)
	2	4	2	2	8
/mm^{-1}	5.773	8.243	5.195	4.970	4.429
o. of rflns collected	23224	34723	21762	29513	50764
o. unique rflns	8245	11428	8346	12243	12686
(int)	0.0211	0.0243	0.0264	0.0503	0.0252
oodness of fit on F^2	1.100	1.042	1.036	1.083	1.069
inal *R* índices	R1 = 0.0202	R1 = 0.0309	R1 = 0.0329	R1 = 0.0380	R1 = 0.0333
$>2\sigma(I)$]	wR2 = 0.0434	wR2 = 0.0601	wR2 = 0.0744	wR2 = 0.1102	wR2 = 0.0756
indices (all data)	R1 = 0.0253	R1 = 0.0450	R1 = 0.0448	R1 = 0.0528	R1 = 0.0469
	wR2 = 0.0455	wR2 = 0.0660	wR2 = 0.0786	wR2 = 0.1169	wR2 = 0.0812

References: p 66

2.3 Crystal structure of 1

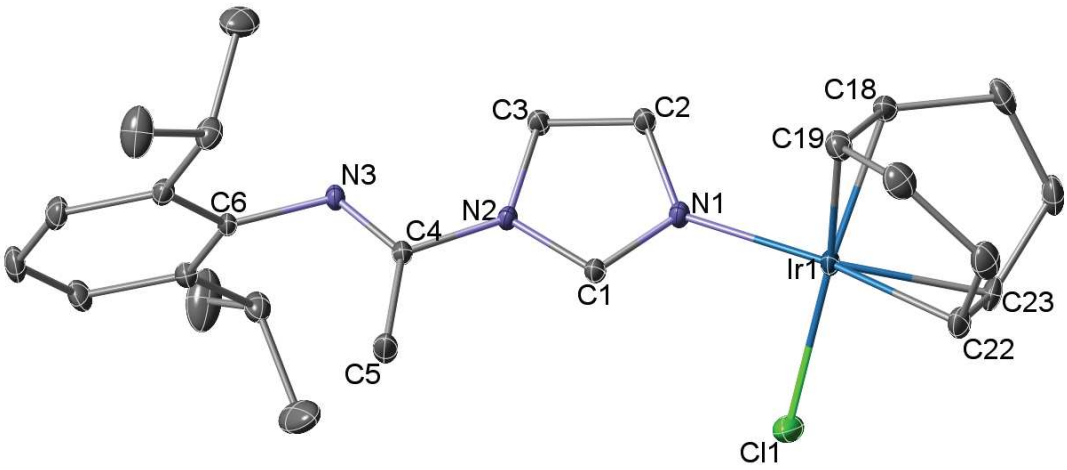

Figure S1. Molecular structure of **1**. H atoms omitted for clarity. Thermal ellipsoids are at the 30% level. Selected bond lengths (Å) and angles (°): C1–N1 1.321(2), C1–N2 1.360(2), C2–N1 1.387(3), C2–C3 1.358(3), C3–N2 1.381(2), C4–N2 1.427(2), C4–N3 1.261(2), C4–C5 1.494(3), C6–N3 1.427(2), Ir1–N1 2.0903(16), Ir1–Cl1 2.3605(6), Ir1–C18 2.111(2), Ir1–C19 2.096(2), Ir1–C22 2.130(2), Ir1–C23 2.121(2), C18–C19 1.418(3), C22–C23 1.405(4); N1–C1–N2 110.79(17), N1–Ir1–Cl1 87.98(5), N1–Ir1–C18 93.71(7), N1–Ir1–C19 90.42(8), Cl1–Ir1–C22 92.51(7), Cl1–Ir1–C23 91.22(7).

2.4 Crystal structure of 2

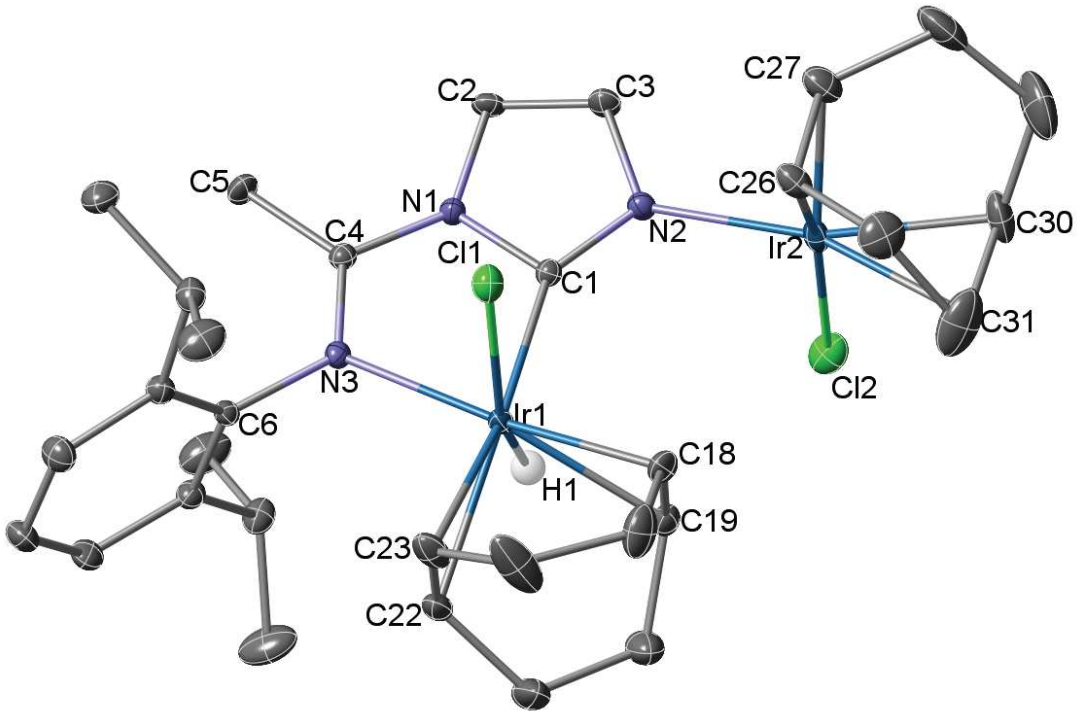

Figure S2. Molecular structure of **2**. H atoms omitted for clarity, except H1(Ir). Thermal ellipsoids are at the 30% level. Selected bond lengths (Å) and angles (°): C1–N1 1.400(4), C1–N2 1.330(5), C2–N1 1.394(5), C2–C3 1.344(5), C3–N2 1.406(5), C4–N1 1.374(5), C4–N3 1.295(5), C4–C5 1.482(5), C6–N3 1.454(4), Ir1–Cl1 2.5017(10), Ir1–C1 2.024(3), Ir1–N3 2.115(3), Ir1–C18 2.186(4), Ir1–C19 2.221(4), Ir1–C22 2.276(4), Ir1–C23 2.258(4), C18–C19 1.391(6), C22–C23 1.363(7), Ir2–Cl2 2.3627(11), Ir2–N2 2.083(3), Ir2–C26 2.108(4), Ir2–C27 2.100(5), Ir2–C30 2.127(4), Ir2–C31 2.118(4), C26–C27 1.412(6), C30–C31 1.394(7); N1–C1–N2 106.6(3), C1–Ir1–N3 78.43(13), C1–Ir1–C18 100.85(15), C1–Ir1–C19 98.67(14), N3–Ir1–C22 95.44(13), N3–Ir1–C23 96.99(15), C1–Ir1–Cl1 80.92(10), N3–Ir1–Cl1 87.03(8), N2–Ir2–Cl2 88.52(9), N2–Ir2–C26 92.18(15), N2–Ir2–C27 91.08(16), Cl2–Ir2–C30 91.80(16), Cl2–Ir2–C31 91.42(16).

References: p 66

2.5 Crystal structure of 3

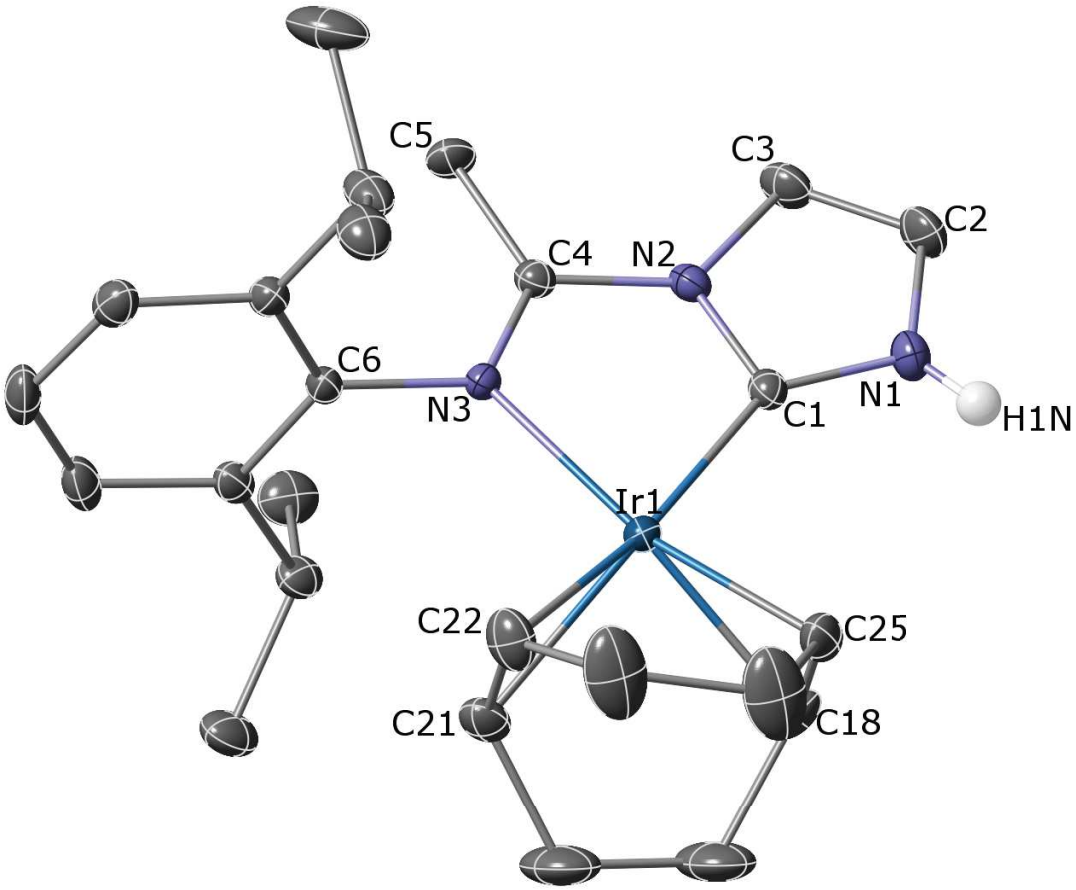

Figure S3. Molecular structure of the cation in $\mathbf{3}^{+}[PF_6]^{-}$. H atoms omitted for clarity, except H1(N1). Thermal ellipsoids are at the 30% level. Selected bond lengths (Å) and angles (°): C1–N1 1.340(4), C1–N2 1.366(5), C2–N1 1.395(6), C2–C3 1.332(6), C3–N2 1.400(4), C4–N2 1.395(4), C4–N3 1.293(4), C4–C5 1.485(5), C6–N3 1.448(4), Ir1–C1 1.984(3), Ir1–N3 2.115(3), Ir1–C18 2.116(4), Ir1–C21 2.232(4), Ir1–C22 2.225(4), Ir1–C25 2.129(4), C18−C25 1.403(7), C21−C22 1.365(7), N1–H1N 0.84(5); N1–C1–N2 103.5(3), C1–Ir1–N3 77.15(13), C1–Ir1–C18 95.60(16), C1–Ir1–C25 96.52(15), N3–Ir1–C21 97.65(13), N3–Ir1–C22 100.53(15).

References: p 66

2.6 Crystal structure of 4

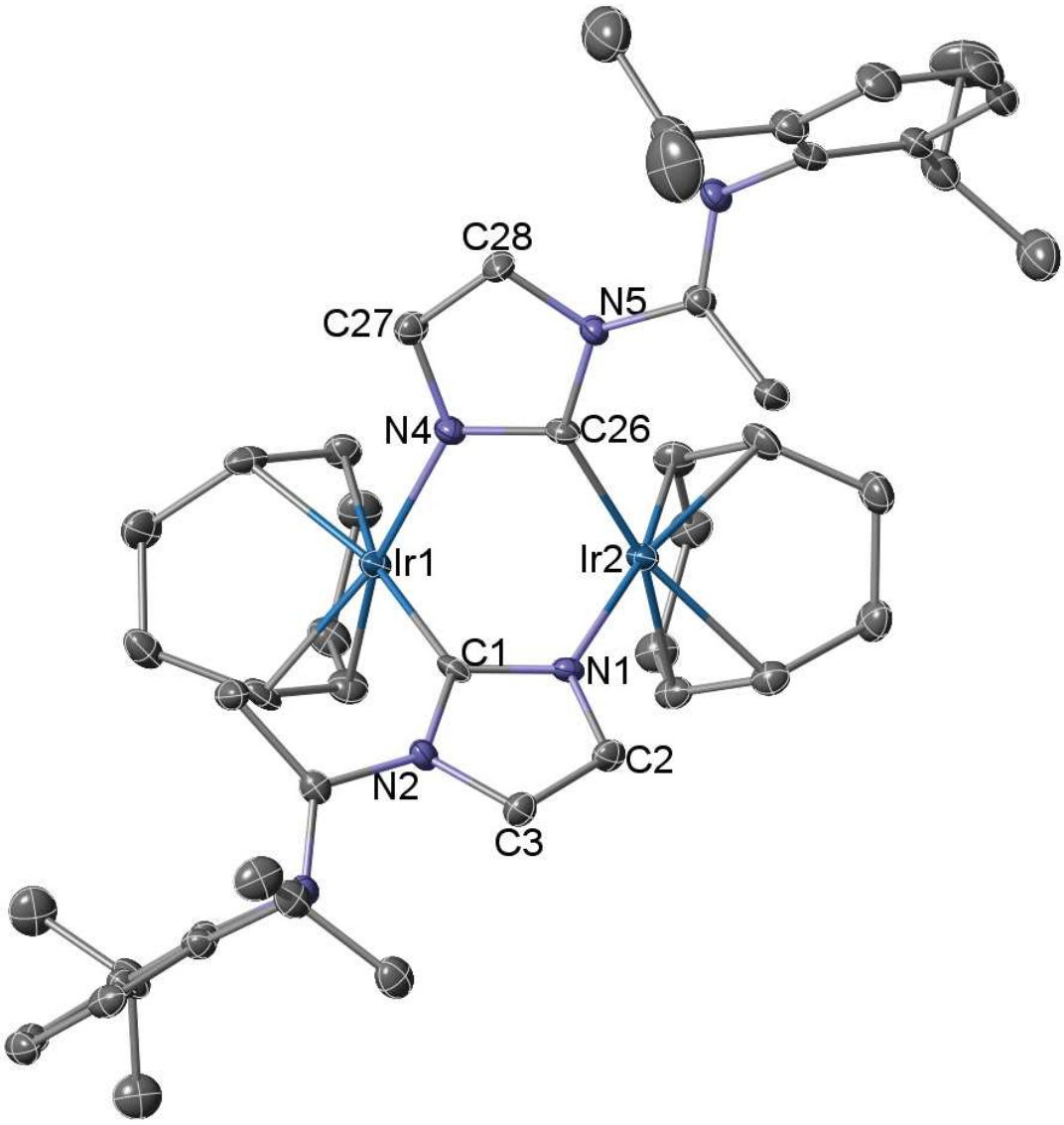

Figure S4. Molecular structure of **4**. H atoms omitted for clarity. Thermal ellipsoids are at the 30% level. Selected bond lengths (Å) and angles (°): C1–N1 1.357(7), C1–N2 1.392(6), C2–N1 1.394(7), C2–C3 1.356(8), C3–N2 1.399(7), C26–N4 1.347(7), C26–N5 1.383(6), C27–N4 1.387(6), C27–C28 1.338(8), C28–N5 1.387(6), Ir1–C1 2.046(5), Ir1–N4 2.066(4), Ir2–C26 2.050(4), Ir2–N1 2.058(4), Ir1···Ir2 3.1844(3); N1–C1–N2 105.3(4), N4–C26–N5 106.3(4), C1–Ir1–N4 88.11(18), C26–Ir2–N1 87.95(18).

References: p 66

2.7 Crystal structure of 8

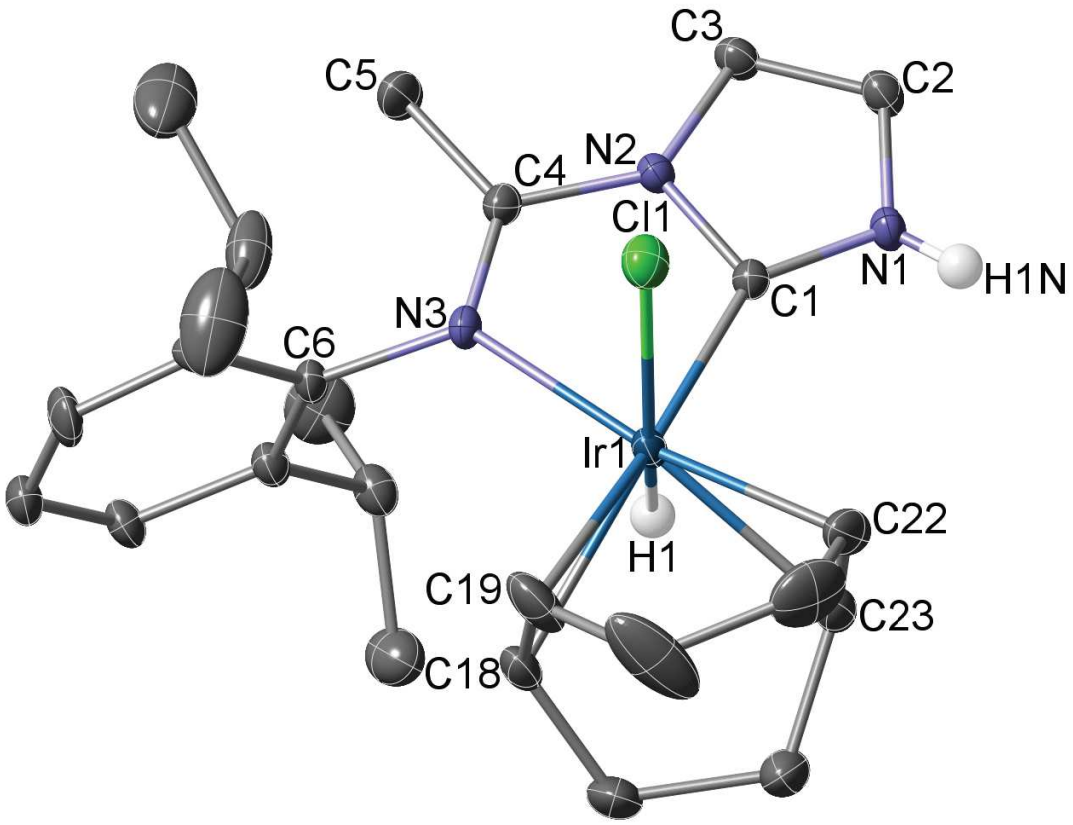

Figure S5. Molecular structure of $\mathbf{8}^{+}$ in $\mathbf{8}^{+}[BF_4]^{-}$. H atoms omitted for clarity, except H1(N1) and H1(Ir). Thermal ellipsoids are at the 30% level. Selected bond lengths (Å) and angles (°): C1–N1 1.327(3), C1–N2 1.371(3), C2–N1 1.397(4), C2–C3 1.345(4), C3–N2 1.392(3), C4–N2 1.391(3), C4–N3 1.290(3), C4–C5 1.486(4), C6–N3 1.452(3), Ir1–Cl1 2.4901(8), Ir1–C1 1.983(2), Ir1–N3 2.125(2), Ir1–C18 2.281(3), Ir1–C19 2.287(3), Ir1–C22 2.180(3), Ir1–C23 2.191(3), C18–C19 1.367(6), C22–C23 1.375(6); N1–C1–N2 105.0(2), C1–Ir1–N3 77.45(9), C1–Ir1–C22 97.10(12), C1–Ir1–C23 97.03(11), N3–Ir1–C18 95.69(10), N3–Ir1–C19 103.11(14), C1–Ir1–Cl1 82.23(8), N3–Ir1–Cl1 87.35(6).

References: p 66

REFERENCES

1. G. M. Sheldrick, *SHELXL-97, Program for crystal structure refinement*, University of Göttingen, Göttingen, Germany, 1997.

Chapitre 4

Homo and heterodinuclear Ir and Rh imine-functionalized protic NHC complexes: synthetic, structural studies and tautomerization/metallotropism insights

Résumé

L'influence d'un groupe imine potentiellement chélatant, présent en tant que groupement fonctionnel dans les ligands imidazoles complexant l'Ir et le Rh, a été étudiée dans la transformation en complexes NHC-protique (pNHC) de ces mêmes métaux. Cette transformation par tautomérisation/métallotropisme ainsi que certaines espèces intermédiaires impliquées ont été décrites. L'abstraction de chlorure dans [Ir(cod)Cl{$C_3H_3N_2$(DippN=CMe)-κN3}] (**1a**) par $TlPF_6$ a permis la formation de [Ir(cod){$C_3H_3N_2$(DippN=CMe)-κ^2(C2,N_{imine})}]$^+$[PF_6]$^-$ (**3a**$^+$[PF_6]$^-$) (Schéma 1).

Schéma 1.

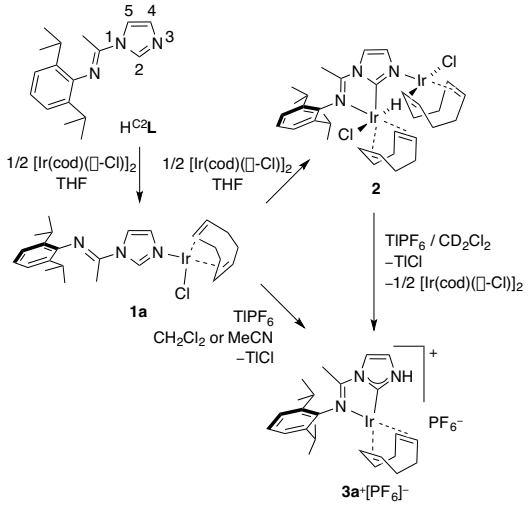

Dans les complexes de l'Ir avec l'imidazole lié à l'azote, tels que [Ir(cod)Cl{$C_3H_3N_2$(R)-κN3}] (**4a**/**b**: R = *n*-Bu/Mes), (Ir: imidazole = 1:1), l'abstraction de chlorure est accompagnée par un transfert de ligands pour donner [Ir(cod){$C_3H_3N_2$(R)-κN3}$_2$]$^+$[PF_6]$^-$ (**5a**/**b**$^+$[PF_6]$^-$) (Ir: imidazole = 1:2) (Schéma 2).

Schéma 2.

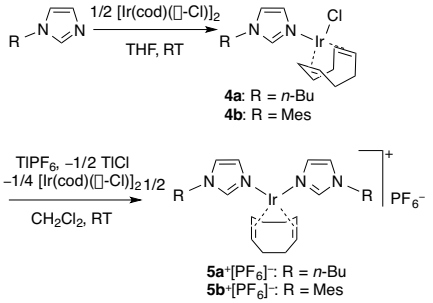

Contrairement à (**5a**/**b**$^+$[PF_6]$^-$), le complexe de l'Ir comportant un imidazole fonctionnalisé par une imine dans un rapport 2:1 [Ir(cod){$C_3H_3N_2$(DippN=CMe)-κN3}$_2$]$^+$[PF_6]$^-$ (**6a**$^+$[PF_6]$^-$) n'est isolable qu'en présence de 1-(2,6-di*iso*propylphenylimino)ethylimidazole additionnel lors de la réaction d'abstraction du chlorure dans (**1a**) (Schéma 3).

Schéma 3.

 References: p 100

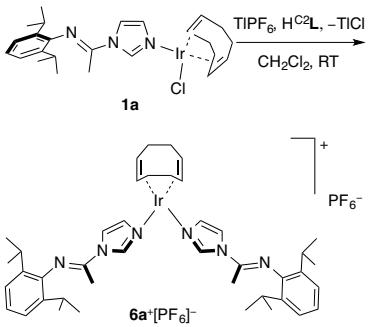

Un mécanisme raisonnable concernant la tautomérisation de (**1a**) en (**3a**$^+$[PF_6]$^-$) qui implique l'activation de la liaison C2–H soit dans (**1a**) soit dans (**6a**$^+$[PF_6]$^-$) a été proposé. L'addition de PR_3 à (**3a**$^+$[PF_6]$^-$) permet l'obtention d'un complexe à 18 électrons de valence [Ir(cod)(PR_3){$C_3H_3N_2$(DippN=CMe)-κ^2(C2,N_{imine})}]$^+$[PF_6]$^-$ (**7a**/**b**$^+$[PF_6]$^-$, R = Ph, Me) (Schéma 4).

Schéma 4.

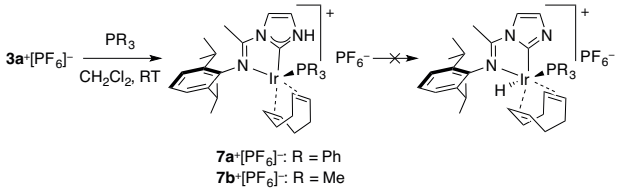

L'abstraction de chlorure de [Ir(cod)Cl{C_3HN_2(DippN=CMe)(DippN=CH)(Me)-κN3}] (**8**) permet l'obtention de [Ir(cod){C_3HN_2(DippN=CMe)(DippN=CH)(Me)-κ^2(N3,N_{imine})}]$^+$[PF_6]$^-$ (**9**$^+$[PF_6]$^-$) où le groupe imine chélate l'Ir (Schéma 5).

Schéma 5.

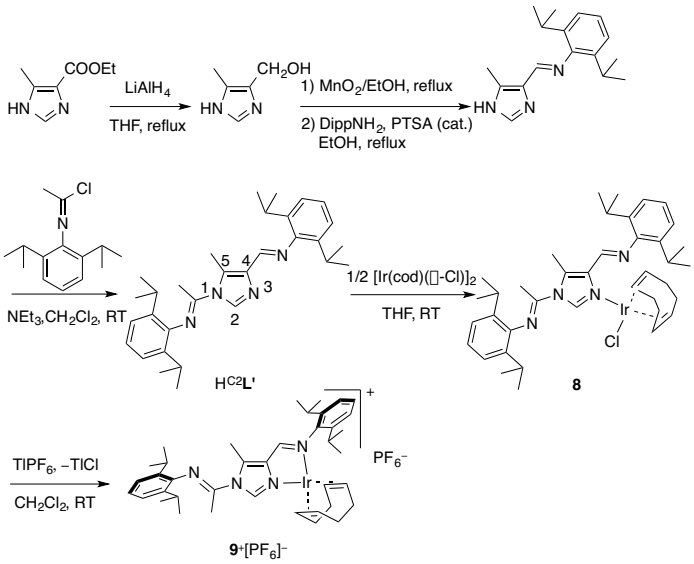

Contrairement à l'Ir, l'abstraction de chlorure de [Rh(cod)Cl{$C_3H_3N_2$(DippN=CMe)-κN3}] (**1b**), à température ambiante, conduit essentiellement à [Rh(cod){$C_3H_3N_2$(DippN=CMe)-κN3}$_2$]$^+$[PF_6]$^-$ (**6b**$^+$[PF_6]$^-$) et seulement à [Rh(cod){$C_3H_3N_2$(DippN=CMe)-κ^2(C2,N_{imine})}]$^+$[PF_6]$^-$ (**3b**$^+$[PF_6]$^-$), tandis qu'à 110°C ce dernier complexe est le seul à se former (Schéma 6).

Schéma 6.

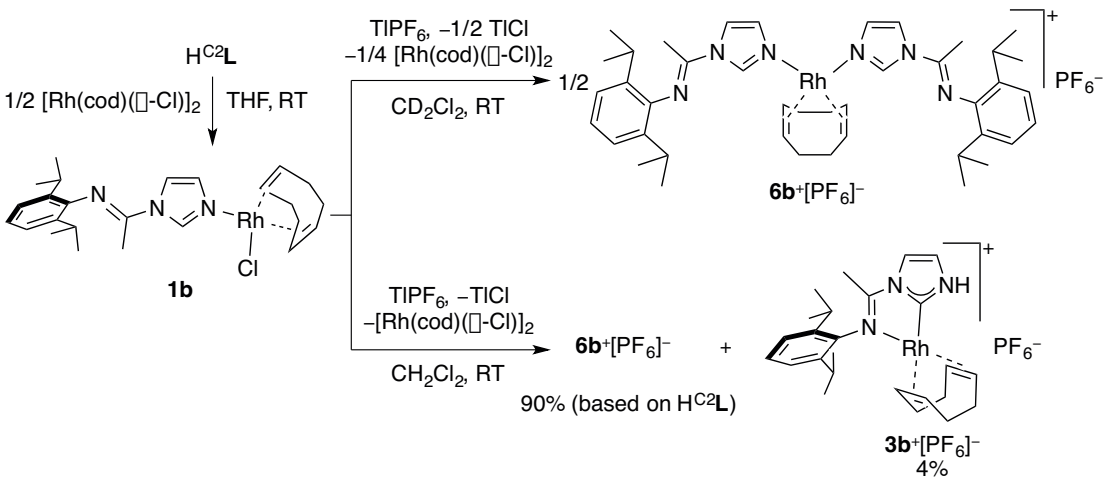

Le complexe homodinucléaire $[Ir_2(cod)_2Cl\{\mu\text{-}C_3H_2N_2(DippN{=}CMe)\text{-}\kappa^2(C2,N_{imine}),\kappa N3\}]$ (**10**) a été formé par déprotonation *in situ* soit de (**1a**) avec $KN(SiMe_3)_2$, soit de ($\mathbf{3a}^+[PF_6]^-$) avec NaO*t*-Bu suivide l'addition de 0.5 équiv. de $[Ir(cod)(\mu\text{-}Cl)]_2$. La réaction de (**10**) avec CO a permis d'isoler $[Ir_2(CO)_4Cl\{\mu\text{-}C_3H_2N_2(DippN{=}CMe)\text{-}\kappa^2(C2,N_{imine}),\kappa N3\}]$ (**11**) (Schéma 7).

Schéma 7.

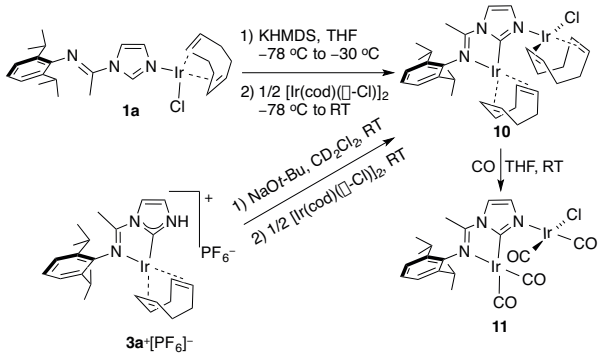

Le complexe hétérodinucléaire $[IrRh(cod)_2Cl\{\mu\text{-}C_3H_2N_2(DippN{=}CMe)\text{-}\kappa^2(C2,N_{imine}),\kappa N3\}]$ (**12**) a été obtenu soit par déprotonation *in situ* de (**1a**) avec $KN(SiMe_3)_2$ suivie de l'addition de 0.5 équiv. de $[Rh(cod)(\mu\text{-}Cl)]_2$, soit par déprotonation de (**1b**) avec $KN(SiMe_3)_2$ suivie de l'addition de 0.5 équiv. de $[Ir(cod)(\mu\text{-}Cl)]_2$ (Schéma 8).

Schéma 8.

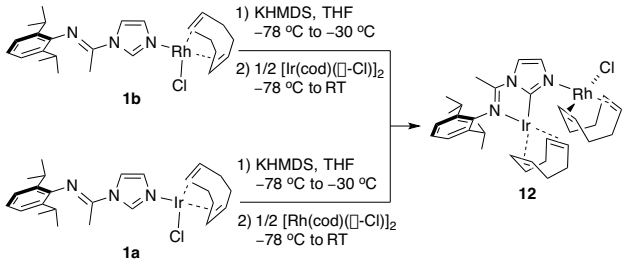

Les structures des complexes (**1b**), ($\mathbf{3b}^+[PF_6]^-$), ($\mathbf{6a}^+[PF_6]^-$), ($\mathbf{7a}^+[PF_6]^-$), ($\mathbf{9}^+[PF_6]^-$), (**10**·Et_2O·toluene), (**11**) et (**12**·2THF) ont été déterminées par radiocristallographie aux rayons X.

Références et synopsis

Homo and heterodinuclear Ir and Rh imine-functionalized protic NHC complexes: synthetic, structural studies and tautomerization/metallotropism insights

Ce chapitre est rédigé comme une version préliminaire d'une publication qui sera soumise prochainement.

He, F.; Wesolek, M.; Danopoulos, A. A.; Braunstein, P., *submitted*.

Ma contribution a porté sur la recherche bibliographique, la partie expérimentale ainsi que la rédaction de la version préliminaire.

References: p 100

Homo and Heterodinuclear Ir and Rh Imine-functionalized Protic NHC Complexes: Synthetic, Structural Studies and Tautomerization/Metallotropism Insights

Fan He,[a] Marcel Wesolek,[a] Andreas A. Danopoulos,*[a, b] and Pierre Braunstein*[a]

Dedication ((optional))

Abstract: The influence of the potentially chelating imino group of imine functionalized Ir and Rh imidazole complexes on the formation of functionalized protic NHC (pNHC) complexes by tautomerization/metallotropism sequences and a number of species involved in the transformation were studied. Chloride abstraction in [Ir(cod)Cl{$C_3H_3N_2$(DippN=CMe)-κN3}] (**1a**) with $TlPF_6$ gave [Ir(cod){$C_3H_3N_2$(DippN=CMe)-κ^2(C2,N_{imine})}]$^+$[PF_6]$^-$ (**3a**$^+$[PF_6]$^-$). However, in the N-bound Ir imidazole complexes [Ir(cod)Cl{$C_3H_3N_2$(R)-κN3}] (**4a/b**: R = *n*-Bu/Mes), (Ir/imidazole = 1:1), analogous chloride abstraction was accompanied by spontaneous ligand transfer to give [Ir(cod){$C_3H_3N_2$(R)-κN3}$_2$]$^+$[PF_6]$^-$ (**5a/b**$^+$[PF_6]$^-$) (Ir/imidazole = 1:2). In contrast to **5a/b**$^+$[PF_6]$^-$, the 2:1 complexes with imine functionalized imidazoles, *i.e.* [Ir(cod){$C_3H_3N_2$(DippN=CMe)-κN3}$_2$]$^+$[PF_6]$^-$ (**6a**$^+$[PF_6]$^-$), were only obtained from **1a** when the chloride abstraction was followed by further addition of 1-(2,6-di*iso*propylphenylimino)ethylimidazole. Plausible mechanisms for the tautomerization of **1a** to **3a**$^+$[PF_6]$^-$ involving C2–H bond activation either in **1a** or in **6a**$^+$[PF_6]$^-$ were postulated. Addition of PR_3 to **3a**$^+$[PF_6]$^-$ afforded the 18 valence electron [Ir(cod)(PR_3){$C_3H_3N_2$(DippN=CMe)-κ^2(C2,N_{imine})}]$^+$[PF_6]$^-$ (**7a/b**$^+$[PF_6]$^-$, R = Ph, Me). Chloride abstraction from [Ir(cod)Cl{C_3HN_2(DippN=CMe)(DippN=CH)(Me)-κN3}] (**8**) led to [Ir(cod){C_3HN_2(DippN=CMe)(DippN=CH)(Me)-κ^2(N3,N_{imine})}]$^+$[PF_6]$^-$ (**9**$^+$[PF_6]$^-$) in which the imino groups is chelated to Ir. In contrast to Ir, chloride abstraction from [Rh(cod)Cl{$C_3H_3N_2$(DippN=CMe)-κN3}] (**1b**) at room temperature afforded [Rh(cod){$C_3H_3N_2$(DippN=CMe)-κN3}$_2$]$^+$[PF_6]$^-$ (**6b**$^+$[PF_6]$^-$) and minor quantities of [Rh(cod){$C_3H_3N_2$(DippN=CMe)-κ^2(C2,N_{imine})}]$^+$[PF_6]$^-$ (**3b**$^+$[PF_6]$^-$); the reaction yielded exclusively latter in toluene at 110 ºC. The homodinuclear complex [Ir_2(cod)$_2$Cl{μ-$C_3H_2N_2$(DippN=CMe)-κ^2(C2,N_{imine}),κN3}] (**10**) was obtained by *in situ* deprotonation of either **1a** with KN($SiMe_3$)$_2$ or **3a**$^+$[PF_6]$^-$ with NaO*t*-Bu, followed by addition of 0.5 equiv. of [Ir(cod)(μ-Cl)]$_2$. Treatment of **10** with CO afforded [Ir_2(CO)$_4$Cl{μ-$C_3H_2N_2$(DippN=CMe)-κ^2(C2,N_{imine}),κN3}] (**11**). The heterodinuclear [IrRh(cod)$_2$Cl{μ-$C_3H_2N_2$(DippN=CMe)-κ^2(C2,N_{imine}),κN3}] (**12**) was isolated by *in situ* deprotonation of either **1a** with KN($SiMe_3$)$_2$ followed by addition of 0.5 equiv. of [Rh(cod)(μ-Cl)]$_2$ or of **1b** with KN($SiMe_3$)$_2$ followed by addition of 0.5 equiv. of [Ir(cod)(μ-Cl)]$_2$. The structures of **1b**, **3b**$^+$[PF_6]$^-$, **6a**$^+$[PF_6]$^-$, **7a**$^+$[PF_6]$^-$, **9**$^+$[PF_6]$^-$, **10**·Et_2O·toluene, **11** and **12**·2THF were determined by X-ray diffraction.

Introduction

Since the isolation of N-heterocyclic carbenes (NHCs),[1] their study and complexation chemistry have generated a rapidly increasing interest.[2] In most of their metal complexes, both N atoms carry substituents R (R = R' or R ≠ R' in **A**) that allow fine-tuning of the steric and electronic properties of the NHC ligands. Protic NHC (pNHC) metal complexes (**B**) are less common. The NH moiety can further be a reactive site, *e.g.* with bases or H-bond acceptors, the latter being relevant to substrate recognition in homogeneous catalysis.[3]

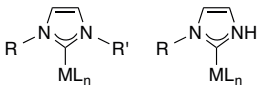

A **B**

pNHCs cannot be generally obtained by simple deprotonation of the corresponding imidazolium salts owing to the presence of sites with acidity comparable to the NH group on the imidazole heterocycle; furthermore, the free pNHCs are not stable and tend to isomerize to the corresponding imidazoles.[4] This has motivated the development of various methods to access pNHC metal complexes, which have been recently summarized and reviewed.[3b,3c,5] The first transition metal complex bearing 1H-imidazol-2-ylidene (R = H in **B**) was obtained by the acid-catalyzed rearrangement of a Ru(II)-imidazole to a Ru(II)-pNHC system (Scheme 1).[6] Recently, the preparation of the parent (benz)imidazole-type pNHC complexes *via* oxidative addition of 2-halogenoazoles to a zerovalent transition metal center was reported by Hahn (Scheme 1).[7]

[a] Dr. F. He, Dr. M. Wesolek, Prof. Dr. A. A. Danopoulos, Prof. Dr. P. Braunstein
Laboratoire de Chimie de Coordination, Institut de Chimie (UMR 7177 CNRS), Université de Strasbourg, 4 rue Blaise Pascal, 67081 Strasbourg Cedex, France
E-mail: braunstein@unistra.fr
[b] Prof. Dr. A. A. Danopoulos
Université de Strasbourg Institute for Advanced Study (USIAS), 4 rue Blaise Pascal, 67081 Strasbourg Cedex, France
E-mail: danopoulos@unistra.fr

Supporting information for this article is available on the WWW under http://dx.doi.org/10.1002/chem.xxxxxx.

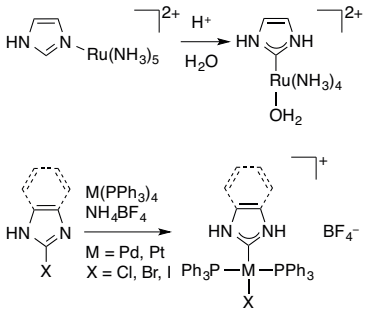

Scheme 1. Examples of transition metal complexes containing 1H-(benz)imidazol-2-ylidenes.[6-7]

The N-substituent (R in **B**) is expected to be crucial for the tuning of the stereoelectronic properties and coordination behavior of the pNHCs, and the stability and catalytic properties of the resulting metal complexes.[8] In most pNHC complexes, the R substituent is an alkyl or an aryl group, but there are relatively few examples where a donor functional group is attached to the N-substituent that could potentially be involved in chelate formation. The number of complexes with functionalized pNHCs is still limited, and some have been found catalytic applications (Scheme 2).

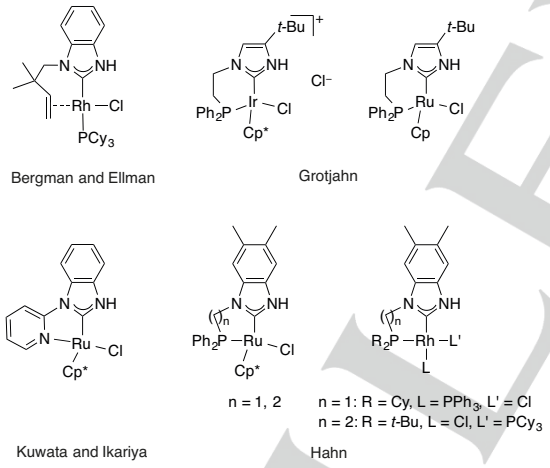

Scheme 2. Transition metal complexes with bidentate functionalized pNHCs.

Thus, Bergman, Ellman and co-workers reported an intramolecular coupling reaction sequence of alkenes to 2-functionalized azole derivatives, in which an alkene-functionalized pNHC Rh(I) complex was isolated as an intermediate (Scheme 2).[9] This intramolecular reaction was extended to an intermolecular coupling reaction.[10] The pyridyl-functionalized pNHC Ru(II) complex reported by Kuwata and Ikariya (Scheme 2) was used as catalyst for the dehydrative condensation of *N*-(2-pyridyl)benzimidazole and allyl alcohol.[11] The phosphorus-functionalized pNHC Ir(III) and Ru(II) complexes reported by Grotjahn (Scheme 2) were developed as catalysts for the activation of dihydrogen and in various transfer hydrogenation reactions.[12] Related phosphorus-functionalized pNHC Ru(II)[13] and Rh(I)[14] complexes have been reported by Hahn, the former revealed intermolecular hydrogen bonding between the N-*H* and the 1,3-dimethyltetrahydropyrimidin-2(1H)-one acting as hydrogen bond acceptor. This property appears to be common and could be utilized for substrate recognition and regioselective catalysis with pNHC complexes.[3b,3c]

In view of the remarkable catalytic properties of α-diimine and pyridine diimine complexes,[15] it appeared attractive to design metal complexes bearing imine-functionalized NHC ligands.[16] The features of the imino-NHCs as hybrid ligands are based on the association of a σ-donor/π-acceptor imine and a strong σ-donor/poor π-acceptor NHC functionalities. It is noteworthy that an imine-functionalized NHC Rh(I) complex shows high activity and *cis*-selectivity in catalytic cyclopropanation of alkenes,[17] and that imine-functionalized pNHC complexes are potentially bifunctional catalysts.[18]

We have recently demonstrated[19] that the reaction of 1-(2,6-di*iso*propylphenylimino)ethylimidazole (H^{C2}**L**)[16f] (where the superscript associated with H indicates its position in the ring) with 0.5 equiv. of $[Ir(cod)(\mu\text{-}Cl)]_2$ afforded $[Ir(cod)Cl\{C_3H_3N_2(DippN{=}CMe)\text{-}\kappa N3\}]$ (**1a**), abbreviated as $Ir(cod)Cl(H^{C2}\mathbf{L}^{N3})$ where $\mathbf{L}^{N3}$ represents a N3-metalated functionalized imidazole (the superscript associated with **L** indicates the site(s) of metalation). Reaction of **1a** with an additional half equivalent of $[Ir(cod)(\mu\text{-}Cl)]_2$, or the direct reaction of H^{C2}**L** with 1.0 equiv. of $[Ir(cod)(\mu\text{-}Cl)]_2$, afforded $[Ir_2(cod)_2HCl_2\{\mu\text{-}C_3H_2N_2(DippN{=}CMe)\text{-}\kappa^2(C2,N_{imine}),\kappa N3\}]$ (**2**), abbreviated as $[Ir_2(cod)_2HCl_2(\mathbf{L}^{C2,Nimine,N3})]$, represents a mixed-valence homodinuclear complex comprising one N-bound Ir(I) center and one C2,N_{imine}-chelated Ir(III) center.

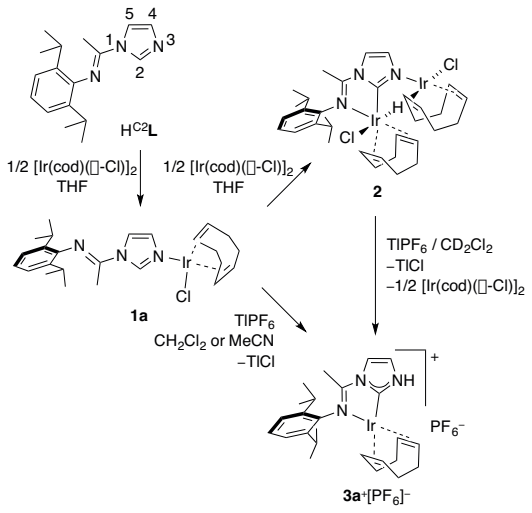

Scheme 3. Tautomerism/metallotropism leading to the pNHC complex $\mathbf{3a}^{+}[PF_6]^{-}$.[19]

The imine-functionalized pNHC Ir(I) complex [Ir(cod){$C_3H_3N_2$(DippN=CMe)-κ^2(C2,N_{imine})}]$^+$[PF_6]$^-$ (**3a**$^+$[PF_6]$^-$), abbreviated as [Ir(cod)(H^{N3}**L**^{C2,Nimine})]$^+$[PF_6]$^-$, was obtained from the reaction of either **1** or **2** with $TlPF_6$ (Scheme 3).[19]

Here we investigate further the synthesis and reactivity of imine-functionalized pNHC iridium complexes by the metalation of the C2–H in N-bonded imidazole iridium complexes, and extend these studies to rhodium and to homo- and hetero-dinuclear complexes.

Results and Discussion

(i) Chelate Assistance of the Imine Functionality in the C2-Metallation of Ir Imidazole Complexes.

In order to examine the influence of the potentially chelating imino group on the reactivity of **1a,** in particular in the course of the chloride abstraction which led to products arising from tautomerization/metallotropism, we prepared the complexes [Ir(cod)Cl{$C_3H_3N_2$(*n*-Bu)-κN3}] (**4a**) and [Ir(cod)Cl{$C_3H_3N_2$(Mes)-κN3}] (**4b**)[20] (Scheme 4), with the N-butyl- and N-mesityl-substituents, respectively.

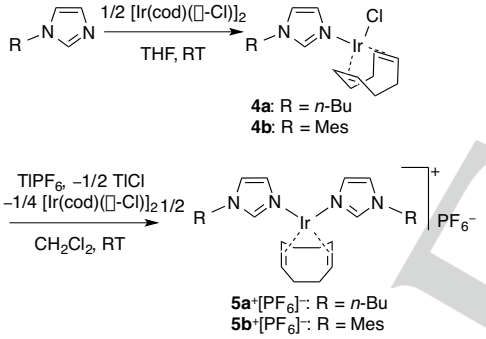

Scheme 4. Synthesis of **4a/b** and **5a/b**$^+$[PF_6]$^-$.

Under conditions similar to those used for the chloride abstraction reaction of **1a**, **4a/b** only afforded the complexes [Ir(cod){$C_3H_3N_2$(R)-κN3}$_2$]$^+$[PF_6]$^-$ (**5a/b**$^+$[PF_6]$^-$: R = *n*-Bu/Mes); this was evidenced by the ratio of the coordinated imidazoles and the 1,5-cyclooctadiene (cod) (2:1) in the ^{1}H NMR spectra. The reaction was accompanied by the formation of [Ir(cod)(μ-Cl)]$_2$ (NMR evidence). These results point to the crucial role of the N-arylimino functional group for the tautomerization/metallotropism manifested by the conversion of the N-bound Ir(I) to Ir(I)-pNHC (Scheme 3).

In comparison, although the formation of [Ir(cod){$C_3H_3N_2$(DippN=CMe)-κN3}$_2$]$^+$[PF_6]$^-$ (**6a**$^+$[PF_6]$^-$), abbreviated as [Ir(cod)(H^{C2}**L**^{N3})$_2$]$^+$[PF_6]$^-$, was observed in the initial stages of the halide abstraction from **1a**, as evidenced by monitoring the reaction of the latter with $TlPF_6$ in CD_2Cl_2 at room temperature by ^{1}H NMR spectroscopy, [Ir(cod)(H^{C2}**L**^{N3})$_2$]$^+$[PF_6]$^-$ (**6a**$^+$[PF_6]$^-$) could not be isolated. Informatively, we show below that **6a**$^+$[PF_6]$^-$ can react further with [Ir(cod)(μ-Cl)]$_2$ to give **3a**$^+$[PF_6]$^-$ (see Scheme 7). In contrast to **5a/b**$^+$[PF_6]$^-$ (Scheme 4), **1a** was fully converted to **3a**$^+$[PF_6]$^-$ at the end of the reaction (Scheme 3). Addition of 1.0 equiv. of H^{C2}**L** was required in order to isolate **6a**$^+$[PF_6]$^-$ (Scheme 5).

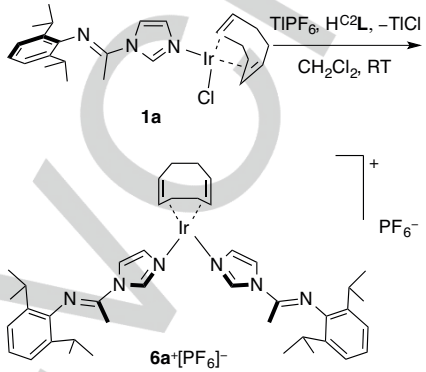

Scheme 5. Synthesis of **6a**$^+$[PF_6]$^-$.

In the ^{1}H NMR spectrum, the 2:1 ratio between the imidazole and the 1,5-cod protons in **6a**$^+$[PF_6]$^-$ is consistent with the molecular structure of **6a**$^+$[PF_6]$^-$ in the solid-state (Figure 1). The 16 valence electron iridium center in **6a**$^+$[PF_6]$^-$ adopts an approximate square-planar coordination geometry, defined by the two olefinic bonds of the 1,5-cod ligand and two nitrogen atoms from the imidazole ligands.

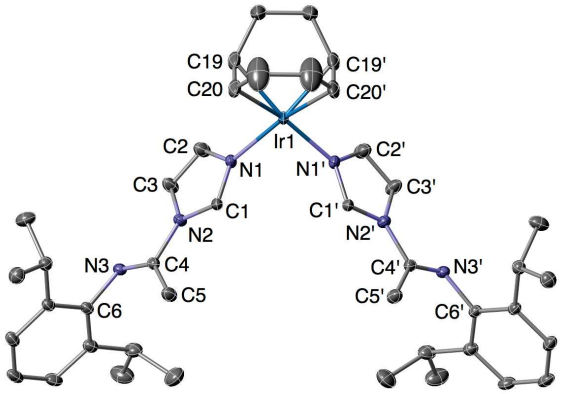

Figure 1. Molecular structure of the cation in **6a**$^+$[PF_6]$^-$. H atoms are omitted for clarity. Thermal ellipsoids are at the 30% level. The crystallographic labels C1 and N1 correspond to the conventional C2 and N3 numbering used in the text. Selected bond distances (Å) and angles (°): C1–N1 1.322(5), C1–N2 1.363(5), C2–N1 1.393(5), C2–C3 1.352(6), C3–N2 1.379(5), C4–N2 1.435(4), C4–N3 1.255(5), C4–C5 1.491(5), C6–N3 1.422(4), Ir1–N1 2.078(3), Ir1–C19 2.125(5), Ir1–C20 2.120(5), C19–C20 1.391(9); N1–C1–N2 110.2(3), N1–Ir1–C19 91.8(2), N1–Ir1–C20 92.3(2), N1–Ir1– N1' 88.3(2).

References: p 100

Complexes with functionalized pNHC ligands, related to **3a**$^+$[PF$_6$]$^-$, and bearing bidentate (benz)imidazolin-2-ylidene/donor ligands, have been obtained by formal tautomerization/metallotropism,[11-13] Hahn proposed the occurrence of a 'redox tautomerization' involving an initial C2–H oxidative addition of azoles followed by reductive elimination of the proton on the metal center.[3b,14,21] In the present case of tautomerization of **1a** to **3a**$^+$[PF$_6$]$^-$, we suggest on the basis of ^{1}H NMR monitoring that complex **2** (Scheme 3) is a reaction intermediate. It was isolated in an separate experiment and can be viewed as the product of C2–H oxidative addition of the N-bound iridium complex **1a** (Scheme 3), requiring the presence of a catalytic amount of [Ir(cod)(μ-Cl)]$_2$. Then, ^{1}H NMR monitoring of the reaction between **2** and TlPF$_6$ in CD_2Cl_2 (Scheme 3) revealed a hydride resonance at δ −14.41, which could be tentatively assigned to the intermediate [**2**−Cl$^-$]$^+$[PF$_6$]$^-$ in Cycle I (*cf.* δ −15.12 in **2**). In a ^{1}H NMR experiment monitoring the chloride abstraction of **1a** with TlPF$_6$ in CD_2Cl_2 at room temperature, the resonances of **6a**$^+$[PF$_6$]$^-$ and of three hydride species were observed in the initial stages of the reaction, in a ratio of *ca.* 1:20:4 at δ −14.41 ([**2**−Cl$^-$]$^+$[PF$_6$]$^-$), −14.99 and −15.12 (**2**) (Figure S1 in ESI), respectively, which progressively disappeared. The hydride species at δ −14.41 ([**2**−Cl$^-$]$^+$[PF$_6$]$^-$) and −15.12 (**2**) are consistent with the suggested steps shown in Cycle I of Scheme 6.

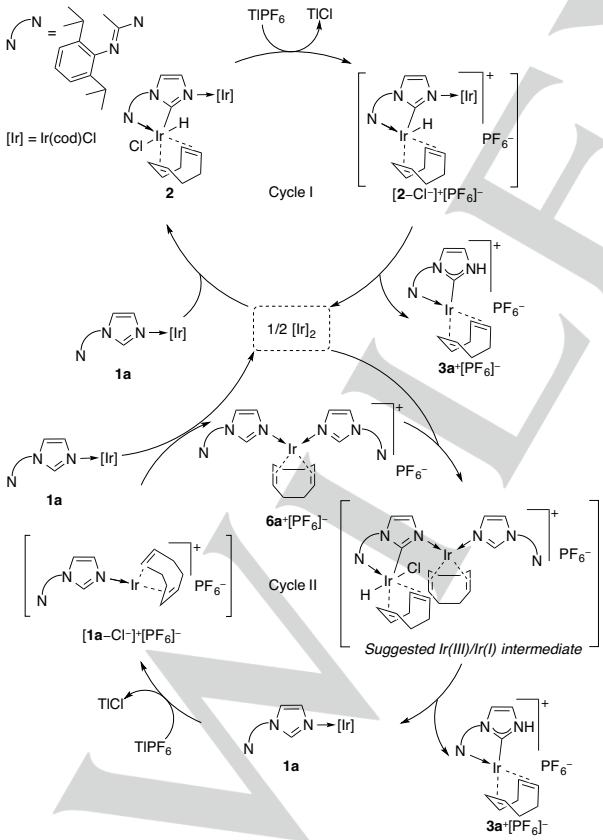

Scheme 6. Proposed mechanism for the tautomerization of **1a** to **3a**$^+$[PF$_6$]$^-$ via a neutral and a cationic Ir(III)/Ir(I) intermediate.

In order to prove that C2–H bond activation can occur on the N3-coordinated imidazole in complexes of type [Ir(cod)(H^{C2}**L**^{N3})$_2$]$^+$ (*cf.* behavior of **4a**/**b** giving **5a**/**b**$^+$, Scheme 4), a reaction between **6a**$^+$[PF$_6$]$^-$ and [Ir(cod)(μ-Cl)]$_2$ in CD_2Cl_2 was monitored by ^{1}H NMR (Scheme 7). Interestingly, we observed the same intermediate hydride species as in the chloride abstraction reaction of **1a** (Figure S2 in ESI). These postulated steps for the tautomerization of **1a** to **3a**$^+$[PF$_6$]$^-$ are summarized in Cycle II of Scheme 6. Furthermore, the observation of **1a** and **3a**$^+$[PF$_6$]$^-$ indicates that **6a**$^+$[PF$_6$]$^-$ is an intermediate in the tautomerization of **1a** to **3a**$^+$[PF$_6$]$^-$ and therefore cannot be isolated by this sequence of steps.

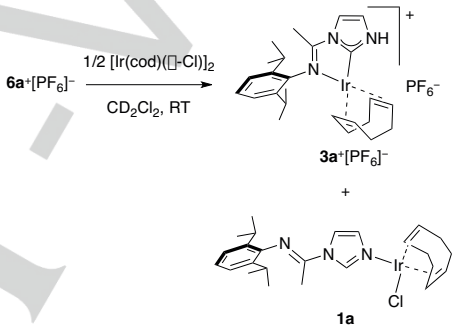

Scheme 7. ^{1}H NMR monitoring of the reaction between **6a**$^+$[PF$_6$]$^-$ and [Ir(cod)(μ-Cl)]$_2$.

The reaction between **1a** and TlPF$_6$ (Cycle II in Scheme 6) would give a reactive Ir species [**1a**−Cl$^-$]$^+$[PF$_6$]$^-$, which could react with **1a** still present to yield **6a**$^+$[PF$_6$]$^-$ by ligand transfer, and [Ir(cod)(μ-Cl)]$_2$. The latter could activate the C2–H bond either of **1a** to give **2** (Cycle I in Scheme 6) or of **6a**$^+$[PF$_6$]$^-$ to give **3a**$^+$[PF$_6$]$^-$ (Scheme 7 and Cycle II in Scheme 6), via a postulated Ir(III)/Ir(I) intermediate, which is supposed to be the hydride species resonating at δ −14.99. Proton transfer from the Ir(III) center to the N3 of the metalated heterocycle with concomitant breaking of the N3–Ir(I) bond would lead to **3a**$^+$[PF$_6$]$^-$ and **1a**, the latter remaining in the cycle until complete conversion to **3a**$^+$[PF$_6$]$^-$. In summary, the species postulated in Cycles I and II point to the different elementary steps that lead to tautomerization (H shift) and "apparent" metallotropism (Ir to N3 shift), the latter formally involving different iridium species.

With the aim to explore the scope of H-shift from N to Ir in pNHC as a way to access valence tautomers, we reacted **3a**$^+$[PF$_6$]$^-$ with phosphine ligands to render the metal center more electron-rich, hoping to favor a transformation from Ir(I) to Ir(III). Addition of triphenylphosphine/trimethylphosphine afforded the 18 valence electron addition products [Ir(cod)(PR$_3$){C$_3$H$_3$N$_2$(DippN=CMe)-κ^2(C2,N$_{imine}$)}]$^+$[PF$_6$]$^-$

(**7a**/**b**$^+$[PF$_6$]$^-$: R = Ph/Me), abbreviated as [Ir(cod)(PR$_3$)(H^{N3}**L**^{C2,Nimine})]$^+$[PF$_6$]$^-$, respectively (Scheme 8).

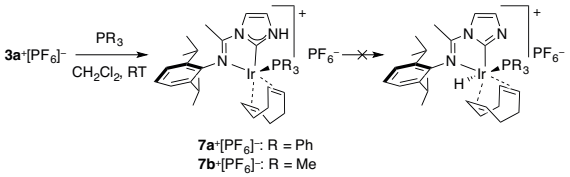

Scheme 8. Synthesis of **7a**/**b**$^+$[PF$_6$]$^-$.

In the ^{31}P{^{1}H} NMR spectrum of **7a**$^+$[PF$_6$]$^-$, the PPh$_3$ ligand gives rise to a singlet at δ −1.9. In **7b**$^+$[PF$_6$]$^-$, a characteristic ^{31}P{^{1}H} NMR singlet at δ −44.8 and the C_{NHC} resonance at δ 171.1 (d, $^2J_{P\text{-}C}$ = 10.9 Hz) in the ^{13}C{^{1}H} NMR spectrum suggest that coordination of the PMe$_3$ ligand occurs in *cis* position to the C_{NHC}. In the structure of **7a**$^+$[PF$_6$]$^-$ (Figure 2), the iridium center adopts a distorted trigonal-bipyramidal coordination geometry, with C1 and the C22–C23 double bond in the apical positions.[22] The Ir1–C1 bond length in **7a**$^+$[PF$_6$]$^-$ (1.982(2) Å) is similar to that in **3a**$^+$[PF$_6$]$^-$ (1.984(3) Å), but the Ir1–N3 bond in **7a**$^+$[PF$_6$]$^-$ is considerably longer than the corresponding bond in **3a**$^+$[PF$_6$]$^-$ (2.347(2) Å *vs.* 2.115(3) Å), which is consistent with the respective electron counts of the metals and the steric hindrance in **7a**$^+$. The closest N−H···F(PF$_5$) distance of 2.21(3) Å is consistent with a hydrogen bonding interaction. Although as expected, phosphine coordination has taken place in the reactions of Scheme 8, a transformation from Ir(I) to Ir(III) species was not observed in these reactions, in contrast to findings involving a 1,9-phenanthroline-derived pNHC system.[22c] The stability of **7a**/**b**$^+$[PF$_6$]$^-$ is consistent with their 18 valence electron count.

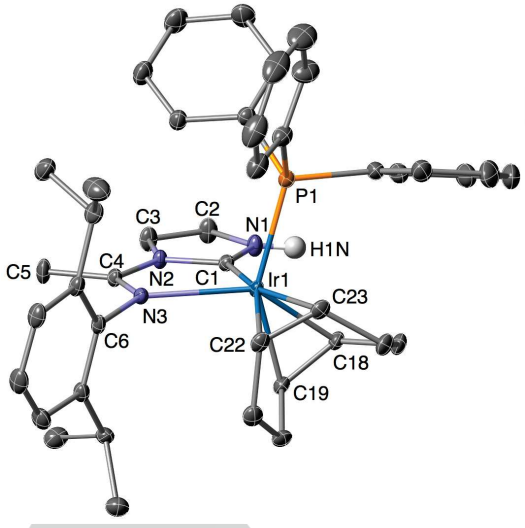

Figure 2. Molecular structure of the cation in **7a**$^+$[PF$_6$]$^-$. H atoms are omitted for clarity, except H1N. Thermal ellipsoids are at the 30% level. Selected bond distances (Å) and angles (°): C1–N1 1.345(2), C1–N2 1.371(2), C2–N1 1.388(3), C2–C3 1.337(3), C3–N2 1.402(2), C4–N2 1.402(2), C4–N3 1.284(2), C4–C5 1.495(3), C6–N3 1.453(2), Ir1–P1 2.3388(5), Ir1–C1 1.982(2), Ir1–N3 2.347(2), Ir1–C18 2.118(2), Ir1–C19 2.142(2), Ir1–C22 2.220(2), Ir1–C23 2.269(2), C18–C19 1.445(3), C22–C23 1.390(3), N1–H1N 0.82(3); N1–C1–N2 104.0(2), C1–Ir1–N3 73.61(6), C1–Ir1–P1 89.59(5), C1–Ir1–C18 89.36(7), C1–Ir1–C19 90.85(8), N3–Ir1–P1 108.63(4).

To further study the possible contribution of the imino group on the tautomerization/metallotropism, ligand H^{C2}**L'**, a derivative of H^{C2}**L**, was designed in which the carbon atoms C5 and C4 of the heterocycle are substituted by methyl and imino groups in order to prevent the formation of abnormal NHC complexes and provide chelate assistance by imine coordination, respectively. Reaction of H^{C2}**L'** with [Ir(cod)(μ-Cl)]$_2$ led to the formation of [Ir(cod)Cl{C$_3$HN$_2$(DippN=CMe)(DippN=CH)(Me)-κN3}] (**8**), abbreviated as [Ir(cod)Cl(H^{C2}**L'**^{N3})] (Scheme 9).

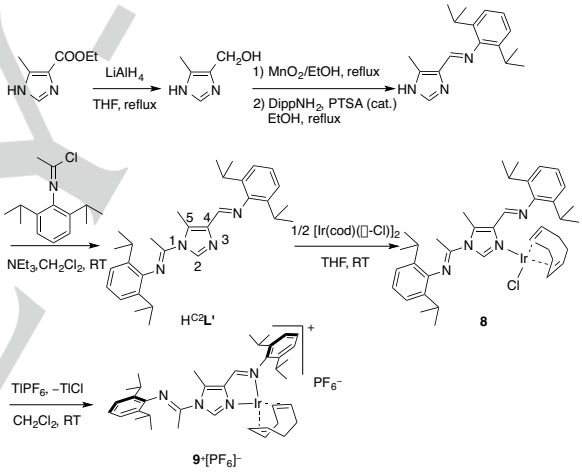

Scheme 9. Synthesis of H^{C2}**L'**, **8** and **9**$^+$[PF$_6$]$^-$.

Abstraction of the chloride ligand from **8** in CH_2Cl_2 did not lead to 'Ir migration' from N to C2, but to rapid chelation of the proximal imino group to give {C$_3$HN$_2$(DippN=CMe)(DippN=CH)(Me)-κ^2(N3,N$_{imine}$)}]$^+$[PF$_6$]$^-$ (**9**$^+$[PF$_6$]$^-$), abbreviated as [Ir(cod) [Ir(cod)(H^{C2}**L'**^{N3,Nimine})]$^+$[PF$_6$]$^-$, the structure of which was confirmed crystallographically (Figure 5). In contrast to **1a** which can lead to the dinuclear Ir(III)/Ir(I) complex **2** (Scheme 3), **9**$^+$[PF$_6$]$^-$ does not react further with [Ir(cod)(μ-Cl)]$_2$, possibly for steric reasons, the orientation of the Ir(cod) moiety being locked owing to N,N chelation.

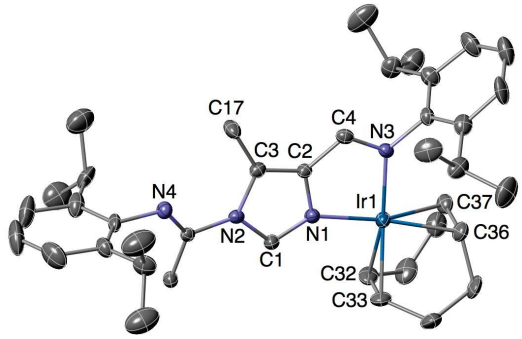

Figure 3. Molecular structure of the cation in **9**$^{+}$[PF_6]$^{-}$. H atoms are omitted for clarity. Thermal ellipsoids are at the 30% level. Selected bond distances (Å) and angles (°): C1–N1 1.31(1), C1–N2 1.38(1), C2–N1 1.394(9), C2–C3 1.37(1), C3–N2 1.41(1), C4–N3 1.31(1), Ir1–N1 2.083(7), Ir1–N3 2.094(6), Ir1–C32 2.154(9), Ir1–C33 2.137(8), Ir1–C36 2.110(9), Ir1–C37 2.123(9), C32–C33 1.43(2), C36–C37 1.38(1); N1–C1–N2 111.1(7), N1–Ir1–N3 78.9(3), N1–Ir1–C32 98.6(3), N1–Ir1–C33 94.2(3), N3–Ir1–C36 97.5(3), N3–Ir1– C37 93.6(3).

(ii) Synthesis of Imine-Functionalized pNHC Rh(I) Complexes.

Similarly to **1a**, the reaction of H^{C2}**L** with 0.5 equiv. of [Rh(cod)(μ-Cl)]$_2$ in THF gave [Rh(cod)Cl{$C_3H_3N_2$(DippN=CMe)-κN3}] (**1b**), abbreviated as [Rh(cod)Cl(H^{C2}**L**^{N3})], in nearly quantitative yield (Scheme 10).

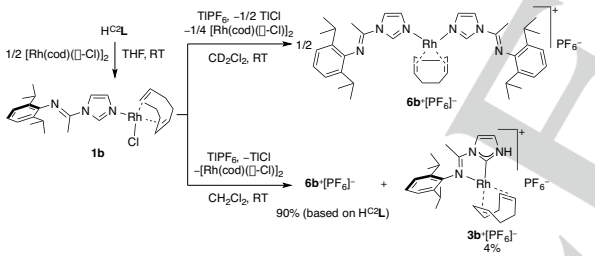

Scheme 10. Synthesis of the Rh(I) complexes **1b**, **3b**$^{+}$[PF_6]$^{-}$ and **6b**$^{+}$[PF_6]$^{-}$.

In the ^{1}H NMR spectrum of **1b** in CD_2Cl_2, the C2–*H* exhibits a broad singlet at δ 8.73 (*cf.* δ 8.11 in H^{C2}**L**). The molecular structure of **1b** is shown in Figure 4.

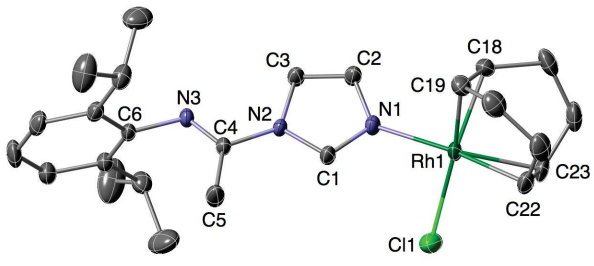

Figure 4. Molecular structure of **1b**. H atoms are omitted for clarity. Thermal ellipsoids are at the 30% level. Selected bond distances (Å) and angles (°): C1–N1 1.315(2), C1–N2 1.359(2), C2–N1 1.383(2), C2–C3 1.355(2), C3–N2 1.381(2), C4–N2 1.428(2), C4–N3 1.260(2), C4–C5 1.496(2), C6–N3 1.428(2), Rh1–N1 2.104(1), Rh1–Cl1 2.3748(5), Rh1–C18 2.120(2), Rh1–C19 2.101(2), Rh1–C22 2.143(2), Rh1–C23 2.127(2), C18–C19 1.399(3), C22–C23 1.396(3); N1–C1–N2 111.1(1), N1–Rh1–Cl1 88.36(4), N1–Rh1–C18 93.69(6), N1–Rh1–C19 90.02(6), Cl1–Rh1–C22 92.20(6), Cl1–Rh1–C23 91.16(6).

Defined by the two double bonds of the 1,5-cod ligand, one nitrogen atom of the imidazole and one terminal chloride ligand, the rhodium center adopts a distorted square planar geometry, as evidenced by the bond angles at Rh *viz.* N1–Rh1–Cl1 88.36(4), N1–Rh1–C18/C19 93.69(6)/90.02(6), Cl1–Rh1–C22/C23 92.20(6)/91.16(6). This is consistent with the IR absorption band at 1685 cm^{-1} assigned to *ν*(C=N) of the dangling imino functionality and the ^{13}C{^{1}H} NMR signal at δ 149.0 assigned to *C*=N.

Inspired by the conversion of **1a** to **3a**$^{+}$[PF_6]$^{-}$, we investigated analogous reactivity with the rhodium complex **1b**. In a ^{1}H NMR monitoring experiment, the reaction of **1b** with 1.0 equiv. of $TlPF_6$ in CD_2Cl_2 at room temperature gave a white precipitate of TlCl and a yellow solution, which (by ^{1}H NMR) contained half one equivalent of a new rhodium species [Rh(cod){$C_3H_3N_2$(DippN=CMe)-κN3}$_2$]$^{+}$[PF_6]$^{-}$ (**6b**$^{+}$[PF_6]$^{-}$), abbreviated as [Rh(cod)(H^{C2}**L**^{N3})$_2$]$^{+}$[PF_6]$^{-}$, and 0.25 equivalent of [Rh(cod)(μ-Cl)]$_2$ resulting from a ligand transfer reaction, but no pNHC Rh complex was detected (Scheme 8). However, when this experiment was repeated on a larger scale in dichloromethane at room temperature, the color of the solution slightly turned to red and the pNHC Rh(I) complex [Rh(cod){$C_3H_3N_2$(DippN=CMe)-κ^2(C2,N$_{imine}$)}]$^{+}$[PF_6]$^{-}$ (**3b**$^{+}$[PF_6]$^{-}$), abbreviated as [Rh(cod)(H^{N3}**L**^{C2,Nimine})]$^{+}$[PF_6]$^{-}$, was isolated in 4% yield as dark red crystals by fractional crystallization (see Experimental Section). The low yield partly explains why **3b**$^{+}$[PF_6]$^{-}$ had not been observed in the ^{1}H NMR experiment. From the supernatant solution, **6b**$^{+}$[PF_6]$^{-}$ was isolated as a pale yellow powder in good yield (90% based on H^{C2}**L**). The ^{1}H NMR data of **6b**$^{+}$[PF_6]$^{-}$ in CD_2Cl_2 established the ratio of the imidazole and the 1,5-cod ligands to be 2:1 and the upfield shift by 0.31 ppm (compared to **1b)** of the resonance of the C2–*H* proton at δ 8.42. In the ^{13}C{H} NMR spectrum, the resonance at δ 137.0 was assigned to the *C*2–H. The IR *ν*(C=N) band for a dangling imine group in **6b**$^{+}$[PF_6]$^{-}$ was observed at 1687 cm^{-1}.

In the ^{1}H NMR spectrum of **3b**$^{+}$[PF_6]$^{-}$ in CD_2Cl_2, the N*H* proton appears as a broad singlet at δ 10.31 and the ^{13}C{^{1}H} NMR spectrum contains resonances for *C*2$_{NHC}$ and *C*$_{imine}$ at δ 176.9 (d, $^{1}J_{Rh-C}$ = 55.1 Hz) and δ 163.7, respectively (*cf.* δ 138.6 and 149.0 in **1b**). The IR absorptions at 3405 and 1627 cm^{-1} can be assigned to N–H[19,22c,23] and coordinated C=N stretching, respectively. All these data indicate that **3b**$^{+}$[PF_6]$^{-}$ is a κ^2(C2,N$_{imine}$) chelated imino-NHC rhodium complex, which was further confirmed crystallographically (Figure 5).

References: p 100

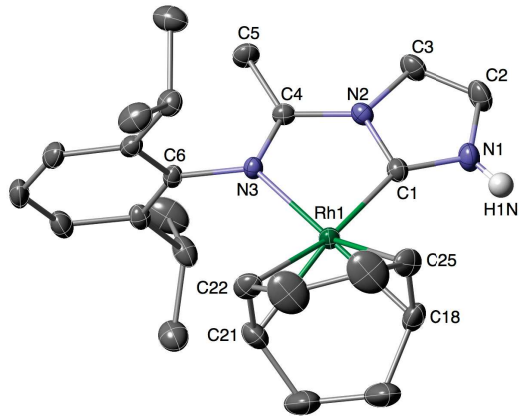

Figure 5. Molecular structure of the cation in **3b**$^+$[PF_6]$^-$. H atoms are omitted for clarity, except H1N. Thermal ellipsoids are at the 30% level. Selected bond distances (Å) and angles (°): C1–N1 1.342(4), C1–N2 1.369(4), C2–N1 1.380(4), C2–C3 1.340(5), C3–N2 1.392(3), C4–N2 1.399(3), C4–N3 1.287(3), C4–C5 1.484(4), C6–N3 1.444(3), Rh1–C1 1.972(3), Rh1–N3 2.125(2), Rh1–C18 2.137(3), Rh1–C21 2.239(3), Rh1–C22 2.256(3), Rh1–C25 2.122(3), C18–C25 1.390(5), C21–C22 1.345(5), N1–H1N 0.82(4); N1–C1–N2 103.0(2), C1–Rh1–N3 77.7(1), C1–Rh1–C18 95.9(1), C1–Rh1–C25 94.8(1), N3–Rh1–C21 100.6(1), N3–Rh1–C22 97.9(1).

In the structure of **3b**$^+$[PF_6]$^-$, the square-planar coordination geometry around the metal center, which is defined by the κ^2(C2,N_{imine}) five membered ring chelate and the two olefinic bonds of the 1,5-cod ligand, is strongly distorted, with an acute C1–Rh1–N3 angle of 77.7(1)°. In agreement with the lower *trans* influence of the imino group compared to the NHC donor, the Rh1–C18/C25 (2.137(3)/2.122(3) Å) bond distances are shorter than Rh1–C21/C22 (2.239(3)/2.256(3) Å) and, consistently, the C18–C25 double bond (1.390(5) Å) is slightly longer than C21–C22 (1.345(5) Å), owing to increased back-bonding from the metal. The Rh–C_{NHC} bond distance of 1.972(3) Å is similar to that found in the κ^2(C2,N_{imine}) chelated imino-NHC rhodium complex with a N-methyl substituent (1.99(1) Å).[17b] Owing to the coordination of the N_{imine} atom to the Rh atom, the C4–N3 bond in **3b**$^+$[PF_6]$^-$ (1.287(3) Å) is longer than that in **1b** (1.260(2) Å), while the C4–N2 bond in **3b**$^+$[PF_6]$^-$ (1.399(3) Å) is shorter than that in **1b** (1.428(2) Å). As expected from the decreased π-delocalization over the azole ring, the bond distances of C1−N1/N2 in **3b**$^+$[PF_6]$^-$ (1.342(4)/1.369(4) Å) are longer than those in **1b** (1.321(2)/1.359(2) Å). As a result, the N1−C1−N2 bond angle in **3b**$^+$[PF_6]$^-$ (103.0(2)°) is also significantly less obtuse than that in **1b** (111.1(1)°). The shortest N−H···F(PF_5) distances of 2.43(4) and 2.49(4) Å are consistent with H-bonding interactions.

In an attempt to improve the yield of **3b**$^+$[PF_6]$^-$, we used toluene as the reaction solvent. In a ^{1}H NMR experiment in toluene-d_8 at room temperature, the reaction of **1b** with 1.0 equiv. of $TlPF_6$ was found to give the same products as in CD_2Cl_2. However, after heating the reaction mixture to 110 °C for 12 h, the yellow solution became colorless and a red precipitate was formed. The ^{1}H NMR spectroscopic data of the solution indicated complete consumption of **6b**$^+$[PF_6]$^-$ and [Rh(cod)(μ-Cl)]$_2$. The red precipitate was isolated by filtration and extracted in CD_2Cl_2 giving pure **3b**$^+$[PF_6]$^-$in solution and white precipitate of TlCl. Repeating the reaction on a larger scale led to the isolation of **3b**$^+$[PF_6]$^-$ in 90% yield (Scheme 11).

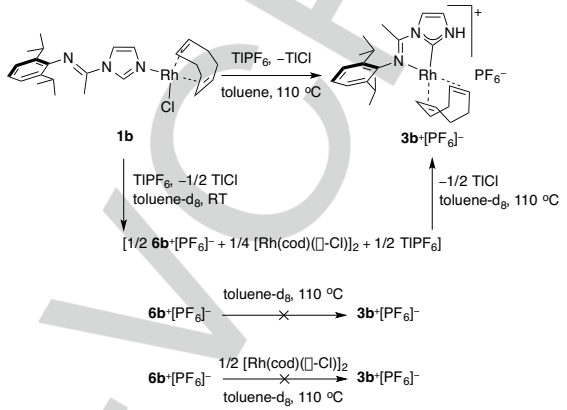

Scheme 11. Improved synthesis of **3b**$^+$[PF_6]$^-$.

When a solution of **6b**$^+$[PF_6]$^-$, in the presence or not of 0.5 equiv. of [Rh(cod)(μ-Cl)]$_2$, was heated at 110 °C for more than 24 h, no **3b**$^+$[PF_6]$^-$ was observed but only a slight decomposition of **6b**$^+$[PF_6]$^-$ occurred (Scheme 11). These results suggest that **6b**$^+$[PF_6]$^-$ is an intermediate in the synthesis of **3b**$^+$[PF_6]$^-$ only in the presence of both [Rh(cod)(μ-Cl)]$_2$ and $TlPF_6$ (*cf.* corresponding Ir complexes described above).

The tautomerization of **1b** to **3b**$^+$[PF_6]$^-$ may apparently proceed in a similar way to the conversion of **1a** to **3a**$^+$[PF_6]$^-$, but a different mechanism may be operative since Rh−H species were not detected in situ by ^{1}H NMR, although this may be attributable to the poor solubility of the cationic hydride species in toluene-d_8.

(iii) Homo and Heterodinuclear Ir and Rh Complexes.

To expand the scope and the reactivity of complexes **1a** and **3a**$^+$[PF_6]$^-$, we considered using them as precursors to dinuclear complexes. The *in situ* deprotonation of **1a** by potassium bis(trimethylsilyl)amide (KHMDS) in THF at −30 ºC initially gave a red solution; after addition of 0.5 equiv. of [Ir(cod)(μ-Cl)]$_2$ the dark green [Ir$_2$(cod)$_2$Cl{μ-$C_3H_2N_2$(DippN=CMe)-κ^2(C2,N_{imine}),κN3}] (**10**), abbreviated as [Ir$_2$(cod)$_2$Cl(**L**^{C2,Nimine,N3})], was isolated (Scheme 12).

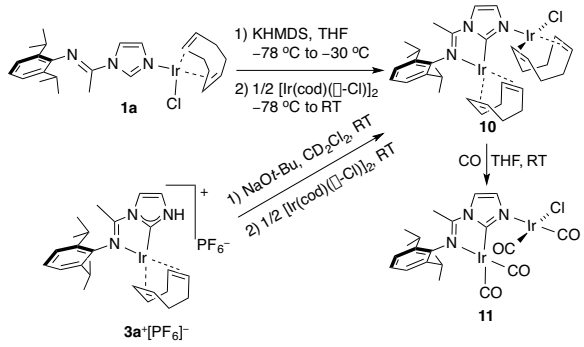

Scheme 12. Synthesis of the dinuclear Ir(I) complexes **10** and **11**.

An IR absorption band at 1577 cm^{-1} for the C=N stretching and the $^{13}C\{^1H\}$ NMR resonance due to *C*=N (δ 166.0) support the coordination of the N_{imine} to the cationic Ir(I) in **10**. In addition, the disappearance of a C2–*H* in the ^1H NMR spectrum of **10** (C_6D_6), and the appearance of a signal at δ 180.6 in the $^{13}C\{^1H\}$ NMR spectrum, confirmed the formation of an Ir–C_{NHC} bond.

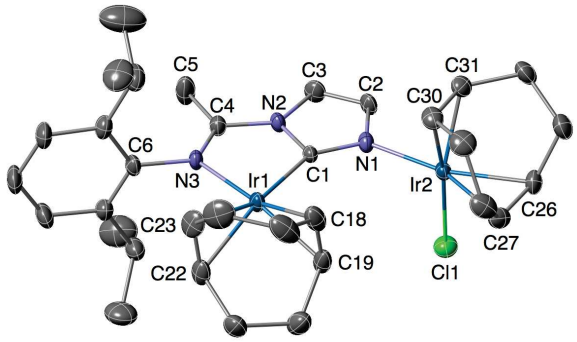

Figure 6. Molecular structure of **10**·Et_2O·toluene. H atoms and the solvent molecules are omitted for clarity. Thermal ellipsoids are at the 30% level. Selected bond distances (Å) and angles (°): C1–N1 1.335(6), C1–N2 1.397(7), C2–N1 1.391(7), C2–C3 1.342(8), C3–N2 1.387(7), C4–N2 1.382(6), C4–N3 1.289(7), C4–C5 1.486(8), C6–N3 1.454(6), Ir1–C1 2.041(5), Ir1–N3 2.112(4), Ir1–C18 2.137(6), Ir1–C19 2.118(6), Ir1–C22 2.185(5), Ir1–C23 2.184(5), C18–C19 1.400(9), C22–C23 1.380(9), Ir2–Cl1 2.367(1), Ir2–C26 2.149(5), Ir2–C27 2.111(6), Ir2–C30 2.113(5), Ir2–C31 2.099(5), C26–C27 1.396(8), C30–C31 1.418(8); N1–C1–N2 105.9(4), C1–Ir1–N3 78.3(2), C1–Ir1–C18 100.2(2), C1–Ir1–C19 95.8(2), N3–Ir1–C22 98.4(2), N3–Ir1–C23 94.3(2), N1–Ir2–Cl1 88.1(1), N1–Ir2–C30 93.4(2), N1–Ir2–C31 91.0(2), Cl1–Ir2–C26 92.3(2), Cl1–Ir2–C27 91.6(2).

The structure of **10**·Et_2O·toluene (Figure 6) revealed a dinuclear complex comprising one N-bound Ir(I) center and one κ^2(C2,N_{imine}) chelated Ir(I) center (*cf.* the κ^2(C2,N_{imine}) chelation of the Ir(III) center in **2**). Both iridium centers adopt distorted square-planar coordination geometries. In a ^1H NMR experiment performed in CD_2Cl_2, **10** was alternatively synthesized from the reaction of **3a**$^+$[PF_6]$^-$ with 1.0 equiv. of NaO*t*-Bu (which led to an equilibrium between a mononuclear neutral complex containing a C-bound 'anionic' imidazolide and its dimer in which the imidazolide binds in a μ-C,N bridging mode)[19] followed by the addition of 0.5 equiv. of [Ir(cod)(μ-Cl)]$_2$. The yield (by ^1H NMR spectroscopy) is higher than 80%.

The two cod ligands in **10** were readily replaced by CO at room temperature to afford the red [Ir_2(CO)$_4$Cl{μ-$C_3H_2N_2$(DippN=CMe)-κ^2(C2,N_{imine}),κN3}] (**11**), abbreviated as [Ir_2(CO)$_4$Cl(**L**^{C2,Nimine,N3})]. Its IR spectrum showed two strong *v*(CO) bands at 2054 (s) and 1971 (vbr), consistent with a mutually *cis* disposition of the CO ligands, which was further confirmed crystallographically (Figure 7).

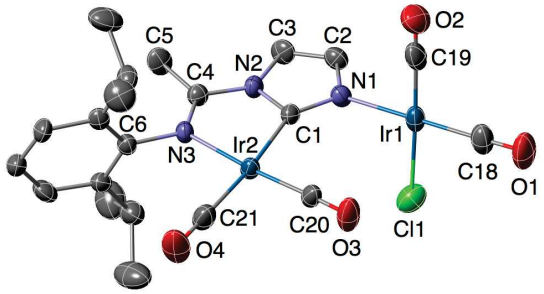

Figure 7. Molecular structure of **11**. Thermal ellipsoids are at the 30% level. Selected bond distances (Å) and angles (°): C1–N1 1.336(9), C1–N2 1.391(9), C2–N1 1.386(9), C2–C3 1.35(1), C3–N2 1.392(8), C4–N2 1.378(9), C4–N3 1.302(9), C4–C5 1.47(1), C6–N3 1.443(8), C1–Ir2 2.052(7), N3–Ir2 2.097(6), C20–Ir2 1.838(8), C21–Ir2 1.907(8), N1–Ir1 2.074(6), Cl1–Ir1 2.339(2), C18–Ir1 1.848(9), C19–Ir1 1.85(1), C18–O1 1.15(1), C19–O2 1.14(1), C20–O3 1.148(9), C21–O4 1.131(9); N1–C1–N2 106.6(6), C1–Ir2–N3 77.5(2), C1–Ir2–C20 97.6(3), C20–Ir2–C21 89.9(3), C21–Ir2–N3 95.0(3); N1–Ir1–Cl1 86.6(2); N1–Ir1–C19 91.8(3); C18–Ir1–C19 88.9(4); C18–Ir1–Cl1 92.7(3).

Unexpectedly, both the *in situ* deprotonation of **1b** by KHMDS followed by the addition of 0.5 equiv. of [Ir(cod)(μ-Cl)]$_2$ and the *in situ* deprotonation of **1a** by KHMDS followed by the addition of 0.5 equiv. of [Rh(cod)(μ-Cl)]$_2$ afforded the same heterodinuclear complex [IrRh(cod)$_2$Cl{μ-$C_3H_2N_2$(DippN=CMe)-κ^2(C2,N_{imine}),κN3}] (**12**), abbreviated as [IrRh(cod)$_2$Cl(**L**^{C2,Nimine,N3})], in 60% and 51% yield, respectively (Scheme 13).

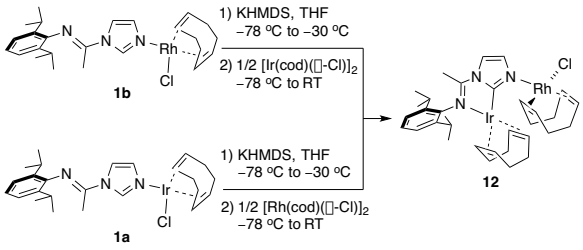

Scheme 13. Synthesis of **12**.

References: p 100

In the $^{13}C\{^1H\}$ NMR spectrum of **12**, a characteristic singlet at δ 179.8 was assigned to the C_{NHC} carbon. The structure of **12**·2THF (Figure 8) revealed a dinuclear complex comprising one N-bound Rh(I) center and one κ^2(C2,N_{imine}) chelated Ir(I) center. Both metals adopted distorted square-planar coordination geometries. The reactions shown in Scheme 14 clearly indicate that the formation of the Ir–C bond represent a thermodynamic driving force.

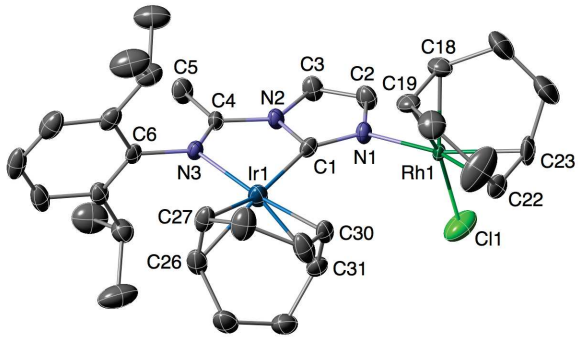

Figure 8. Molecular structure **12** in **12**·2THF. H atoms and the solvent molecules are omitted for clarity. Thermal ellipsoids are at the 30% level. Selected bond distances (Å) and angles (°): C1–N1 1.331(7), C1–N2 1.418(7), C2–N1 1.392(8), C2–C3 1.349(9), C3–N2 1.387(7), C4–N2 1.381(7), C4–N3 1.303(7), C4–C5 1.480(8), C6–N3 1.434(7), Ir1–C1 2.004(6), Ir1–N3 2.111(4), Ir1–C26 2.202(6), Ir1–C27 2.189(6), Ir1–C30 2.140(5), Ir1–C31 2.113(6), C26–C27 1.38(1), C30–C31 1.39(1), Rh1–N1 2.079(5), Rh1–Cl1 2.371(2), Rh1–C18 2.091(6), Rh1–C19 2.113(6), Rh1–C22 2.134(6), Rh1–C23 2.127(6), C18–C19 1.407(9), C22–C23 1.38(1); N1–C1–N2 105.0(5), C1–Ir1–N3 78.4(2), C1–Ir1–C30 98.4(2), C1–Ir1–C31 95.0(2), N3–Ir1–C26 95.7(2), N3–Ir1–C27 99.7(2), N1–Rh1–Cl1 88.4 (2), N1–Rh1–C18 90.3(2), N1–Rh1–C19 91.2(2), Cl1–Rh1–C22 94.1(2), Cl1–Rh1–C23 90.5(3).

A comparative ^1H NMR experiment was performed with either **1a** and 0.5 equiv. of [Rh(cod)(μ-Cl)]$_2$ or **1b** with 0.5 equiv. of [Ir(cod)(μ-Cl)]$_2$ in CD_2Cl_2 at room temperature, in the absence of KHMDS. A mixture of **1a**, **1b** and **2** in 3:1:1 ratio was obtained, indicating the occurrence of competing reactions (Scheme 14).

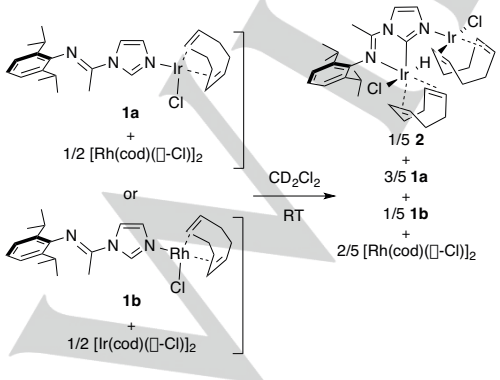

Scheme 14. ^1H NMR monitoring of the reactions between **1a** and [Rh(cod)(μ-Cl)]$_2$, **1b** and [Ir(cod)(μ-Cl)]$_2$ in the absence of KHMDS.

The reaction between **1a** and 0.5 equiv. of [Rh(cod)(μ-Cl)]$_2$ could be viewed as a two-step process (Scheme 14), the first step would be partial N-bound metal exchange, liberating some [Ir(cod)(μ-Cl)]$_2$ that could react in a second step with **1a** to give **2** as a result of the C2–H bond activation. Starting from **1b** and [Ir(cod)(μ-Cl)]$_2$ metal exchange is thermodynamically favored and the resulting **1a** reacts then with [Ir(cod)(μ-Cl)]$_2$ as described above. Somewhat surprisingly, C2–H bond activation of **1b** by [Ir(cod)(μ-Cl)]$_2$ to give a κ^2(C2,N_{imine})Ir^{III},κ(N3)Rh^{I} complex was never observed.

Conclusions

A comparative study between Ir(I) and Rh(I) using imine-functionalized imidazoles as potential precursors to functionalized pNHC complexes, has revealed details of the mechanistic steps prior and during the C2–H metallation that leads to the pNHC complexes. In the case of iridium, the observation of Ir–H intermediates by ^1H NMR is consistent with the involvement of the (isolable) $N_{imidazole}$–Ir complex precursors undergoing tautomerization/metallotropism, followed by a chelate assisted C2–H bond activation in a neutral and a cationic intermediate. In the case of rhodium, C2-metallation proceeded only under forcing conditions at higher temperatures and intermediates analogous to those observed for Ir remained elusive. A new Rh(I)-Ir(I) heterodinuclear complex was obtained in a stepwise manner, which allowed the chemoselectivity of the synthetic approach to be investigated and understood. The κ^2(C2,N_{imine})Ir^{I},κ(N3)Rh^{I} complex was selectively isolated, either starting from the N-bound Ir or from the N-bound Rh precursor. These results are in agreement with the preferred formation of strong, inert Ir–C bonds and can rationalize the carbophilic migration of the iridium (from **1a** to **10**, Scheme 13). It is anticipated that the results described above could be useful for the further development of synthetic methodologies to pNHC, C-bound 'anionic' imidazolide, and relevant homo and heterodinuclear complexes.

Experimental Section

General Considerations. All manipulations involving organometallics were performed under argon in a Braun glove-box or using standard Schlenk techniques. Solvents were dried using standard methods and distilled over sodium/benzophenone under argon prior use or passed through columns of activated alumina and subsequently purged with argon. [Ir(cod)(μ-Cl)]$_2$ is commercially available from Johnson Matthey PLC. [Rh(cod)(μ-Cl)]$_2$,[24] 1-(2,6-di*iso*propylphenylimino)ethylimidazole (H^{C2}**L**),[16f] 4(5)-carbethoxy-5(4)-methylimidazole,[25] N-(2,6-diisopropylphenyl)acetimidoyl chloride,[16f] complexes **1a**,[19] **2**,[19] **3a**$^+$[PF_6]$^-$[19] and **4b**[20] were prepared according to the literature. NMR spectra of organic compounds and complexes were recorded on a Bruker 300 MHz, 400 MHz or 500 MHz instrument

at ambient temperature and referenced using the proton (^{1}H) or carbon (^{13}C) resonance of the residual solvent. Assignments are based on ^{1}H, ^{1}H-COSY, ^{1}H-NOESY, ^{1}H/^{13}C-HSQC, and ^{1}H/^{13}C-HMBC experiments. ^{31}P{^{1}H} NMR spectra were recorded on a Bruker Avance 300 instrument at 121.49 MHz using H_3PO_4 (85% in D_2O) as external standard. IR spectra were recorded in the region 4000–100 cm^{-1} on a Nicolet 6700 FT-IR spectrometer (ATR mode, diamond crystal). Elemental analyses were performed by the "Service de microanalyses", Université de Strasbourg.

Synthesis of 4(5)-methyl-5(4)-hydroxymethylimidazole. To a stirred suspension of 4(5)-carbethoxy-5(4)-methylimidazole (1.54 g, 10.00 mmol) in THF (100 mL) at 0 ºC was added slowly lithium aluminium hydride (1.00 g, 26.35 mmol). The reaction mixture was heated to reflux for 4 h and then quenched by 1 mL of H_2O, 1 mL of 15% NaOH solution and 3 mL of H_2O at 0 ºC. After an appropriate amount of sodium sulfate was added to the mixture, it was further stirred for 30 min. The resultant solution was filtered through Celite and the filtrate was evaporated under reduced pressure to yield a white solid (1.00 g, 8.92 mmol, 89%).

Synthesis of 4(5)-methyl-5(4)-(2,6-di*iso*propylphenylimino) methylimidazole. To a stirred solution of 4(5)-methyl-5(4)-hydroxymethylimidazole (0.56 g, 5.00 mmol) in EtOH (50 mL) was added MnO_2 (0.87 g, 10.00 mmol). The reaction mixture was heated to reflux for 12 h. After filtration through Celite, 2,6-diisopropylaniline (0.89 g, 5.00 mmol) and a catalytic amount of 4-methylbenzenesulfonic acid were added to the filtrate. The reaction mixture was further heated to reflux for 6 h. After the solvent was evaporated under reduced pressure, the residue was washed with petroleum ether (3 × 3 mL) and dried under vacuum to give a white powder (0.68 g, 2.52 mmol, 50%). ^{1}H NMR (500 MHz, $CDCl_3$): δ 11.90 (br s, 1H, N*H*), 8.13 (s, 1H, N=C*H*), 7.19 (m, 3H, C*H*$_{(Dipp)}$), 6.75 (br s, 1H, NC*H*NH), 3.00 (sept, ^3J = 6.9 Hz, 2H, C*H*$(CH_3)_2$), 2.36 (s, 3H, C$H_{3(imidazole)}$), 1.12 (d, ^3J = 6.9 Hz, 12H, CH(C$H_3)_2$). ^{13}C{^{1}H} NMR (125 MHz, $CDCl_3$): δ 151.3 (N=*C*H), 147.9 (*C*$_{(Dipp)}$), 144.2 (br s, *C*$_{(imidazole)}$), 138.8 (*C*$_{(Dipp)}$), 138.3 (N*C*HNH), 125.5 (br s, *C*$_{(imidazole)}$), 125.3 (*C*H$_{(Dipp)}$), 123.6 (*C*H$_{(Dipp)}$), 28.1 (*C*H$(CH_3)_2$), 23.7 (CH(*C*$H_3)_2$), 12.7 (*C*$H_{3(imidazole)}$). IR: ν_{max} (pure, orbit diamond)/cm^{-1} 1637 ν(C=N). Anal. Calcd for $C_{17}H_{23}N_3$ (269.39): C, 75.80; H, 8.61; N, 15.60. Found: C, 75.41; H, 8.64; N, 15.93.

Synthesis of 1-(2,6-di*iso*propylphenylimino)ethyl-4- (2,6-di*iso*propylphenylimino)methyl-5-methylimidazole ($H^{C2}L'$). To a stirred solution of 4(5)-methyl-5(4)-(2,6-di*iso*propylphenylimino) methylimidazole (1.00 g, 3.71 mmol) and triethylamine (1.0 mL, 7.17 mmol) in CH_2Cl_2 (10 mL) was added N-(2,6-diisopropylphenyl) acetimidoyl chloride (0.88 g, 3.71 mmol). The reaction mixture was stirred for 12 h at room temperature. After removal of the volatiles under reduced pressure, the residue was extracted with Et_2O and the solution was filtered through Celite. The filtrate was evaporated under reduced pressure. Then the residue was washed with pentane (3 × 1 mL) and dried under vacuum to give a yellow powder (1.57 g, 3.34 mmol, 90%). ^{1}H NMR (500 MHz, $CDCl_3$): δ 8.68 (s, 1H, N=C*H*), 8.00 (s, 1H, NC*H*N$_{(near\ imine)}$), 7.23–7.00 (m, 6H, C*H*$_{(Dipp)}$), 3.00 (sept, ^3J = 6.9 Hz, 2H, C*H*$(CH_3)_2$), 2.79 (sept, ^3J = 6.9 Hz, 2H, C*H*$(CH_3)_2$), 2.61 (s, 3H, C$H_{3(imidazole)}$), 2.28 (s, 3H, C$H_{3(imine)}$), 1.12 (d, ^3J = 6.9 Hz, 18H, CH(C$H_3)_2$), 1.05 (d, ^3J = 6.9 Hz, 6H, CH(C$H_3)_2$). ^{13}C{^{1}H} NMR (125 MHz, $CDCl_3$): δ 153.2 (N=*C*H), 152.3 (N=*C*CH$_3$), 149.9 (*C*$_{(Dipp)}$), 146.9 (*C*$_{(imidazole)}$), 142.5 (*C*$_{(Dipp)}$), 137.9 (N*C*HN$_{(near\ imine)}$), 137.7 (*C*$_{(Dipp)}$), 136.8 (*C*$_{(Dipp)}$), 125.2 (*C*$_{(imidazole)}$), 124.7 (*C*H$_{(Dipp)}$), 124.1 (*C*H$_{(Dipp)}$), 123.4 (*C*H$_{(Dipp)}$), 123.0 (*C*H$_{(Dipp)}$), 28.4 (*C*H$(CH_3)_2$), 27.9 (*C*H$(CH_3)_2$), 23.7 (CH(*C*$H_3)_2$), 23.5 (CH(*C*$H_3)_2$), 23.2 (CH(*C*$H_3)_2$), 19.1 (*C*$H_{3(imine)}$), 15.0 (*C*$H_{3(imidazole)}$). IR: ν_{max} (pure, orbit diamond)/cm^{-1} 1670 ν(C=N). Anal. Calcd for $C_{31}H_{42}N_4$ (470.71): C, 79.10; H, 8.99; N, 11.90. Found: C, 78.67; H, 8.94; N, 12.33.

Synthesis of [Rh(cod)Cl($H^{C2}L^{N3}$)] (1b). A solution of 1-(2,6-diisopropylphenylimino)ethylimidazole (0.054 g, 0.20 mmol) in THF (2 mL) was added to a stirred solution of [Rh(cod)(μ-Cl)]$_2$ (0.050 g, 0.10 mmol) in THF (3 mL). The reaction mixture was stirred for 1 h at room temperature and then the solvent was removed under reduced pressure. The residue was washed with pentane (3 × 1 mL) and dried under vacuum to give a yellow solid (0.093 g, 0.18 mmol, 90%). Single crystals of **1b** suitable for X-ray diffraction were obtained by slow evaporation of a saturated solution of **1b** in Et_2O at ambient temperature. ^{1}H NMR (500 MHz, CD_2Cl_2): δ 8.72 (s, 1H, NC*H*N$_{(near\ imine)}$), 7.80 (apparent t, $^{3,4}J$ = 1.5 Hz, 1H, NCHC*H*N$_{(near\ imine)}$), 7.20–7.09 (m, 3H, C*H*$_{(Dipp)}$), 6.95 (apparent t, $^{3,4}J$ = 1.5 Hz, 1H, NC*H*CHN$_{(near\ imine)}$), 4.80–3.70 (an overlap of two br s, 4H, C*H*$_{(cod)}$), 2.68 (sept, ^3J = 6.9 Hz, 2H, C*H*$(CH_3)_2$), 2.48 (m, 4H, C*H*$_{2(cod)}$), 2.17 (s, 3H, C*H*$_{3(imine)}$), 1.85 (m, 4H, C*H*$_{2(cod)}$), 1.14 (d, ^3J = 6.9 Hz, 6H, CH(C$H_3)_2$), 1.10 (d, ^3J = 6.9 Hz, 6H, CH(C$H_3)_2$). ^{13}C{^{1}H} NMR (125 MHz, CD_2Cl_2): δ 149.0 (*C*=N), 142.2 (*ipso*-*C*$_{(Dipp)}$), 138.6 (N*C*HN$_{(near\ imine)}$), 137.2 (*o*-*C*$_{(Dipp)}$), 127.9 (N*C*HC*H*N$_{(near\ imine)}$), 125.0 (*p*-*C*H$_{(Dipp)}$), 123.7 (*m*-*C*H$_{(Dipp)}$), 117.0 (NCHC*H*N$_{(near\ imine)}$), 83.0 (br, *C*H$_{(cod)}$), 76.2 (br, *C*H$_{(cod)}$), 31.2 (br, *C*H$_{2(cod)}$), 28.7 (*C*H$(CH_3)_2$), 23.3 (CH(*C*$H_3)_2$), 23.0 (CH(*C*$H_3)_2$), 16.4 (*C*$H_{3(imine)}$). IR: ν_{max} (pure, orbit diamond)/cm^{-1} 1687 ν(C=N) and 280 ν(Rh–Cl). Anal. Calcd for $C_{25}H_{35}ClN_3Rh$ (515.92): C, 58.20; H, 6.84; N, 8.14. Found: C, 58.18; H, 6.77; N, 8.27.

Synthesis of [Rh(cod)($H^{N3}L^{C2,Nimine}$)]$^+$[PF_6]$^-$ (3b$^+$[PF_6]$^-$) and [Rh(cod)($H^{C2}L^{N3}$)$_2$]$^+$[PF_6]$^-$ (6b$^+$[PF_6]$^-$). To a stirred solution of **1b** (0.103 g, 0.20 mmol) in CH_2Cl_2 (5 mL) was added $TlPF_6$ (0.070 g, 0.20 mmol). The reaction mixture was stirred for 12 h at room temperature. After filtration through Celite, the filtrate was concentrated under reduced pressure to *ca.* 2 mL and then was stratified with Et_2O to yield **3b**$^+$[PF_6]$^-$ as dark red crystals, which were collected by filtration and dried in vacuo (0.005 g, 0.008 mmol, 4%). ^{1}H NMR (500 MHz, CD_2Cl_2): δ 10.31 (br s, 1H, N*H*), 7.36–7.25 (m, 4H, NHCHC*H*N$_{(near\ imine)}$ and C*H*$_{(Dipp)}$), 7.23 (apparent t, ^3J = 2.3 Hz, 1H, NHC*H*CHN$_{(near\ imine)}$), 4.64 (m, 2H, C*H*$_{(cod)}$), 4.23 (m, 2H, C*H*$_{(cod)}$), 3.10 (sept, ^3J = 6.8 Hz, 2H, C*H*$(CH_3)_2$), 2.44–2.32 (m, 5H, C*H*$_{2(cod)}$ and C*H*$_{3(imine)}$), 2.29–2.17 (m, 4H, C*H*$_{2(cod)}$), 2.12–2.00 (m, 2H, C*H*$_{2(cod)}$), 1.37 (d, ^3J = 6.8 Hz, 6H, CH(C$H_3)_2$), 1.13 (d, ^3J = 6.8 Hz, 6H, CH(C$H_3)_2$). ^{13}C{^{1}H} NMR (125 MHz, CD_2Cl_2): δ 176.9 (d, $^1J_{Rh\text{-}C}$ = 55.1 Hz, NHC*N*$_{(near\ imine)}$), 163.7 (*C*=N), 140.6 (*o*-*C*$_{(Dipp)}$), 138.7 (*ipso*-*C*$_{(Dipp)}$), 128.5 (*p*-*C*H$_{(Dipp)}$), 124.9 (*m*-*C*H$_{(Dipp)}$), 121.4 (NHC*H*C*H*N$_{(near\ imine)}$), 116.1 (NHC*H*C*H*N$_{(near\ imine)}$), 105.6 (d, $^1J_{Rh\text{-}C}$ = 6.8 Hz, *C*H$_{(cod)}$), 78.9 (d, $^1J_{Rh\text{-}C}$ = 12.6 Hz, *C*H$_{(cod)}$), 32.0 (*C*H$_{2(cod)}$), 29.0 (*C*H$_{2(cod)}$), 28.9 (*C*H$(CH_3)_2$), 25.0 (CH(*C*$H_3)_2$), 23.3 (CH(*C*$H_3)_2$), 16.3 (*C*$H_{3(imine)}$). ^{31}P{^{1}H} NMR (121.5 MHz, CD_2Cl_2): δ −144.1 (sept, $^1J_{P\text{-}F}$ = 712 Hz, *P*F_6^-). ^{19}F{^{1}H} NMR (282.4 MHz, CD_2Cl_2): δ −73.5 (d, $^1J_{P\text{-}F}$ = 712 Hz, P*F*$_6^-$). IR: ν_{max} (pure, orbit diamond)/cm^{-1} 3405 ν(N-H), 1627 ν(C=N) and 827 ν(P–F). Anal. Calcd for $C_{25}H_{35}F_6RhN_3P$ (625.45): C, 48.01; H, 5.64; N, 6.72. Found: C, 47.92; H, 5.65; N, 6.71.

The above filtrate was further concentrated under reduced pressure to *ca.* 2 mL. A yellow precipitate was formed after 5 mL of pentane was added to the solution. The precipitate was filtered, washed with pentane (2 × 3 mL) and dried under vacuum to give **6b**$^+$[PF_6]$^-$ as a pale yellow powder (0.081 g, 0.090 mmol, 90% (based on **L**)). ^{1}H NMR (500 MHz, CD_2Cl_2): δ 8.42 (br s, 2H, NC*H*N$_{(near\ imine)}$), 7.80 (s, 2H, NCHC*H*N$_{(near\ imine)}$), 7.23–7.09 (m, 6H, C*H*$_{(Dipp)}$), 7.04 (s, 2H, NC*H*CHN$_{(near\ imine)}$), 4.24 (br s, 4H, C*H*$_{(cod)}$), 2.67 (sept, ^3J = 6.7 Hz, 4H, C*H*$(CH_3)_2$), 2.57 (m, 4H, C*H*$_{2(cod)}$), 2.19 (s, 6H, C*H*$_{3(imine)}$), 1.94 (m, 4H, C*H*$_{2(cod)}$), 1.14 (d, ^3J = 6.7 Hz, 12H, CH(C$H_3)_2$), 1.09 (d, ^3J = 6.7 Hz, 12H, CH(C$H_3)_2$). ^{13}C{^{1}H} NMR (125 MHz, CD_2Cl_2): δ 149.2 (*C*=N),

142.2 (*ipso*-$C_{(Dipp)}$), 137.2 (*o*-$C_{(Dipp)}$), 137.0 (NCHN$_{(near\ imine)}$), 129.0 (NCHCHN$_{(near\ imine)}$), 125.1 (*p*-$CH_{(Dipp)}$), 123.7 (*m*-$CH_{(Dipp)}$), 117.6 (NCHCHN$_{(near\ imine)}$), 83.8 (br, $CH_{(cod)}$), 31.1 ($CH_{2(cod)}$), 28.7 ($CH(CH_3)_2$), 23.3 ($CH(CH_3)_2$), 22.9 ($CH(CH_3)_2$), 16.3 ($CH_{3(imine)}$). $^{31}P\{^1H\}$ NMR (121.5 MHz, CD_2Cl_2): δ −144.3 (sept, $^1J_{P\text{-}F}$ = 712 Hz, PF_6^-). $^{19}F\{^1H\}$ NMR (282.4 MHz, CD_2Cl_2): δ −73.4 (d, $^1J_{P\text{-}F}$ = 712 Hz, PF_6^-). IR: ν_{max} (pure, orbit diamond)/cm^{-1} 1685 ν(C=N) and 840 ν(P–F). Anal. Calcd for $C_{42}H_{58}F_6N_6PRh$ (894.84): C, 56.37; H, 6.53; N, 9.39. Found: C, 56.90; H, 6.75; N, 9.74.

Improved synthesis of [Rh(cod)($H^{N3}L^{C2,Nimine}$)]$^+[PF_6]^-$ (3b$^+[PF_6]^-$). To a stirred solution of **1b** (0.044 g, 0.086 mmol) in toluene (2 mL) was added $TlPF_6$ (0.030 g, 0.086 mmol). The reaction mixture was stirred for 12 h at 110 °C. The resulting red precipitate was collected by filtration and dissolved in CH_2Cl_2 (3 mL). After filtration through Celite, the filtrate was evaporated under reduced pressure to yield a dark red crystalline solid (0.048 g, 0.077 mmol, 90%).

Synthesis of [Ir(cod)Cl{$C_3H_3N_2$(*n*-Bu)-*κ*N3}] (4a). A solution of 1-*n*-butylimidazole (0.019 g, 0.15 mmol) in THF (2 mL) was added to a stirred solution of [Ir(cod)(μ-Cl)]$_2$ (0.050 g, 0.074 mmol) in THF (3 mL). The reaction mixture was stirred for 1 h at room temperature and then the solvent was removed in vacuo. The residue was washed with pentane (3 × 1 mL) and dried under vacuum to give a yellow solid (0.062 g, 0.13 mmol, 90%). ^1H NMR (500 MHz, CD_2Cl_2): δ 8.08 (br s, 1H, NC*H*N$_{(n\text{-}Bu)}$), 7.01 (s, 1H, NC*H*CHN$_{(n\text{-}Bu)}$), 6.96 (s, 1H, NCHC*H*N$_{(n\text{-}Bu)}$), 3.94 (t, ^3J = 7.4 Hz, 2H, NCH_2CH$_2$CH$_2$CH$_3$), 3.89 (br s, 4H, C$H_{(cod)}$), 2.22 (m, 4H, C$H_{2(cod)}$), 1.75 (quint, ^3J = 7.4 Hz, 2H, NCH$_2$CH_2CH$_2$CH$_3$), 1.54 (m, 4H, C$H_{2(cod)}$), 1.31 (sext, ^3J = 7.4 Hz, 2H, NCH$_2$CH$_2$CH_2CH$_3$), 0.92 (t, ^3J = 7.4 Hz, 3H, NCH$_2$CH$_2$CH$_2$CH_3). $^{13}C\{^1H\}$ NMR (125 MHz, CD_2Cl_2): δ 139.1 (*N*CHN$_{(n\text{-}Bu)}$), 127.2 (*N*CHCHN$_{(n\text{-}Bu)}$), 119.8 (NCH*C*HN$_{(n\text{-}Bu)}$), 62.5 (br, *C*H$_{(cod)}$), 48.1 (*N*CH$_2$CH$_2$CH$_2$CH$_3$), 33.0 (NCH$_2$*C*H$_2$CH$_2$CH$_3$), 31.8 (*C*H$_{2(cod)}$), 20.0 (NCH$_2$CH$_2$*C*H$_2$CH$_3$), 13.6 (NCH$_2$CH$_2$CH$_2$*C*H$_3$). Anal. Calcd for $C_{15}H_{24}ClIrN_2$ (460.04): C, 39.16; H, 5.26; N, 6.09. Found: C, 38.64; H, 5.43; N, 6.55.

Synthesis of [Ir(cod){$C_3H_3N_2$(*n*-Bu)-*κ*N3}$_2$]$^+[PF_6]^-$ (5a$^+[PF_6]^-$). To a stirred solution of **4a** (0.046 g, 0.10 mmol) in CH_2Cl_2 (5 mL) was added $TlPF_6$ (0.035 g, 0.10 mmol). The reaction mixture was stirred for 12 h at room temperature. After filtration through Celite, the filtrate was evaporated to dryness under reduced pressure. The residue was washed with Et_2O (3 × 1 mL) and dried under vacuum to give a yellow solid (0.028 g, 0.041 mmol, 82%). ^1H NMR (500 MHz, CD_2Cl_2): δ 7.42 (s, 2H, NC*H*N$_{(n\text{-}Bu)}$), 7.07 (s, 2H, NC*H*CHN$_{(n\text{-}Bu)}$), 6.81 (s, 2H, NCHC*H*N$_{(n\text{-}Bu)}$), 3.99 (t, ^3J = 7.4 Hz, 4H, NCH_2CH$_2$CH$_2$CH$_3$), 3.83 (br s, 4H, C$H_{(cod)}$), 2.33 (m, 4H, C$H_{2(cod)}$), 1.73 (m, 8H, NCH$_2$CH_2CH$_2$CH$_3$ and C$H_{2(cod)}$), 1.27 (sext, ^3J = 7.4 Hz, 4H, NCH$_2$CH$_2$CH_2CH$_3$), 0.91 (t, ^3J = 7.4 Hz, 6H, NCH$_2$CH$_2$CH$_2$CH_3). $^{13}C\{^1H\}$ NMR (125 MHz, CD_2Cl_2): δ 138.0 (*N*CHN$_{(n\text{-}Bu)}$), 127.9 (*N*CHCHN$_{(n\text{-}Bu)}$), 121.2 (NCH*C*HN$_{(n\text{-}Bu)}$), 67.2 (*C*H$_{(cod)}$), 48.6 (*N*CH$_2$CH$_2$CH$_2$CH$_3$), 32.7 (NCH$_2$*C*H$_2$CH$_2$CH$_3$), 31.6 (*C*H$_{2(cod)}$), 19.9 (NCH$_2$CH$_2$*C*H$_2$CH$_3$), 13.6 (NCH$_2$CH$_2$CH$_2$*C*H$_3$). $^{31}P\{^1H\}$ NMR (121.5 MHz, CD_2Cl_2): δ −144.4 (sept, $^1J_{P\text{-}F}$ = 712 Hz, PF_6^-). $^{19}F\{^1H\}$ NMR (282.4 MHz, CD_2Cl_2): δ −73.4 (d, $^1J_{P\text{-}F}$ = 712 Hz, PF_6^-). Anal. Calcd for $C_{22}H_{36}F_6IrN_4P$ (693.74): C, 38.09; H, 5.23; N, 8.08. Found: C, 37.61; H, 5.70; N, 8.55.

Synthesis of [Ir(cod){$C_3H_3N_2$(Mes)-*κ*N3}$_2$]$^+[PF_6]^-$ (5b$^+[PF_6]^-$). To a stirred solution of **4b** (0.052 g, 0.10 mmol) in CH_2Cl_2 (5 mL) was added $TlPF_6$ (0.035 g, 0.10 mmol). The reaction mixture was stirred for 12 h at room temperature. After filtration through Celite, the filtrate was evaporated to dryness under reduced pressure. The residue was washed with with Et_2O (3 × 1 mL) and dried under vacuum to give a yellow solid (0.038 g, 0.046 mmol, 92%). ^1H NMR (500 MHz, CD_2Cl_2): δ 7.52 (apparent t, ^4J = 1.3 Hz, 2H, NC*H*N$_{(Mes)}$), 7.11 (apparent t, $^{3,4}J$ = 1.3 Hz, 1H, NC*H*CHN$_{(Mes)}$), 7.07 (apparent t, $^{3,4}J$ = 1.3 Hz, 2H, NCHC*H*N$_{(Mes)}$), 7.02 (s, 4H, *m*-C*H*$_{(Mes)}$), 3.93 (m, 4H, C*H*$_{(cod)}$), 2.39 (m, 4H, C$H_{2(cod)}$), 2.34 (s, 6H, *p*-C$H_{3(Mes)}$), 1.92 (s, 12H, *o*-C$H_{3(Mes)}$), 1.81 (m, 4H, C$H_{2(cod)}$). $^{13}C\{^1H\}$ NMR (125 MHz, CD_2Cl_2): δ 141.0 (*p*-$C_{(Mes)}$), 138.4 (*N*CHN$_{(Mes)}$), 134.9 (*o*-$C_{(Mes)}$), 131.9 (*ipso*-$C_{(Mes)}$), 129.8 (*m*-$CH_{(Mes)}$), 128.5 (NCHCHN$_{(Mes)}$), 123.1 (NCH*C*HN$_{(Mes)}$), 68.2 (*C*H$_{(cod)}$), 31.7 (*C*H$_{2(cod)}$), 21.2 (*p*-C$H_{3(Mes)}$), 17.4 (*o*-C$H_{3(Mes)}$). $^{31}P\{^1H\}$ NMR (121.5 MHz, CD_2Cl_2): δ −144.5 (sept, $^1J_{P\text{-}F}$ = 712 Hz, PF_6^-). $^{19}F\{^1H\}$ NMR (282.4 MHz, CD_2Cl_2): δ −73.4 (d, $^1J_{P\text{-}F}$ = 712 Hz, PF_6^-). Anal. Calcd for $C_{32}H_{40}F_6IrN_4P$ (817.88): C, 46.99; H, 4.93; N, 6.85. Found: C, 47.07; H, 4.60; N, 7.24.

Synthesis of [Ir(cod)($H^{C2}L^{N3}$)$_2$]$^+[PF_6]^-$ (6a$^+[PF_6]^-$). To a stirred solution of **1a** (0.030 g, 0.050 mmol) and 1-(2,6-diiospropylphenylimino) ethylimidazole (0.014 g, 0.052 mmol) in CH_2Cl_2 (2 mL) was added $TlPF_6$ (0.018 g, 0.052 mmol). The reaction mixture was stirred for 2 h at room temperature. After filtration through Celite, the filtrate was evaporated to dryness under reduced pressure. The residue was washed with Et_2O (3 × 1 mL) and dried under vacuum to give a yellow powder (0.045 g, 0.046 mmol, 92%). Single crystals of **6a**$^+[PF_6]^-$ suitable for X-ray diffraction were obtained by slow evaporation of a saturated solution in Et_2O at ambient temperature. ^1H NMR (500 MHz, CD_2Cl_2): δ 8.41 (s, 2H, NC*H*N$_{(near\ imine)}$), 7.91 (s, 2H, NCHC*H*N$_{(near\ imine)}$), 7.20–7.07 (m, 8H, C*H*$_{(Dipp)}$ and NC*H*CHN$_{(near\ imine)}$), 3.98 (br s, 4H, C*H*$_{(cod)}$), 2.67 (sept, ^3J = 6.9 Hz, 4H, C*H*(CH$_3$)$_2$), 2.43 (m, 4H, C$H_{2(cod)}$), 2.22 (s, 6H, C$H_{3(imine)}$), 1.83 (m, 4H, C$H_{2(cod)}$), 1.14 (d, ^3J = 6.9 Hz, 12H, CH(CH_3)$_2$), 1.08 (d, ^3J = 6.9 Hz, 12H, CH(CH_3)$_2$). $^{13}C\{^1H\}$ NMR (125 MHz, CD_2Cl_2): δ 149.2 (*C*=N), 141.9 (*ipso*-$C_{(Dipp)}$), 137.1 (*o*-$C_{(Dipp)}$), 136.7 (*N*CHN$_{(near\ imine)}$), 129.0 (*N*CHCHN$_{(near\ imine)}$), 125.3 (*p*-C$H_{(Dipp)}$), 123.7 (*m*-C$H_{(Dipp)}$), 118.4 (NCH*C*HN$_{(near\ imine)}$), 68.9 (*C*H$_{(cod)}$), 31.7 (*C*H$_{2(cod)}$), 28.7 (*C*H(CH$_3$)$_2$), 23.4 (CH(*C*H$_3$)$_2$), 22.9 (CH(*C*H$_3$)$_2$), 16.2 (*C*H$_{3(imine)}$). $^{31}P\{^1H\}$ NMR (121.5 MHz, CD_2Cl_2): δ −144.4 (sept, $^1J_{P\text{-}F}$ = 712 Hz, PF_6^-). $^{19}F\{^1H\}$ NMR (282.4 MHz, CD_2Cl_2): δ −73.4 (d, $^1J_{P\text{-}F}$ = 712 Hz, PF_6^-). IR: ν_{max} (pure, orbit diamond)/cm^{-1} 1687 ν(C=N) and 833 ν(P–F). Anal. Calcd for $C_{42}H_{58}F_6N_6PIr$ (984.15): C, 51.26; H, 5.94; N, 8.54. Found: C, 50.81; H, 5.93; N, 8.44.

Synthesis of [Ir(cod)(PPh$_3$)($H^{N3}L^{C2,Nimine}$)]$^+[PF_6]^-$ (7a$^+[PF_6]^-$). To a stirred solution of **3a**$^+[PF_6]^-$ (0.040 g, 0.056 mmol) in CH_2Cl_2 (3 mL) was added a solution of PPh_3 (0.015 g, 0.057 mmol) in CH_2Cl_2 (2 mL). The reaction mixture was stirred for 1 h at room temperature. After it was concentrated under reduced pressure to *ca.* 2 mL, the solution was stratified with Et_2O to yield after diffusion green crystals, which were collected by filtration and dried in vacuo (0.046 g, 0.047 mmol, 84%). ^1H NMR (500 MHz, CD_2Cl_2): δ 9.69 (br s, 1H, N*H*), 7.53–7.26 (m, 12H, C*H*$_{(Ar)}$), 7.22 (apparent t, ^3J = 2.3 Hz, 1H, NHCHC*H*N$_{(near\ imine)}$), 7.06 (br s, 6H, C*H*$_{(Ar)}$), 6.99 (apparent t, ^3J = 2.3 Hz, 1H, NHC*H*CHN$_{(near\ imine)}$), 5.10–4.00 (br s, 2H, C*H*$_{(cod)}$), 4.00–3.20 (br s, 2H, C*H*$_{(cod)}$), 2.75 (br s, , 2H, C*H*(CH$_3$)$_2$), 2.37 (s, 3H, C$H_{3(imine)}$), 1.89 (br s, 4H, C$H_{2(cod)}$), 1.71 (br s, 4H, C$H_{2(cod)}$), 1.48–0.56 (br s, 12H, CH(CH_3)$_2$). $^{13}C\{^1H\}$ NMR (125 MHz, CD_2Cl_2): δ 173.8 (NHC*N*$_{(near\ imine)}$), 158.7 (br, *C*=N), 141.7 (*C*$_{(Dipp)}$), 141.2 (br, *C*$_{(Dipp)}$), 134.7 (d, $^1J_{P\text{-}C}$ = 39.4 Hz, *ipso*-$C_{(PPh3)}$), 133.1 (d, $J_{P\text{-}C}$ = 5.3 Hz, *C*H$_{(PPh3)}$), 130.5 (*C*H$_{(PPh3)}$), 129.2 (d, $J_{P\text{-}C}$ = 9.1 Hz, *C*H$_{(PPh3)}$), 127.9 (*C*H$_{(Dipp)}$), 125.0 (br, *C*H$_{(Dipp)}$), 122.0 (NH*C*HCHN$_{(near\ imine)}$), 117.0 (NHCH*C*HN$_{(near\ imine)}$), 88.7 (br, *C*H$_{(cod)}$), 30.1 (*C*H$_{2(cod)}$), 28.4 (br, *C*H(CH$_3$)$_2$), 25.3 (CH(*C*H$_3$)$_2$), 24.2 (br, CH(*C*H$_3$)$_2$), 19.3 (*C*H$_{3(imine)}$). $^{31}P\{^1H\}$ NMR (121.5 MHz, CD_2Cl_2): δ −1.9 (s, *P*Ph$_3$), −144.1 (sept, $^1J_{P\text{-}F}$ = 712 Hz, PF_6^-). $^{19}F\{^1H\}$ NMR (282.4 MHz, CD_2Cl_2): δ −73.5 (d, $^1J_{P\text{-}F}$ = 712 Hz, PF_6^-). IR: ν_{max} (pure, orbit diamond)/cm^{-1} 3390 ν(N-H), 1617 ν(C=N) and 839 ν(P–F). Anal. Calcd for $C_{43}H_{50}F_6IrN_3P_2$ (977.05): C, 52.86; H, 5.16; N, 4.30. Found: C, 52.39; H, 5.33; N, 4.14.

Synthesis of [Ir(cod)(PMe$_3$)(H^{N3}L^{C2,Nimine})]$^+$[PF$_6$]$^-$ (7b$^+$[PF$_6$]$^-$). To a stirred solution of **3a**$^+$[PF$_6$]$^-$ (0.040 g, 0.056 mmol) in CH_2Cl_2 (3 mL) was added a solution of PMe_3 (0.1 M in Et_2O, 0.60 mL, 0.060 mmol). The reaction mixture was stirred for 1 h at room temperature. After removal of the volatiles under reduced pressure, the residue was washed with Et_2O (3 × 1 mL) to yield a yellow powder, which was collected by filtration and dried in vacuo (0.038 g, 0.048 mmol, 86%). ^{1}H NMR (500 MHz, CD_2Cl_2): δ 10.08 (br s, 1H, N*H*), 7.47 (apparent t, *J* = 2.4 Hz, 1H, NHCHC*H*N$_{(near\ imine)}$), 7.36 (apparent t, ^3J = 2.4 Hz, 1H, NHC*H*CHN$_{(near\ imine)}$), 7.35–7.21 (m, 3H, C*H*$_{(Dipp)}$), 3.93 (m, 1H, C*H*$_{(cod)}$), 3.56 (m, 2H, C*H*$_{(cod)}$), 2.82 (m, 1H, C*H*$_{(cod)}$), 2.72 (sept, ^3J = 6.7 Hz, 1H, C*H*(CH$_3$)$_2$), 2.58 (sept, ^3J = 6.7 Hz, 1H, C*H*(CH$_3$)$_2$), 2.45 (m, 2H, C*H*$_{2(cod)}$), 2.26 (d, $^5J_{H\text{-}P}$ = 4.3 Hz, 3H, C*H*$_{3(imine)}$), 2.20–1.94 (m, 3H, C*H*$_{2(cod)}$), 1.46–1.32 (m, 3H, C*H*$_{2(cod)}$), 1.30 (d, ^3J = 6.7 Hz, 3H, CH(C*H*$_3$)$_2$), 1.23 (m, 12H, P(C*H*$_3$)$_3$ and CH(C*H*$_3$)$_2$), 1.09 (d, ^3J = 6.7 Hz, 3H, CH(C*H*$_3$)$_2$), 1.02 (d, ^3J = 6.7 Hz, 3H, CH(C*H*$_3$)$_2$). ^{13}C{^{1}H} NMR (125 MHz, CD_2Cl_2): δ 171.1 (d, $^2J_{P\text{-}C}$ = 10.9 Hz, NH*C*N$_{(near\ imine)}$), 155.3 (d, $^3J_{P\text{-}C}$ = 6.2 Hz, *C*=N), 142.6 (*C*$_{(Dipp)}$), 140.9 (*C*$_{(Dipp)}$), 140.2 (*C*$_{(Dipp)}$), 128.1 (*C*H$_{(Dipp)}$), 125.5 (*C*H$_{(Dipp)}$), 124.5 (*C*H$_{(Dipp)}$), 121.8 (NH*C*HCHN$_{(near\ imine)}$), 115.3 (NHCH*C*HN$_{(near\ imine)}$), 94.4 (d, $^2J_{P\text{-}C}$ = 4.6 Hz, *C*H$_{(cod)}$), 73.4 (*C*H$_{(cod)}$), 58.2 (d, $^2J_{P\text{-}C}$ = 16.6 Hz, *C*H$_{(cod)}$), 42.0 (*C*H$_{2(cod)}$), 41.1 (d, $^2J_{P\text{-}C}$ = 2.3 Hz, *C*H$_{(cod)}$), 33.3 (*C*H$_{2(cod)}$), 30.0 (*C*H$_{2(cod)}$), 29.5 (*C*H$_{2(cod)}$), 27.8 (d, $^5J_{P\text{-}C}$ = 3.9 Hz, *C*H(CH$_3$)$_2$), 27.5 (*C*H(CH$_3$)$_2$), 24.8 (CH(*C*H$_3$)$_2$), 24.7 (CH(*C*H$_3$)$_2$), 24.4 (CH(*C*H$_3$)$_2$), 24.2 (CH(*C*H$_3$)$_2$), 17.5 (*C*H$_{3(imine)}$), 16.1 (d, $^1J_{P\text{-}C}$ = 28.1 Hz, P*C*H$_3$). ^{31}P{^{1}H} NMR (121.5 MHz, CD_2Cl_2): δ −44.8 (s, *P*(CH$_3$)$_3$), −144.3 (sept, $^1J_{P\text{-}F}$ = 712 Hz, *P*F$_6^-$). ^{19}F{^{1}H} NMR (282.4 MHz, CD_2Cl_2): δ −73.5 (d, $^1J_{P\text{-}F}$ = 712 Hz, P*F*$_6^-$). IR: ν_{max} (pure, orbit diamond)/cm^{-1} 3381 *v*(N-H), 1608 *v*(C=N) and 835 *v*(P–F). Anal. Calcd for $C_{28}H_{44}F_6IrN_3P_2$ (790.84): C, 42.53; H, 5.61; N, 5.31. Found: C, 42.32; H, 5.71; N, 5.11.

Synthesis of [Ir(cod)Cl(H^{C2}L'^{N3})] (8). A solution of H^{C2}**L**' (0.071 g, 0.15 mmol) in THF (2 mL) was added to a stirred solution of [Ir(cod)(μ-Cl)]$_2$ (0.050 g, 0.074 mmol) in THF (3 mL). The reaction mixture was stirred for 1 h at room temperature and then the solvent was removed under reduced pressure. The residue was washed with pentane (3 × 1 mL) and dried under vacuum to give a yellow solid (0.103 g, 0.13 mmol, 85%). ^{1}H NMR (500 MHz, CD_2Cl_2): δ 8.70 (s, 1H, N=C*H*), 8.19 (s, 1H, NC*H*N$_{(near\ imine)}$), 7.20–7.00 (m, 6H, C*H*$_{(Dipp)}$), 4.38 (m, 2H, C*H*$_{(cod)}$), 3.34 (m, 2H, C*H*$_{(cod)}$), 2.96 (m, 5H, C*H*(CH$_3$)$_2$ and C*H*$_{3(imidazole)}$), 2.69 (sept, ^3J = 6.9 Hz, 2H, C*H*(CH$_3$)$_2$), 2.32 (m, 4H, C*H*$_{2(cod)}$), 2.28 (s, 3H, C*H*$_{3(imine)}$), 1.61 (m, 4H, C*H*$_{2(cod)}$), 1.11 (d, ^3J = 6.9 Hz, 6H, CH(C*H*$_3$)$_2$), 1.09 (d, ^3J = 6.9 Hz, 12H, CH(C*H*$_3$)$_2$), 0.98 (d, ^3J = 6.9 Hz, 6H, CH(C*H*$_3$)$_2$). ^{13}C{^{1}H} NMR (125 MHz, CD_2Cl_2): δ 153.5 (N=*C*H), 151.6 (N=*C*CH$_3$), 149.6 (*C*$_{(Dipp)}$), 144.5 (*C*$_{(imidazole)}$), 142.0 (*C*$_{(Dipp)}$), 137.8 (*C*$_{(Dipp)}$), 136.9 (*C*$_{(Dipp)}$), 136.7 (N*C*HN$_{(near\ imine)}$), 126.4 (*C*$_{(imidazole)}$), 125.3 (*C*H$_{(Dipp)}$), 124.7 (*C*H$_{(Dipp)}$), 123.8 (*C*H$_{(Dipp)}$), 123.2 (*C*H$_{(Dipp)}$), 70.1 (*C*H$_{(cod)}$), 58.5 (*C*H$_{(cod)}$), 32.8 (*C*H$_{2(cod)}$), 31.5 (*C*H$_{2(cod)}$), 28.6 (*C*H(CH$_3$)$_2$), 28.1 (*C*H(CH$_3$)$_2$), 23.7 (CH(*C*H$_3$)$_2$), 23.2 (CH(*C*H$_3$)$_2$), 23.2 (CH(*C*H$_3$)$_2$), 18.8 (*C*H$_{3(imine)}$), 16.0 (*C*H$_{3(imidazole)}$). IR: ν_{max} (pure, orbit diamond)/cm^{-1} 1684 *v*(C=N). Anal. Calcd for $C_{39}H_{54}ClIrN_4$ (806.56): C, 58.08; H, 6.75; N, 6.95. Found: C, 58.29; H, 6.39; N, 6.58.

Synthesis of [Ir(cod)(H^{C2}L'^{N3,Nimine})]$^+$[PF$_6$]$^-$ (9$^+$[PF$_6$]$^-$). $TlPF_6$ (0.035 g, 0.10 mmol) was added to a stirred solution of **8** (0.081 g, 0.10 mmol) in CH_2Cl_2 (5 mL). The reaction mixture was further stirred for 2 h at room temperature. After filtration through Celite, the filtrate was evaporated under reduced pressure. Then the residue was washed with pentane (3 × 1 mL) and dried under vacuum to give a dark red crystalline solid (0.080 g, 0.087 mmol, 87%). Single crystals of **9**$^+$[PF$_6$]$^-$ suitable for X-ray diffraction were obtained by slow diffusion of a layer of pentane into a solution of **9**$^+$[PF$_6$]$^-$ in THF at ambient temperature under argon. ^{1}H NMR (500 MHz, CD_2Cl_2): δ 8.30 (s, 2H, N=C*H* and NC*H*N$_{(near\ imine)}$), 7.36–7.12 (m, 6H, C*H*$_{(Dipp)}$), 4.84 (m, 2H, C*H*$_{(cod)}$), 3.31 (m, 2H, C*H*$_{(cod)}$), 3.22 (sept, ^3J = 6.9 Hz, 2H, C*H*(CH$_3$)$_2$), 2.87 (s, 3H, C*H*$_{3(imidazole)}$), 2.69 (sept, ^3J = 6.9 Hz, 2H, C*H*(CH$_3$)$_2$), 2.36 (s, 3H, C*H*$_{3(imine)}$), 2.29 (m, 2H, C*H*$_{2(cod)}$), 2.21 (m, 2H, C*H*$_{2(cod)}$), 1.91 (m, 2H, C*H*$_{2(cod)}$), 1.74 (m, 2H, C*H*$_{2(cod)}$), 1.40 (d, ^3J = 6.9 Hz, 6H, CH(C*H*$_3$)$_2$), 1.21 (d, ^3J = 6.9 Hz, 6H, CH(C*H*$_3$)$_2$), 1.14 (d, ^3J = 6.9 Hz, 6H, CH(C*H*$_3$)$_2$), 1.13 (d, ^3J = 6.9 Hz, 6H, CH(C*H*$_3$)$_2$). ^{13}C{^{1}H} NMR (125 MHz, CD_2Cl_2): δ 165.1 (N=*C*H), 151.8 (N=*C*CH$_3$), 142.3 (*C*$_{(Ar)}$), 141.7 (*C*$_{(Ar)}$), 141.5 (*C*$_{(Ar)}$), 141.1 (N*C*HN$_{(near\ imine)}$), 140.8 (*C*$_{(Ar)}$), 139.0 (*C*$_{(Ar)}$), 136.6 (*C*$_{(Ar)}$), 129.1 (*C*H$_{(Ar)}$), 125.7 (*C*H$_{(Ar)}$), 124.1 (*C*H$_{(Ar)}$), 123.9 (*C*H$_{(Ar)}$), 71.1 (*C*H$_{(cod)}$), 70.3 (*C*H$_{(cod)}$), 31.6 (*C*H$_{2(cod)}$), 31.4 (*C*H$_{2(cod)}$), 28.8 (*C*H(CH$_3$)$_2$), 28.6 (*C*H(CH$_3$)$_2$), 25.9 (CH(*C*H$_3$)$_2$), 23.8 (CH(*C*H$_3$)$_2$), 22.8 (CH(*C*H$_3$)$_2$), 22.4 (CH(*C*H$_3$)$_2$), 18.1 (*C*H$_{3(imine)}$), 14.6 (*C*H$_{3(imidazole)}$). ^{31}P{^{1}H} NMR (121.5 MHz, CD_2Cl_2): δ −144.2 (sept, $^1J_{P\text{-}F}$ = 712 Hz, *P*F$_6^-$). ^{19}F{^{1}H} NMR (282.4 MHz, CD_2Cl_2): δ −73.3 (d, $^1J_{P\text{-}F}$ = 712 Hz, P*F*$_6^-$). IR: ν_{max} (pure, orbit diamond)/cm^{-1} 1689 *v*(C=N), 1623 *v*(C=N). Anal. Calcd for $C_{39}H_{54}F_6IrN_4P$ (916.07): C, 51.13; H, 5.94; N, 6.12. Found: C, 50.56; H, 5.96; N, 5.88.

Synthesis of [Ir$_2$(cod)$_2$Cl(L^{C2,Nimine,N3})] (10). To a stirred yellow solution of **1a** (0.151 g, 0.25 mmol) in THF (10 mL) was added slowly a solution of KHMDS (0.55 g, 0.28 mmol) in THF (5 mL) at −78 ºC. The reaction mixture was stirred for 1 h at −30 ºC and the color of solution turned to red. Then a solution of [Ir(cod)(μ-Cl)]$_2$ (0.084 g, 0.13 mmol) in THF (5 mL) was added to the reaction mixture at −78 ºC. The reaction mixture was further stirred for 12 h at room temperature during which time the color of the solution turned dark green. After removal of the solvent under reduced pressure, the residue was extracted with toluene and the solution was filtered through Celite. The filtrate was concentrated to *ca*. 3 mL. After Et_2O (3 mL) was added, the solution was cooled to −30 ºC to yield dark green crystals which were collected by filtration and dried in vacuo (0.145 g, 0.16 mmol, 64%). Single crystals of **10**·Et_2O·toluene suitable for X-ray diffraction were obtained by crystallization from a toluene/Et_2O (1:1) solution at −30 ºC. ^{1}H NMR (400 MHz, C_6D_6): δ 7.29 (d, ^3J = 2.0 Hz, 1H, NC*H*CHN$_{(near\ imine)}$), 7.07–6.86 (m, 3H, C*H*$_{(Dipp)}$), 6.30 (d, ^3J = 2.0 Hz, 1H, NCHC*H*N$_{(near\ imine)}$), 6.23 (m, 2H, C*H*$_{(cod)}$), 4.93 (m, 1H, C*H*$_{(cod)}$), 4.84 (m, 1H, C*H*$_{(cod)}$), 3.61 (m, 1H, C*H*$_{(cod)}$), 3.40 (m, 1H, C*H*$_{(cod)}$), 3.32 (m, 1H, C*H*$_{(cod)}$), 3.23 (m, 1H, C*H*$_{(cod)}$), 2.92 (sept, ^3J = 6.7 Hz, 2H, C*H*(CH$_3$)$_2$), 2.60–2.08 (m, 7H, C*H*$_{2(cod)}$), 2.06–1.76 (m, 3H, C*H*$_{2(cod)}$), 1.72–1.30 (m, 9H, C*H*$_{2(cod)}$ and C*H*$_{3(imine)}$), 1.18 (d, ^3J = 6.7 Hz, 3H, CH(C*H*$_3$)$_2$), 1.11 (d, ^3J = 6.7 Hz, 3H, CH(C*H*$_3$)$_2$), 0.86 (d, ^3J = 6.7 Hz, 3H, CH(C*H*$_3$)$_2$), 0.54 (d, ^3J = 6.7 Hz, 3H, CH(C*H*$_3$)$_2$). ^{13}C{^{1}H} NMR (75 MHz, C_6D_6): δ 180.6 (N*C*N$_{(near\ imine)}$), 166.0 (*C*=N), 142.0 (*o*-*C*$_{(Dipp)}$), 141.8 (*o*-*C*$_{(Dipp)}$), 138.8 (*ipso*-*C*$_{(Dipp)}$), 131.8 (N*C*HCHN$_{(near\ imine)}$), 128.5 (*p*-*C*H$_{(Dipp)}$), 124.3 (*m*-*C*H$_{(Dipp)}$), 123.9 (*m*-*C*H$_{(Dipp)}$), 114.9 (NCH*C*HN$_{(near\ imine)}$), 83.1, 82.1, 70.8, 69.3, 68.1, 66.0, 59.0 and 56.3 (*C*H$_{(cod)}$), 35.0, 33.8, 33.1, 32.6, 32.3, 31.6, 30.8 and 29.4 (*C*H$_{2(cod)}$), 28.4 and 28.0 (*C*H(CH$_3$)$_2$), 25.0, 24.7, 23.6 and 23.0 (CH(*C*H$_3$)$_2$), 15.2 (*C*H$_{3(imine)}$). IR: ν_{max} (pure, orbit diamond)/cm^{-1} 1577 *v*(C=N) and 292 *v*(Ir–Cl). Anal. Calcd for $C_{33}H_{46}ClIr_2N_3$ (904.64): C, 43.81; H, 5.13; N, 4.65. Found: C, 43.38; H, 4.85; N, 4.21.

Synthesis of [Ir$_2$(CO)$_4$Cl(L^{C2,Nimine,N3})] (11). A solution of **10** (0.090 g, 0.10 mmol) in THF (2 mL) was stirred under CO (1 bar) at room temperature for 30 min and then filtered through a cannula. After removal of the volatiles under reduced pressure, the residue was washed with cold Et_2O (2 × 1 mL) to yield a red crystalline solid, which was collected by filtration and dried in vacuo (0.066 g, 0.082 mmol, 82%). Single crystals of **11** suitable for X-ray diffraction were obtained by slow diffusion of a layer of Et_2O into a dichloromethane solution of **11** at ambient temperature under argon. ^{1}H NMR (500 MHz, CD_2Cl_2): δ 7.40–7.30 (m, 3H, C*H*$_{(Dipp)}$), 7.22 (d, ^3J = 2.1 Hz, 1H, NCHC*H*N$_{(near\ imine)}$), 7.19 (d, ^3J = 2.1 Hz, 1H, NC*H*CHN$_{(near\ imine)}$), 3.09 (sept, ^3J = 6.8 Hz, 2H, C*H*(CH$_3$)$_2$), 2.34 (s, 1H, C*H*$_{3(imine)}$), 1.34 (d, ^3J = 6.8 Hz, 6H, CH(C*H*$_3$)$_2$), 1.18 (d, ^3J = 6.8 Hz, 6H, CH(C*H*$_3$)$_2$). ^{13}C{^{1}H} NMR (125

MHz, CD_2Cl_2): δ 186.5 (NCN$_{(near\ imine)}$), 183.0 (*C*O), 174.5 (*C*O), 172.3 (*C*O), 168.8 (*C*=N), 168.5 (*C*O), 142.7 (*ipso*-*C*$_{(Dipp)}$), 140.8 (*o*-*C*$_{(Dipp)}$), 133.0 (NCHCHN$_{(near\ imine)}$), 129.5 (*p*-*C*H$_{(Dipp)}$), 125.1 (*m*-*C*H$_{(Dipp)}$), 117.5 (NCH*C*HN$_{(near\ imine)}$), 28.9 (*C*H(CH$_3$)$_2$), 24.2 (CH(*C*H$_3$)$_2$), 23.7 (CH(*C*H$_3$)$_2$), 15.0 (*C*H$_{3(imine)}$). IR: ν_{max} (pure, orbit diamond)/cm^{-1} 2054, 1971 ν(CO), 1606 ν(C=N) and 320 ν(Ir–Cl). Anal. Calcd for $C_{21}H_{22}ClIr_2N_3O_4$ (800.30): C, 31.52; H, 2.77; N, 5.25. Found: C, 32.06; H, 3.23; N, 5.32.

Synthesis of [IrRh(cod)$_2$Cl(L^{C2,Nimine,N3})] (12). From complex **1b**: To a stirred, yellow solution of **1b** (0.103 g, 0.20 mmol) in THF (10 mL) was added a solution of KHMDS (0.044 g, 0.22 mmol) in THF (5 mL) slowly at −78 ºC. The mixture was stirred for 1 h at −30 ºC and the color of solution turned to orange. Then a solution of [Ir(cod)(μ-Cl)]$_2$ (0.067 g, 0.10 mmol) in THF (5 mL) was added to the mixture at −78 ºC. The mixture was further stirred for 12 h at room temperature during which time the color of the solution turned to maroon. After removal of the volatiles under reduced pressure, the residue was extracted with toluene and the solution was filtered through Celite. The filtrate was evaporated to dryness under reduced pressure. The residue was dissolved in THF (2 mL) and Et_2O (2 mL) was added. Then the solution was cooled to −30 ºC to yield a maroon crystalline solid, which was collected by filtration and dried in vacuo (0.098 g, 0.12 mmol, 60%). Single crystals of **12**·2THF suitable for X-ray diffraction were obtained by crystallization in a THF/Et_2O (1:1) solution at −30 ºC. ^{1}H NMR (500 MHz, CD_2Cl_2): δ 7.30 (d, ^3J = 1.8 Hz, 1H, NC*H*CHN$_{(near\ imine)}$), 7.29–7.21 (m, 3H, C*H*$_{(Dipp)}$), 6.92 (d, ^3J = 1.8 Hz, 1H, NCHC*H*N$_{(near\ imine)}$), 6.22 (m, 1H, C*H*$_{(cod)}$), 5.53 (m, 1H, C*H*$_{(cod)}$), 4.53 (m, 1H, C*H*$_{(cod)}$), 4.42 (m, 1H, C*H*$_{(cod)}$), 3.60 (m, 2H, C*H*$_{(cod)}$), 3.46 (m, 1H, C*H*$_{(cod)}$), 3.27 (m, 1H, C*H*$_{(cod)}$), 3.21 (sept, ^3J = 6.7 Hz, 1H, C*H*(CH$_3$)$_2$), 3.07 (sept, ^3J = 6.7 Hz, 1H, C*H*(CH$_3$)$_2$), 2.63 (m, 2H, C*H*$_{2(cod)}$), 2.36 (m, 4H, C*H*$_{2(cod)}$), 2.27–2.07 (m, 5H, C*H*$_{2(cod)}$ and C*H*$_{3(imine)}$), 2.02 (m, 2H, C*H*$_{2(cod)}$), 1.91 (m, 2H, C*H*$_{2(cod)}$), 1.78–1.56 (m, 4H, C*H*$_{2(cod)}$), 1.35 (d, ^3J = 6.7 Hz, 3H, CH(C*H*$_3$)$_2$), 1.34 (d, ^3J = 6.7 Hz, 3H, CH(C*H*$_3$)$_2$), 1.12 (d, ^3J = 6.7 Hz, 3H, CH(C*H*$_3$)$_2$), 1.03 (d, ^3J = 6.7 Hz, 3H, CH(C*H*$_3$)$_2$). ^{13}C{^{1}H} NMR (125 MHz, CD_2Cl_2): δ 179.8 (NC*N*$_{(near\ imine)}$), 166.3 (*C*=N), 142.2 (*o*-*C*$_{(Dipp)}$), 142.0 (*o*-*C*$_{(Dipp)}$), 138.8 (*ipso*-*C*$_{(Dipp)}$), 131.7 (NCHCHN$_{(near\ imine)}$), 128.2 (*p*-*C*H$_{(Dipp)}$), 124.5 (*m*-*C*H$_{(Dipp)}$), 124.2 (*m*-*C*H$_{(Dipp)}$), 115.2 (NCH*C*HN$_{(near\ imine)}$), 84.8 (d, $^1J_{Rh\text{-}C}$ = 11.2 Hz, *C*H$_{(cod)}$), 84.2 (*C*H$_{(cod)}$), 83.4 (d, $^1J_{Rh\text{-}C}$ = 11.4 Hz, *C*H$_{(cod)}$), 83.0 (*C*H$_{(cod)}$), 77.9 (d, $^1J_{Rh\text{-}C}$ = 14.6 Hz, *C*H$_{(cod)}$), 73.8 (d, $^1J_{Rh\text{-}C}$ = 13.8 Hz, *C*H$_{(cod)}$), 69.2 (*C*H$_{(cod)}$), 65.4 (*C*H$_{(cod)}$), 34.5, 33.1, 32.8, 31.9, 31.3, 30.7, 29.5 and 29.4 (*C*H$_{2(cod)}$), 28.6 and 28.3 (*C*H(CH$_3$)$_2$), 25.3, 23.7 and 23.4 (CH(*C*H$_3$)$_2$), 15.9 (*C*H$_{3(imine)}$). IR: ν_{max} (pure, orbit diamond)/cm^{-1} 1600 ν(C=N) and 290 ν(Rh–Cl). Anal. Calcd for $C_{33}H_{46}ClIrRhN_3$ (815.32): C, 48.61; H, 5.69; N, 5.15. Found: C, 48.40; H, 6.19; N, 4.63.

From complex **1a**: To a stirred solution of **1a** (0.121 g, 0.20 mmol) in THF (10 mL) was added slowly a solution of KHMDS (0044 g, 0.22 mmol) in THF (5 mL) at −78 ºC. The reaction mixture was stirred for 1 h at −30 ºC and the color of solution turned to red. Then a solution of [Rh(cod)(μ-Cl)]$_2$ (0.050 g, 0.10 mmol) in THF (5 mL) was added to the mixture at −78 ºC. The reaction mixture was further stirred for 12 h at room temperature during which time the color of the solution turned maroon. After removal of the volatiles under reduced pressure, the residue was extracted with toluene and the solution was filtered through Celite. The filtrate was evaporated to dryness under reduced pressure. The residue was dissolved in THF (2 mL) and Et_2O (2 mL) was added. The solution was cooled to −30 ºC to yield a maroon crystalline solid, which was collected by filtration and dried in vacuo (0.083 g, 0.10 mmol, 51%).

X-ray Data Collection, Structure Solution, and Refinement for All Compounds. Suitable crystals for the X-ray analysis of all compounds were obtained as described above. Data for **1b**, **3b**$^+$[PF$_6$]$^-$, **7a**$^+$[PF$_6$]$^-$, **10**·Et_2O·toluene and **12**·2THF were collected on an APEX-II CCD (graphite-monochromated Mo-Kα radiation, λ = 0.71073 Å) at 173(2) K, data for **6a**$^+$[PF$_6$]$^-$, **9**$^+$[PF$_6$]$^-$ and **11** were collected on a Kappa CCD diffractometer (graphite-monochromated Mo-Kα radiation, λ = 0.71073 Å) at 173(2) K. Crystallographic and experimental details for these structures are summarized in Table S1 and S2 (ESI). The structures were solved by direct methods (SHELXS-97[26]) and refined by full-matrix least-squares procedures (based on F^2, SHELXL-97) with anisotropic thermal parameters for all the non-hydrogen atoms. The hydrogen atoms were introduced into the geometrically calculated positions (SHELXS-97 procedures). Details of the specific comments applied for the structures are provided in ESI. CCDC 1426156 (**1b**), CCDC 1426157 (**3b**$^+$[PF$_6$]$^-$), CCDC 1426158 (**6a**$^+$[PF$_6$]$^-$), CCDC 1426159 (**7a**$^+$[PF$_6$]$^-$), CCDC 1426160 (**9**$^+$[PF$_6$]$^-$), CCDC 1426161 (**10**·Et_2O·toluene), CCDC 1426162 (**11**) and CCDC 1426163 (**12**·2THF) contain the supplementary crystallographic data for this paper. These data can be obtained free of charge from The Cambridge Crystallographic Data Centre.

Acknowledgements

The USIAS, CNRS, UdS, Région Alsace and Communauté Urbaine de Strasbourg are gratefully acknowledged for the award of fellowships and a Gutenberg Excellence Chair (2010–11) to A.A.D. and support. We also thank the ucFRC (www.icfrc.fr) for support and the China Scholarship Council for a PhD grant to F.H., and the Service de Radiocristallographie (Institut de Chimie, Strasbourg) for the determination of the crystal structures.

Keywords: protic N-heterocyclic carbenes • imidazole • iridium • rhodium • C-H activation

[1] a) A. J. Arduengo, III, R. L. Harlow, M. Kline, *J. Am. Chem. Soc.* **1991**, *113*, 361–363; b) A. J. Arduengo, III, H. V. R. Dias, R. L. Harlow, M. Kline, *J. Am. Chem. Soc.* **1992**, *114*, 5530–5534; c) D. Bourissou, O. Guerret, F. P. Gabbaï, G. Bertrand, *Chem. Rev.* **2000**, *100*, 39–92.

[2] a) F. E. Hahn, M. C. Jahnke, *Angew. Chem. Int. Ed.* **2008**, *47*, 3122–3172; b) P. de Frémont, N. Marion, S. P. Nolan, *Coord. Chem. Rev.* **2009**, *253*, 862–892; c) M. Melaimi, M. Soleilhavoup, G. Bertrand, *Angew. Chem. Int. Ed.* **2010**, *49*, 8810–8849; d) R. H. Crabtree, *Coord. Chem. Rev.* **2013**, *257*, 755–766.

[3] a) N. Meier, F. E. Hahn, T. Pape, C. Siering, S. R. Waldvogel, *Eur. J. Inorg. Chem.* **2007**, *2007*, 1210–1214; b) F. E. Hahn, *ChemCatChem* **2013**, *5*, 419–430; c) M. C. Jahnke, F. E. Hahn, *Coord. Chem. Rev.* **2015**, *293–294*, 95–115.

[4] S. Karmakar, A. Datta, *Angew. Chem. Int. Ed.* **2014**, *53*, 9587–9591.

[5] F. E. Hahn, in *Advances in Organometallic Chemistry and Catalysis*, John Wiley & Sons, Inc., **2013**, pp. 111–132.

[6] R. J. Sundberg, R. F. Bryan, I. F. Taylor, H. Taube, *J. Am. Chem. Soc.* **1974**, *96*, 381–392.

[7] a) R. Das, C. G. Daniliuc, F. E. Hahn, *Angew. Chem. Int. Ed.* **2014**, *53*, 1163–1166; b) R. Das, A. Hepp, C. G. Daniliuc, F. E. Hahn, *Organometallics* **2014**, *33*, 6975–6987.

[8] J. Tornatzky, A. Kannenberg, S. Blechert, *Dalton Trans.* **2012**, *41*, 8215–8225.

[9] a) K. L. Tan, R. G. Bergman, J. A. Ellman, *J. Am. Chem. Soc.* **2001**, *123*, 2685–2686; b) K. L. Tan, R. G. Bergman, J. A. Ellman, *J. Am.*

Chem. Soc. **2002**, *124*, 3202–3203; c) K. L. Tan, A. Vasudevan, R. G. Bergman, J. A. Ellman, A. J. Souers, *Org. Lett.* **2003**, *5*, 2131–2134.

[10] a) K. L. Tan, R. G. Bergman, J. A. Ellman, *J. Am. Chem. Soc.* **2002**, *124*, 13964–13965; b) K. L. Tan, S. Park, J. A. Ellman, R. G. Bergman, *J. Org. Chem.* **2004**, *69*, 7329–7335; c) J. C. Lewis, R. G. Bergman, J. A. Ellman, *Acc. Chem. Res.* **2008**, *41*, 1013–1025.

[11] K. Araki, S. Kuwata, T. Ikariya, *Organometallics* **2008**, *27*, 2176–2178.

[12] a) V. Miranda-Soto, D. B. Grotjahn, A. G. DiPasquale, A. L. Rheingold, *J. Am. Chem. Soc.* **2008**, *130*, 13200–13201; b) V. Miranda-Soto, D. B. Grotjahn, A. L. Cooksy, J. A. Golen, C. E. Moore, A. L. Rheingold, *Angew. Chem. Int. Ed.* **2011**, *50*, 631–635.

[13] F. E. Hahn, A. R. Naziruddin, A. Hepp, T. Pape, *Organometallics* **2010**, *29*, 5283–5288.

[14] A. R. Naziruddin, A. Hepp, T. Pape, F. E. Hahn, *Organometallics* **2011**, *30*, 5859–5866.

[15] a) L. K. Johnson, C. M. Killian, M. Brookhart, *J. Am. Chem. Soc.* **1995**, *117*, 6414–6415; b) B. L. Small, M. Brookhart, A. M. A. Bennett, *J. Am. Chem. Soc.* **1998**, *120*, 4049–4050; c) G. J. P. Britovsek, V. C. Gibson, S. J. McTavish, G. A. Solan, A. J. P. White, D. J. Williams, G. J. P. Britovsek, B. S. Kimberley, P. J. Maddox, *Chem. Commun.* **1998**, 849–850; d) C. C. H. Atienza, T. Diao, K. J. Weller, S. A. Nye, K. M. Lewis, J. G. P. Delis, J. L. Boyer, A. K. Roy, P. J. Chirik, *J. Am. Chem. Soc.* **2014**, *136*, 12108–12118.

[16] a) K. S. Coleman, S. Dastgir, G. Barnett, M. J. P. Alvite, A. R. Cowley, M. L. H. Green, *J. Organomet. Chem.* **2005**, *690*, 5591–5596; b) M. Frøseth, K. A. Netland, C. Rømming, M. Tilset, *J. Organomet. Chem.* **2005**, *690*, 6125–6132; c) S. Dastgir, K. S. Coleman, A. R. Cowley, M. L. H. Green, *Organometallics* **2006**, *25*, 300–306; d) J. Al Thagfi, S. Dastgir, A. J. Lough, G. G. Lavoie, *Organometallics* **2010**, *29*, 3133–3138; e) J. Al Thagfi, G. G. Lavoie, *Organometallics* **2012**, *31*, 2463–2469; f) P. Liu, M. Wesolek, A. A. Danopoulos, P. Braunstein, *Organometallics* **2013**, *32*, 6286–6297.

[17] a) M. L. Rosenberg, A. Krivokapic, M. Tilset, *Org. Lett.* **2009**, *11*, 547–550; b) M. L. Rosenberg, K. Vlašaná, N. S. Gupta, D. Wragg, M. Tilset, *J. Org. Chem.* **2011**, *76*, 2465–2470.

[18] a) S. Kuwata, T. Ikariya, *Chem.–Eur. J.* **2011**, *17*, 3542–3556; b) S. Kuwata, T. Ikariya, *Chem. Commun.* **2014**, *50*, 14290–14300; c) B. Zhao, Z. Han, K. Ding, *Angew. Chem. Int. Ed.* **2013**, *52*, 4744–4788.

[19] F. He, P. Braunstein, M. Wesolek, A. A. Danopoulos, *Chem. Commun.* **2015**, *51*, 2814–2817.

[20] F. He, L. Ruhlmann, J.-P. Gisselbrecht, S. Choua, M. Orio, M. Wesolek, A. Danopoulos, P. Braunstein, *Dalton Trans.* **2015**, *44*, 17030–17044.

[21] T. Kösterke, J. Kösters, E.-U. Würthwein, C. Mück-Lichtenfeld, C. Schulte to Brinke, F. Lahoz, F. E. Hahn, *Chem.–Eur. J.* **2012**, *18*, 14594–14598.

[22] a) C. Bianchini, E. Farnetti, M. Graziani, G. Nardin, A. Vacca, F. Zanobini, *J. Am. Chem. Soc.* **1990**, *112*, 9190–9197; b) M. T. Whited, R. H. Grubbs, *Organometallics* **2008**, *27*, 5737–5740; c) G. Song, Y. Su, R. A. Periana, R. H. Crabtree, K. Han, H. Zhang, X. Li, *Angew. Chem. Int. Ed.* **2010**, *49*, 912–917.

[23] G. E. Dobereiner, C. A. Chamberlin, N. D. Schley, R. H. Crabtree, *Organometallics* **2010**, *29*, 5728–5731.

[24] G. Giordano, R. H. Crabtree, R. M. Heintz, D. Forster, D. E. Morris, *Inorg. Synth.* **1990**, *28*, 88–90.

[25] H. Graboyes, T. J. Kasper, P. D. Vaidya, *Eur. Pat. Appl.* **1982**, EP49638.

[26] G. M. Sheldrick, *SHELXL-97, Program for crystal structure refinement*, University of Göttingen, Göttingen, Germany, **1997**.

FULL PAPER

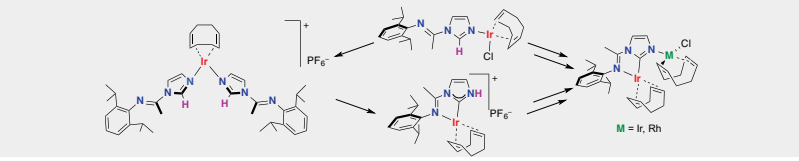

The Ir imine-functionalized protic NHC complex was obtained via a chelate assisted C2–H bond activation in the cationic $N_{imidazole}$–Ir complex. The homo/heterodinuclear complexes could be prepared by *in situ* deprotonation of either the neutral $N_{imidazole}$–Ir complex or the Ir pNHC complex followed by addition of metal precursors.

F. He, M. Wesolek, A. A. Danopoulos, P. Braunstein**

Page 1 – Page 14

Homo and Heterodinuclear Ir and Rh Imine-functionalized Protic NHC Complexes: Synthetic, Structural Studies and Tautomerization/ Metallotropism Insights

SUPPORTING INFORMATION

Homo and Heterodinuclear Ir and Rh Imine-functionalized Protic NHC Complexes: Synthetic, Structural Studies and Tautomerization/Metallotropism Insights

Fan He,[a] Marcel Wesolek,[a] Andreas A. Danopoulos,*[a, b], and Pierre Braunstein*[a]

[a] Laboratoire de Chimie de Coordination, Institut de Chimie (UMR 7177 CNRS), Université de Strasbourg, 4 rue Blaise Pascal, 67081 Strasbourg Cedex, France

[b] Université de Strasbourg Institute for Advanced Study (USIAS), 4 rue Blaise Pascal, 67081 Strasbourg Cedex, France

* Corresponding authors. E-mail: danopoulos@unistra.fr, braunstein@unistra.fr

 References: p 100

Contents

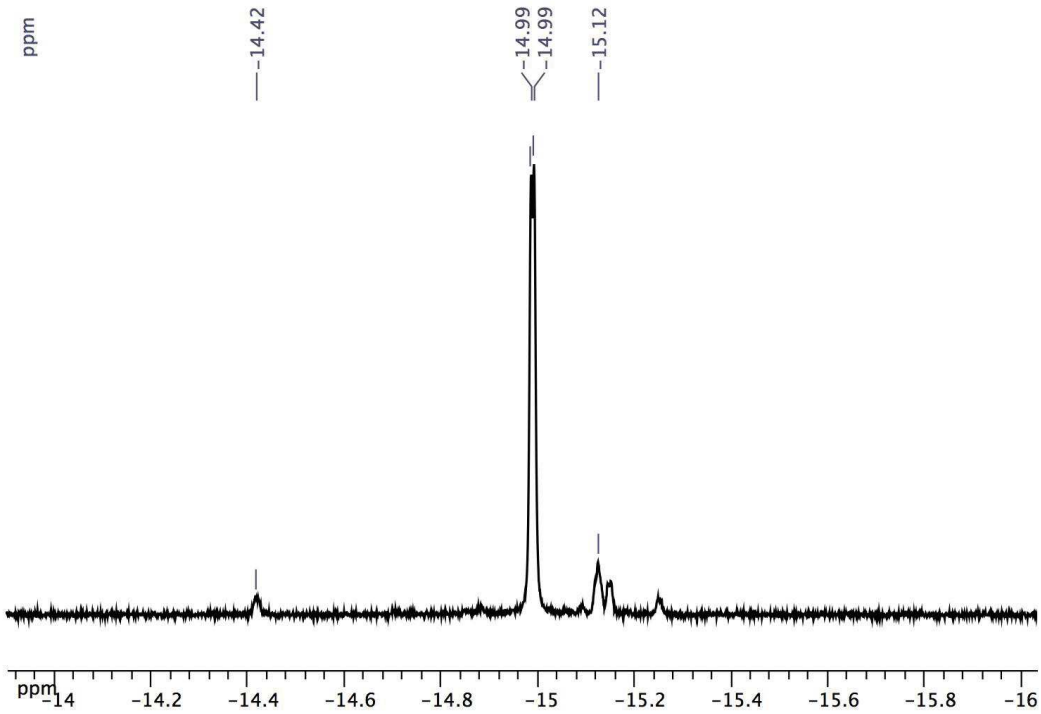

Figure S1. Hydride species observed by ^{1}H NMR monitoring of the reaction between **1a** and $TlFP_6$ in CD_2Cl_2.

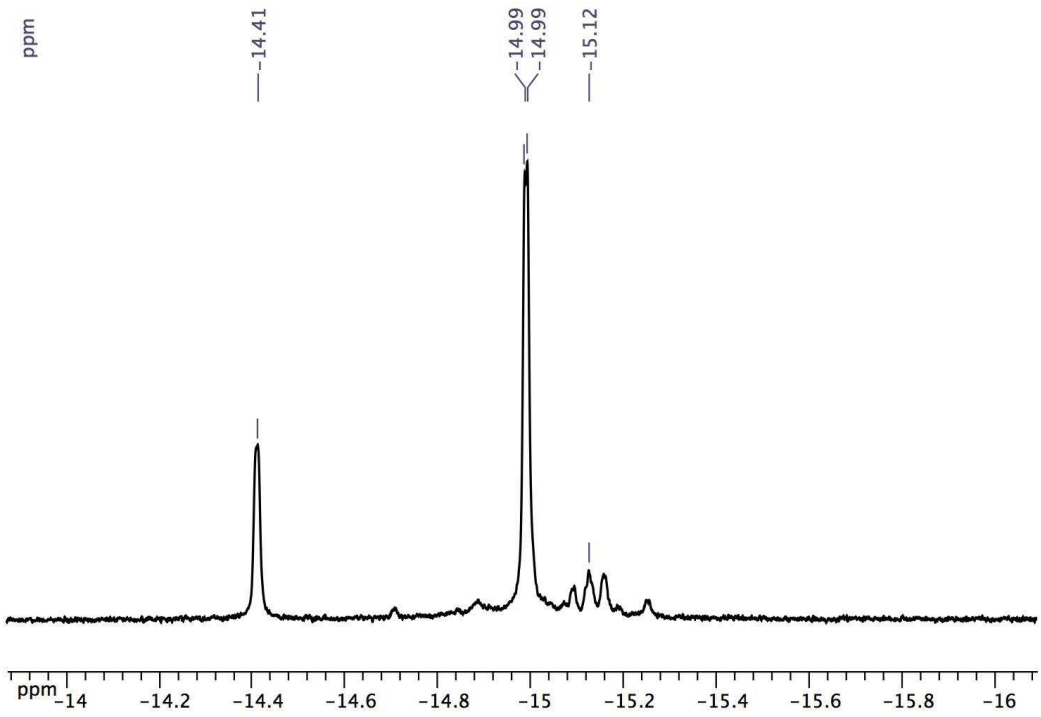

Figure S2. Hydride species observed by ^{1}H NMR monitoring of the reaction between **6a**$^{+}[PF_6]^{-}$ and $[Ir(cod)(\mu\text{-}Cl)]_2$ in CD_2Cl_2.

Table S1. Crystal data and structure refinement for **1b**, **3b**$^{+}$[PF_6]$^{-}$, **6a**$^{+}$[PF_6]$^{-}$ and **7a**$^{+}$[PF_6]$^{-}$.

	1b	**3b**$^{+}$[PF_6]$^{-}$	**6a**$^{+}$[PF_6]$^{-}$	**7a**$^{+}$[PF_6]$^{-}$
CCDC number	1426156	1426157	1426158	1426159
Empirical formula	$C_{25}H_{35}ClN_3Rh$	$C_{25}H_{35}F_6N_3PRh$	$C_{42}H_{58}F_6IrN_6P$	$C_{43}H_{50}F_6IrN_3P_2$
Fw	515.92	625.44	984.11	977.00
T/K	173(2)	173(2)	173(2)	173(2)
Crystal system	Triclinic	Triclinic	Monoclinic	Monoclinic
Space group	P -1	P -1	P 21/m	C 2/c
a/Å	8.5634(3)	10.257(4)	8.9998(2)	41.4775(17)
b/Å	11.4171(4)	10.725(4)	24.2454(6)	10.2741(4)
c/Å	13.6703(5)	13.696(5)	10.2140(2)	22.5405(9)
α/°	69.7350(10)	106.152(9)	90	90
β/°	87.2870(10)	109.992(9)	102.670(2)	118.1240(10)
γ/°	71.1190(10)	97.398(10)	90	90
V/Å^3	1183.18(7)	1317.4(9)	2174.46(9)	8471.4(6)
Z	2	2	2	8
μ/mm^{-1}	0.851	0.771	3.169	3.288
No. of rflns collected	25970	24279	15687	58047
No. unique rflns	7024	9207	5093	14693
R(int)	0.0201	0.0342	0.0434	0.0225
Goodness of fit on F^2	1.042	1.047	1.153	1.053
Final *R* indices [$I>2\sigma(I)$]	R1 = 0.0262 wR2 = 0.0647	R1 = 0.0480 wR2 = 0.1267	R1 = 0.0366 wR2 = 0.1039	R1 = 0.0247 wR2 = 0.0523
R indices (all data)	R1 = 0.0330 wR2 = 0.0680	R1 = 0.0634 wR2 = 0.1365	R1 = 0.0428 wR2 = 0.1104	R1 = 0.0339 wR2 = 0.0551

References: p 100

Table S2. Crystal data and structure refinement for $\mathbf{9}^{+}[PF_6]^{-}$, $\mathbf{10}\cdot Et_2O\cdot$Toluene, **11** and $\mathbf{12}\cdot$2THF.

	$\mathbf{9}^{+}[PF_6]^{-}$	$\mathbf{10}\cdot Et_2O\cdot$Toluene	**11**	$\mathbf{12}\cdot$2THF
CCDC number	1426160	1426161	1426162	1426163
Empirical formula	$C_{39}H_{54}F_6IrN_4P$	$C_{44}H_{64}ClIr_2N_3O$	$C_{21}H_{22}ClIr_2N_3O_4$	$C_{41}H_{62}ClIrN_3O_2Rh$
Fw	916.03	1070.83	800.27	959.50
T/K	173(2)	173(2)	173(2)	173(2)
Crystal system	Monoclinic	Monoclinic	Monoclinic	Triclinic
Space group	P 21/c	P 21/c	P 21/c	P -1
a/Å	15.5012(6)	12.3548(5)	12.8201(5)	13.6319(13)
b/Å	16.8194(4)	22.3808(8)	13.7204(5)	13.6628(10)
c/Å	16.6028(6)	15.0390(6)	13.5396(5)	13.6964(13)
α/°	90	90	90	65.328(3)
β/°	99.483(2)	95.9200(10)	91.510(2)	73.603(2)
γ/°	90	90	90	60.138(18)
V/Å^3	4269.5(2)	4136.3(3)	2380.75(15)	2001.3(3)
Z	4	4	4	2
μ/mm^{-1}	3.221	6.529	11.311	3.838
No. of rflns collected	31159	39933	12804	43813
No. unique rflns	9778	14188	5429	11707
R(int)	0.0930	0.0340	0.0452	0.0407
Goodness of fit on F^2	1.087	1.184	1.066	1.049
Final *R* indices [$I>2\sigma(I)$]	R1 = 0.0632 wR2 = 0.1761	R1 = 0.0456 wR2 = 0.0798	R1 = 0.0340 wR2 = 0.0727	R1 = 0.0532 wR2 = 0.1328
R indices (all data)	R1 = 0.1106 wR2 = 0.2178	R1 = 0.0774 wR2 = 0.0932	R1 = 0.0565 wR2 = 0.0986	R1 = 0.0714 wR2 = 0.1478

References: p 100

Specific comments concerning these structures:

3b^{+}[PF_6]$^{-}$: Instead of being placed in a calculated position, the hydrogen atom H1N was found. There are inter-molecular hydrogen bond interactions between the NH group and F4/F5 in the [PF_6]$^{-}$.

6a^{+}[PF_6]$^{-}$: The asymmetric unit contains half a molecule of **6a**$^{+}$ and half a molecule of [PF_6]$^{-}$. The atoms F1, F3, P1 and Ir1 are in special position (population 50%).

7a^{+}[PF_6]$^{-}$: Instead of being placed in a calculated position, the hydrogen atom H1N was found. There is an inter-molecular hydrogen bond interaction between the NH group and F3 in the [PF_6]$^{-}$. The SQUEEZE instruction in PLATON was applied for **7a**$^{+}$[PF_6]$^{-}$. The residual electron density was assigned to half a molecule of diethyl ether for **7**$^{+}$[PF_6]$^{-}$.

9^{+}[PF_6]$^{-}$: There is an Alert B in checkcif because it remains the residual electron density corresponding to the disordered solvent. The squeeze could not be applied.

10·Et_2O·toluene: The asymmetric unit contains one molecule of **10**, one molecule of Et_2O and one molecule of toluene.

12·2THF: The asymmetric unit contains one molecule of **12** and two molecules of THF.

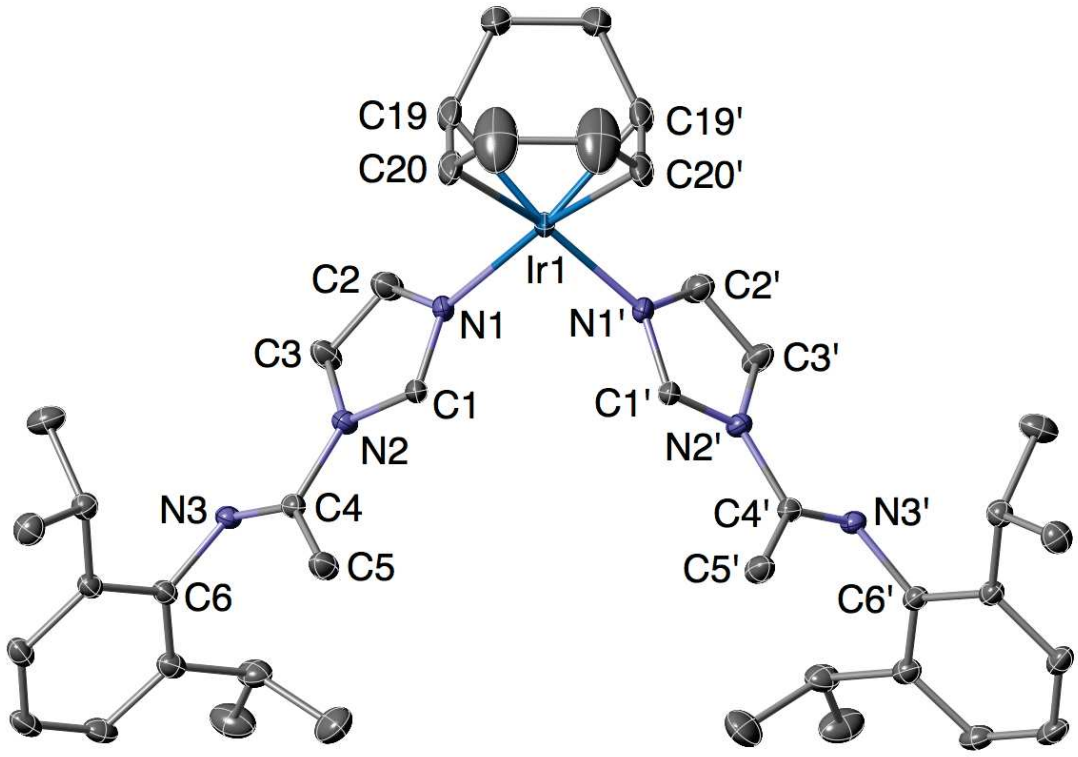

Figure S3. Molecular structure of the cation in **6a**$^{+}$[PF_6]$^{-}$. H atoms are omitted for clarity. Thermal ellipsoids are at the 30% level. The crystallographic labels C1 and N1 correspond to the conventional C2 and N3 numbering used in the text. Selected bond distances (Å) and angles (°): C1–N1 1.322(5), C1–N2 1.363(5), C2–N1 1.393(5), C2–C3 1.352(6), C3–N2 1.379(5), C4–N2 1.435(4), C4–N3 1.255(5), C4–C5 1.491(5), C6–N3 1.422(4), Ir1–N1 2.078(3), Ir1–C19 2.125(5), Ir1–C20 2.120(5), C19–C20 1.391(9); N1–C1–N2 110.2(3), N1–Ir1–C19 91.8(2), N1–Ir1–C20 92.3(2), N1–Ir1– N1' 88.3(2).

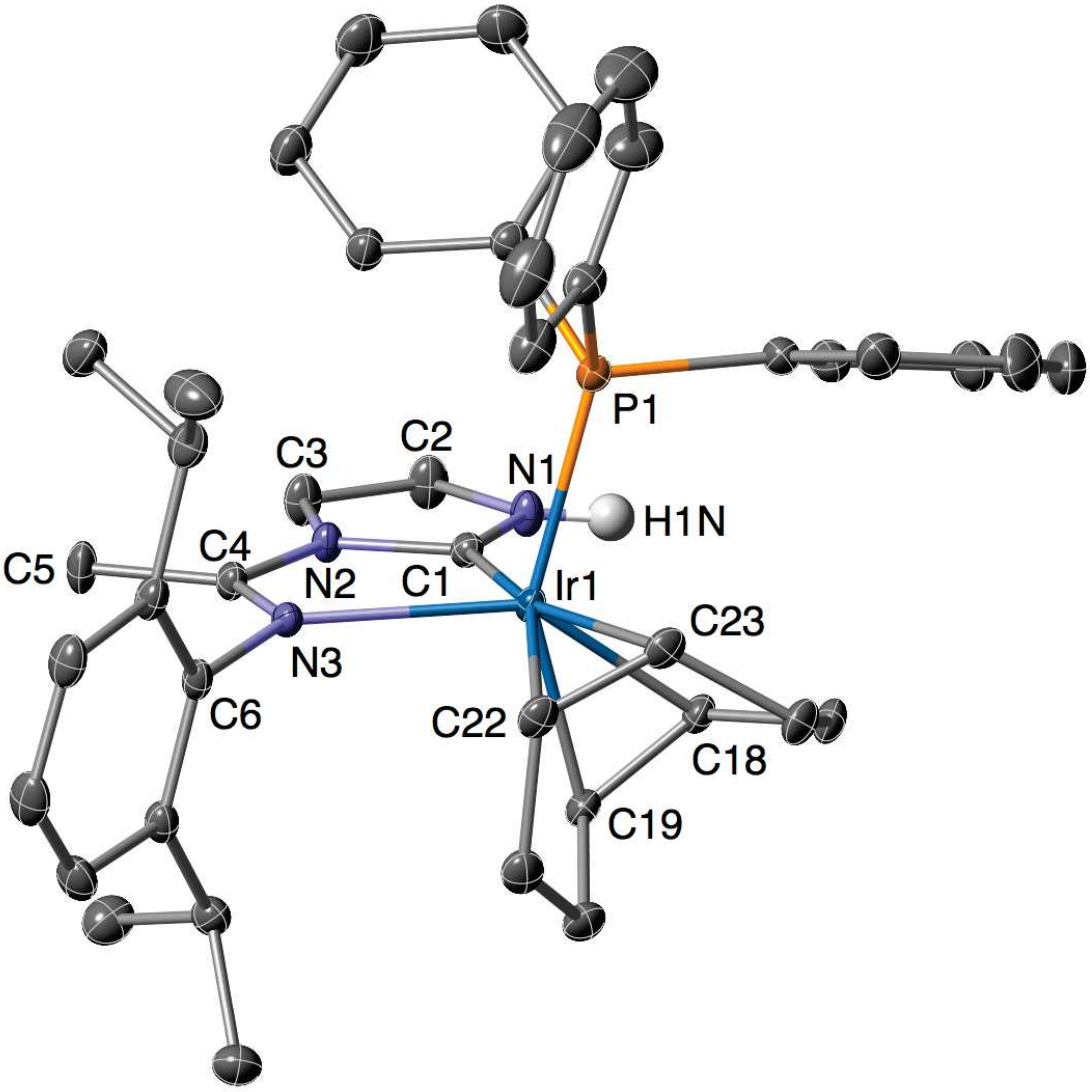

Figure S4. Molecular structure of the cation in **7a**$^{+}$[PF_6]$^{-}$. H atoms are omitted for clarity, except H1N. Thermal ellipsoids are at the 30% level. Selected bond distances (Å) and angles (°): C1–N1 1.345(2), C1–N2 1.371(2), C2–N1 1.388(3), C2–C3 1.337(3), C3–N2 1.402(2), C4–N2 1.402(2), C4–N3 1.284(2), C4–C5 1.495(3), C6–N3 1.453(2), Ir1–P1 2.3388(5), Ir1–C1 1.982(2), Ir1–N3 2.347(2), Ir1–C18 2.118(2), Ir1–C19 2.142(2), Ir1–C22 2.220(2), Ir1–C23 2.269(2), C18–C19 1.445(3), C22–C23 1.390(3), N1–H1N 0.82(3); N1–C1–N2 104.0(2), C1–Ir1–N3 73.61(6), C1–Ir1–P1 89.59(5), C1–Ir1–C18 89.36(7), C1–Ir1–C19 90.85(8), N3–Ir1–P1 108.63(4).

References: p 100

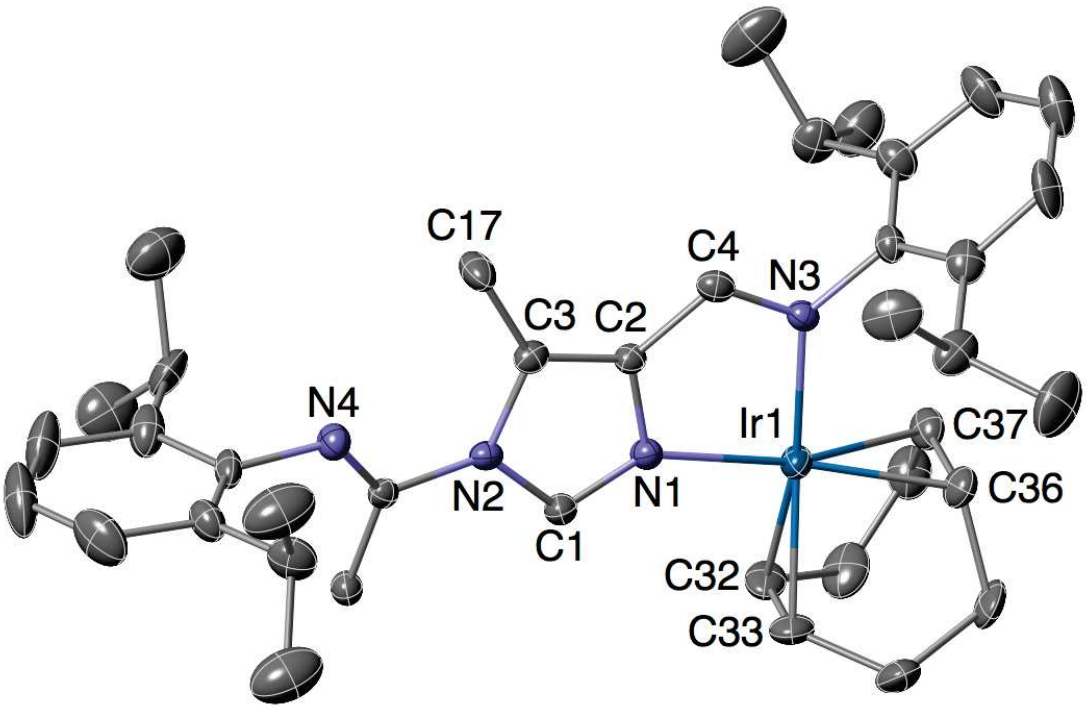

Figure S5. Molecular structure of the cation in $\mathbf{9}^{+}[PF_6]^{-}$. H atoms are omitted for clarity. Thermal ellipsoids are at the 30% level. Selected bond distances (Å) and angles (°): C1–N1 1.31(1), C1–N2 1.38(1), C2–N1 1.394(9), C2–C3 1.37(1), C3–N2 1.41(1), C4–N3 1.31(1), Ir1–N1 2.083(7), Ir1–N3 2.094(6), Ir1–C32 2.154(9), Ir1–C33 2.137(8), Ir1–C36 2.110(9), Ir1–C37 2.123(9), C32–C33 1.43(2), C36–C37 1.38(1); N1–C1–N2 111.1(7), N1–Ir1–N3 78.9(3), N1–Ir1–C32 98.6(3), N1–Ir1–C33 94.2(3), N3–Ir1–C36 97.5(3), N3–Ir1– C37 93.6(3).

References: p 100

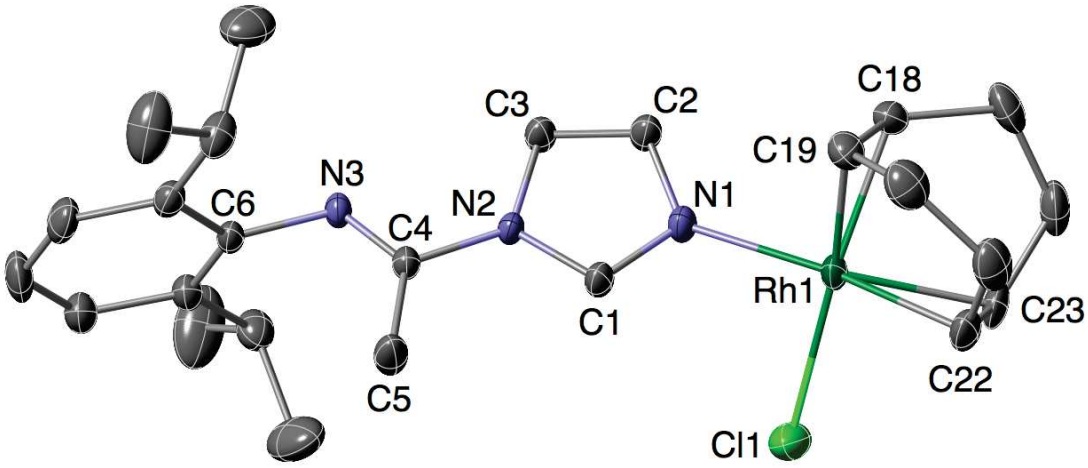

Figure S6. Molecular structure of **1b**. H atoms are omitted for clarity. Thermal ellipsoids are at the 30% level. Selected bond distances (Å) and angles (°): C1–N1 1.315(2), C1–N2 1.359(2), C2–N1 1.383(2), C2–C3 1.355(2), C3–N2 1.381(2), C4–N2 1.428(2), C4–N3 1.260(2), C4–C5 1.496(2), C6–N3 1.428(2), Rh1–N1 2.104(1), Rh1–Cl1 2.3748(5), Rh1–C18 2.120(2), Rh1–C19 2.101(2), Rh1–C22 2.143(2), Rh1–C23 2.127(2), C18–C19 1.399(3), C22–C23 1.396(3); N1–C1–N2 111.1(1), N1–Rh1–Cl1 88.36(4), N1–Rh1–C18 93.69(6), N1–Rh1–C19 90.02(6), Cl1–Rh1–C22 92.20(6), Cl1–Rh1–C23 91.16(6).

References: p 100

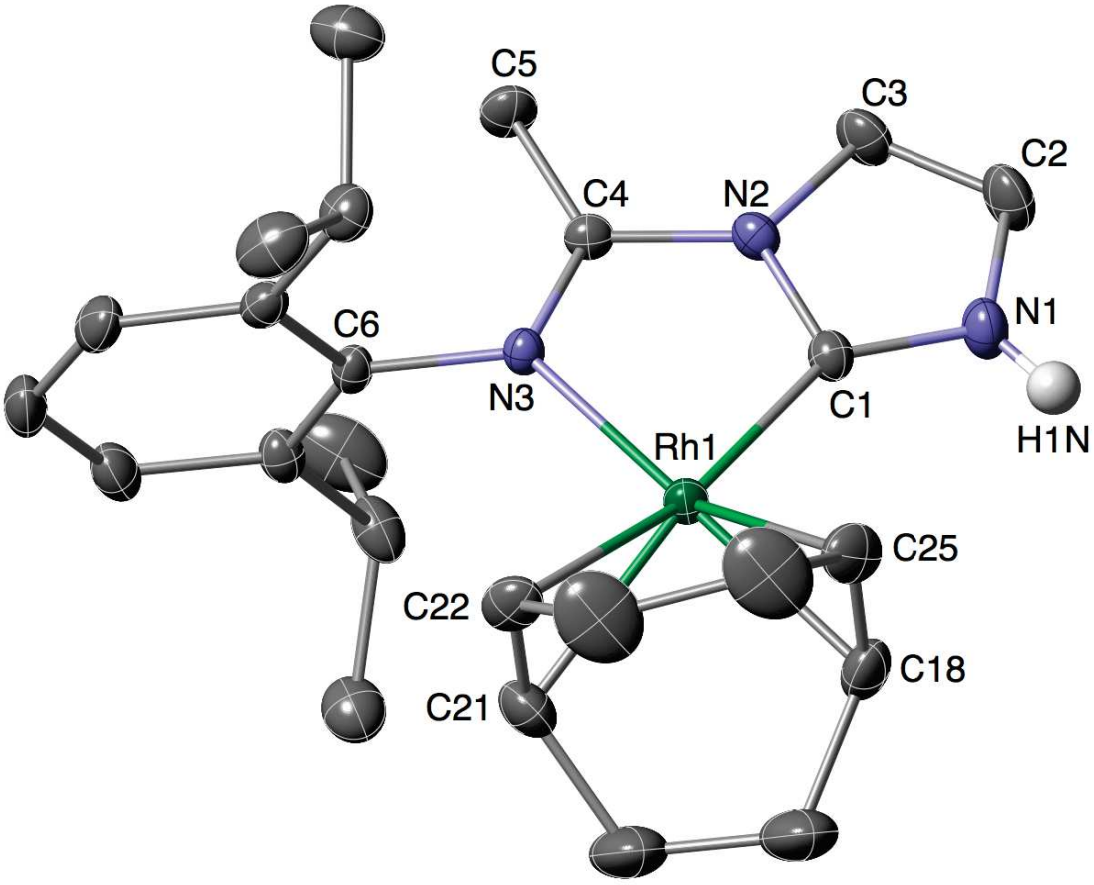

Figure S7. Molecular structure of the cation in $\mathbf{3b}^{+}[PF_6]^{-}$. H atoms are omitted for clarity, except H1N. Thermal ellipsoids are at the 30% level. Selected bond distances (Å) and angles (°): C1–N1 1.342(4), C1–N2 1.369(4), C2–N1 1.380(4), C2–C3 1.340(5), C3–N2 1.392(3), C4–N2 1.399(3), C4–N3 1.287(3), C4–C5 1.484(4), C6–N3 1.444(3), Rh1–C1 1.972(3), Rh1–N3 2.125(2), Rh1–C18 2.137(3), Rh1–C21 2.239(3), Rh1–C22 2.256(3), Rh1–C25 2.122(3), C18–C25 1.390(5), C21–C22 1.345(5), N1–H1N 0.82(4); N1–C1–N2 103.0(2), C1–Rh1–N3 77.7(1), C1–Rh1–C18 95.9(1), C1–Rh1–C25 94.8(1), N3–Rh1–C21 100.6(1), N3–Rh1–C22 97.9(1).

References: p 100

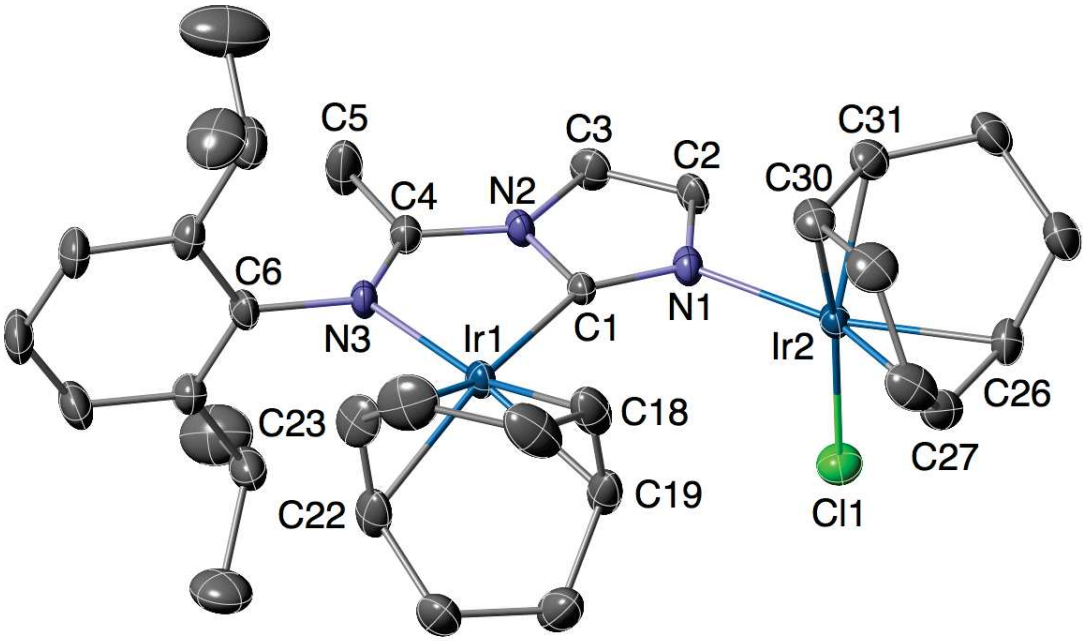

Figure S8. Molecular structure of **10** in **10**·Et_2O·toluene. H atoms and the solvent molecules are omitted for clarity. Thermal ellipsoids are at the 30% level. Selected bond distances (Å) and angles (°): C1–N1 1.335(6), C1–N2 1.397(7), C2–N1 1.391(7), C2–C3 1.342(8), C3–N2 1.387(7), C4–N2 1.382(6), C4–N3 1.289(7), C4–C5 1.486(8), C6–N3 1.454(6), Ir1–C1 2.041(5), Ir1–N3 2.112(4), Ir1–C18 2.137(6), Ir1–C19 2.118(6), Ir1–C22 2.185(5), Ir1–C23 2.184(5), C18–C19 1.400(9), C22–C23 1.380(9), Ir2–Cl1 2.367(1), Ir2–C26 2.149(5), Ir2–C27 2.111(6), Ir2–C30 2.113(5), Ir2–C31 2.099(5), C26–C27 1.396(8), C30–C31 1.418(8); N1–C1–N2 105.9(4), C1–Ir1–N3 78.3(2), C1–Ir1–C18 100.2(2), C1–Ir1–C19 95.8(2), N3–Ir1–C22 98.4(2), N3–Ir1–C23 94.3(2), N1–Ir2–Cl1 88.1(1), N1–Ir2–C30 93.4(2), N1–Ir2–C31 91.0(2), Cl1–Ir2–C26 92.3(2), Cl1–Ir2–C27 91.6(2).

References: p 100

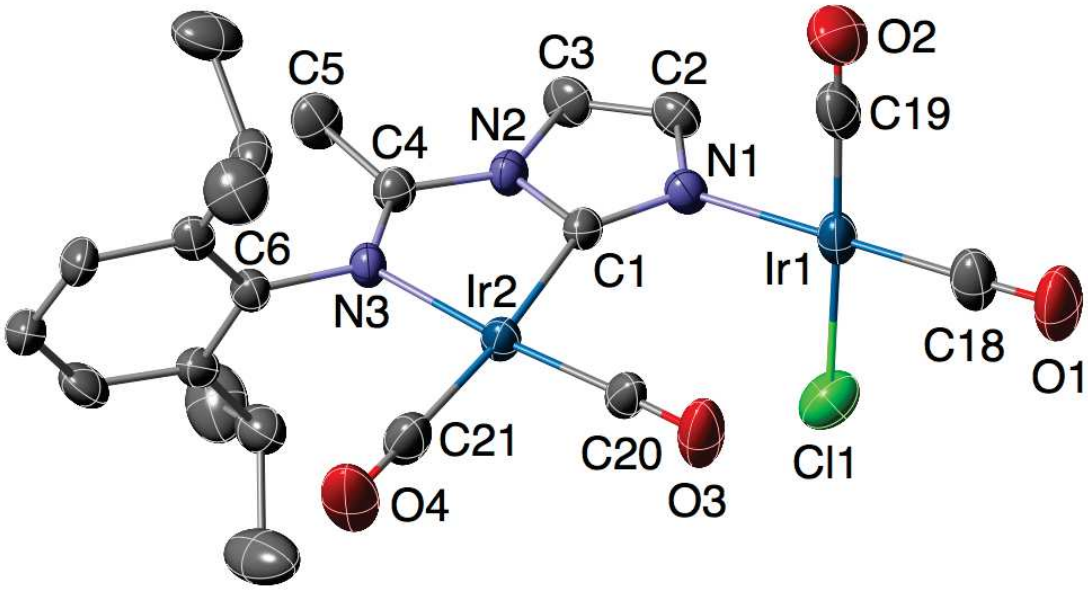

Figure S9. Molecular structure of **11**. Thermal ellipsoids are at the 30% level. Selected bond distances (Å) and angles (°): C1–N1 1.336(9), C1–N2 1.391(9), C2–N1 1.386(9), C2–C3 1.35(1), C3–N2 1.392(8), C4–N2 1.378(9), C4–N3 1.302(9), C4–C5 1.47(1), C6–N3 1.443(8), C1–Ir2 2.052(7), N3–Ir2 2.097(6), C20–Ir2 1.838(8), C21–Ir2 1.907(8), N1–Ir1 2.074(6), Cl1–Ir1 2.339(2), C18–Ir1 1.848(9), C19–Ir1 1.85(1), C18–O1 1.15(1), C19–O2 1.14(1), C20–O3 1.148(9), C21–O4 1.131(9); N1–C1–N2 106.6(6), C1–Ir2–N3 77.5(2), C1–Ir2–C20 97.6(3), C20–Ir2–C21 89.9(3), C21–Ir2–N3 95.0(3); N1–Ir1–Cl1 86.6(2); N1–Ir1–C19 91.8(3); C18–Ir1–C19 88.9(4); C18–Ir1–Cl1 92.7(3).

References: p 100

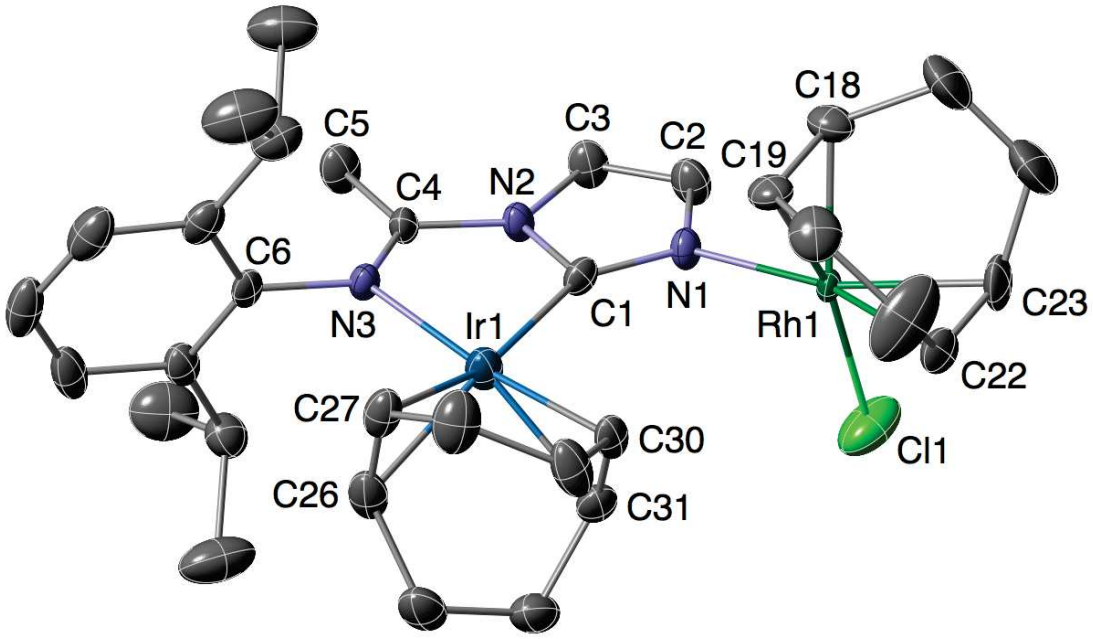

Figure S10. Molecular structure **12** in **12**·2THF. H atoms and the solvent molecules are omitted for clarity. Thermal ellipsoids are at the 30% level. Selected bond distances (Å) and angles (°): C1–N1 1.331(7), C1–N2 1.418(7), C2–N1 1.392(8), C2–C3 1.349(9), C3–N2 1.387(7), C4–N2 1.381(7), C4–N3 1.303(7), C4–C5 1.480(8), C6–N3 1.434(7), Ir1–C1 2.004(6), Ir1–N3 2.111(4), Ir1–C26 2.202(6), Ir1–C27 2.189(6), Ir1–C30 2.140(5), Ir1–C31 2.113(6), C26–C27 1.38(1), C30–C31 1.39(1), Rh1–N1 2.079(5), Rh1–Cl1 2.371(2), Rh1–C18 2.091(6), Rh1–C19 2.113(6), Rh1–C22 2.134(6), Rh1–C23 2.127(6), C18–C19 1.407(9), C22–C23 1.38(1); N1–C1–N2 105.0(5), C1–Ir1–N3 78.4(2), C1–Ir1–C30 98.4(2), C1–Ir1–C31 95.0(2), N3–Ir1–C26 95.7(2), N3–Ir1–C27 99.7(2), N1–Rh1–Cl1 88.4 (2), N1–Rh1–C18 90.3(2), N1–Rh1–C19 91.2(2), Cl1–Rh1–C22 94.1(2), Cl1–Rh1–C23 90.5(3).

References: p 100

Chapitre 5

Unsymmetrical pincer-type Ir(III) pNHC complexes: synthetic, structural and reactivity studies

Résumé

L'imidazole fonctionnalisé 2-(1-(2,6-diisopropylphenylimino)ethyl)-6-(1-imidazolyl)pyridine (**L**) a été préparé avec un rendement satisfaisant. Le composé **L** est ensuite protoné à l'aide de $HBF_4 \cdot Et_2O$ pour donner le sel de diazolium correspondant $[\mathbf{L}H]^+[BF_4]^-$ (Schéma 1).

Schéma 1.

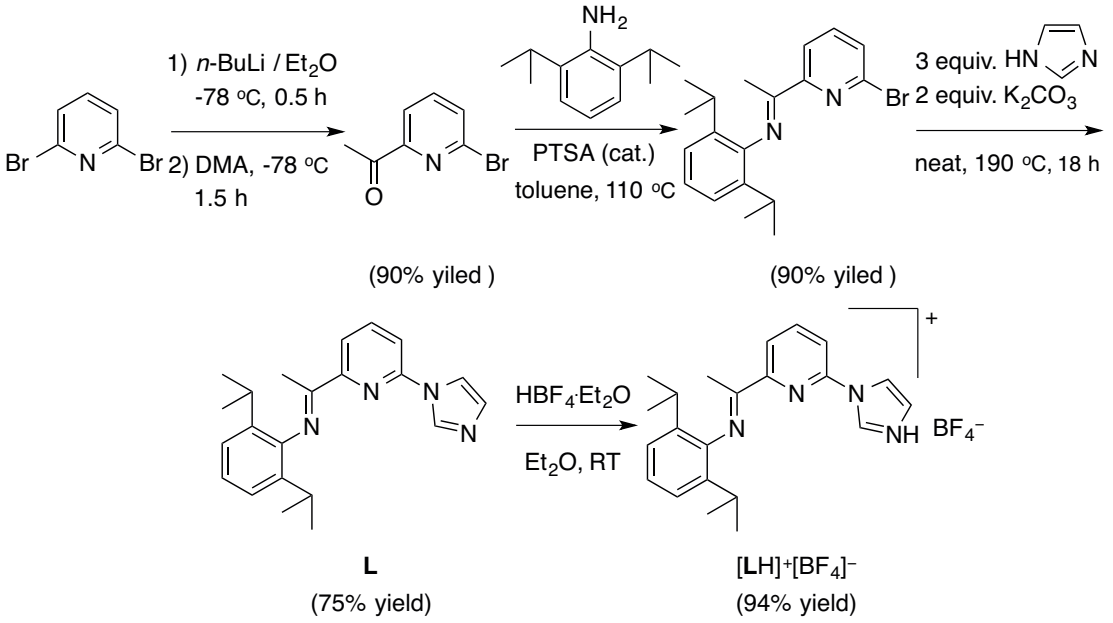

La réaction de métallation du sel de diazolium $[\mathbf{L}H]^+[BF_4]^-$ avec $[Ir(cod)(\mu\text{-}Cl)]_2$ a été conduite dans l'acétonitrile à 80 °C pendant 12 h et a conduit à la formation de $[Ir(NCMe)HCl\{(DippN{=}CMe)(C_5H_3N)(C_3H_3N_2)\text{-}\kappa^3(N_{imine},N_{Py},C2)\}]^+[BF_4]^-$ ($\mathbf{1}^+[BF_4]^-$). Le complexe $[IrP(i\text{-}Pr)_3HCl\{(DippN{=}CMe)(C_5H_3N)(C_3H_3N_2)\text{-}\kappa^3(N_{imine},N_{Py},C2)\}]^+[BF_4]^-$ ($\mathbf{2}^+[BF_4]^-$) a été obtenu par réaction de $\mathbf{1}^+[BF_4]^-$ avec la triisopropylphosphine sous reflux dans le THF pendant 12 h. La réaction d'abstraction de chlorure de $\mathbf{1}^+[BF_4]^-$ par $AgBF_4$ a permis l'obtention de $[Ir(NCMe)_2H\{(DippN{=}CMe)(C_5H_3N)(C_3H_3N_2)\text{-}\kappa^3(N_{imine},N_{Py},C2)\}]^{2+}2[BF_4]^-$ ($\mathbf{3}^{2+}2[BF_4]^-$). Le complexe $[Ir(NCMe)H\{(DippN{=}CMe)(C_5H_3N)(\mu\text{-}C_3H_2N_2\text{-}\kappa C2,\kappa N3)\text{-}\kappa^3(N_{imine},N_{Py},C2)\}]_2^{2+}2[B(ArF_5)_3F]^-$ ($\mathbf{4}^{2+}2[B(ArF_5)_3F]^-$) a été isolé après déprotonation de $\mathbf{3}^{2+}2[BF_4]^-$ à l'aide de KO*t*-Bu et addition ultérieure de $B(ArF_5)_3$ (Schéma 2).

Schéma 2.

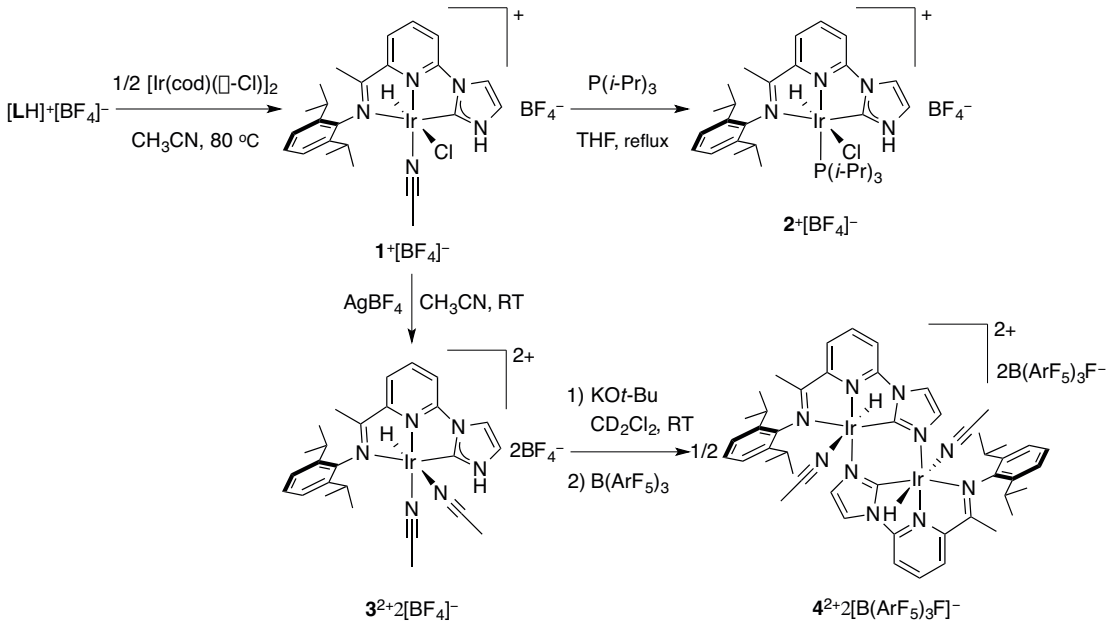

Les structures moléculaires de $\mathbf{1}^{+}[BF_4]^{-}\cdot CH_2Cl_2$, $\mathbf{2}^{+}[BF_4]^{-}\cdot CH_2Cl_2$, $\mathbf{3}^{2+}2[BF_4]^{-}\cdot 2CH_2Cl_2$ et $\mathbf{4}^{2+}2[B(ArF_5)_3F]^{-}\cdot 4CH_2Cl_2$ ont été déterminées par diffraction des rayons X.

Références et synopsis

Unsymmetrical pincer-type Ir(III) pNHC complexes: synthetic, structural and reactivity studies

Ce chapitre est rédigé comme une version préliminaire pour une publication. Ma contribution a porté sur la recherche bibliographique, sur la partie expérimentale ainsi que la rédaction de la version préliminaire. La partie expérimentale est incomplète, cependant la description des résultats dans ce chapitre ne tient compte que des composés organiques et des complexes complètement caractérisés.

References: p 138

Unsymmetrical pincer-type Ir(III) pNHC complexes: synthetic, structural and reactivity studies

Abstract

The functionalized imidazole 2-(1-(2,6-diisopropylphenylimino)ethyl)-6-(1-imidazolyl)pyridine (**L**) was protonated by $HBF_4 \cdot Et_2O$ to give the imidazolium salt $[\mathbf{L}H]^+[BF_4]^-$, which was then metalated with $[Ir(cod)(\mu\text{-}Cl)]_2$ in acetonitrile at 80 °C to give $[Ir(NCMe)HCl\{(DippN{=}CMe)(C_5H_3N)(C_3H_3N_2)\text{-}\kappa^3(N_{imine},N_{Py},C2)\}]^+[BF_4]^-$ ($\mathbf{1}^+[BF_4]^-$). $[IrP(i\text{-}Pr)_3HCl\{(DippN{=}CMe)(C_5H_3N)(C_3H_3N_2)\text{-}\kappa^3(N_{imine},N_{Py},C2)\}]^+[BF_4]^-$ ($\mathbf{2}^+[BF_4]^-$) was prepared by treatment of $\mathbf{1}^+[BF_4]^-$ with tri*iso*propylphosphine in refluxing THF for 12 h. The chloride abstraction reaction of $\mathbf{1}^+[BF_4]^-$ by $AgBF_4$ led to the isolation of $[Ir(NCMe)_2H\{(DippN{=}CMe)(C_5H_3N)(C_3H_3N_2)\text{-}\kappa^3(N_{imine},N_{Py},C2)\}]^{2+}2[BF_4]^-$ ($\mathbf{3}^{2+}2[BF_4]^-$). The dinuclear complex $[Ir(NCMe)H\{(DippN{=}CMe)(C_5H_3N)(\mu\text{-}C_3H_2N_2\text{-}\kappa C2,\kappa N3)\text{-}\kappa^3(N_{imine},N_{Py},C2)\}]_2^{2+}2[B(ArF_5)_3F]^-$ ($\mathbf{4}^{2+}2[B(ArF_5)_3F]^-$) was isolated after deprotonation of $\mathbf{3}^{2+}2[BF_4]^-$ by KO*t*-Bu followed by addition of $B(ArF_5)_3$. It contains two Ir pincer moieties which are connected by the Ir–N bonds in a μ-C,N bridging mode. The molecular structures of $\mathbf{1}^+[BF_4]^- \cdot CH_2Cl_2$, $\mathbf{2}^+[BF_4]^- \cdot CH_2Cl_2$, $\mathbf{3}^{2+}2[BF_4]^- \cdot 2CH_2Cl_2$ and $\mathbf{4}^{2+}2[B(ArF_5)_3F]^- \cdot 4CH_2Cl_2$ have been determined by X-ray diffraction.

Introduction

As tunable and strong σ-donor ligands, N-heterocyclic carbenes (NHCs) have triggered a fast growing interest in organometallic chemistry in the last two decades.[1] A considerable number of NHC metal complexes have been produced and in most cases, both N sites carry a substituent R (R = alkyl or aryl in **I**) that allows a fine-tuning of the steric and electronic properties of the NHC ligand. In contrast, protic NHC (R = alkyl, aryl or H in **II**) metal complexes are less common.

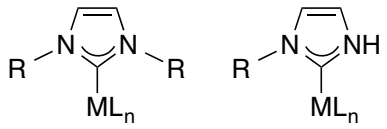

I **II**

Owing to the presence of an acidic NH group, pNHCs cannot generally be readily obtained by simple deprotonation of the corresponding imidazolium salts and they are not stable as free ligands and tend to isomerize to the corresponding imidazoles by H migration from C2 to N.[2] Thus pNHCs have been comparatively much less investigated and the synthesis of pNHC complexes is still a challenge. The presence of a NH moiety in a pNHC complex can act as a reactive site of potential relevance to bifunctional catalysis[3] and substrate recognition.[4] This feature has motivated the development of various synthetic methods to access pNHC metal complexes, and they have been recently reviewed.[4b,4c,5] Among the limited number of pNHC metal complexes reported, those of the pincer type often possesses interesting properties which make them attractive targets (Scheme 1).

Scheme 1. Transition metal complexes containing pincer-type pNHC ligands.[6]

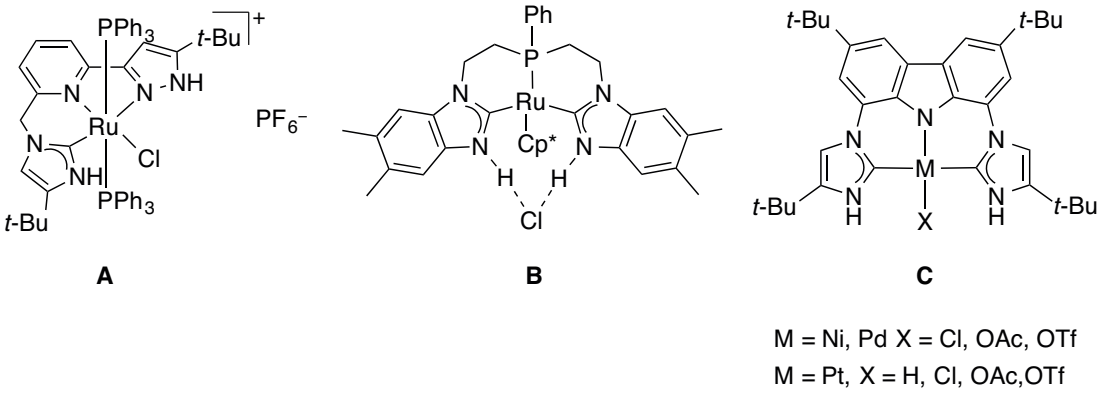

A **B** **C**

M = Ni, Pd X = Cl, OAc, OTf
M = Pt, X = H, Cl, OAc,OTf

References: p 138

The Ru(II) unsymmetrical pincer-type pNHC complex reported by Kuwata and Ikariya (**A** in Scheme 1) has two different NH groups, one belongs to the pNHC ligand and the other to the pyrazole. Treatment of this complex with one equivalent of base led to deprotonation of the pyrazole, indicating that the pNHC arm is less acidic.[6b] The Ru(II) pincer pNHC complex reported by Flowers and Cossairt (**B** in Scheme 1) shows in the solid state hydrogen bonding interactions between the two NH groups and the chloride counterion. A double deprotonation of this complex followed by salt metathesis afforded Ru(II)/Fe(II) and Ru(II)/Co(II) bimetallic complexes.[6a] The Ni(II) pincer pNHC complex reported by Grotjahn (**C** in Scheme 1) is the first such example for a first-row metal. The Pt(II) triflate analog was successfully applied to the anti-Markovnikov addition of O−H bonds to alkynes and the catalytic hydration of alkynes.[6c]

We have recently reported a one step procedure to prepare bidentate Ir(III) imine-functionalized pNHC complexes by direct metalation of the imidazolium salt (Scheme 2).[7] In order to extend this reaction, we have now investigated the synthesis and properties of unsymmetrical pincer-type pNHC Ir(III) complexes.

Scheme 2. One step access to a bidentate imine-functionalized pNHC Ir(III) complex.[7]

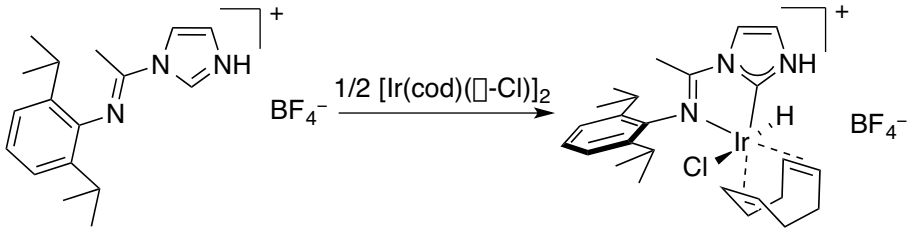

Results and discussion

Synthesis of the ligand. The compounds 2-acetyl-6-bromopyridine[8] and 2-1-(2,6-diisopropylphenylimino)ethyl-6-bromopyridine[9] were prepared from the commercially available 2,6-dibromopyridine. According to the synthetic methodology of 2-imidazolylpyridines reported by Herrmann and Kühn,[10] the reaction of 2-1-(2,6-diisopropylphenylimino)ethyl-6-bromopyridine with 3 equiv. of imidazole and 2 equiv. of K_2CO_3 at 190 °C for 18 h led to the isolation of

2-(1-(2,6-diisopropylphenylimino)ethyl)-6-(1-imidazolyl)pyridine (**L**) in satisfactory yields (Scheme 3).

Scheme 3. Synthesis of **L** and $[\mathbf{L}H]^+[BF_4]^-$.

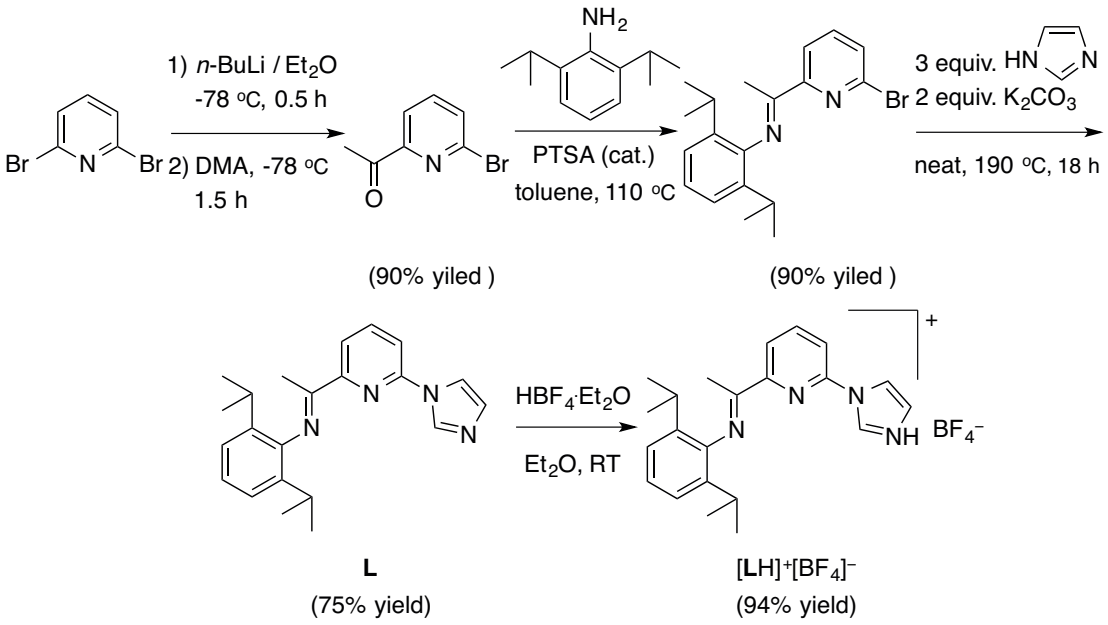

Then **L** was protonated by $HBF_4 \cdot Et_2O$ to give the imidazolium salt $[\mathbf{L}H]^+[BF_4]^-$ in high yield. In the ^1H NMR spectrum of $[\mathbf{L}H]^+[BF_4]^-$ in DMSO-d_6, the C2–*H* proton of the imidazole exhibits a characteristic apparent triplet resonance at δ 10.06 (^4J = 1.7 Hz) which is considerably downfield shifted compared to that in **L** (δ 8.44 in $CDCl_3$). It is also noteworthy that the shift of the $^{13}C\{^1H\}$ NMR resonances due to C_{imine} and *C*2 (at δ 165.9 and 134.7 in $[\mathbf{L}H]^+[BF_4]^-$) is useful to determine the formation of a pincer-type metal complex, in which C2 is metalated and the metal is coordinated by the imine functional group.

Synthesis of Ir(III) complexes. Attempts to metalate $[\mathbf{L}H]^+[BF_4]^-$ with either $[Ir(coe)_2(\mu\text{-}Cl)]_2$ or $[Ir(C_2H_4)_2(\mu\text{-}Cl)]_2$, which were monitored by ^1H NMR spectroscopy in different deuterated solvents such as CD_3CN, C_6D_6, toluene-d_8 or THF-d_8, resulted in intractable mixtures regardless of reaction time or temperature. The metalation by $[Ir(cod)(\mu\text{-}Cl)]_2$ was best performed in acetonitrile. After heated its solution up at 80 °C for 12 h,

[Ir(NCMe)HCl{(DippN=CMe)(C_5H_3N)($C_3H_3N_2$)-κ^3(N_{imine},N_{Py},C2)}]$^+$[BF_4]$^-$ (**1**$^+$[BF_4]$^-$) was isolated from the reaction mixture in good yield (Scheme 4).

Scheme 4. Synthesis of Ir(III) complexes.

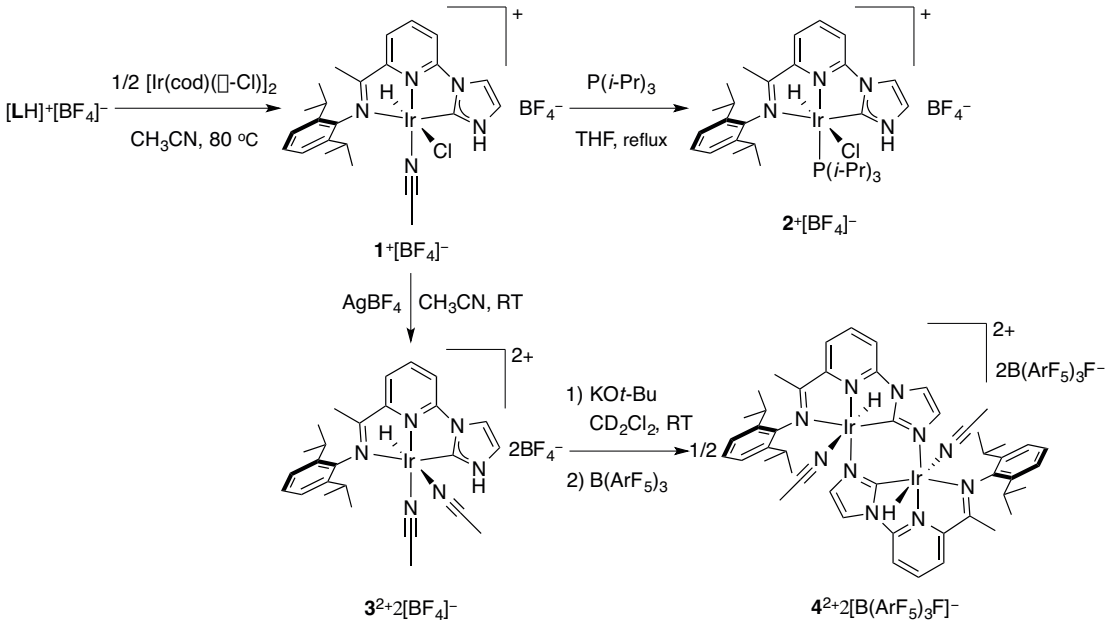

In the ^{1}H NMR spectrum of **1**$^+$[BF_4]$^-$ in CD_2Cl_2, the N*H* proton gives rise to a broad singlet at δ 11.59. There were no signals for the cod ligand and C2–*H* proton, but two characteristic new singlet resonances were found at δ 2.31 and -22.73 and assigned to the coordinated C*H*$_3$CN and Ir–*H*, respectively The ^{13}C{^{1}H} NMR spectrum contains resonances for C_{imine} at δ 176.9 and $C2_{NHC}$ at δ 141.9. All these data are consistent with **1**$^+$[BF_4]$^-$ being an Ir(III) pincer complex. This was confirmed by the structural determination of **1**$^+$[BF_4]$^-$·CH_2Cl_2 by X-ray diffraction (Figure 1, with selected bond distances and angles).

References: p 138

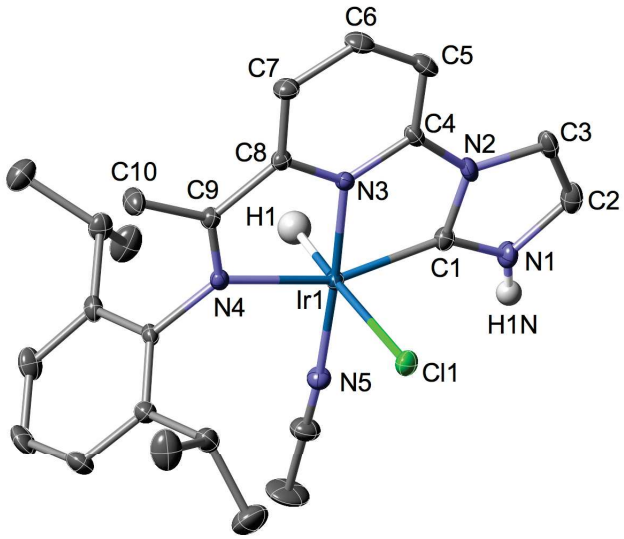

Figure 1. View of the molecular structure of the cation in $\mathbf{1}^{+}[BF_4]^{-}\cdot CH_2Cl_2$. H atoms are omitted for clarity, except H1 and H1N. Thermal ellipsoids are at the 30% level. Selected bond distances (Å) and angles (°): C1–N1 1.332(4), C1–N2 1.380(4), Ir1–C1 1.970(3), Ir1–N3 1.956(2), Ir1–N4 2.124(2), Ir1–N5 2.006(3), Ir1–Cl1 2.4990(8); N1–C1–N2 104.3(3), C1–Ir1–N3 79.8(1), N3–Ir1–N4 77.9(1), N4–Ir1–N5 100.5(1), N5–Ir1–C1 101.7(1), Cl1–Ir1–C1 88.5(1), Cl1–Ir1–N3 89.50(8), Cl1–Ir1–N4 93.57(7), Cl1–Ir1–N5 93.56(9).

The structure of $\mathbf{1}^{+}[BF_4]^{-}\cdot CH_2Cl_2$ shows tridentate $\kappa^3(N_{imine},N_{Py},C2)$ coordination of the ligand and a distorted octahedral coordination geometry for the metal. The *cis* disposition of the Ir–C and Ir–H bonds is consistent with this 18 valence electron Ir(III) complex resulting from C–H oxidative addition to Ir(I).The Ir1–C1 bond distance of 1.970(3) Å is similar to that in the bidentate imine functionalized pNHC Ir(III) complex (1.983(2) Å).[7] The shortest N−H···F(BF_3) distance of 2.01(4) Å is consistent with a hydrogen bonding interaction.

Deprotonation of $\mathbf{1}^{+}[BF_4]^{-}$ by KO*t*-Bu at room temperature was monitored by ^{1}H NMR spectroscopy in CD_2Cl_2. After addition of a stoichiometric amount of KO*t*-Bu, the disappearance of the N*H* proton and the characteristic doublet resonance due to C5–*H* at δ 7.75 (d, ^3J = 2.3 Hz) (*cf.* 7.77 (dd, J = 2.2, 0.9 Hz) in $\mathbf{1}^{+}[BF_4]^{-}$) indicate the formation of the Ir(III) complex containing a C-bound 'anionic' imidazolide ligand in solution. Unfortunately, attempts to isolate this iridium species under different conditions (KO*t*-Bu / DCM, RT or KHMDS / THF, −78 °C) led to intractable reaction mixtures. Therefore, in order to stabilize the iridium centre,

[IrP(*i*-Pr)$_3$HCl{(DippN=CMe)(C_5H_3N)($C_3H_3N_2$)-κ^3(N_{imine},N_{Py},C2)}]$^+$[BF_4]$^-$ (**2**$^+$[BF_4]$^-$) was prepared by treatment of **1**$^+$[BF_4]$^-$ with tri*iso*propylphosphine in refluxing THF for 12 h (Scheme 4). The ^{1}H NMR spectrum of **2**$^+$[BF_4]$^-$ shows the Ir–*H* resonance at δ −22.41 (d, $^2J_{H\text{-}P}$ = 19.5 Hz). The coordinated tri*iso*propylphosphine ligand gives rise to a singlet in ^{31}P{^{1}H} NMR at δ 12.8. The C_{NHC} resonance at δ 146.4 (d, $^2J_{C\text{-}P}$ = 9.9 Hz) in the ^{13}C{^{1}H} NMR spectrum suggests that coordination of the tri*iso*propylphosphine ligand has occurred in *cis* position with respect to the C_{NHC}. As expected, the structure of **2**$^+$[BF_4]$^-$·CH_2Cl_2 (Figure 2, with selected bond distances and angles), in which the acetonitrile ligand has been replaced by a triisopropylphosphine ligand, is similar to that of **1**$^+$[BF_4]$^-$·CH_2Cl_2.

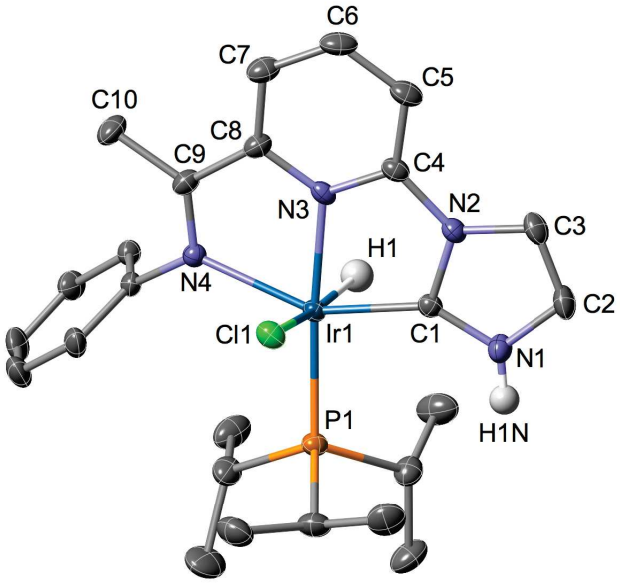

Figure 2. View of the molecular structure of the cation in **2**$^+$[BF_4]$^-$·CH_2Cl_2. Two isopropyl groups in Dipp and H atoms are omitted for clarity, except H1 and H1N. Thermal ellipsoids are at the 30% level. Selected bond distances (Å) and angles (°): C1–N1 1.348(4), C1–N2 1.391(3), Ir1–C1 1.973(3), Ir1–N3 2.052(2), Ir1–N4 2.206(2), Ir1–P1 2.3259(9), Ir1–Cl1 2.487(1); N1–C1–N2 102.5(2), C1–Ir1–N3 78.9(1), N3–Ir1–N4 74.40(9), N4–Ir1–P1 109.51(6), P1–Ir1–C1 97.00(8), Cl1–Ir1–C1 92.24(8), Cl1–Ir1–N3 82.45(7), Cl1–Ir1–N4 88.92(6), Cl1–Ir1–P1 99.23(3).

The coordination geometry of Ir in **2**$^+$ is distorted octahedral and comprises a κ^3(N_{imine},N_{Py},C2) ligand, one tri*iso*propylphosphine ligand and mutually *trans* hydride and chloride ligands. The Ir1–C1 bond distance of 1.973(3) Å is similar to that in

$\mathbf{1}^{+}[BF_4]^{-}\cdot CH_2Cl_2$. The presence of a N−H···F(BF_3) hydrogen bonding interaction can also be deduced from the metrical data (N−H···F(BF_3) distance 2.03 Å).

Chloride abstraction from $\mathbf{1}^{+}[BF_4]^{-}$ by $AgBF_4$ was performed in acetonitrile at room temperature to afford $[Ir(NCMe)_2H\{(DippN{=}CMe)(C_5H_3N)(C_3H_3N_2)\text{-}\kappa^3(N_{imine},N_{Py},C2)\}]^{2+}2[BF_4]^{-}$ ($\mathbf{3}^{2+}2[BF_4]^{-}$) (Scheme 4). According to its NMR spectra in CD_2Cl_2, this complex contains two acetonitrile ligands, and the resonance of Ir–*H* at is slightly upfield shifted compared to $\mathbf{1}^{+}[BF_4]^{-}$ (δ −23.11 *vs*. −22.73), while the resonance of C_{NHC} is downfield shifted (δ 146.1 *vs*. 141.9). The 18 valence electron Ir(III) center in $\mathbf{3}^{2+}2[BF_4]^{-}$ adopts a distorted octahedral coordination geometry (Figure 3, with selected bond distances and angles). Two acetonitrile ligands are *cis* to each other. The bond distance of Ir1–C1 is 1.982(4) Å.

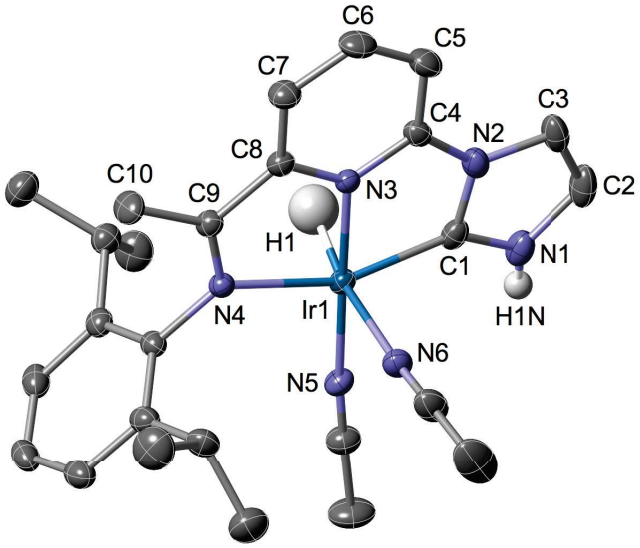

Figure 3. View of the molecular structure of the cation in $\mathbf{3}^{2+}2[BF_4]^{-}\cdot 2CH_2Cl_2$. H atoms are omitted for clarity, except H1 and H1N. Thermal ellipsoids are at the 30% level. Selected bond distances (Å) and angles (°): C1–N1 1.328(5), C1–N2 1.382(6), Ir1–C1 1.982(4), Ir1–N3 1.984(3), Ir1–N4 2.122(3), Ir1–N5 2.015(3), Ir1–N6 2.154(4); N1–C1–N2 105.5(4), C1–Ir1–N3 78.8(2), N3–Ir1–N4 78.3(1), N4–Ir1–N5 102.8(1), N5–Ir1–C1 100.1(2), N6–Ir1–C1 91.4 (2), N6–Ir1–N3 92.7(1), N6–Ir1–N4 92.7(1), N5–Ir1–N6 87.7(2).

Initially, for the purpose of obtaining a pincer-type anionic NHC complex which contains a N–$B(ArF_5)_3$ moiety, the deprotonation of $\mathbf{3}^{2+}2[BF_4]^{-}$ with KO*t*-Bu

followed by addition of $B(ArF_5)_3$ was performed in a ^1H NMR experiment in CD_2Cl_2. Unexpectedly, the dinuclear complex [Ir(NCMe)H{(DippN=CMe)(C_5H_3N)(μ-$C_3H_2N_2$-κC2,κN3)-κ^3(N_{imine},N_{Py},C2)}]$_2^{2+}$2[B(ArF_5)$_3$F]$^-$ (**4**$^{2+}$2[B(ArF_5)$_3$F]$^-$) was isolated in this reaction mixture. In its ^1H NMR spectrum in CD_2Cl_2, the protons at the imidazolide backbone C4 and C5 positions give rise to an AX pattern at δ 5.31 (d) and 7.30 (d, ^3J = 1.6 Hz). In the $^{13}C\{^1H\}$ NMR spectrum, the resonances at δ 129.2 and 116.3 are assigned to C4 and C5, respectively. The $^{13}C\{^1H\}$ NMR resonance of the imidazolide C2 carbon in **4**$^{2+}$2[B(ArF_5)$_3$F]$^-$ (δ 154.1) is downfield shifted compared to C_{NHC} in **3**$^{2+}$2[BF_4]$^-$ (δ 146.1). The structure of **4**$^{2+}$2[B(ArF_5)$_3$F]$^-$·4CH_2Cl_2 was further confirmed crystallographically (Figure 4, with selected bond distances and angles).

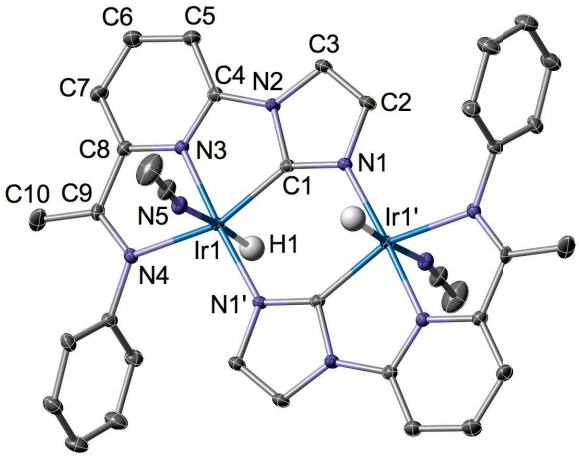

Figure 4. View of the molecular structure of the cation in **4**$^{2+}$2[B(ArF_5)$_3$F]$^-$·4CH_2Cl_2. Two isopropyl groups in Dipp and H atoms are omitted for clarity, except H1. Thermal ellipsoids are at the 30% level. Selected bond distances (Å) and angles (°): C1–N1 1.328(3), C1–N2 1.404(3), Ir1–C1 1.980(2), Ir1–N3 1.978(2), Ir1–N4 2.155(2), Ir1–N1' 2.059(2), Ir1–N5 2.161(2); N1–C1–N2 107.3(2), C1–Ir1–N3 80.33(8), N3–Ir1–N4 76.88(7), N4–Ir1–N1' 105.85(7), N1'–Ir1–C1 96.86(7), N5–Ir1–C1 90.38(8), N5–Ir1–N3 92.29(7), N5–Ir1–N4 94.80(7), N5–Ir1–N1' 88.60(7).

The structure of **4**$^{2+}$ reveals a dinuclear complex containing two Ir(III) pincer-type imidazolide complexes in a μ-C,N bridging mode, each Ir has a distorted octahedral coordination geometry defined by a κ^3(N_{imine},N_{Py},C2) ligand, *trans* hydride and acetonitrile ligands and one nitrogen atom from another ligand. The separation

between the metal atoms is 3.992 Å, which is too long to allow direct interaction between the metal centers. The C1–N1 distance of 1.328(3) Å is shorter than C1–N2 1.404(3) Å, which would be consistent with a more pronounced double bond character for the C–N bond in the bridging part of the ligands.

Conclusion

We have extended the one step procedure of metalation of functionalized imidazolium salts to synthesize pincer-type Ir(III) pNHC complexes and explored their reactivity. These results are useful for the further development of synthetic methodologies giving access to pNHC, C-bound 'anionic' imidazolide complexes.

Experimental Section

General Considerations. All manipulations involving organometallics were performed under argon in a Braun glove-box or using standard Schlenk techniques. Solvents were dried using standard methods and distilled over sodium/benzophenone under argon prior use or passed through columns of activated alumina and subsequently purged with argon. $[Ir(cod)(\mu\text{-}Cl)]_2$ is commercially available from Johnson Matthey PLC. NMR spectra of complexes were recorded on a Bruker 300 MHz, 400 MHz or 500 MHz instrument at ambient temperature and referenced using the proton (^1H) or carbon (^{13}C) resonance of the residual solvent. Assignments are based on ^1H, ^1H-COSY, ^1H-NOESY, $^1H/^{13}C$-HSQC, and $^1H/^{13}C$-HMBC experiments. $^{31}P\{^1H\}$ NMR spectra were recorded on a Bruker Avance 300 instrument at 121.49 MHz using H_3PO_4 (85% in D_2O) as external standard. IR spectra were recorded in the region 4000–100 cm^{-1} on a Nicolet 6700 FT-IR spectrometer (ATR mode, diamond crystal). Elemental analyses were performed by the "Service de microanalyses", Université de Strasbourg.

Synthesis of 2-(1-(2,6-diisopropylphenylimino)ethyl)-6-(1-imidazolyl)pyridine (L). A 50 mL round Schlenk flask equipped with a stirring bar was loaded with 2-1-(2,6-di*iso*propylphenylimino)ethyl-6-bromopyridine (1.00 g, 2.78 mmol), imidazole (0.57 g, 8.37 mmol) and K_2CO_3 (0.77 g, 5.56 mmol). The reaction mixture

was degassed under 10^{-3} mbar and placed under argon atmosphere, this cycle was repeated three times. Then the mixture was stirred at 190 °C for 18 h. After cooling to room temperature, the mixture was diluted in 10 mL of water, extracted with dichloromethane (3 × 10 mL) and the extract was washed with a saturated aqueous Na_2CO_3 solution (3 × 20 mL). The combined organic phases were dried over $NaSO_4$, filtered and the solvent was removed under reduced pressure to leave a crude brown solid. It was dissolved in 50 mL of Et_2O and the solution was passed through a plug of Celite, then the solvent was removed under reduced pressure and the resultant solid was washed with pentane (3 × 5 mL) to yield a yellowish powder (0.72 g, 75%). ^{1}H NMR (500 MHz, $CDCl_3$): δ 8.44 (apparent t, ^4J = 1.4 Hz, 1H, NC*H*N$_{(near\ Py)}$), 8.31 (dd, J = 7.8, 0.5 Hz, 1H, C*H* Py), 7.95 (apparent t, ^3J = 7.8 Hz, 1H, C*H* Py), 7.72 (apparent t, $^{3,4}J$ = 1.4 Hz, 1H, NC*H*CHN$_{(near\ Py)}$), 7.46 (dd, J = 7.8, 0.5 Hz, 1H, C*H* Py), 7.24 (apparent t, $^{3,4}J$ = 1.4 Hz, 1H, NCHC*H*N$_{(near\ Py)}$), 7.20–7.08 (m, 3H, C*H* Ar), 2.72 (sept, ^3J = 6.9 Hz, 2H, C*H*(CH$_3$)$_2$), 2.23 (s, 3H, C*H*$_{3(imine)}$), 1.16 (d, ^3J = 6.9 Hz, 6H, CH(C*H*$_3$)$_2$), 1.15 (d, ^3J = 6.9 Hz, 6H, CH(C*H*$_3$)$_2$). ^{13}C{^{1}H} NMR (125 MHz, $CDCl_3$): δ 166.1 (*C*=N), 155.9 (*C* Ar), 148.2 (*C* Ar), 146.3 (*C* Ar), 139.6 (*C*H Ar), 135.8 (*C* Ar), 135.1 (N*C*HN$_{(near\ Py)}$), 131.0 (N*C*HCHN$_{(near\ Py)}$), 123.9 (*C*H Ar), 123.2 (*C*H Ar), 119.4 (*C*H Ar), 116.3 (NCH*C*HN$_{(near\ Py)}$), 113.1 (*C*H Ar), 28.5 (*C*H(CH$_3$)$_2$), 23.3 (CH(*C*H$_3$)$_2$), 23.0 (CH(*C*H$_3$)$_2$), 17.3 (*C*H$_{3(imine)}$). Anal. Calcd for $C_{22}H_{26}N_4$ (346.48): C, 76.27; H, 7.56; N, 16.17. Found: C, 75.97; H, 7.73; N, 16.12.

Synthesis of [LH]$^+$[BF$_4$]$^-$. To a stirred solution of 2-(1-(2,6-di*iso*propylphenylimino)ethyl)-6-(1-imidazolyl)pyridine (0.34 g, 1.00 mmol) in Et_2O (30 mL) was added dropwise a solution of $HBF_4 \cdot Et_2O$ (0.16 g, 1.00 mmol) in Et_2O (5 mL). The reaction mixture was stirred for 2 h at room temperature. Then the resultant precipitate was collected by filtration, washed with Et_2O and dried in vacuo to obtain a yellow powder (0.41 g, 0.94 mmol, 94%). ^{1}H NMR (500 MHz, DMSO-d$_6$): δ 10.06 (apparent t, ^4J = 1.7 Hz, 1H, NHC*H*N$_{(near\ Py)}$), 8.61 (apparent t, $^{3,4}J$ = 1.7 Hz, 1H, NHCHC*H*N$_{(near\ Py)}$), 8.44 (d, J = 7.9 Hz, 1H, C*H* Py), 8.35 (apparent t, ^3J = 7.9 Hz, 1H, C*H* Py), 8.21 (d, J = 7.9 Hz, 1H, C*H* Py), 7.99 (apparent t, $^{3,4}J$ = 1.7 Hz, 1H, NHC*H*CHN$_{(near\ Py)}$), 7.21–7.07 (m, 3H, C*H* Ar), 2.65 (sept, ^3J = 6.9 Hz, 2H, C*H*(CH$_3$)$_2$), 2.23 (s, 3H, C*H*$_{3(imine)}$), 1.11 (d, ^3J = 6.9 Hz, 6H, CH(C*H*$_3$)$_2$), 1.09 (d, ^3J = 6.9 Hz, 6H, CH(C*H*$_3$)$_2$). The N*H* resonance was not observed. ^{13}C{^{1}H} NMR (125

MHz, DMSO-d_6): δ 165.9 (*C*=N), 154.7 (*C* Ar), 146.0 (*C* Ar), 145.5 (*C* Ar), 141.4 (*C*H Ar), 135.1 (*C* Ar), 134.7 (NH*C*HN$_{(near\ Py)}$), 124.0 (*C*H Ar), 123.1 (*C*H Ar), 121.5 (NH*C*HCHN$_{(near\ Py)}$), 121.2 (*C*H Ar), 119.2 (*C*H Ar), 116.0 (NHCH*C*HN$_{(near\ Py)}$), 27.9 (*C*H(CH$_3$)$_2$), 23.1 (CH(*C*H$_3$)$_2$), 22.7 (CH(*C*H$_3$)$_2$), 17.1 (*C*H$_{3(imine)}$). Anal. Calcd for $C_{22}H_{27}BF_4N_4$ (434.29): C, 60.84; H, 6.27; N, 12.90. Found: C, 60.46; H, 6.19; N, 12.66.

Synthesis of [Ir(NCMe)HCl{(DippN=CMe)(C$_5$H$_3$N)(C$_3$H$_3$N$_2$)-κ^3(N$_{imine}$,N$_{Py}$,C2)}]$^+$[BF$_4$]$^-$ (1$^+$[BF$_4$]$^-$). To a stirred solution of [**L**H]$^+$[BF$_4$]$^-$ (0.065 g, 0.15 mmol) in acetonitrile (3 mL) was added to a solution of [Ir(cod)(μ-Cl)]$_2$ (0.050 g, 0.075 mmol) in acetonitrile (2 mL). The reaction mixture was stirred for 12 h at 80 °C and then the volatiles were removed under reduced pressure. The residue was washed with Et_2O (3 × 2 mL) to yield a red solid, which was collected by filtration and dried in vacuo (0.086 g, 0.12 mmol, 82%). ^{1}H NMR (400 MHz, CD_2Cl_2): δ 11.59 (br s, 1H, N*H*), 8.05 (apparent t, ^3J = 8.0 Hz, 1H, C*H* Py), 7.87 (dd, J = 8.0, 0.6 Hz, 1H, C*H* Py), 7.84 (dd, J = 8.0, 0.6 Hz, 1H, C*H* Py), 7.77 (dd, J = 2.2, 0.9 Hz, 1H, NHCHC*H*N$_{(near\ Py)}$), 7.40–7.26 (m, 3H, C*H* Ar), 7.23 (apparent t, ^3J = 2.2 Hz, 1H, NHC*H*CHN$_{(near\ Py)}$), 3.59 (sept, ^3J = 6.8 Hz, 1H, C*H*(CH$_3$)$_2$), 2.73 (sept, ^3J = 6.8 Hz, 1H, C*H*(CH$_3$)$_2$), 2.58 (s, 3H, C*H*$_{3(imine)}$), 2.31 (s, 3H, C*H*$_3$CN), 1.28 (d, ^3J = 6.8 Hz, 3H, CH(C*H*$_3$)$_2$), 1.18 (d, ^3J = 6.8 Hz, 3H, CH(C*H*$_3$)$_2$), 1.16 (d, ^3J = 6.8 Hz, 3H, CH(C*H*$_3$)$_2$), 1.12 (d, ^3J = 6.8 Hz, 3H, CH(C*H*$_3$)$_2$), −22.73 (s, 1H, Ir–*H*). ^{13}C{^{1}H} NMR (100 MHz, CD_2Cl_2): δ 176.9 (*C*=N), 157.5 (*C* Ar), 154.9 (*C* Ar), 141.9 (NH*C*N$_{(near\ Py)}$), 141.7 (*C*H Ar), 141.2 (*C* Ar), 139.4 (*C* Ar), 128.6 (*C*H Ar), 125.2 (*C*H Ar), 122.4 (*C*H Ar), 120.9 (NH*C*HCHN$_{(near\ Py)}$), 120.6 (CH$_3$*C*N), 117.5 (NHCH*C*HN$_{(near\ Py)}$), 112.0 (*C*H Ar), 28.6 (*C*H(CH$_3$)$_2$), 27.7 (*C*H(CH$_3$)$_2$), 25.6 (CH(*C*H$_3$)$_2$), 24.8 (CH(*C*H$_3$)$_2$), 24.3 (CH(*C*H$_3$)$_2$), 24.2 (CH(*C*H$_3$)$_2$), 18.8 (*C*H$_{3(imine)}$), 3.4 (*C*H$_3$CN). Anal. Calcd for $C_{24}H_{30}BClF_4IrN_5$ (703.01): C, 41.00; H, 4.30; N, 9.96. Found: C, 40.57; H, 4.31; N, 9.75.

Synthesis of [IrP(*i*-Pr)$_3$HCl{(DippN=CMe)(C$_5$H$_3$N)(C$_3$H$_3$N$_2$)-κ^3(N$_{imine}$,N$_{Py}$,C2)}]$^+$[BF$_4$]$^-$ (2$^+$[BF$_4$]$^-$). To a stirred solution of **1** (0.070 g, 0.10 mmol) in THF (5 mL), was added dropwise a solution of tri*iso*propylphosphine (0.1 M in toluene, 1.1 mL, 1.1 mmol).

The reaction mixture was refluxed with stirring for 12 h. The volatiles were removed under reduced pressure and the residue was washed with Et_2O (3 × 2 mL) to yield an orange solid, which was collected by filtration and dried in vacuo (0.062 g, 0.075 mmol, 75%). ^{1}H NMR (300 MHz, CD_2Cl_2): δ 10.26 (br s, 1H, N*H*), 8.18 (apparent t, ^3J = 8.0 Hz, 1H, C*H* Py), 7.99 (dt, *J* = 8.0, 0.9 Hz, 1H, C*H* Py), 7.93 (dt, *J* = 8.0, 0.9 Hz, 1H, C*H* Py), 7.84 (dd, *J* = 2.3, 0.9 Hz, 1H, NHCHC*H*N$_{(near\ Py)}$), 7.40–7.22 (m, 4H, C*H* Ar and NHC*H*CHN$_{(near\ Py)}$), 3.50 (sept, ^3J = 6.7 Hz, 1H, C*H*(CH$_3$)$_2$), 2.64 (sept, ^3J = 6.7 Hz, 1H, C*H*(CH$_3$)$_2$), 2.45 (s, 3H, C*H*$_{3(imine)}$), 2.27 (m, 3H, PC*H*(CH$_3$)$_2$), 1.34–1.18 (m, 15H, PC*H*(CH$_3$)$_2$ CH(C*H*$_3$)$_2$), 1.16–1.00 (m, 15H, PC*H*(CH$_3$)$_2$ CH(C*H*$_3$)$_2$), −22.41 (d, $^2J_{H\text{-}P}$ = 19.5 Hz, 1H, Ir–*H*). ^{13}C{^{1}H} NMR (75 MHz, CD_2Cl_2): δ 180.4 (d, $^3J_{C\text{-}P}$ = 2.5 Hz, *C*=N), 155.1 (d, $^3J_{C\text{-}P}$ = 1.3 Hz, *C* Ar), 151.5 (d, $^3J_{C\text{-}P}$ = 1.9 Hz, *C* Ar), 146.4 (d, $^2J_{C\text{-}P}$ = 9.9 Hz, NH*C*N$_{(near\ Py)}$), 142.7 (*C*H Ar), 141.0 (*C* Ar), 139.8 (*C* Ar), 139.7 (*C* Ar), 129.0 (*C*H Ar), 125.6 (*C*H Ar), 124.7 (*C*H Ar), 123.1 (d, $^4J_{C\text{-}P}$ = 2.5 Hz, *C*H Ar), 122.0 (NH*C*HCHN$_{(near\ Py)}$), 117.0 (NHCH*C*HN$_{(near\ Py)}$), 112.5 (d, $^4J_{C\text{-}P}$ = 1.9 Hz, *C*H Ar), 28.9 (*C*H(CH$_3$)$_2$), 27.8 (*C*H(CH$_3$)$_2$), 26.1 (d, $^1J_{C\text{-}P}$ = 30.2 Hz, P*C*H(CH$_3$)$_2$), 24.9 (CH(*C*H$_3$)$_2$), 24.8 (CH(*C*H$_3$)$_2$), 23.9 (CH(*C*H$_3$)$_2$), 22.3 (*C*H$_{3(imine)}$), 19.9 (PCH(*C*H$_3$)$_2$), 19.3 (PCH(*C*H$_3$)$_2$). ^{31}P{^{1}H} NMR (121.5 MHz, CD_2Cl_2): δ 12.8. Anal. Calcd for $C_{31}H_{48}BClF_4IrN_4P$ (822.20): C, 45.29; H, 5.88; N, 6.81. Found: C, 44.92; H, 5.63; N, 6.45.

Synthesis of [Ir(NCMe)$_2$H{(DippN=CMe)(C$_5$H$_3$N)(C$_3$H$_3$N$_2$)-κ^3(N$_{imine}$,N$_{Py}$,C2)}]$^{2+}$2[BF$_4$]$^-$ (3^{2+}2[BF$_4$]$^-$). To a solution of **1** (0.070 g, 0.10 mmol) in acetonitrile (5 mL), was added $AgBF_4$ (0.020 g, 0.10 mmol). The reaction mixture was stirred in the absence of light for 3 h at room temperature. After filtration through Celite, the filtrate was evaporated to dryness and then the residue was washed with Et_2O (3 × 2 mL) to yield an orange solid, which was collected by filtration and dried in vacuo (0.063 g, 0.079 mmol, 79%). ^{1}H NMR (500 MHz, CD_2Cl_2): δ 11.98 (br s, 1H, N*H*), 8.27 (apparent t, ^3J = 8.0 Hz, 1H, C*H* Py), 8.07 (dd, *J* = 8.0, 0.5 Hz, 1H, C*H* Py), 8.03 (dd, *J* = 8.0, 0.5 Hz, 1H, C*H* Py), 7.92 (dd, *J* = 2.3, 1.3 Hz, 1H, NHCHC*H*N$_{(near\ Py)}$), 7.43 (apparent t, ^3J = 2.3 Hz, 1H, NHC*H*CHN$_{(near\ Py)}$), 7.42–7.30 (m, 3H, C*H* Ar), 2.98 (sept, ^3J = 6.7 Hz, 1H, C*H*(CH$_3$)$_2$), 2.73 (sept, ^3J = 6.7 Hz, 1H, C*H*(CH$_3$)$_2$), 2.64 (s, 3H, C*H*$_{3(imine)}$), 2.35 (s, 3H, C*H*$_3$CN), 2.23 (s, 3H, C*H*$_3$CN), 1.26 (d, ^3J = 6.7 Hz, 3H, CH(C*H*$_3$)$_2$), 1.25

(d, ^3J = 6.7 Hz, 3H, CH(CH_3)$_2$), 1.15 (d, ^3J = 6.7 Hz, 3H, CH(CH_3)$_2$), 1.12 (d, ^3J = 6.7 Hz, 3H, CH(CH_3)$_2$), −23.11 (s, 1H, Ir–*H*). ^{13}C{^{1}H} NMR (125 MHz, CD_2Cl_2): δ 180.7 (*C*=N), 157.5 (*C* Ar), 154.9 (*C* Ar), 146.1 (NH*C*N$_{(near\ Py)}$), 143.7 (*C*H Ar), 140.7 (*C* Ar), 139.7 (*C* Ar), 139.6 (*C* Ar), 129.1 (*C*H Ar), 125.6 (*C*H Ar), 125.2 (*C*H Ar), 124.5 (*C*H Ar), 121.3 (NH*C*HCHN$_{(near\ Py)}$), 120.5 (CH_3*C*N), 120.4 (CH_3*C*N), 118.4 (NHCH*C*HN$_{(near\ Py)}$), 113.7 (*C*H Ar), 28.5 (*C*H(CH$_3$)$_2$), 27.8 (*C*H(CH$_3$)$_2$), 24.9 (CH(*C*H$_3$)$_2$), 24.7 (CH(*C*H$_3$)$_2$), 24.2 (CH(*C*H$_3$)$_2$), 23.9 (CH(*C*H$_3$)$_2$), 18.9 (*C*H$_{3(imine)}$), 3.7 (*C*H$_3$CN), 3.3 (*C*H$_3$CN). Anal. Calcd for $C_{26}H_{33}B_2F_8IrN_6$ (795.42): C, 39.26; H, 4.18; N, 10.57. Found: C, 38.85; H, 4.14; N, 10.82.

Synthesis of [Ir(NCMe)H{(DippN=CMe)(C$_5$H$_3$N)(μ-C$_3$H$_2$N$_2$-κC2,κN3)-κ^3(N$_{imine}$,N$_{Py}$,C2)}]$_2^{2+}$2[B(ArF$_5$)$_3$F]$^-$ (4^{2+}2[B(ArF$_5$)$_3$F]$^-$). To a CD_2Cl_2 (0.5 mL) solution of **3**$^{2+}$2[BF_4]$^-$ (0.014 g, 0.018 mmol) in a Young NMR tube, was added KO*t*-Bu (0.002 g, 0.018 mmol), the disappearance of the N*H* resonance was confirmed by ^{1}H NMR spectroscopic data. Then B(ArF$_5$)$_3$ (0.010 g, 0.019 mmol) was added to this reaction mixture. The product crystallized in the NMR tube at 0 °C (0.013 g, 0.006 mmol, 65%). ^{1}H NMR (500 MHz, CD_2Cl_2): δ 7.90 (apparent t, ^3J = 8.2 Hz, 1H, C*H* Py), 7.78 (d, ^3J = 8.0 Hz, 1H, C*H* Py), 7.58–7.36 (m, 4H, C*H* Ar), 7.30 (d, ^3J = 2.2 Hz, 1H, NCHC*H*N$_{(near\ Py)}$), 5.31 (d, ^3J = 2.2 Hz, 1H, NC*H*CHN$_{(near\ Py)}$), 2.88 (sept, ^3J = 6.9 Hz, 1H, C*H*(CH$_3$)$_2$), 2.77 (sept, ^3J = 6.9 Hz, 1H, C*H*(CH$_3$)$_2$), 2.63 (s, 3H, C*H*$_{3(imine)}$), 1.93 (s, 3H, C*H*$_3$CN), 1.25 (d, ^3J = 6.9 Hz, 3H, CH(C*H*$_3$)$_2$), 1.16 (d, ^3J = 6.9 Hz, 3H, CH(C*H*$_3$)$_2$), 1.12 (d, ^3J = 6.9 Hz, 3H, CH(C*H*$_3$)$_2$), 0.94 (d, ^3J = 6.9 Hz, 3H, CH(C*H*$_3$)$_2$), -24.02 (s, 1H, Ir–*H*). ^{13}C{^{1}H} NMR (125 MHz, CD_2Cl_2): δ 178.3 (*C*=N), 156.7 (*C* Ar), 156.3 (*C* Ar), 154.1 (N*C*N$_{(near\ Py)}$), 149.2 (*C* C_6F_5), 147.3 (*C* C_6F_5), 143.0 (*C* Ar), 141.1 (*C*H Ar), 139.8 (*C* Ar), 139.1 (*C* Ar), 138.0 (*C* C_6F_5),136.0 (*C* C_6F_5), 129.2 (N*C*HCHN$_{(near\ Py)}$), 128.6 (*C*H Ar), 126.3 (*C*H Ar), 125.6 (*C*H Ar), 121.3 (*C*H Ar), 117.4 (CH_3*C*N), 116.3 (NCH*C*HN$_{(near\ Py)}$), 110.9 (*C*H Ar), 28.6 (*C*H(CH$_3$)$_2$), 27.6 (*C*H(CH$_3$)$_2$), 24.7 (CH(*C*H$_3$)$_2$), 24.4 (CH(*C*H$_3$)$_2$), 24.0 (CH(*C*H$_3$)$_2$), 23.3 (CH(*C*H$_3$)$_2$), 18.7 (*C*H$_{3(imine)}$), 3.0 (*C*H$_3$CN). ^{11}B{^{1}H} NMR (128 MHz, CD_2Cl_2): δ -0.31 (br s) ^{19}F{^{1}H} NMR (282 MHz, CD_2Cl_2): δ -136.6 (pentet, $^3J_{F\text{-}F}$ = 12.9 Hz, 6F, *o*-C$_6$*F*$_5$), -163.3 (t, $^3J_{F\text{-}F}$ = 20.1 Hz, 3F, *p*-C$_6$*F*$_5$), -167.8 (td, $^3J_{F\text{-}F}$ = 20.4 Hz, $^4J_{F\text{-}F}$ = 4.3 Hz, 6F, *m*-C$_6$*F*$_5$), -190.8 (br s, 1F, B*F*). Anal. Calcd for $C_{84}H_{58}B_2F_{32}Ir_2N_{10}$ (2221.46): C, 45.42;

H, 2.63; N, 6.31. Found: C, 44.99; H, 2.79; N, 6.12.

X-ray Data Collection, Structure Solution, and Refinement for All Compounds. Suitable crystals for the X-ray analysis of all compounds were obtained as described above. Data for $\mathbf{1}^{+}[BF_4]^{-}\cdot CH_2Cl_2$, $\mathbf{2}^{+}[BF_4]^{-}\cdot CH_2Cl_2$, $\mathbf{3}^{2+}2[BF_4]^{-}\cdot 2CH_2Cl_2$ and $\mathbf{4}^{2+}2[B(ArF_5)_3F]^{-}\cdot 4CH_2Cl_2$ were collected on an APEX-II CCD (graphite-monochromated Mo-Kα radiation, λ = 0.71073 Å) at 173(2) K. Crystallographic and experimental details for these structures are summarized in Table 1. The structures were solved by direct methods (SHELXS-97[11]) and refined by full-matrix least-squares procedures (based on F^2, SHELXL-97) with anisotropic thermal parameters for all the non-hydrogen atoms. The hydrogen atoms were introduced into the geometrically calculated positions (SHELXS-97 procedures).

The following specific comments apply for the structures:

$\mathbf{1}^{+}[BF_4]^{-}\cdot CH_2Cl_2$: The asymmetric unit contains one molecule of CH_2Cl_2. The hydrogen atom H1N was found (not located in calculated position). There is an inter-molecular hydrogen bond interaction between the NH group and F2 in the $[BF_4]^{-}$. The hydride H1 was found and then fixed, otherwise the bond distance Ir1–H1 changes during the refinement.

$\mathbf{2}^{+}[BF_4]^{-}\cdot CH_2Cl_2$: The asymmetric unit contains one molecule of CH_2Cl_2. The hydrogen atom H1N was found (not located in calculated position). There is an inter-molecular hydrogen bond interaction between the NH group and F2 in the $[BF_4]^{-}$. The hydride H1 was found (not located in calculated position) then fixed. The SQUEEZE instruction in PLATON was applied to eliminate residual electronic density. The residual electron density was assigned to half a molecule of diethyl ether disordered.

$\mathbf{3}^{2+}2[BF_4]^{-}\cdot 2CH_2Cl_2$: One $[BF_4]^{-}$ is disordered. The asymmetric unit contains 2 molecules of CH_2Cl_2. The hydrogen atom H1N and the hydride H1 were found (not located in calculated position). There is an inter-molecular hydrogen bond interaction between the NH group and F4 in the $[BF_4]^{-}$.

$\mathbf{4}^{2+}2[B(ArF_5)_3F]^{-}\cdot 4CH_2Cl_2$: The asymmetric unit contains half a molecule of the iridium dimer, one molecule of $[B(ArF_5)_3F]^{-}$ and two molecules of CH_2Cl_2. By symmetry, there are 2 molecules of $[B(ArF_5)_3F]^{-}3$ for 1 entire Ir dimer and 4 molecules of CH_2Cl_2. The hydride H1 was found and then fixed. Although the

ellipsoid of C10 is distorted (alert B in the checkcif), it is a CH_3 group confirmed by the NMR spectra.

Table 1. Crystal data and structure refinement for $\mathbf{1}^{+}[BF_4]^{-}\cdot CH_2Cl_2$, $\mathbf{2}^{+}[BF_4]^{-}\cdot CH_2Cl_2$, $\mathbf{3}^{2+}2[BF_4]^{-}\cdot 2CH_2Cl_2$ and $\mathbf{4}^{2+}2[B(ArF_5)_3F]^{-}\cdot 4CH_2Cl_2$.

	$\mathbf{1}^{+}[BF_4]^{-}\cdot CH_2Cl_2$	$\mathbf{2}^{+}[BF_4]^{-}\cdot CH_2Cl_2$	$\mathbf{3}^{2+}2[BF_4]^{-}\cdot 2CH_2Cl_2$	$\mathbf{4}^{2+}2[B(ArF_5)_3F]^{-}\cdot 4CH_2Cl_2$
Empirical formula	$C_{25}H_{32}BCl_3F_4IrN_5$	$C_{32}H_{50}BCl_3F_4IrN_4P$	$C_{28}H_{37}B_2Cl_4F_8IrN_6$	$C_{88}H_{66}B_2Cl_8F_{32}Ir_2N_{10}$
Fw	787.91	907.09	965.25	2561.12
T/K	173(2)	173(2)	173(2)	173(2)
Crystal system	Monoclinic	Triclinic	Triclinic	Triclinic
Space group	P 21/c	P -1	P -1	P -1
a/Å	18.4630(6)	9.234(5)	12.037(9)	12.3805(5)
b/Å	8.4248(3)	12.118(5)	12.849(10)	14.7768(6)
c/Å	24.8389(7)	18.115(5)	14.281(10)	14.8245(6)
α/°	90	93.175(5)	77.179(18)	79.6020(10)
β/°	127.008(2)	93.492(5)	71.935(17)	69.5660(10)
γ/°	90	93.730(5)	66.434(18)	71.7040(10)
V/Å^3	3085.30(18)	2015.4(15)	1913(2)	2405.26(17)
Z	4	2	2	1
μ/mm^{-1}	4.635	3.596	3.838	3.099
No. of rflns collected	52902	52682	50012	63046
No. unique rflns	10720	13891	13241	16590
R(int)	0.0322	0.0336	0.0307	0.0239
Goodness of fit on F^2	1.187	1.024	1.061	1.131
Final *R*	R1 = 0.0364	R1 = 0.0319	R1 = 0.0401	R1 = 0.0268
indices [$I>2\sigma(I)$]	wR2 = 0.0691	wR2 = 0.0743	wR2 = 0.1119	wR2 = 0.0548
R indices (all data)	R1 = 0.0474	R1 = 0.0423	R1 = 0.0485	R1 = 0.0355
	wR2 = 0.0716	wR2 = 0.0774	wR2 = 0.1176	wR2 = 0.0599

References: p 138

ACKNOWLEDGMENTS

The USIAS, CNRS, UdS, Région Alsace and Communauté Urbaine de Strasbourg are gratefully acknowledged for the award of fellowships and a Gutenberg Excellence Chair (2010–11) to AAD and support. We also thank the ucFRC (www.icfrc.fr) for support and the China Scholarship Council for a PhD grant to F. H., and the Service de Radiocristallographie (Institut de Chimie, Strasbourg) for the determination of the crystal structures.

References: p 138

REFERENCES

(1) (a) Crabtree, R. H., *Coord. Chem. Rev.* **2013,** *257*, 755–766. (b) Melaimi, M.; Soleilhavoup, M.; Bertrand, G., *Angew. Chem. Int. Ed.* **2010,** *49*, 8810–8849. (c) de Frémont, P.; Marion, N.; Nolan, S. P., *Coord. Chem. Rev.* **2009,** *253*, 862–892. (d) Hahn, F. E.; Jahnke, M. C., *Angew. Chem. Int. Ed.* **2008,** *47*, 3122–3172.

(2) Karmakar, S.; Datta, A., *Angew. Chem. Int. Ed.* **2014,** *53*, 9587–9591.

(3) (a) Kuwata, S.; Ikariya, T., *Chem.–Eur. J.* **2011,** *17*, 3542–3556. (b) Kuwata, S.; Ikariya, T., *Chem. Commun.* **2014,** *50*, 14290–14300. (c) Zhao, B.; Han, Z.; Ding, K., *Angew. Chem. Int. Ed.* **2013,** *52*, 4744–4788.

(4) (a) Meier, N.; Hahn, F. E.; Pape, T.; Siering, C.; Waldvogel, S. R., *Eur. J. Inorg. Chem.* **2007,** *2007*, 1210–1214. (b) Hahn, F. E., *ChemCatChem* **2013,** *5*, 419–430. (c) Jahnke, M. C.; Hahn, F. E., *Coord. Chem. Rev.* **2015,** *293–294*, 95–115.

(5) Hahn, F. E., *Advances in Organometallic Chemistry and Catalysis* **2013**, 111–132.

(6) (a) Flowers, S. E.; Cossairt, B. M., *Organometallics* **2014,** *33*, 4341–4344. (b) Toda, T.; Kuwata, S.; Ikariya, T., *Chem.–Eur. J.* **2014,** *20*, 9539-9542. (c) Marelius, D. C.; Darrow, E. H.; Moore, C. E.; Golen, J. A.; Rheingold, A. L.; Grotjahn, D. B., *Chem.–Eur. J.* **2015,** *21*, 10988–10992.

(7) He, F.; Braunstein, P.; Wesolek, M.; Danopoulos, A. A., *Chem. Commun.* **2015,** *51*, 2814–2817.

(8) Parks, J. E.; Wagner, B. E.; Holm, R. H., *J. Organomet. Chem.* **1973,** *56*, 53–66.

(9) Bianchini, C.; Mantovani, G.; Meli, A.; Migliacci, F.; Laschi, F., *Organometallics* **2003,** *22*, 2545–2547.

(10) Raba, A.; Anneser, M. R.; Jantke, D.; Cokoja, M.; Herrmann, W. A.; Kühn, F. E., *Tetrahedron Lett.* **2013,** *54*, 3384–3387.

(11) Sheldrick, G. M., *SHELXL-97, Program for crystal structure refinement*. University of Göttingen: Göttingen, Germany, 1997.

Conclusion générale

Conclusion générale

Des complexes NHC-protique de l'iridium et du rhodium sont étudiés dans cette thèse.

Dans le cas des 1-arylimidazoles non fonctionnalisés nous avons approfondi l'étude des complexes homo bi-nucléaire des complexes de l'Ir(I) et du Rh(I) contenant un ligand 1-arylimidazolide pontant les centres métalliques par C2 et N3, dans le chapitre 2. Les données obtenues par radiocristallographie aux rayons X suggèrent une délocalisation électronique dans le système et un caractère partiellement carbènique pour le carbone de l'imidazolide lié à l'Ir. L'imidazolide lié au métal peut être vu comme un système pNHC déprotoné.

Le cas des imidazoles fonctionnalisés par des imines est étudié dans les chapitres 2 et 3. Dans la formation des complexes de l'Ir(I) et du Rh(I) avec des ligands pNHC fonctionnalisés par des imines, nous avons étudié l'effet du métal. Dans le cas de l'iridium, on a pu observ par RMN ^{1}H des hydrures intermédiaires suggérant fortement que la transformation par tautomérisation/métallotropisme observée passait par une activation par l'iridium de la liaison C2-H assistée par une chélation de l'imine dans les complexes neutre ou cationique ayant un iridium lié au N. Dans le cas du Rh cependant de tels intermédiaires n'ont pas pu être observés. Dans l'étude des complexes homo et hétéro-di-nucléaire, de nouveaux complexes hétéro-di-nucléaire Rh-Ir ont pu être obtenus séquentiellement ; ceci a permis d'étudier la métallosélectivité dans ces réactions. Le complexe C–Ir/N–Rh a été isolé sélectivement à partir soit du précurseur lié au N par l'Ir, soit de celui dont le N est lié par le Rh. Ces résultats montrent la préférence de la formation de la liaison Ir-C et révèlent la migration de l'iridium de N au C.

Dans le chapitre 4 nous avons étendu nos précédents résultats complexes pNHC fonctionnalisés bidente à la synthèse de complexes pNHC bis fonctionnalisé tridente et étudié leur réactivité. Tous ces résultats sont utiles pour un développement ultérieur des méthodologies de synthèse donnant accès aux complexes homo et hétéro-nucléaire des pNHC ayant une liaison C imidazolide anionique.

Les applications potentielles en catalyse bifonctionnelle pour ces complexes pNHC fonctionnalisés restent à développer.

Fan HE

Complexes de métaux de transition avec des ligands carbènes N-hétérocycliques : synthèse et réactivité

Résumé

L'objectif de ce travail est la synthèse de complexes contenant des ligands NHC protiques fonctionnalisés avec un groupement imine dans le but de développer des méthodologies de synthèse donnant accès à des ligands pNHC ainsi que la synthèse des groupes imidazolide anioniques liés par le C et leurs complexes homo et hétéro-dinucléaires. Dans le cas des imidazoles sans groupe fonctionnel, la déprotonation à l'aide de *n*-butyl lithium a permis l'obtention de (1-aryl-1*H*-imidazol-2-yl)lithium avec de bons rendements. La réaction de (1-aryl-1*H*-imidazol-2-yl)lithium avec $[Ir(cod)(\mu\text{-}Cl)]_2$ ou $[Rh(cod)(\mu\text{-}Cl)]_2$ a conduit à des complexes dinucléaires bipontés en C2,N3. Dans le cas de l'imidazole possédant une fonctionnalité imine, le complexe de l'Ir(I) lié au N de l'imidazole peut se tautomériser en complexe de l'Ir(I) imine avec un ligand pNHC suite à la réaction d'abstraction du chlorure à température ambiante, alors que la tautomérisation de l'analogue du Rh(I) nécessite une température de 110°C. La déprotonation des complexes de l'Ir(I) et Rh(I) liés par le N de l'imidazole avec addition de $[Ir(cod)(\mu\text{-}Cl)]_2$ ou de $[Rh(cod)(\mu\text{-}Cl)]_2$ *in situ* permet l'obtention de complexes homo et hétéro-dinucléaires. La métallation des sels d'imidazolium fonctionnalisés avec un groupement imine s'est avére être une méthode efficace pour la synthèse de complexes métallés ayant un ligand pNHC et a été étendue des complexes bidentes aux complexes chélatants pNHC.

Mots clés : carbènes N-hétérocyclique protique, fonctionnalitéimine, complexes de l'iridium, complexes du rhodium, activation C-H.

Résumé en anglais

The purpose of this work is the synthesis of complexes containing imine-functionalized protic NHC ligands in order to further develop synthetic methodologies giving access to pNHC, C-bound 'anionic' imidazolide, and homo- and heterodinuclear complexes. In the case of imidazoles without functional group, deprotonation with *n*-butyl lithium afforded (1-aryl-1*H*-imidazol-2-yl)lithium in good yield. Reaction of (1-aryl-1*H*-imidazol-2-yl)lithium with $[Ir(cod)(\mu\text{-}Cl)]_2$ or $[Rh(cod)(\mu\text{-}Cl)]_2$ yielded a doubly C2,N3-bridged dinuclear complex. In the case of imine-functionalized imidazole, the Ir(I) N-bound imidazole complex can tautomerize to Ir(I) imine-functionalized pNHC complex chloride abstraction at room temperature, while in the Rh(I) analog the tautomerization can be achieved at 110 °C. *In situ* deprotonation of the N-bound imidazole Ir(I) or Rh(I) complexes, followed by addition of $[Ir(cod)(\mu\text{-}Cl)]_2$ or $[Rh(cod)(\mu\text{-}Cl)]_2$ led to the isolation of homo- and heterodinuclear complexes. The metalation of imine-functionalized imidazolium salts is also an effective procedure for synthesis of pNHC metal complexes, and it was extended from bidentate to pincer-type pNHC complexes.

Kewords: protic N-heterocyclic carbenes, imine-functionalizations, iridium complexes, rhodium complexes, C-H activation.